

PROCESSING AND CHARACTERISATION OF ALUMINIUM METAL MATRIX COMPOSITES

Thesis submitted to
The University of Kerala
in fulfilment of the requirements
for the Degree of
DOCTOR OF PHILOSOPHY
in the **Faculty of Engineering and Technology**

By
T.P.D. RAJAN



REGIONAL RESEARCH LABORATORY
COUNCIL OF SCIENTIFIC AND INDUSTRIAL RESEARCH
THIRUVANANTHAPURAM - 695 019
INDIA

June 2002



COUNCIL OF SCIENTIFIC AND INDUSTRIAL RESEARCH
REGIONAL RESEARCH LABORATORY
Industrial Estate P.O., Thiruvananthapuram – 695 019, India
Telegram: Consearch, Fax: 0471-490186, 491712
Email: root@csrtrd.ren.nic.in; Phone: 0471-490674, 490811

CERTIFICATE

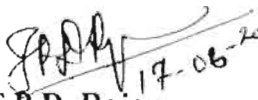
This is to certify that the thesis entitled '**Processing and Characterisation of Aluminium Metal Matrix Composites**' embodies the results of bonafide research work carried out by **Mr. T.P.D. Rajan** for the degree of **Doctor of Philosophy** in the Faculty of Engineering and Technology of the University of Kerala under our guidance. The content of this thesis or part thereof has not been submitted to any other university or institute for the award of any degree or diploma.

Dr. B.C. Pai
Senior Deputy Director
Metal Processing Division
Regional Research Laboratory
CSIR, Thiruvananthapuram
India.

Dr. R.M. Pillai
Deputy Director and Head
Metal Processing Division
Regional Research Laboratory
CSIR, Thiruvananthapuram
India.

DECLARATION

I hereby declare that this thesis entitled '**Processing and Characterisation of Aluminium Metal Matrix Composites**' embodies the results of bonafide research work done by me for the degree of **Doctor of Philosophy** in Faculty of Engineering and Technology of the University of Kerala under the guidance of **Dr. B.C. Pai** and **Dr. R.M. Pillai**, Regional Research Laboratory (CSIR), Thiruvananthapuram. I further declare that this thesis or part thereof has not previously been formed the basis for the award of any degree or diploma.


17-06-200
T.P.D. Rajan

*Dedicated to
My Parents
and Teachers*

ABSTRACT

Metal Matrix Composites (MMC) are an important class of high performance advanced materials with potential engineering applications especially in the areas of aerospace, defence and automotive industries. The advantages of MMC over traditional alloys are their high specific strength and modulus, increased wear resistance, high temperature strength, low coefficient of thermal expansion and good damping capacity. The metal matrix composites currently used are monocomposites, wherein only one type of reinforcement is used. Hybrid metal matrix composites are the new type of MMC where more than one type of reinforcements are used. These materials provide better properties compared to conventional mono composites. Among the various matrix material available, aluminium and its alloys are widely used as the matrix in the fabrication of MMC. Discontinuously reinforced aluminium matrix composites are most commonly studied due to their isotropic properties, wide application, cost effectiveness, simple fabrication techniques and feasibility of large scale production. Stir casting technique is the simplest and economical processing route.

The present investigation is on the processing and characterisation of mono and hybrid composites based on cast Al-7Si-0.35Mg [Al(356)] matrix alloy reinforced with silicon carbide particles, graphite particles, carbon short fibres, aluminosilicate short fibres and flyash particles. The composites fabricated are evaluated with respect to structural, interfacial, solidification, physical and mechanical characteristics. Correlations are made on the effect of various processing parameters on the structure and properties of the composites. The utilization of the indigenously available low cost aluminosilicate fibres and the fine spherical flyash particles as reinforcements for the fabrication of aluminium matrix composites are assessed. The study also compares the effect of reinforcement with different morphology such as carbon in the form of graphite particle and short fibre, and aluminosilicate in the form of short fibre and fly ash particle on the processing, structure and properties. The structure of the thesis and details of the studies are given below.

The Chapter 1 deals with the general introduction to MMC. The Chapter 2 deals with the extensive literature survey carried out on aluminium matrix composites, their processing, properties, interfacial and solidification characteristics and applications with respect to mono and hybrid composites.

The Chapter 3 gives the details of the materials and the experimental methods used in the present investigation. Liquid metal stir casting technique is used in general, while compocasting and squeeze casting are adopted for processing specific systems of the composites. The structural characteristics of all the composites systems synthesised are evaluated by optical microscopy, SEM, EDS, AFM and XRD and solidification behaviour by Thermal analysis. The physical properties such as density and electrical conductivity are measured. The mechanical properties such as hardness by Brinell hardness tester and tensile and compression strengths using Instron Universal testing machine are evaluated.

The Chapter 4 deals with the processing and characterisation of SiC and Graphite reinforced mono and hybrid aluminium matrix composites. The mixed mode of particle addition during hybrid composite synthesis results in better dispersion and distribution of particles. There is no remarkable interfacial reaction at SiC – matrix interface, where as there is formation of $MgAl_2O_4$ spinel due to the presence of SiO_2 layer over SiC. Introduction of silicon carbide and graphite reinforcements into the Al(356) matrix alloy reduces the liquidus temperature. Incorporation of additional Mg to the composite melt has multifunctional behaviour such as promotion of ceramic particle wetting with the aluminium alloy matrix, better contact at metal/mould interface, there by enhancing heat transfer rate and precipitation hardening of the matrix. The compression strength of mono and hybrid composites is higher than those of the base alloy. Hybridization with synthetic graphite particles has resulted in lower compression strength than natural graphite particles.

The Chapter 5 deals with the processing and characterisation of SiC and carbon short fibre reinforced mono and hybrid composites. The surface treatments of carbon fibre are discussed. Addition of as received carbon short fibre to the matrix alloy leads to agglomeration and rejection. The sodium silicate surface treatment is

effective in deflocculation of the fibres and making them free flow during the addition into the matrix. Interfacial reaction occurs at the carbon fibre – matrix interface with the formation of aluminium carbide providing better wetting, but it degrades the fibre surface. This brittle reaction products increase the hardness of the hybrid composite compared to the monocomposite. Carbon short fibres are highly reactive compared to the graphite particle.

The Chapter 6 deals with the processing and characterisation of standard and zirconia grade alumino silicate short fibre reinforced aluminium matrix composites. Among the various surface treatments studied, the ultrasonic treatment in aqueous acidic solution of pH 4-5 range has given better dispersion, and less agglomeration and porosity in the composite castings. All the major constituents of the fibre such as Al_2O_3 , SiO_2 and ZrO_2 react with the matrix elements. MgAl_2O_4 spinel formation is observed in both the standard and zirconia grade fibres. The interfacial reaction depletes the Mg content in the matrix, thus reducing the amounts of Mg_2Si available during precipitation hardening and resulting in lower hardness for the composites after aging. The addition of aluminosilicate fibre reduces the liquidus temperature of the matrix and peak heat flux values.

The Chapter 7 discusses the processing and characterisation of cenosphere or spherical type fly ash particle reinforced aluminium matrix composites. Addition of 5wt% of $13\mu\text{m}$ (average size) fly ash particles in as received condition leads to their agglomeration in 356 Al alloy composites processed by liquid metal processing technique. Surface treatment given to the fly ash particles has deflocculated them leading to better dispersion of individual particles in the composite. Further, improvement in the dispersion and distribution has been achieved by modified compocasting i.e., by reheating the semisolid/compocast composite slurry just above the liquidus and then casting by permanent mould or squeeze casting. The interfacial reaction between the fly ash and the matrix alloy is higher with liquid metal processed composites than semisolid processed ones. In addition to giving the conclusion drawn under each chapter (4 to 7) separately, Chapter 8 summarises all of them together and also gives the significant contributions of the present investigation leading to the areas for the future work.

ACKNOWLEDGEMENTS

It is with great respect and profound gratefulness that I record my indebtedness and deep felt devotion to my supervising teachers **Dr. B.C. Pai**, Senior Deputy Director and **Dr. R.M. Pillai**, Deputy Director and Head, Metal Processing Division, Regional Research Laboratory, Trivandrum for their precious and encouraging supervision, valuable discussions, never failing kindness and inspiring guidance throughout the course of this research work.

I express my sincere gratitude to Dr. K.G. Satyanarayana, Senior Deputy Director for his persistent encouragement and timely counsel. I greatly acknowledge Prof. Javed Iqbal, present Director, RRL and Ex-director Dr. G. Vijay Nair for their permission and support during the course of research work.

I am very much grateful to Council of Scientific and Industrial Research (CSIR), New Delhi for granting Senior Research Fellowship and Research Associateship for carrying out this research work.

I wish to express my sincere thanks to Mr. K. Sukumaran, Dr. U.T.S. Pillai and Mr. K.K. Ravikumar for their help in mechanical testing, Mr. S.G.K. Pillai for the optical metallography, Dr. V. John and Mr. M.C. Shaji for foundry facilities, Mr. M. Ravi for image analysis and data logger. Also I extend my gratefulness to all of them for the valuable and useful technical discussions.

I am most grateful to Dr. Peter Koshy and Mr. Prabhakar Rao, RRL, Thiruvananthapuram, Prof. M. Chakraborty and Dr. S.A. Kori, Indian Institute of Technology, Kharagpur, Dr. H.K. Varma and Mr. Sree Kumar, Sree Chithra Thirunal Institute of Medical Science and Technology, Thiruvananthapuram and Dr. R.V. Krishnan and Dr. T.A. Bhaskaran, National Aerospace Laboratory, Bangalore for extending their facilities for SEM and EDS work. I also extend my thanks to Dr. Richard Lin, University of Auckland, New Zealand for AFM, SEM and EDS work. I am also grateful to Dr. Manoj Raama Varma and Dr. Roschen Saikumar, RRL, Trivandrum for providing the data logger. I wish to thank Dr. U. Symaprasad and Mr. P. Gurusami for the XRD work.

I profoundly express my heartfelt thanks to Dr. K. Narayan Prabhu, KREC, Surathkal for his kind encouragement and help in the heat transfer studies. My sincere thanks to Prof. P.K. Rohatgi, University of Wisconsin, Milwaukee, USA, for providing the fine spherical fly ash particles. I am thankful to M/s Murugappa Morgan Ltd, Chennai for supplying aluminosilicate fibres. My sincere thanks to Mr. Hugh Davies, Thermodynamics and Process Modelling Group, Materials Centre, National Physical Laboratory, Teddington, Middlesex, United Kingdom for computing the thermodynamic calculations using MTDATA software and Dr. A.E.M. Warner, INCO Ltd., Ontario, Canada for sending photographs and data related to hybrid metal matrix composites.

I am very much indebted to Dr. P.P. Sinha, General Manager, Rocket Fabrication Facility, and Dr. T. Lakshmanan, Former Head, Materials Characterisation Division, Vikram Sarabhai Space Centre, ISRO, Trivandrum for their valuable advice and encouragement.

My heartfelt thanks to Mr. V. Antony for the help received from him throughout the research work. I am very much thankful to Mr. T. Soman, Mr. B. Parameshwaran Nair, Mrs. M.B. Madhavikutty Amma and Mrs. Sreelatha Nair. I acknowledge with thanks the help received from Mr. P. Balan, Mr. S. Ramakrishnan, Mr. N. Narayanan, Mr. T.A. Balakrishnan, Mr. P. Sisupalan and P. Soman for the machining, fabrication and other works at workshop.

I am very much grateful to Miss. S.S. Sreeja Kumari for the kind help and the fruitful technical discussions. I extend my sincere thanks to Mrs. Kavithaa Shanamugam, Mrs. L. Sandhya Rani, Mr. V.M. Sreekumar, Mr. K.R. Ravi, Miss. Sindhu, Mrs. Prajila, Mr. P. Jawahar and Mr. Prince Bovas for their assistance in my work.

I greatly acknowledge the support received from my friends, especially from Dr. P. Shanmugham, Miss. J. Mary Gladis, Mr. K. S. Shibu and Mr. S.R. Santhosh.

T.P.D. RAJAN

CONTENTS

Abstract	i
Acknowledgements	iv
Contents	vi
List of Tables	xi
List of Figures	xii
CHAPTER 1: INTRODUCTION	1
1.1. CONSTITUENTS OF MMC	3
1.1.1. Matrix	3
1.1.2. Reinforcements	3
1.1.3. Interface	4
1.2. TYPES OF MMC	7
1.3. IMPORTANCE AND PROSPECTS OF MMC	8
CHAPTER 2: LITERATURE REVIEW	9
2.1. INTRODUCTION	9
2.2. PROCESSING OF MMC AND HYBRIDISATION	9
2.2.1. Hybridisation	10
2.2.2. Primary Liquid State Processes	11
2.2.3. Primary Solid State Processing	16
2.3. CLASSIFICATION OF HMMC	17
2.4. HYBRID SYSTEMS	18
2.4.1. Aluminium	18
2.4.2. Magnesium	27
2.4.3. Smart Hybrids	27
2.4.4. Functionally Gradient Hybrids	29
2.5. PROPERTIES OF MONO AND HYBRID COMPOSITES	30
2.5.1 Physical Properties	30
2.5.2. Mechanical Properties	31
2.5.3. Tribological Properties	36

2.5.4. Corrosion Resistance Properties	38
2.6. SOLIDIFICATION BEHAVIOUR OF MMC	39
2.6.1. Solidification and Structure Formation	39
2.6.2. Characteristics of Solidification curve	41
2.6.3. Casting/Mould Interfacial Heat transfer	41
2.7. INTERFACIAL CHARACTERISTICS OF MMC	42
2.7.1. Wetting	43
2.7.2 Interfacial chemical reaction	43
2.7.3. Interfaces and Composite properties	47
2.8. APPLICATIONS	49
2.9. GENERAL DISCUSSION	53
2.10. FUTURE RESEARCH AVENUES	54
2.11. SUMMARY	55
2.12 SCOPE OF THE INVESTIGATION	56
CHAPTER 3: MATERIALS AND EXPERIMENTAL METHODS	58
3.1. MATERIALS	58
3.1.1. Matrix:	58
3.1.2. Reinforcements	58
3.2. COMPOSITE PROCESSING	62
3.3. SOLIDIFICATION STUDIES	65
3.4. HEAT TREATMENT STUDIES	65
3.5. STRUCTURAL STUDIES	67
3.5.1. Optical Microscopy	67
3.5.2. Image Analysis	68
3.5.3. Scanning Electron Microscopy (SEM)	68
3.5.4. Energy Dispersive X-ray Spectroscopy (EDS)	68
3.5.5. Atomic Force Microscope (AFM)	68
3.6. PHYSICAL CHARACTERISTICS	69
3.6.1. Density Measurement	69

3.6.2. Electrical Conductivity Measurement	69
3.7. MECHANICAL CHARACTERISTICS	69
3.7.1. Hardness Measurement	69
3.7.2. Mechanical Testing	70
CHAPTER 4: Al (356) - SiC_(p) - GRAPHITE MONO AND HYBRID COMPOSITES	72
4.1. INTRODUCTION	72
4.2. METHODOLOGY	73
4.2.1. Estimation of Heat Flux	75
4.3. RESULTS	75
4.3.1. Structural Characteristics	75
4.3.2. Solidification Characteristics	86
4.3.3. Heat Treatment Characteristics	93
4.3.4. Physical Properties	94
4.3.5. Mechanical Properties	95
4.4. DISCUSSION	110
4.4.1. Processing and Microstructural Evolution	110
4.4.2. Solidification Behaviour	113
4.4.3. Heat Treatment Characteristics	116
4.4.4. Physical Properties	116
4.4.5. Mechanical Properties	117
4.5. SUMMARY	117
CHAPTER 5: Al(356) - SiC_(p) - C_(sf) MONO AND HYBRID COMPOSITES	119
5.1. INTRODUCTION	119
5.2. METHODOLOGY	120
5.3. RESULTS	121
5.3.1. Optical Microstructures and Image Analysis	121
5.3.2. SEM Microstructures and EDS Analysis	122
5.3.3. Ageing Behaviour	125
5.3.4. Density	125

5.3.5. Mechanical Characteristics	126
5.4. DISCUSSION	142
5.4.1. Fibre treatments	142
5.4.2. Structural and Interfacial Characteristics	143
5.4.3. Ageing Characteristics	149
5.4.4. Physical and Mechanical Characteristics	149
5.5. SUMMARY	150
CHAPTER 6: Al(356) - ALUMINOSILICATE SHORT FIBER REINFORCED COMPOSITES	151
6.1. INTRODUCTION	151
6.2. METHODOLOGY	152
6.3. RESULTS	153
6.3.1. Fibre Treatments	153
6.3.2. Optical Microstructures	154
6.3.3. SEM Microstructures and EDS Analysis	155
6.3.4. Heat Treatment	157
6.3.5. Solidification Behaviour	157
6.4. DISCUSSION	173
6.4.1. Fibre Treatments	173
6.4.2. Microstructural Behaviour	173
6.4.3. Interfacial Behaviour	174
6.4.4. Heat Treatment Response	178
6.4.5. Solidification Behaviour	178
6.5. SUMMARY	179
CHAPTER 7: Al(356) – FLY ASH COMPOSITES	181
7.1. INTRODUCTION	181
7.2. METHODOLOGY	182
7.3. RESULTS	183

7.3.1. Optical Microstructures and Image Analysis	184
7.3.2. SEM Microstructures and EDS Analysis	186
7.3.3. Physical Properties	188
7.3.4. Mechanical Properties	188
7.4. DISCUSSION	206
7.4.1. Liquid Metal Stir Casting	206
7.4.2. Compocasting	207
7.4.3. Modified Compocasting	207
7.4.4. Interfacial Reactions	209
7.5. SUMMARY	210
CHAPTER 8: CONCLUSIONS	212
8.1 SIGNIFICANT OBSERVATIONS/CONTRIBUTIONS OF THE PRESENT INVESTIGATION	215
8.2 SCOPE FOR THE FUTURE WORK	216
REFERENCES	217
AWARDS, PATENTS AND PUBLICATIONS	232

LIST OF TABLES

Figure Number	Caption	Page Number
1.1	Widely used aluminium matrices and their mechanical properties	5
1.2	Common reinforcements and their characteristics	6
2.1	Types of hybrid metal matrix composite systems	18
2.2	Possible reaction products and precipitates at the interface in various aluminum alloy matrix and reinforcement combinations	46
2.3	Comparison of indexed finished part cost for cylinder liner: Grey cast iron versus GrA-Ni TM	50
3.1	Chemical composition of the matrix alloy	58
3.2	Thermophysical properties of the matrix	59
3.3	Thermophysical properties of the reinforcements chosen	60
3.4	Composition of aluminosilicate fibres	61
3.5	Chemical composition of fly ash particles	62
3.6	Thermophysical properties of the mould materials	65
4.1	Variation in structural morphology of primary aluminium and eutectic silicon phases in the matrices of base alloy and different composite system	85
7.1	Measured areas of primary α -aluminum phase in Al(356) - 5% fly ash (treated particles) composites synthesized by different routes	185

LIST OF FIGURES

Figure Number	Caption	Page Number
1.1	Comparison between conventional monolithic materials and composite materials	2
2.1	Wear rate and applied load diagram for Al(356)-20% SiC _(p) -10% Gr and Al(356)-20% SiC _(p) -3% Gr HMMC in comparison with (a) Al(356) alloy and Al(356)-20% SiC _(p) mono composite	20
2.2	Variation of the weight loss with sliding distance for SiC + BN-Al-4% Cu hybrid composites under an applied load of 35 N and a sliding velocity of 1m/s	23
2.3	Microstructures of Al-15% SiC _(p) -15% mullite short fibres HMMC using (a) as received SiC _(p) and (b) oxidised SiC _(p)	23
2.4	Effect of sliding speeds on wear behaviour of Al-Al ₂ O _{3(sf)} -C _(sf) HMMC	24
2.5	SEM micrograph of Al-SiC _(p) -C _(sf) (a) mono and (b) hybrid composites	24
2.6	Schematic illustration of contact angle in a (a) non-wetting, and (b) wetting system	45
2.7	Silicon levels required in the matrix to prevent the formation of aluminium carbide as a function of melt temperature	45
2.8	Photographs of GrA-Ni TM HMMC components (a) cylindrical liners, (b) sand cast rotors and (c) Drisc TM brake system	51
2.9	Properties comparison of Al-12% Al ₂ O _{3(sf)} -9% C _(sf) HMMC with ordinary engine block liners	52
3.1	Schematic diagram of composite fabrication setup for liquid metal stir casting.	63
3.2	Typical permanent mould composite castings made with (a) 500 gm and (b) 10 Kg level	64
3.3	Dimensions of cylindrical mould and thermocouple positions	66
3.4	Experimental setup of computer-aided data acquisition system	66

3.5	Dimensions of specimens used for mechanical testing (a) Standard tensile specimen (b) Hounsfield Tensometer Specimen and (c) Compression testing specimen.	71
4.1	Scanning electron micrograph of various reinforcements used for composite fabrication. (a) Silicon carbide, (b) Natural graphite, and (c) Synthetic graphite particles.	78
4.2	XRD pattern of two different types of carbon used as reinforcements (a) Natural graphite and (b) Synthetic graphite	79
4.3	Microstructures of 356 aluminium silicon alloy used (a) Gravity cast and (b) Squeeze cast.	80
4.4	Microstructure of gravity cast Al (356)-15% SiC _(p) mono composite	81
4.5	Microstructures of gravity cast Al(356) -5% Graphite mono composite. (a) Natural (b) Synthetic	81
4.6	Photomicrographs of gravity cast Al(356)-15% SiC _(p) -3% graphite (natural) hybrid composites (a) SiC _(p) followed by graphite addition (b) Graphite followed by SiC _(p) addition and (c) Mixed mode of addition	82
4.7	Microstructures of gravity cast Al(356)-15% SiC _(p) - 5% graphite hybrid composites (a) natural graphite and (b) synthetic graphite	83
4.8	Microstructure showing encircling of graphite by SiC particles in gravity cast Al(356) -15% SiC _(p) - 5% graphite hybrid composites	83
4.9	Photomicrograph of squeeze cast Al(356)-15% SiC _(p) mono composite	84
4.10	Microstructures of Al(356) -15% SiC _(p) - 5% graphite hybrid composites solidified by squeeze casting (a) natural graphite and (b) synthetic graphite	84
4.11	Scanning electron micrograph of Al(356)-15% SiC _(p) mono composites. (a) SiC particles in the matrix, (b) Single SiC particle in the matrix and fibrous iron intermetallics and (c) An iron intermetallic phase with eutectic phase surrounding it	87
4.12	EDS elemental X-ray mapping of Al(356)-15% SiC _(p) mono composite	88
4.13	SEM micrograph of Al(356)-15% SiC _(p) - 5% graphite hybrid composites	89

4.14	Tensile fractograph of (a) Al(356) base alloy and (b) Al(356)-15% SiC _(p) composite	89
4.15	Compression fractograph of (a) and (b) Al(356) base alloy and (c) and (d) Al(356)-15% SiC _(p) composite	90
4.16	Thermal analysis parameter of 356 aluminium silicon alloy	91
4.17	Cooling curve of 356 Al alloy solidified in metal, graphite and sand moulds	96
4.18	Cooling curve of 356 Al alloy-1% Mg solidified in metal, graphite and sand moulds	96
4.19	Cooling curve of Al (356)-SiC _(p) composites with varying weight percentages (a) 10% and (b) 20% solidified in metal, graphite and sand moulds	97
4.20	Cooling curve of Al(356)-5% Graphite particle reinforced composite solidified in metal, graphite and sand moulds	98
4.21	Cooling curve of Al(356)-15% SiC _p -5% graphite hybrid composite solidified in metal, graphite and sand moulds	98
4.22	Cooling curves of base alloy, 10 and 20% SiC _(p) reinforced 356 aluminium matrix composites determined using Aluminium Meltlab data logger system using the standard steel cup	99
4.23	Variation in liquidus temperature with the increase in SiC _(p) weight fraction	99
4.24	Variation in total solidification time with increase in SiC _(p) weight fraction	100
4.25	Variation in cooling rate with increase in SiC _(p) percentage in metal, graphite and sand mould	100
4.26	Variation of (a) total heat content of the composite and (b) thermal conductivity of composite in liquid (l) (727 °C) and solidified (s) (25 °C) conditions with increase in vol % of SiC _(p)	101
4.27	Variation in interfacial heat flux with time for 356 alloy with and without 1% Mg and 10% SiC _(p) reinforced composite cast in steel mould	102
4.28	Variation in interfacial heat flux with time for 356 alloy with and without 1% Mg and 10% SiC _(p) reinforced composite cast in graphite mould	102

4.29	Variation in interfacial heat flux with time for 356 alloy with and without 1% Mg and 10% SiC _(p) reinforced composite cast in sand mould	103
4.30	Variation in interfacial heat flux with time for 356 alloy reinforced with 5% Gr and 15% SiC _(p) -5% Gr composites cast in steel mould.	104
4.31	Variation in interfacial heat flux with time for 356 alloy reinforced with 5% Gr and 15% SiC _(p) -5% Gr composites cast in sand mould	104
4.32	Estimated casting / mould interface temperatures during solidification of various alloys and composites (a) steel and (b) sand mould	105
4.33	Ageing characteristics of 356 aluminium alloy and Al (356)-15% SiC _(p) mono and Al (356)-15% SiC _(p) -5% graphite hybrid composites	106
4.34	Variations in densities of base alloy and composites solidified under gravity and squeeze cast conditions	106
4.35	Variation in electrical conductivity of Al(356)-SiC _(p) composite with varying (a) weight fraction and (b) at different positions of the casting	107
4.36	Variation in electrical conductivity of Al(356)-SiC _(p) composite with varying weight fraction and particle size of SiC	108
4.37	Hardness values of base alloy and composite systems in as cast and aged conditions	108
4.38	Ultimate tensile strength of base alloy and composite systems	109
4.39	Compressive strength of base alloy and composite systems	109
5.1	SEM photomicrographs of (a) and (b) as received and (c) and (d) surface treated carbon fibres	127
5.2	Variation of the height of the carbon fibre column with settling time in different treatments	128
5.3	X-ray diffraction pattern of carbon fibre	128
5.4	Photomicrographs of Al(356)-3% C _(sf) mono composite	129

5.5	Photomicrographs of Al(356)-15% SiC _(p) -3% C _(sf) hybrid composite	129
5.6	Photomicrographs of (a) Al(356)-3% C _(sf) mono composite and (b) Al(356)-15% SiC _(p) -3% C _(sf) hybrid composite from image analyser	130
5.7	SEM photomicrographs of Al(356)-3% C _(sf) mono composite	131
5.8	SEM photomicrographs of Al(356)-15% SiC _(p) -3% C _(sf) hybrid composite	132
5.9	SEM photomicrographs of Al(356)-3% C _(sf) mono composite showing a single carbon fibre oriented in (a) lateral and (b) longitudinal direction with respect to the ingot	133
5.10	EDS X-ray elemental mapping of Al(356)-3% C _(sf) mono composite	134
5.11	EDS line scan of Al(356)-3% C _(sf) mono composite	135
5.12	EDS X-ray elemental mapping of Al(356)-15% SiC _(p) -3% C _(sf) hybrid composite	136
5.13	EDS line scan of Al(356)-15%SiC _(p) -3C _(sf) hybrid composite	137
5.14	EDS spectrogram of Al(356)-15% SiC _(p) -3% C _(sf) hybrid composite for (a) overall matrix, (b) SiC particle in the matrix and (c) carbon short fibre in the matrix	138
5.15	Atomic Force Microscopic structures of Al(356)-15% SiC _(p) -3% C _(sf) hybrid composite	139
5.16	Ageing characteristics of alloy and composites with respect to hardness measurements	140
5.17	Density of base alloy and composite systems	140
5.18	Hardness of base alloy and composite systems	141
5.19	Compression strength of base alloy and composite systems	141
6.1	SEM photomicrographs of standard grade aluminosilicate fibre (a) and (b) as received fibre and (c) and (d) surface treated fibre.	158
6.2	SEM photomicrographs of zirconia grade aluminosilicate fibre surface (a) and (b) as received fibre and (c) and (d) treated fibre	159

6.3	Polished cross section of Al(356)-15% zirconia grade aluminosilicate fibre composites: (a) as received fibre (b) ultrasonically dispersed in sodium silicate and (c) treated in acidic solution	160
6.4	Polished cross section of Al(356)-15% standard grade aluminosilicate fibre composites: (a) as received fibre, (b) acidic solution treated, and (c) chopped and acidic solution treated	160
6.5	Photomicrographs of Al(356)- zirconia grade aluminosilicate fibre reinforced composite (a) sodium silicate treated (b) acidic solution treated fibre	161
6.6	Photomicrographs of Al(356)- acidic solution treated standard grade aluminosilicate fibre reinforced composite (a) distribution of fibres and shots (b) cracked aluminosilicate shot.	161
6.7	(a) Microstructure of Al(356)-15% SiC _(p) -5% Al ₂ O ₃ .SiO ₂ hybrid composite (b) Microstructure of Al(356)-15%SiC _(p) -5% Al ₂ O ₃ .SiO ₂ hybrid composite showing a cracked shot in the matrix	162
6.8	X-ray diffraction patterns of zirconia grade fibre in (a) as received, (b) heat treated (750 °C, 2 h), and (c) extracted from the composite (heated in Al alloy at 750 °C for 2 h).	163
6.9	EDS spectra of as received (a) standard and (b) zirconia grade aluminosilicate fibre	163
6.10	SEM photomicrographs of the surface of the fibres observed in the composites (a) standard grade (b) zirconia grade.	164
6.11	(a) SEM photomicrograph of standard aluminosilicate fiber in the composite, (b) EDS spectra showing the presence of MgAl ₂ O ₄ on the fibre surface in the composite (position 1 in Fig 6.11a) and (c) EDS spectra of the matrix alloy (position 2 in Figure 6.11a)	165
6.12	SEM photomicrograph of aluminosilicate fibre reinforced composites showing presence of silicon over fibre surface	166
6.13	Elemental X-ray dot maps of standard aluminosilicate fiber dispersed composite showing the spinel formed segregating near to eutectic silicon region in the matrix	166

6.14	(a) SEM photomicrograph of $ZrAl_3$ phase formed by the reaction between matrix and reinforcement (b) the EDS spectra at position 1 in Figure 6.14a and (c) EDS spectra of position 2 in Figure 6.14a.	167
6.15	(a) SEM photomicrograph of zirconia grade fibre reinforced aluminium matrix composite showing the presence of intermetallic compounds in the matrix, (b) the EDS spectra at position 1 in Figure 6.15a and (c) EDS spectra of position 2 in Figure 6.15a.	168
6.16	Aging curves for Al(356) base alloy and 10% standard aluminosilicate fibre reinforced composite	169
6.17	Solidification curve of Al(356)-10% standard aluminosilicate fibre cast in (a) metal, (b) graphite and sand moulds.	169
6.18	Solidification curve of Al(356)-10% $SiC_{(p)}$ -10% standard aluminosilicate fibre solidified in graphite and sand moulds	170
6.19	Variation of interfacial heat flux with time for 356 alloy with ceramic fibre and its hybrid composite cast in (a) graphite and (b) steel and sand mould	171
6.20	Microstructures of Al(356)-10% standard aluminosilicate short fibre composite cast in (a) Metal (b) graphite and (c) sand moulds.	172
7.1	SEM photomicrographs of fly ash particles (a) as-received and (b) surface treated	189
7.2	SEM photomicrographs of fly ash particles showing (a) broken cenosphere particle containing smaller particles inside and (b) non spherical fly ash particle with fine globular particles sticking	190
7.3	Photomicrographs of Al(356)-5% (a) as-received and (b) surface treated fly ash composite synthesised by liquid metal stir casting and cast in metal mould	191
7.4	Frequency distribution in the interparticle distance measured in Al(356)-5% fly ash (surface treated) composite synthesised by liquid metal stir casting and cast in metal mould	191
7.5	Photomicrographs of Al(356)-5% fly ash (treated) composite processed by compocasting and cast in (a) metal mould, (b) graphite mould and (c) crucible	192

7.6	Frequency distribution in the interparticle distance in Al(356)-5% fly ash (treated) composite processed by compocasting and cast in (a) Metal mould, (b) Graphite mould and (c) Crucible	193
7.7	Photomicrographs of Al (356)-5% fly ash composite processed by compocasting and cast in metal mould showing coarse primary phases.	194
7.8	Photomicrographs of Al(356)-5% Fly ash composite processed by modified compocasting and cast in metal mould.	194
7.9	Frequency distribution in the interparticle distance (a) Al (356)-5% fly ash composite processed by modified compocasting and cast in metal mould and (b) Al(356)-15% fly ash composite processed by modified compocasting and cast by squeeze casting.	195
7.10	Photomicrographs of Al(356)-15% fly ash composite processed by modified compocasting followed by squeeze casting. (a) Distribution of fly ash particle in the matrix and (b) hollow fly ash particle showing solidification of the matrix alloy in the cavity.	196
7.11	SEM photomicrographs of Al(356)-15% fly ash composite processed by modified semisolid stir casting followed by squeeze casting. (a) solid fly ash particle, (b) hollow cenospherical fly ash particle and (c) Fly ash particle detached from the matrix showing $MgAl_2O_4$ phase and eutectic silicon.	197
7.12	SEM photomicrographs of Al(356)-15% fly ash composite processed by modified semisolid stir casting followed by squeeze casting showing the solidification of infiltrated matrix alloy into a hollow space of broken cenospherical particle containing fine solid fly ash particle.	198
7.13	SEM photomicrograph (a) and EDS spectra of modified compocast Al(356)-15% fly ash composite of different phases marked as 1 - (b), 2 - (c), 3 - (d), and 4 - (e) in (a).	199
7.14	SEM photomicrograph (a) of modified compocast Al(356)-15% fly ash composites and EDS spectra of phases marked as 1 (b) and 2 (c)	201
7.15	SEM photomicrographs of tensile fracture of Al(356)-15% fly ash composite processed by modified semisolid stir casting followed by squeeze casting	202

7.16	SEM photomicrographs of fractured compression specimens (a) Al(356) matrix alloy and (b) Al(356)-15% fly ash composite processed by modified semisolid stir casting followed by squeeze casting.	203
7.17	Densities of Al(356)-5% fly ash composites fabricated by different processing techniques	204
7.18	Electrical conductivities of Al(356)-5% fly ash composites fabricated by different techniques	205

CHAPTER 1

INTRODUCTION

The major classifications of engineering materials are metals, polymers, ceramics and composites. The development of composite materials is one of the major innovations in the field of science and engineering. Composites of varying types and sizes based on different materials have been developed through the ages of their evolution. Composites based on metals and their alloys, known as metal matrix composites (MMC) have become one of the most important advanced materials used for aerospace, automotive, defence and general engineering applications. They can be tailored to have superior properties such as high specific strength and stiffness, increased wear resistance, enhanced high temperature performance, better thermal and mechanical fatigue and creep resistance than those of monolithic alloys. Figure 1.1 shows the comparison between conventional monolithic materials such as aluminium and steel, and composite materials [1]. This figure indicates the possible improvements one can obtain over conventional materials by the use of composite materials. MMCs have an edge over polymer matrix composites because of their capability to withstand high temperatures, better transverse mechanical properties, superior electrical and thermal conductivities, excellent resistance to moisture, flame and radiation and zero out-gassing at vacuum.

One of the oldest examples of the use of metal matrix composites in ancient civilisation is the copper awls from Cayonu (Turkey) dating back to about 7000 BC and made by repeated lamination and hammering process, resulting in elongated non-metallic inclusions [2]. Among the first composite materials to attract scientific as well as practical attention is the dispersion hardened metal systems. In 1924, Schmidt [3] have consolidated mixtures of aluminium - alumina powders to produce the dispersion hardened metal system, which later led to an extensive research in the 1950's and 1960's [4]. More recent developments have brought the concept of metal matrix composites closer to engineering practice. One important example is the 'dual

phase' steels developed in 1970's by annealing low carbon steels in the $\alpha + \gamma$ phase field and then quenching so as to convert the γ phase to martensite [5]. This product is similar to what is now referred as 'particulate MMC', with about 20% of very hard, relatively coarse martensite particles distributed in a soft ferrite matrix. Development of fibre reinforced metal matrix composites started in 1960's mainly of Al and Cu matrix systems reinforced with tungsten and boron fibres. However, research on these systems waned during the 1970's, largely for the reasons of high cost and production limitations. Investigations on discontinuously reinforced composites have shown a rapid growth in 1980's with main focus on Al based composites reinforced with SiC and alumina particles and short fibres. The combination of good transverse properties, low cost, amenability to conventional metal shaping processes and improved performance over unreinforced alloys has made them the most commercially attractive systems for many applications. The interest on the development of hybrid metal matrix composites has originated in mid-1990's and presently they are a promising advanced futuristic material for various applications in the new millennium.

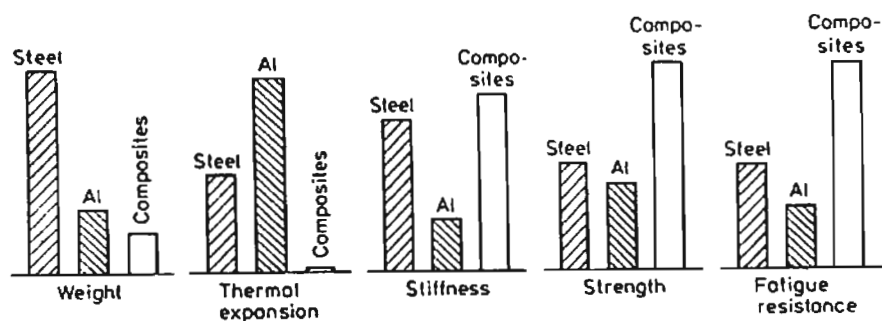


Figure 1.1: Comparison between conventional monolithic materials and composite materials [1].

The conventional metal matrix composites currently used are monocomposites, wherein only one type of reinforcement is used. The hybrid metal matrix composites (HMMC) are the second generation composites, wherein more than one type, shape and size of reinforcements are used to obtain synergistic properties of the reinforcements and matrix chosen. Although the hybrid MMC encompasses the composite system containing two types of alloys to produce laminated structures, current focus is on the former type only. Studies have shown that hybridisation of reinforcements enhanced the structural, physical, mechanical and

tribological behaviour of hybrid composites than mono MMCs. The details are discussed in Chapter 2.

1.1 CONSTITUENTS OF MMC

The major constituents of MMC are the matrix and the reinforcements. The interface between the matrix and the reinforcement is also considered as one of the constituent as it plays a crucial role in determining the properties of the composite.

1.1.1 Matrix

The matrix is the continuous phase (i) binding and keeping the reinforcements in position and orientation, (ii) transferring the load to and between the reinforcements and (iii) protecting reinforcement from the environment and handling. Further, the matrix determines the overall service temperature limitations of composites as well as their resistance to environment. Important requirements of a matrix alloy are compatibility with reinforcements during composite production and product service, high strength and sufficient plasticity at room and elevated temperatures.

The major metal matrices used for the fabrication of composites include aluminium-, magnesium-, titanium- and copper- based alloys. The other matrices studied are based on zinc, tin, steel, super alloys and intermetallics. Among the various matrix materials available, aluminium and its alloys are widely used for the fabrication of MMC due to the fact that they are light in weight, economically viable, amenable for production by various processing techniques and possess high specific strength and good corrosion resistance. In the case of aluminium, both cast (Al-Si, Al-Mg, and Al-Cu) and wrought (Al-Cu, Al-Mg-Si and Al-Zn-Mg) alloys are commonly used. Table 1.1 lists the composition and properties of widely used Al matrix alloys.

1.1.2 Reinforcements

The reinforcements are the second phase materials added to the matrix alloys, which normally enhance strength, stiffness, wear and creep resistances of the

composites. The choice of reinforcements always depends on the final property requirements of the composite system or component to be fabricated. Certain **dispersoids** normally impart some special properties to composites such as enhanced wear resistance and reduced density at the expense of strength. Generally, the dispersoids are refractory materials, such as, oxides, carbides, and nitrides of different elements. Basically, they are stable and non-reactive in most of the matrix alloys. In addition, they do not mostly undergo any change in phase or shape during composite synthesis or in use except those produced by in-situ methods. At present, there are a wide range of reinforcement materials, which can provide varying combinations of properties to the composites synthesized. The most common dispersoids and their characteristics and forms are given in Table 1.2.

1.1.3 Interface

Interface is the region that lies between the matrix and the reinforcement. It plays a crucial role in determining the composite properties. It may contain a simple row of atomic bonds (e.g., the interface between alumina and pure aluminium), or reaction products between the matrix and the reinforcement (e.g., aluminium carbide between aluminium and carbon fibres), or reinforcement coatings (e.g., interfacial coatings between SiC monofilaments and titanium matrices). In composites, (i) stiffening and strengthening rely on load transfer across the interface, (ii) toughness is influenced by crack deflection/ fibre pull-out, and (iii) ductility is affected by relaxation of peak stresses near the interface.

The types of interface bonding are mechanical, physical and chemical in nature. Mechanical bonding is the simple mechanical keying or interlocking effects between two surfaces which could lead to a considerable degree of bonding. Any contraction of the matrix onto the fibre would result in a gripping of the fibre by the matrix. The physical bonding is those involving weak, secondary or Van der Waals forces, dipolar interactions and hydrogen bonding. Chemical bonding involves the atomic or molecular transport by diffusional process. Solid solution and compound formation may occur at the interface, resulting in a reinforcement / matrix interfacial reaction zone with a certain thickness. This encompasses all type of covalent, ionic and metallic bonding.

Table 1.1: Widely used aluminium matrices and their mechanical properties

Matrix Alloy Designation	Composition	Mechanical properties		
		UTS (MPa)	Modulus (GPa)	Elongation (%)
Cast Alloys				
A356 (T6)	Al-7Si-0.3Mg-0.2Fe(Max)	278	71	5
A357 (T6)	Al-7Si-0.5Mg-0.05Be	365	71	5
LM4 (T6)	Al-4Cu-6Si-0.3Mn	310	71	3
LM6	Al-12Si	200	71	13
LM13 (T6)	Al-11Si-1Cu-1Mg	290	71	1
LM25 (T6)	Al-6Si-0.4Mg	300	71	3
LM30	Al-18Si-0.7Mg	150	71	-
Wrought Alloys				
2014 (T6)	Al-4.4Cu-0.9-Si-0.8Mn-0.5Mg	495	74	13
2024 (T6)	Al-4.5Cu-1.5Mg -0.6Mn	485	74	10
6061 (T6)	Al-1Mg-0.6Si-0.2Cu-0.25Cr	320	74	12
7075 (T6)	Al-5.6Zn-2.5Mg-1.6Cu-0.3Cr	580	74	11

Table 1.2: Common reinforcements and their characteristics

Reinforcements	Diameter (μm)	Density (g/cc)	CTE (μm/m°C)	Thermal Conductivity (w/m°C)	Young's Modulus (Gpa)
Discontinuous (Particles (p), Whiskers (w) and Short fibers (sf))					
Graphite flakes	20-60	1.8	7.9	5	207
SiC _(p)	1-50	3.2	4.0	~100	450
SiC _(w)	0.1-1	3.2	4.0	>16	450-700
Al ₂ O _{3(p)}	1-50	3.8	7	100	430
B ₄ C _(p)	1-50	2.5	-	-	480
TiB _{2(p)}	-	4.5	8.1	~100	350-570
Si ₃ Ni _{4(w)}	0.1-10	3.1	-	-	350-385
Continuous fibres (f)					
Al ₂ O ₃ (Saffil)	3	3.5	7.7	-	285
Al ₂ O ₃ (Dupont FP)	20	4.0	8.3	-	380
SiC (Nicalon)	15	2.55	3.0	-	180
C pitch	5-13	2.0	-1.4 (axial) 10 (trans)	355 (axial)	380-690
C PAN (high strength)	7	1.9	-1.2(axial) 10(trans)	-	230
C PAN (high modulus)	7	1.8	-do-	-	412
Al ₂ O ₃ .SiO ₂ (Kaowool)	2.8	2.56	-	-	120
Al ₂ O ₃ .SiO ₂ (Fiber max)	3	3.0	-	-	3.0
Al ₂ O ₃ .B ₂ O ₃ .SiO ₂ (Nextel)	10-12	2.7	-	-	150

1.2. TYPES OF MMC

Metal matrix composites can be classified depending on the nature and number of reinforcements, type of metal matrix and the functional behaviour of composites.

Depending upon the nature of reinforcements used, metal matrix composites can be classified as (a) Dispersion strengthened (b) Discontinuously reinforced and (c) Continuous fibre reinforced composites.

Dispersion strengthened composites are those in which fine particles are dispersed in elemental matrix. The particle size and the volume concentration range from about 0.01 to 0.1 μm and 0 to 15% respectively.

Discontinuously reinforced metal matrix composite is characterized by dispersed particles greater than 1 μm in size with a low aspect ratio, which falls between the range of dispersion strengthened and continuous fibre reinforced composite extremes. They differ from dispersion-strengthened composites in having relatively high volume fraction of reinforcements in the range 5 – 50% with larger size particles of 1–100 μm size and contribute negligible to Orowan strengthening. They exhibit isotropic behaviour in their physical and mechanical characteristics unless the reinforcement is aligned. In these systems, both matrix and reinforcement bear substantial proportions of the load. The discontinuous dispersoids are in the form of particulates, short fibres or whiskers. However, particulates are less expensive compared to whiskers or short fibres.

Continuous fibres are identified as one of the important reinforcements in the early stages of MMC evolution because of their wide use in the fabrication of polymer matrix composites. Their concentration in composites varies from a few to 80% of volume. However, processing of continuous fibre reinforced composites is expensive.

Depending on the number of reinforcements, MMC are classified as mono and hybrid metal matrix composites. In mono composites, only one type of reinforcement is used. In the case of hybrid MMC, more than one type and shape of reinforcement are used. Similarly classification is made on the type of matrix alloy chosen such as Aluminium, Magnesium, Titanium, Copper and Intermetallic MMC. Based on the functional behaviour, they are classified as 'functionally graded' composites, 'smart' composites etc.

1.3 IMPORTANCE AND PROSPECTS OF MMC

MMCs now have a proven track record as successful "high-tech" materials in a range of applications, bringing significant benefits (in terms of energy savings, or component lifetime) and having documented engineering viability. These often relate to niche applications, where achievable property combinations (e.g. high specific stiffness and weldability; high thermal conductivity and low thermal expansion, or high wear resistance and low weight and high thermal conductivity) are attractive for the component concerned. Many such niches, ranging from diesel engine pistons to automotive engine cylinder liners, are of considerable industrial significance. Barriers to their wider exploitation include price (which is, of course, inter-related with global and specific usage levels), shortage of property data and design guidelines and (perceived) limitations to their ductility and toughness. The use of low cost reinforcements, cost effective processing techniques and standardization of processing parameters could facilitate in its wide application. The development of new composite systems containing specific property requirements for particular application with different combination of matrix and reinforcement materials such as HMMC, functionally graded composites and smart composites and consolidation of property data can improve the prospects of MMC.

CHAPTER 2

LITERATURE REVIEW

2.1 INTRODUCTION

Studies have been carried out on monocomposites over the past three decades on synthesis, secondary processing, structure-property correlations, microstructural aspects and application including component identification and evaluation. These details have been compiled in the form of books [6-9], monographs [10,11] and reviews dealing with processing and properties [12-17], solidification behaviour [18,19], interfacial characteristics [20-26], tribological behaviour [27-28], corrosion characteristics [29], joining [30] and systems like functionally gradient composites [31,32] and smart composite [33,34]. However, similar reviews on hybrid metal matrix composites are scarce or not documented. Hence, apart from covering the general features and characteristics of monocomposites, this chapter reviews the state of art knowledge available on constituents, processing, characterisation, classification and application avenues of hybrid metal matrix composites as well as foresees the scope of this new second generation composite system as an emerging advanced material. The chapter also emphasises on the solidification and interfacial characteristics of metal matrix composites.

2.2 PROCESSING OF MMC AND HYBRIDISATION

The evolution of different metal matrix composite systems led to the development of newer processing techniques, in addition to conventional metal processing techniques. The major criteria for the selection of a process rely on the type of composite system to be fabricated, the properties to be achieved and the component to be produced. The processing methods can be widely classified into primary and secondary processes. The primary process combines matrix and reinforcements to produce the basic composite systems and their structures. The secondary process involves processing of primary processed composites with the

objective of improving their mechanical properties by further consolidation (reduction or elimination of porosity), break up of dispersoid agglomerates, improved interfacial bonding, generating dispersoid alignment and/or forming into a required shape to obtain semi finished products.

The primary processing techniques may be classified into liquid and solid state processes. The former utilises either fully or partially molten matrix material during the fabrication of the composite. The major primary liquid state processes are stir casting or vortex method, infiltration, in-situ and spray deposition processes. Despite creation of better interfacial bonding than the solid state processes, liquid state processes lead to unwanted interfacial reactions deteriorating the properties of the composites. Among these, the stir casting is the most simple and economical route and the resulting composite melt can be subsequently shaped by conventional casting techniques as well.

The primary solid state processes use only solid matrix and reinforcement during synthesis of the composites. The important solid state processes are powder metallurgy and diffusion bonding. These processes are generally used for fabricating discontinuous MMCs with better mechanical properties. The reduction in the formation of segregation and interfacial reaction is the important advantage over liquid state processing. However, this route is expensive than liquid state route.

The most commonly used secondary processes for MMCs are extrusion, rolling forging, superplastic deformation, machining and joining.

2.2.1 Hybridisation

Hybridisation of metal matrix composites is the introduction of more than one type/kind, size and shape of reinforcement during processing of composites. It is carried out to obtain synergistic properties of different reinforcements and matrix used, which may not be realised in monolithic alloy or in conventional mono composites. Hybridisation of monocomposites with second reinforcement i.e., introduction of more than one reinforcements simultaneously during processing, can be carried out by most of the conventional monocomposite fabrication techniques.

The primary composite processing techniques, such as, stir casting, infiltration, spray deposition, *in-situ* and powder metallurgy, can be used.

The hybridisation of aluminium-graphite composites with SiC could provide improved abrasive wear resistance in addition to enhanced sliding wear resistance offered by the soft graphite particle [35]. Similarly, the wear resistance of Al(6061) – Al₂O_{3(s)} – SiC_(w) hybrid composites is greater than that of composites containing one of the reinforcements [36]. Hybridisation also helps in enhancing certain inferior properties of monocomposites. For example, the addition of graphite particles alone to aluminium matrix would reduce the strength and hardness of the composite, while hybridisation with SiC could regain the reduced hardness and strength. Defects such as fibre contacts, acting as failure initiation points in continuous fibre reinforced composites, can be rectified by hybridising with discontinuous dispersoids. The average strength and stiffness of Al-SiC_(f) fibres monocomposites are 260 MPa and 144 GPa respectively [37]. The stiffness is in agreement with the rule of mixtures value, while the low strength is attributed to the high volume fraction of fibre (70 vol%) resulting in fibre contacts acting as failure initiation points. Hybridisation of Al-SiC fibre composites with SiC particles reduced the costly fibre volume fraction to 33% and increased the strength and stiffness to 450 MPa and 150 GPa respectively [37]. Studies by Cheng et al [38] on hybridisation of Al-C_(f) composite with small amounts of silicon carbide particles/whiskers have shown improved longitudinal tensile strength with reduced fibre volume fraction compared to conventional monocomposites.

The important fabrication methods used for the fabrication of mono- and hybrid- composites are briefly described below.

2.2.2 Primary Liquid State Processes

2.2.2.1 Stir casting or vortex method

This is the most simplest and economic process available for the fabrication of MMCs in large quantities. In this process, the molten metal is stirred vigorously and dispersoids are added through the vortex [12]. This method is commonly used for fabricating discontinuous dispersoids reinforced MMC. The process of mixing silicon

carbide particle ($\text{SiC}_{(p)}$) in aluminium melt under vacuum using a specially designed stirrer developed by Skibo and Schuster [39] has the advantage in reducing oxide impurities, and gases because of the vacuum and reduced vortex. This process is now commercially used for the production of Al- $\text{SiC}_{(p)}$ and Al- $\text{Al}_2\text{O}_{3(p)}$ composites [39-42]. The companies involved in the production of aluminium matrix composites with different dispersoids based on this method are Duralcan, Canada [40-41], Hydroaluminium, Norway [43] and Comalco, Australia [44].

The other dispersoids introduction techniques studied are (i) gas injection method, in which the particles are injected into the metal using a carrier gas [45], (ii) bottom mixing process, in which a stirrer is progressively lowered into an evacuated bed of particles covered with molten Al [46], (iii) pellet method [47] and (iv) ultrasonic dispersion [12]. The development of rheocasting, in which the alloy is stirred between the liquidus and solidus temperatures to produce non-dendritic microstructure [48, 49], led to the evolution of compocasting technique. In compocasting, the particles are mixed into a semisolid alloy slurry, whose high viscosity inhibits particle settling or floating [50-54].

All the above processes can be used for the synthesis of hybrid composites. In addition, the hybridisation can be carried out either by melting the monocomposite and introduction of the second reinforcement or by simultaneously introducing both the dispersoids during the initial processing of the composites from the base matrix alloy. Ames and Alpas [35] synthesized Al(356)- $\text{SiC}_{(p)}$ -Graphite $_{(p)}$ hybrid composites by remelting Al(356)-20 wt% SiC (Duralcan F3S20S) monocomposites and introducing nickel coated graphite particles by stirring. Rohatgi *et al* [55] have also used Ni coated graphite particle for the synthesis of Al-Si-SiC-NiAl₃-graphite hybrid composite. The nickel coating improved the surface wetting of the graphite during mixing.

2.2.2.2 Infiltration processes

Infiltration process involves the synthesis of composites by infiltrating the liquid metal through the interstitials of a porous preform made out of reinforcement material. The infiltration of liquid metal could be made with or without the

application of an external force. The infiltration processes are classified depending on the nature and type of force applied, as pressure, pressureless, vacuum, combination of pressure and vacuum, etc. Functionally gradient metallic composites can be synthesised using infiltration process [31].

In PrimexTM process developed by Lanxide Corporation [56, 57], the Al-Mg alloy is infiltrated into a packed bed of ceramic powder kept at a temperature in the range of 750 to 1050 °C in nitrogen atmosphere without any applied pressure. In Ti-B process, the Al is infiltrated through the fibres coated with Ti and B by chemical vapour deposition [58-60]. By these processes, composites with better wetting between reinforcement and matrix alloy can be fabricated successfully although rate of infiltration is very low.

In pressure infiltration process, application of an external force enables infiltration of even non wetting systems. The additional advantages include reduced interfacial reaction, increased processing speed, refined matrix microstructures and better soundness of the product. The process can be termed as squeeze infiltration or squeeze casting. The external pressure is imposed either mechanically or by a gas. The mechanical force in the range of 10-100 MPa is generally applied hydraulically [61, 62]. The deformation and breakage of preform are the common problems associated with this process [63-65]. In the case of gas assisted infiltration, inert gas, such as Ar and pressures in the range of 1-10 MPa are generally applied. This process was first patented by Cochran and Roy [66] in 1970 and at present widely used for fabricating aluminium alloys and intermetallic based composites [67, 68].

In vacuum infiltration, the liquid metal is infiltrated by providing a large pressure difference by creating a vacuum around reinforcement. This process was applied in infiltrating Al-Li alloy into alumina preforms [69] and magnesium into Al₂O₃ or SiC preforms [70, 71]. The other applied forces aiding infiltration are vibration [72], centrifugal force [73] and electromagnetic agitation [74].

Infiltration process is commonly used for the synthesis of hybrid composites, since a wide range of reinforcements from particulates to fibres can be incorporated by this method. Hybrid preforms are prepared with different reinforcement types and

the liquid metal is infiltrated through the preform with or without application of pressure. Cheng *et al* [38] synthesized Al-C_(f)-SiC_(p)/SiC_(w) hybrid composites by infiltration process. Carbon fibres were impregnated into an aqueous suspension of particulates or whisker of SiC using a polymer as binding agent and an organometallic compound as dispersion agent. After this treatment, particulates / whiskers were uniformly distributed among carbon fibres. When the whisker concentration in the suspension is high, they get agglomerated in some areas because of their long length. The impregnated fibres were dried to certain extent, then cut to required size and pre-pegged in one direction into a Shirasu balloon (expanded volcanic glass) preform mould to obtain a fibre preform. The preforms along with the cast iron mould were preheated to 375 °C and then pressure casting was carried at a pressure of 49 MPa, melt temperature of 780 °C and pressure keeping time of 60 s. Similar method of squeeze infiltration was adopted by Song *et al* [75] and Towata *et al* [76] for the fabrication of hybrid aluminium matrix composites. In non-wetting systems, surface coatings and treatments can be given to dispersoids to promote wetting. The former also prevents the surface degradation by interfacial reactions [26]. Treating aluminium matrix melt with reactive elements like Mg improves wettability between dispersoids and the matrix [24].

Infiltration process can also be assisted by ultrasonic vibration in case of non wetting systems. Nakanishi *et al.* [77] with the help of ultrasonic agitation infiltrated molten aluminium in alumina particle preform, assisted by exothermic reaction between aluminium and titanium to form titanium aluminide. This is a hybrid process of infiltration, wherein in-situ reaction leads to the formation of hybrid composite system. Similarly, a combined process of reinforcement coating and hybridising for the fabrication of carbon fibre-SiC_(p) hybrid aluminium matrix composite have been carried out by Wang *et al.* [78]. Both SiC coating on carbon fibre and SiC particle hybridisation were carried out simultaneously by sol-gel technique prior to consolidation by squeeze casting.

2.2.2.3 Spray deposition processes

In spray deposition process, the molten metal is atomised and mixed with the reinforcement stream and deposited on a substrate to produce composite product. In

some cases, the molten metal is sprayed on to the reinforcement placed on a substrate alternatively. The Osprey process is one of the commercialised spray forming process involving the deposition of atomised molten metal on to a substrate [79-81]. Later, the process was adopted for the fabrication of composites by injecting the particles into the stream of atomised liquid metal [81-82]. This process is successfully applied by Alcan for producing ingots of 200 kg with a deposition rate $6-10 \text{ kgmin}^{-1}$ [81]. Other techniques of spray deposition are thermal spraying in which metal drops are generated by arc melting [83], flame spraying by gas combustion [84] or by plasma spraying [85]. Spray deposition methods can be used for producing bulk MMC or graded MMC coatings, which provide good wear resistance in ceramic rich region and strong adhesion to metallic substrate in metal-rich region. The advantages of these processes are fine grain structure, strong bonding with less or no interfacial reaction and low oxide content. However, the higher porosity level associated needs further consolidation which in-turn increases the processing cost compared to dispersion and infiltration processes.

Spray deposition process can be used for fabricating hybrid metal matrix composites by mixing a hybrid reinforcement stream with atomised molten metal stream and depositing on a substrate. Zhang *et al* [86] processed Al(6061)-SiC_(p) - Gr_(p) hybrid metal matrix composites by this technique and evaluated their damping behaviour.

2.2.2.4 In-situ processes

The process of generating the reinforcement material by chemical reactions from the matrix alloy with the introduction of selective additives is termed as 'in-situ' process and the composites thus produced are known as in-situ composites. The process is also termed as 'self-propagating synthesis' of composites. The reaction may be between a liquid and gaseous or solid phase. In XD (exothermic dispersion) process developed and patented by Martin Marietta Corp. [87], TiB₂ reinforced aluminium composites have been made by heating Ti, B and Al powders at 800 °C to form TiB₂ [88]. Similarly, Al/Al₂O_{3(w)} composites are prepared by internal oxidation reaction between Al and MoO₃ at 850 °C [89]. In the DIMOX (Direct melt oxidation) process developed by Lanxide Corp., the melt is directly oxidized to produce the composite [90]. By this method, Al/Al₂O_{3(p)} and Al-Cu/TiC_(p) composites are

prepared by oxidation of Al [91] and by bubbling CH₄ and Ar through a melt of Al-Cu-Ti respectively. The gas injection method can also be used to produce varieties of carbides and nitride reinforced composites [92]. The advantages of this process are the uniform distribution of reinforcing phase and good interfacial bonding owing to the nascent nature of the dispersoids. However, the limitations include choice of systems, difficulties in controlling the shape of reinforcement and formation of very fine particles leading to high viscosity and difficulty in handling.

In-situ hybridisation of reinforcements could be made by the reaction between selective additives to produce two or more dispersoids, which contribute to the properties of the composites. In situ hybridisation can also be made by the reaction between the surface coating of a reinforcement with the matrix to produce a second type dispersoids [26]. Al-10% ZrB_{2(p)}-9.2% Al₂O_{3(p)} in-situ hybrid MMC is produced by Feng and Froyer starting from Al+ZrO₂+B by reactive sintering and subsequent hot-pressing [93].

2.2.3 Primary Solid State Processing

2.2.3.1 Powder metallurgy

Powder Metallurgy (PM) is one of the common and versatile process used in the fabrication of metal matrix composites by mixing the metallic matrix powder and ceramic reinforcements followed by compaction and high temperature consolidation. The blending of powder is carried out in liquid suspension or dry condition. The compaction is carried out by cold isostatic pressing followed by degassing and consolidation by hot isostatic pressing (HIP) or extrusion. Various studies have been carried out in the synthesis of MMC by PM technique [94-96]. The use of lower temperature compared to liquid state processes minimises the undesirable interfacial reactions and enhances the mechanical properties. PM route is ideal for making composites, wherein reinforcement dissolves in the matrix such as SiC in tantalum. The problems associated are increased cost compared to dispersion processes and difficulties in removing organic binder leading to residual contamination and poor mechanical properties.

Hybrid composites are also prepared by mixing metallic matrix powder and hybrid ceramic dispersoids followed by compaction and high temperature consolidation. Tjong *et al.* [97] synthesized Al based hybrid composites containing BN and SiC particulates by ultrasonic mixing of the powders in alcohol, drying, cold compacting and subsequently hot pressing and sintering isostatically at 620 °C for 1 hour under an argon pressure of 100 MPa.

2.2.3.2 Diffusion bonding

Diffusion bonding process is used for fabricating hybrid composites by placing alternative layers of hybrid fibres and thin metallic foils followed by hot pressing. A hybrid composite made of boron and steel fibres in aluminium was fabricated by Vishnyakov and Vodopianov [98-99] by hot pressing stacks consisting of boron/aluminium monolayers and knitted nets of stainless steel. ARALL (Aramid Aluminium Laminates) and GLARE (Glass Fibre Reinforced Epoxy) are important class of hybrid composites containing alternate layers of high strength aluminium alloy sheets and unidirectional aramid / glass fibre reinforced in epoxy sheets. GLARE has been cleared for its application in 'A3XX' series jumbo aircrafts of Airbus Industrie, to achieve operating economics around 15% better than anything possible with current generation jumbos [100].

2.3 CLASSIFICATION OF HMMC

Hybrid metal matrix composites can be classified based on the type of reinforcements or the type of matrix alloy used. On the basis of reinforcements, it can be categorized as continuous hybrid metal matrix composites (C-HMMC), discontinuous hybrid metal matrix composites (D-HMMC) and continuous-discontinuous hybrid metal matrix composites (CD-HMMC). C-HMMC are those in which two or more continuous fibres alone are used as reinforcements. In the case of D-HMMC, the dispersoids used are discontinuous types such as particulates, whiskers and short fibres. In CD-HMMC, both continuous and discontinuous type reinforcements are used. Table 2.1 depicts the different HMMCs fabricated and various reinforcements combinations utilised for fabricating the composites. The most commonly used matrix systems are aluminium, magnesium, titanium and copper.

Apart from these systems, nickel, zinc, tin, steel and intermetallics are also used. Depending upon the functional behaviour of composites such as intelligent and functionally gradient properties, they can be grouped under smart and functionally gradient hybrid composites respectively [31-34]. The term hybrid metal matrix composites can also be implied to composites where more than one matrix materials are used as laminated structures.

Table 2.1: Types of hybrid metal matrix composite systems.

Type of HMMC	Type of reinforcement combinations	Composite systems
Discontinuous – HMMC	Particle(p) - particle	Al-SiC _(p) -Graphite _(p) Al-SiC _(p) - BN _(p)
	Particle – short fibres(sf)	Al-SiC _(p) – C _(sf) Al-Al ₂ O _{3(p)} – C _(sf)
	Particle – whiskers(w)	Al-SiC _(p) – SiC _(w) Al-SiC _(p) - Al ₂ O _{3(w)}
	Short fibres - short fibres	Al – C _(sf) -Al ₂ O _{3(sf)} Al - C _(sf) -Al ₂ O ₃ .SiO _{2 (sf)}
	Short fibres – whiskers Whiskers - whiskers	Al - C _(sf) - SiC _(w) Al-SiC _(w) - Al ₂ O _{3(w)}
Continuous – HMMC	Fibre(f) - fibre	Al-Boron _(f) -Steel _(f)
Continuous-Discontinuous-HMMC	Fibre – particle	Al-C _(f) -SiC _(p) Al-C _(f) – Al ₂ O _{3(p)}
	Fibre – short fiber	Al-C _(f) – Al ₂ O _{3(sf)}
	Fibre - whisker	Al-C _(f) – Al ₂ O _{3(w)} Al-C _(f) – SiC _(w)

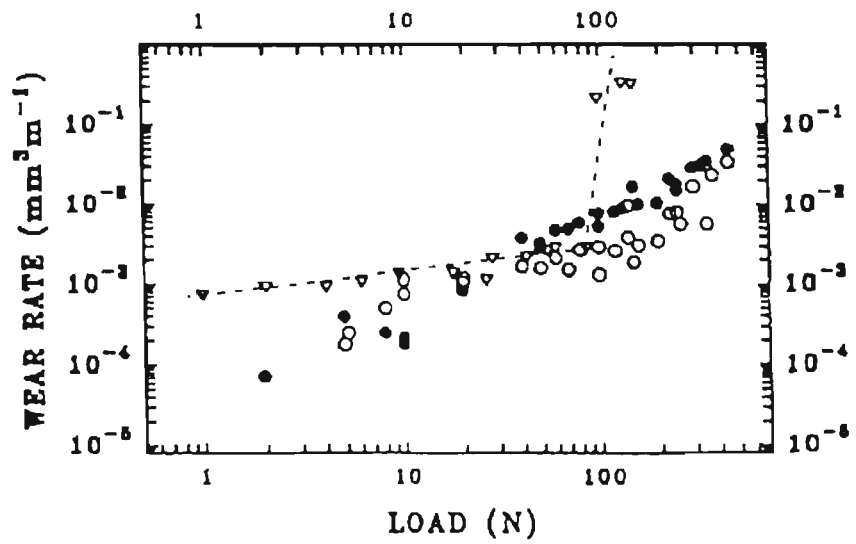
2.4 HYBRID SYSTEMS

2.4.1 Aluminium

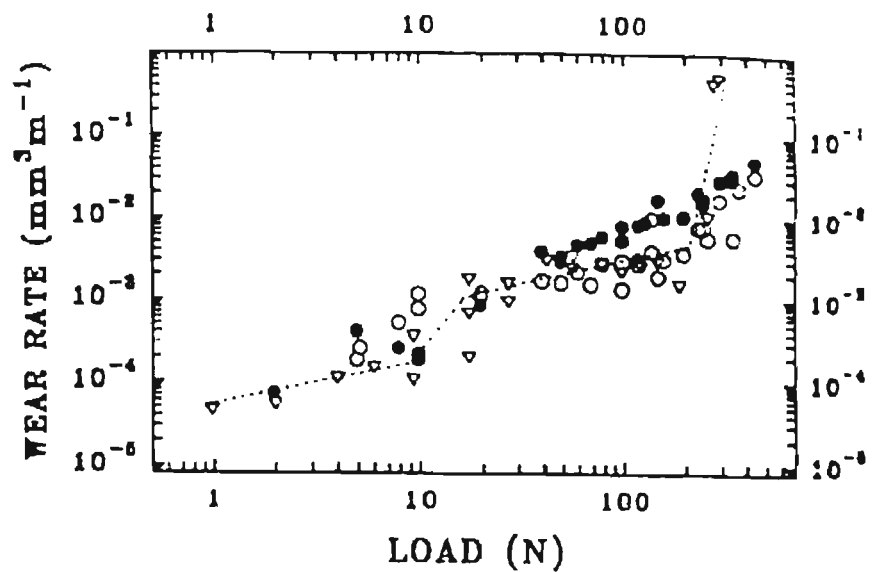
Aluminium and its alloys are the most commonly used matrix materials for the fabrication of MMCs. This is because of their light weight, economic viability, amenability to production by various conventional processing techniques, high strength, good corrosion resistance and availability in wide range of alloy systems. HMMCs are not an exception to the wide use of aluminium and its alloys as matrix.

2.4.1.1 D-HMMC

Among the various hybrid systems, discontinuous hybrid reinforced aluminium matrix composites are extensively studied. SiC and graphite particulates reinforced hybrid aluminium composites are fabricated and characterised mainly for their enhanced wear behaviour [35, 101-111]. Incorporation of SiC and graphite particles in Al alloy represents the merging of two philosophies in tribological alloy design i.e., hard particle reinforcement and soft particle lubrication [35]. The wear resistances of Al(356)-20% SiC_(p)-3% Graphite_(p) and Al(356)-20% SiC_(p) are comparable at low and medium loads. At loads below 20N, both mono and hybrid composites demonstrated wear rates upto 10 times lower than unreinforced Al(356) alloy due to the load-carrying capacity of SiC particles. The wear resistance of Al(356)-20% SiC_(p)-3%Graphite_(p) is 1 to 2 times higher than 10% graphite containing hybrid composites at higher loads. However, the graphite addition reduced the counter face wear. Both unreinforced Al(356) and Al(356)-20% SiC_(p) composite showed a transition from mild to severe wear at 95 and 225N load respectively as shown in Figures 2.1(a) and (b). However, hybrid composites with 3 and 10% graphite does not show such a transition over the entire load range indicating improved seizure resistance of composites induced by graphite [35]. On the other hand, introduction of graphite particle decrease the hardness and fracture toughness of hybrid composites [107]. Increase in graphite particle hybridisation reduces the CTE of composites [107]. Al-SiC-nickel coated graphite particle reinforced hybrid composite, GrA-NiTM, synthesised by Stephenson *et al.* [55, 101] have exhibited higher wear resistance, seizure resistance and load bearing capacity at elevated temperature than non-graphitic composites. Also, nickel present as Al₃Ni precipitates in the matrix enhances wear resistance and high temperature strength. The nickel coating promotes the wetting of graphite with aluminium alloy. It is also proposed that hindered settling between two particles, one more denser and the other less denser than the suspending melt, could provide homogeneous distribution of particles [55, 101] and the relation $V_{SiC} = 1.8V_{Gr}$ (V = volume percentage) is derived for a neutrally buoyant mixture. In most of the studies coated graphite particles have been added to the remelted monocomposites of SiC [35, 101-105].



(a)



(b)

Figure 2.1: Wear rate and applied load diagram for Al(356)-20% SiC_(p)-10%Gr_(p) (○) and Al(356)-20% SiC_(p)-3% Gr_(p) (●) HMMC in comparison with (a) Al(356) alloy (∇) and (b) Al(356)-20% SiC_(p) (∇) monocomposite (Ames and Alpas [35])

Studies by Tjong *et al.* [97] on hybridisation of boron nitride particles on Al-4Cu-10% SiC_(p) composite have enhanced the wear resistance behaviour of the composites due to the self-lubrication property of the BN particle. Also, addition of low density (2.3 g/cm³) BN particle reduce the density of composite. The variation of the weight loss with sliding distance for Al-4Cu-SiC-BN hybrid composites is given in Figure 2.2. Prasad and Mecklenburg [112] have synthesised D-HMMC by powder metallurgy and squeeze infiltration techniques and patented a self lubricating hybrid aluminium matrix composite consisting of a hard ceramic particle and a solid lubricant material as reinforcements. The hard ceramic particle can be SiC, Al₂O₃, SiO₂, TiC or WC and the solid lubricant is described by the general formula MX₂, wherein M is molybdenum, tungsten or niobium and X is sulphur, selenium or tellurium, for example Tungsten disulphide (WS₂), Molybdenum ditelluride (MoTe₂) and Tungsten ditelluride (WTe₂).

Hybrid composites with SiC reinforcements in two different forms, viz., whiskers and particulates at different ratios of 1:1, 1:2 and 1:3 have been fabricated by Ko and Yoo [113] using powder metallurgy technique. Studies by Long *et al.* [114] showed aluminium composites reinforced with a hybrid of SiC whisker, SiC_(p) and C_(sf) exhibited excellent wear resistance. SiC_(p) has been found to be a barrier against slipping of relatively large reinforcements. The liquid metal infiltration technique can be used for producing various combinations of short fibre/particulate hybrid composites [115]. Tanaka *et al.* [116] synthesised a hybrid aluminium matrix composites reinforced with potassium titanate/ aluminium borate whiskers and alumina short fibres. These hybrid composite offers good properties such as anti seizure property, wear resistance and rigidity.

Evaluation of tribological properties of 2024 alloy and Al(2024)-Al₂O_{3(sf)}-SiC_(p) hybrid composite by Fang *et al.* [117] has revealed that the latter exhibited better wear resistance than the former under the test conditions. Studies by Baker *et al.* [118] on Al(6061)-SiC_(p)-Al₂O₃ (saffil fibres) hybrid composites, prepared by direct hot pressing of blended pre-alloyed powder, have shown that the sliding wear resistance of SiC_(p) mono composite is better than hybrid composite.

Commercial pure Al hybrid composites with 15 vol% SiC_(p) and 15 vol% mullite (72% Al₂O₃ and 28% SiO₂) short fibres are fabricated by squeeze casting

technique using as received [Figure 2.3(a)] and artificially oxidized $\text{SiC}_{(p)}$ particles [Figure 2.3(b)] [119].

Today, weight-saving in automobiles is of paramount importance. In order to produce a lighter engine, an aluminium block with cast iron liners and a hypereutectic aluminium silicon alloy has been developed as an alternative to cast-iron blocks [120-122]. To replace the cast iron liners, a new engine block was developed in which the cylinder liners of aluminium based composite reinforced with short hybrid fibres of alumina and carbon are used [123-125]. The self lubricating effect of carbon fibre contributes to improvements in antiseizure when there is no oil film in the cylinder bore surfaces. The sliding tests have shown that once a scratch appears in the alumina fibre MMC, it is easily aggravated, where as in the case of carbon-alumina hybrid composite, small scratches do not grow. Among carbon fibres, PAN carbon fibre is better than low-grade pitch carbon fibre. In addition, it has been observed that the strength tends to drop with the use of carbon fibre alone, whereas if alumina is blended with $\text{C}_{(sf)}$, there is only marginal reduction in strength [123]. Similar trend in decrease of tensile strength and elongation with increase in carbon short fibre in Al- $\text{Al}_2\text{O}_{3(sf)}$ - $\text{C}_{(sf)}$ system fabricated by squeeze casting method have been observed [75, 126, 127]. On the contrary, a slight increase in elastic modulus of Al- $\text{Al}_2\text{O}_{3(sf)}$ - $\text{C}_{(sf)}$ compared with that of unreinforced alloy have been observed. The wear behaviour of Al- $\text{Al}_2\text{O}_{3(sf)}$ - $\text{C}_{(sf)}$ composites have been improved by 20~30% more than that of Al- $\text{Al}_2\text{O}_{3(sf)}$ composites as depicted in Figure 2.4.

Alumina - aluminosilicate fibre reinforced aluminium-silicon matrix hybrid composites are fabricated by Jiang *et al.* [128, 129] using pressure infiltration method. The highest ultimate tensile strength (UTS) have been obtained at an alumina-aluminosilicate ratio of 3:2 [128]. Hybridisation with alumina and aluminosilicate in the ratio of 2:3 has resulted in good wear resistance especially at higher loads.

During processing of in-situ MMCs, more than one reaction products are obtained in many cases. However, those reaction products contributing to any properties of the composites similar to other reinforcements would be considered as a

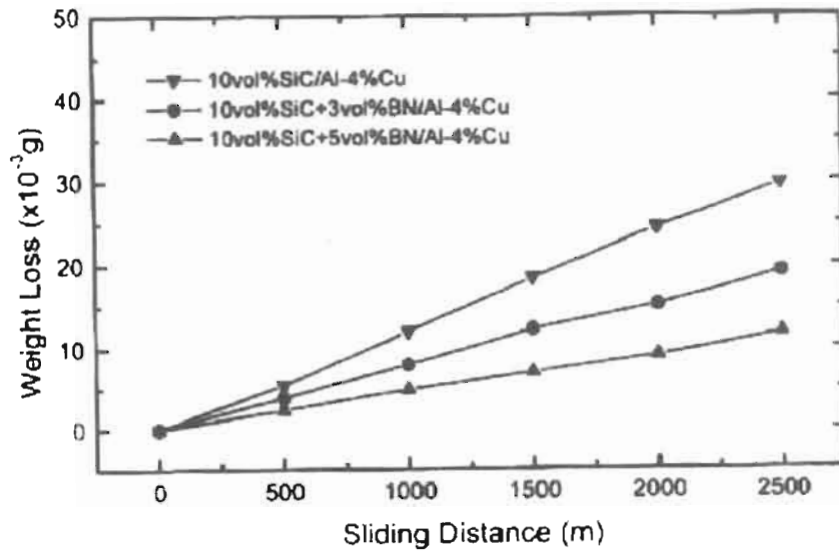


Figure 2.2: Variation of the weight loss with sliding distance for SiC + BN-Al-4% Cu hybrid composites under an applied load of 35 N and a sliding velocity of 1 m/s (Tjong et al. [97])

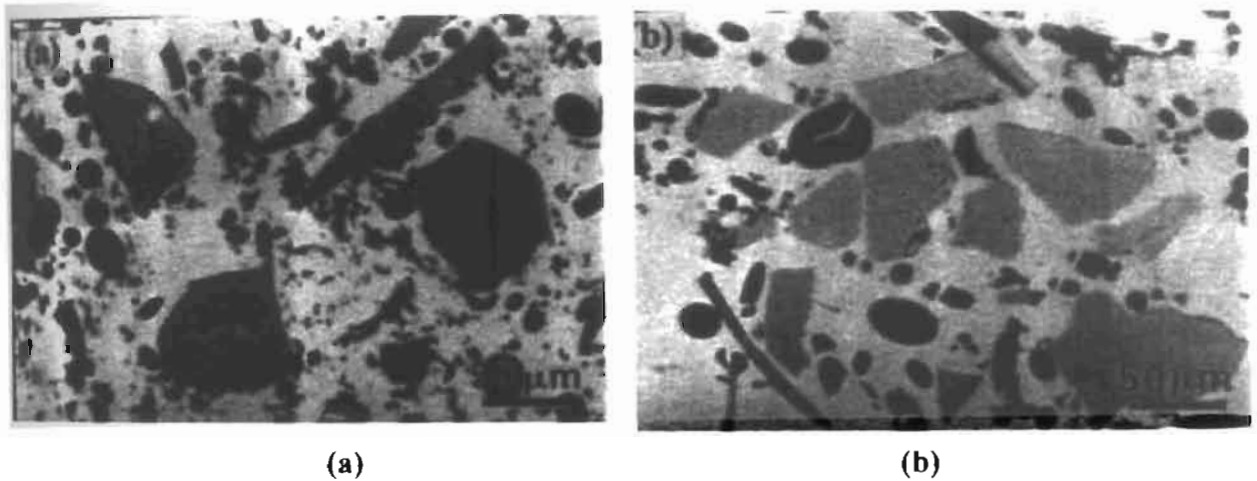


Figure 2.3 : Microstructures of Al-15% SiC_(p)-15% mullite short fibres HMMC using (a) as received SiC_(p) and (b) oxidised SiC_(p) (Guo and Tsao[107])

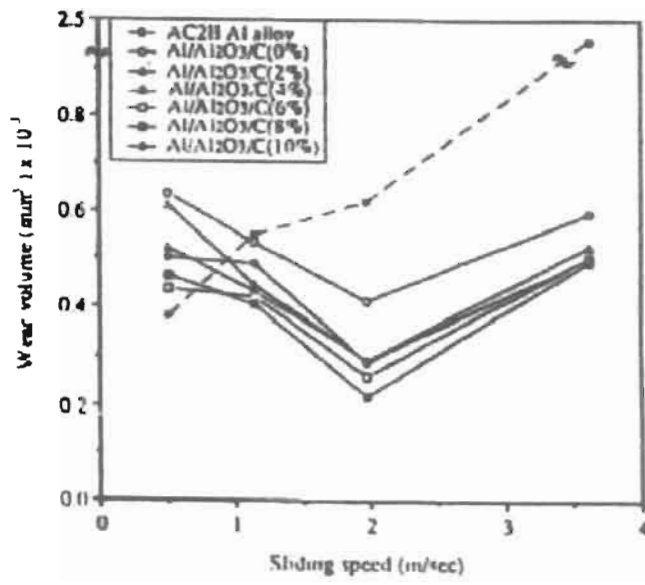


Figure 2.4: Effect of sliding speeds on wear behaviour of Al-Al₂O₃-C HMMC (Song et al. [75])

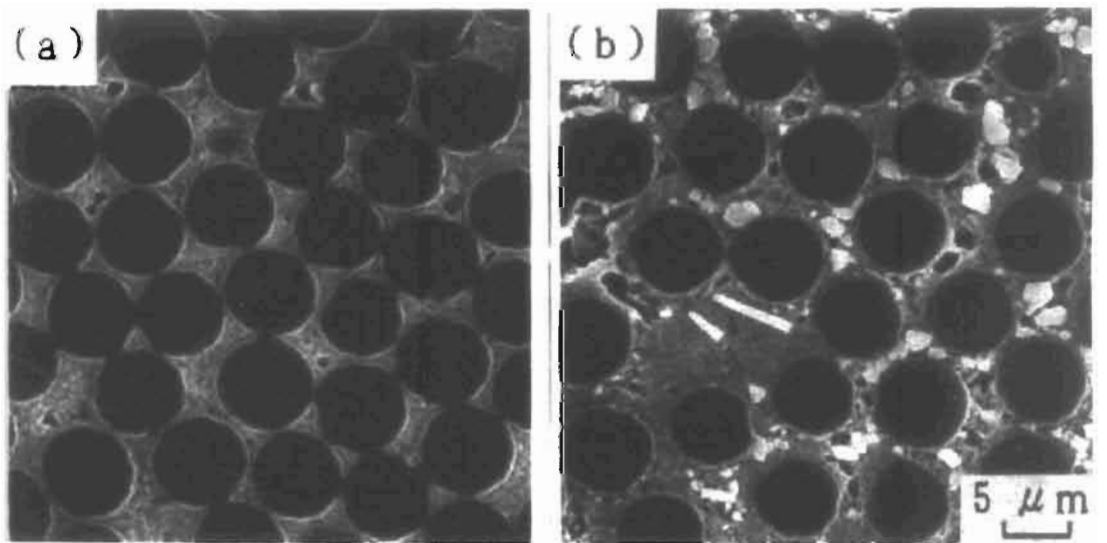


Figure 2.5: SEM micrograph of Al-C-SiC (a) mono and (b) hybrid composites (S. Towata et al. [76])

dispersoid. To be an in-situ hybrid metal matrix composites, more than one dispersoids should be present and at least one should be formed through in-situ reaction. Most of the in-situ HMMC are discontinuous systems. However, there are few cases, where coating on continuous fibre reacts with matrix elements forming a second dispersoid. These processes are termed as 'in-situ hybridisation' by reinforcement coating [26]. Feng and Froyer [93] synthesised Al-10 vol% ZrB₂-9.2 vol% Al₂O₃ from Al+ZrO₂+B mixture by reactive sintering and subsequent densification by hot pressing. The hybrid composite has shown increased properties compared to Al, viz., Young's Modulus (72 to 105 GPa) and bending strength (132 to 320 MPa). However, the ductility of composite is 3.1% against 21% for pure Al. Aluminium based hybrid composites of Al₃Ti platelets and Al₃Ni granular particles possessing functionally gradient properties have been prepared by centrifugal casting method [130].

2.4.1.2 CD-HMMC

The continuous-discontinuous HMMC systems are generally processed to improve the properties of a continuous fibre reinforced metal matrix composites. The hybridisation of particulates or whiskers in a continuous fibre systems improves the infiltration of liquid metal, tailors the fibre volume fraction, reduces the volume fraction of costly fibre and greatly enhances the tensile and longitudinal flexural strength compared to monocomposites [38, 76, 131, 132]. Towata *et al.* [76, 133] have prepared a preform of 150 mm length and 2 mm thick by hybridising whiskers and particulate of SiC in continuous carbon fibre bundles and infiltrated pure Al and Al-5% Mg alloy by squeeze casting process at a pressure of 90 MPa and pressing time of 60s. This hybridisation with 0.07 volume fraction of SiC particulates and whiskers has reduced volume fraction of costly continuous carbon fibre from 0.7 to 0.52. Longitudinal flexural strength of the hybrid composite increased by about 50% from 0.5 to 1 GPa compared to carbon fibre monocomposites. The carbon fibres are uniformly distributed in the matrix without direct fibre-to-fibre contacts because of hybridisation effect [Figure 2.5]. Further, the hybridisation enables the molten aluminium to completely infiltrate into fibre preform and suppresses the stress concentration caused by the failure of the adjacent fibres. The failure of hybrid composites have been caused by the accumulation of micro-cracks, whereas, in case

of conventional fibre composites, the fibre failure is mainly initiated at the direct fibre-to-fibre contact points, resulting in drastic failure. Similarly, the hybridisation improves the transverse flexural strength by 50%. The hybrid composites also exhibit higher longitudinal strength. But, the strength of carbon fibres extracted from the hybrid composites are lower than that extracted from conventional composite due to higher degradation of fibres in hybrid composite. The degradation of fibres in hybrid composite may be due to possible mechanical damage caused by adhering whiskers and particulates during pre-treatment. These results suggest that the strength of composites is not 'so attributable' to the fibre strength as usually reported, but to the 'fracture mechanism' [76, 134]. Cheng *et al.* [38] have observed that the longitudinal tensile strengths of hybrid composites are improved greatly, although fibre volume fractions are very low compared to those of monocomposite. Yoshida *et al.* [132] hybridised SiC whiskers with higher modulus graphite fibre reinforced pure Al matrix composites and evaluated their wear characteristics. Wear rates and friction coefficients of composite with 0.55 V_f high-modulus graphite fibre are very high during the initial state of sliding. The wear rate decreases and becomes constant after about 100 m of sliding. Compared to un-reinforced aluminium, the wear rate is found to be three to four times higher regardless of fibre orientation.

The hybridisation technique by reinforcement coating combines the fibre coating and particles hybridisation. SiC hybridised carbon fibre reinforced aluminium CD-HMMC are synthesized by this technique [78]. SiC coating on $C_{(f)}$ have been made using sol-gel method and the composite fabricated by squeeze cast process have shown good distribution of carbon fibre in the matrix due to hybridisation of particles. The hybridisation improves the mechanical properties especially the axial strength and the coating is an effective barrier for the C/Al interfacial reaction.

2.4.1.3 C-HMMC

As discussed above, many studies have been carried out on particulate or whisker hybridisation on continuous fibre systems leading to formation of CD-HMMC. However, studies on continuous fibre hybridisation leading to C-HMMC are limited. C-HMMC are fabricated mainly to replace a portion of costly fibres by cheaper ones or to enhance certain properties of the monocomposites containing one

type of fibre. For example, the addition of steel network structure to boron fibre reinforced aluminium matrix composite tends to enhance the mechanical properties especially under cyclic loading [98, 99].

2.4.2 Magnesium

Magnesium alloys are one of the low density materials preferred for the structural applications in the areas of aerospace and automotives, where weight saving is necessary. The main disadvantages include relatively low strength at room and elevated temperatures, low stiffness and low wear and corrosion resistances, compared to Al and Ti alloys. The introduction of reinforcements to Mg matrix can improve most of the above critical properties. The properties achieved depend on the matrix alloy, type, composition, volume fraction and distribution of reinforcements, manufacturing methods and subsequent treatments given [135]. Conventional casting alloys such as Mg-Al and Mg-Zn systems can be used as the matrix alloys.

Various studies have been carried out on synthesis of monocomposites based on magnesium matrix with continuous and discontinuous dispersoids such as SiC [135-141], carbon [138, 139], and alumina [135, 140, 141]. However, studies on magnesium based hybrid systems are limited. Schroder and Kainer [141] synthesized Mg hybrid composites reinforced with alumina short fibre (Saffil) and SiC particles using Mg-2.5%Ag-2%RE-0.6%Zr alloy (RE – Rare Earth) matrix. High cost of preform production and reinforcements (e.g. short fibres and whiskers) could be overcome by hybridisation of low cost particles. The hardness value of matrix is increased by 70-85% on reinforcing with a hybrid of 10 wt% of Saffil fibre and 15 wt% SiC particles. Similarly, hybridisation enhances the Young's Modulus from 45 to 77 GPa, tensile strength from 240 to 330 MPa and bending strength from 370 to 560 MPa. The Mg-5.5Zn-0.45Zr (ZK60A)-SiC_(w)- B₄C_(p) hybrid magnesium composite provides excellent mechanical properties with reduced cost [142-144].

2.4.3 Smart Hybrids

The materials with intrinsic sensing, actuating and controlling or information processing capabilities in their microstructure are termed as 'smart' or 'intelligent'

materials. They respond to the environmental changes at the most optimum conditions and manifest their own functions according to the change [145, 146]. Advanced materials are available with multi-functions or primitive intelligence inherent in their structures such as shape-memory alloys, piezo electric ceramics, fibre optics, magneto-(electro) strictive materials, magneto-(electro)-rheological fluids and some functional polymers. To integrate and hybridise the materials with smart behaviour, these advanced materials may lead to composite materials with intrinsic mechanisms for sensing, control and multi responses [146]. Metal matrix composite with intelligent characteristics can be fabricated by incorporating smart materials. Shape memory alloys (SMA) can be used as the reinforcement in fabricating smart composites due to their unusual characteristics such as shape memory effect, pseudoelasticity or large recoverable strain and high damping capacity. Shape memory materials sense thermal, mechanical, magnetic or electric stimulus and exhibit actuation or corresponding change in some technical parameters such as shape, position, strain, stiffness, natural frequency, damping, friction and other static or dynamical characteristics of material systems. Smart MMCs can be prepared in two ways : (a) incorporating SMA reinforcement in a metal matrix and (b) reinforcing ceramic dispersoids in the SMA matrix.

The concept of strengthening the Al-MMC by dispersing Ti-Ni SMA particles was proposed by Yamada *et al.* [147]. The pre-strained SMA particles will try to recover the original shape upon the reverse transformation from martensite to parent austenite state by heating. This will generate compressive stresses in the matrix along the pre-strain direction enhancing the tensile properties of the composite at the austenitic stage. Shape memory particulate reinforced composites can be fabricated by consolidating aluminium and SMA particulates or pre-alloyed powders of size varying from nanometers to micrometers prepared by conventional processes such as atomisation method and spray or rapid solidification process [34]. Shape memory alloy fibres of Ti-Ni reinforced aluminium matrix composites were prepared by Furuya *et al.* [148-149]. The incorporation of Ti-Ni fibres to pure Al (1100) matrix increased Young's modulus and tensile yield stress with increasing volume fraction of fibres. Addition of 9 vol.% of 4% prestrained Ti-Ni fibres to Al (1100) matrix enhanced the yield stress by 100% compared to the matrix alloy. Literature on smart hybrid metal matrix composites are limited. Smart HMMC can be designed and

fabricated by incorporating shape memory materials in fibrous or particulate form into a conventional MMC system.

2.4.4 Functionally Gradient Hybrids

Functionally gradient materials (FGM) are used to produce components featuring engineered gradual transitions in microstructure or composition, which is warranted by the varying functional performance requirements at different locations within a part [31, 150-154]. FGM can be fabricated by various processing methods such as powder densification (conventional solid state powder deposition, liquid phase sintering and reactive powder process), coating (plasma spray forming, vapour deposition, laser cladding and electroforming), lamination, infiltration (infiltration of liquid through gradient porous preform and infiltration combined with liquid phase sintering or self propagating high temperature synthesis), thermal process, mass transport process (diffusion from surface: steel carburisation and nitriding and inter diffusion), settling and centrifugal separation. Functionally gradient metallic composites suitably designed with hybrid reinforcements could provide gradient properties in structures. Gradient structures are produced with selectively reinforcing in a particular position of a component. Diesel engine pistons with selective reinforcement of Al_2O_3 fibre insert in Al alloy prepared by squeeze casting technique [31, 155, 156], is one of the example where monocomposite is used. These composites reduced the weight by 5-10% compared to Ni cast iron insert.

Functionally gradient hybrid composite of nickel base alloy with $\text{Al}_2\text{O}_{3(p)}$ - $\text{Cr}_2\text{O}_{3(p)}$ was prepared by plasma spraying method [157]. FGM structures based on Al- Al_2O_3 - TiB_2 hybrid system have been fabricated by self propagating high temperature synthesis [158]. Automotive components such as pistons with graded transitions from pure aluminium matrix to hybrid ceramic reinforced aluminium at surface were produced. Hybrid reinforcements of alumina short fibres blended with aluminium titanate particles were used to produce aluminium pistons selectively reinforced along with crown surface with preforms containing four layers of distinct volume fraction [159]. Watanabe and Nakamura [160] have synthesised hybrid Al- Al_3Ti - Al_3Ni functionally gradient composite with improved wear resistance by centrifugal casting method.

2.5 PROPERTIES OF MONO AND HYBRID COMPOSITES

The mono composites of different alloy matrices have been synthesised with a wide range of physical, mechanical and tribological properties. As discussed earlier, in addition to the properties of the matrix alloy and reinforcement, other factors influencing the properties of composites are the type, size and volume fraction of the reinforcement, their distribution in the matrix and good interfacial continuity. By hybridisation, further fine tuning and synergistic effect on properties are possible. In continuous fibre reinforced composites, the fibre-to-fibre contact is caused by low wetting of fibres and improper infiltration of liquid metal into the preforms. This is one of the major structural defect leading to failure of the composite at very low stress levels. The hybridisation with particulates or whiskers in these composites leads to more interfibre spacing leading to proper infiltration of liquid metals and hence better properties even with reduced volume fraction of costly fibre [38, 75, 76]. The properties of discontinuous dispersoid reinforced composites are isotropic in nature whereas that of continuous dispersoid reinforced composites are anisotropic. The mechanical properties of mono composites are dealt in detail in many of the reviews mentioned earlier. On the other hand, only very limited literature available on the properties of hybrid composites, are discussed below.

2.5.1 Physical Properties

The composite being a homogeneous mixture of two or more phases, the physical properties of the composites can be predicted fairly accurately using the rule of mixtures (ROM). In general, the density of both mono- and hybrid- composite strictly obeys ROM, whereas other physical properties such as electrical and thermal conductivities and coefficient of thermal expansion (CTE) show deviation from ROM due to the interface and other effects.

In monocomposite, the presence of 30 vol% SiC whisker in pure Al reduce its thermal conductivity to half [161]. Similarly, the presence of 30 vol% SiC whisker reduce the CTE of 7075 Al alloy to half, which is 50% higher than that of 7075-25wt%. Al₂O₃ fibre composite [162]. The graphite particle dispersed Al alloy matrix composites have shown lower density than the base alloy. The use of nickel coated

graphite particles increases the density of the composite [101]. In this case, it is difficult to estimate the density of the composite by ROM since Ni dissolves in Al and precipitates as NiAl₃ having higher density than Al. Further, the GrA-NiTM hybrid composite (Al(356) – 10 vol% SiC_(p) – 5 vol% graphite_(p)) have shown lower CTE than either Al(356) or the Al9Si-20vol%SiC composite due to the formation of NiAl₃ intermetallic out of the reaction between aluminium matrix and nickel coating on graphite. The hybridisation of Al-Al₂O_{3(sf)} system with C_(sf) have reduced its density. The thermal conductivity of Al-Al₂O₃ composite reduces with increase in Al₂O₃ volume fraction. However, in the case of Al-C_(sf), the volume fraction of C_(sf) have shown little effect on thermal conductivity [124].

2.5.2 Mechanical Properties

The effects of different reinforcements on modulus of elasticity, strength, elongation, fatigue, fracture toughness and creep are briefly discussed.

2.5.2.1 Modulus of Elasticity

The introduction of reinforcement always enhances the stiffness of the composite significantly, which is proportional to the elastic modulus. The predominant factors influencing elastic behaviour are the type and volume fraction of reinforcement. In an unidirectionally reinforced continuous fibre MMC, the longitudinal Young's modulus increases linearly as a function of the fibre volume fraction and is in agreement with ROM value, where ROM is given by

$$E_c = V_r E_r + V_m E_m \quad (4.1)$$

where, E is the elastic modulus, V is the volume fraction and c, m and r are the composite, matrix and reinforcement respectively. The increase in modulus along the transverse direction of the fibres is low. In discontinuously reinforced MMC, the actual modulus is very low compared to that predicted by rule of mixtures. For discontinuous reinforcement, the ROM expression is modified as Halpi-Tsai equation.

$$E_c = \frac{Em(1 + 2sqVr)}{1 - qVr} \quad (4.2)$$

$$\text{Where } q = \frac{(Er / Em - 1)}{(Er / Em) + 2s} \quad (4.3)$$

and 's' is the particle aspect ratio.

The accuracy of quantitative determination of Young's modulus is dependent on the method of measurement. Dynamic methods tend to give larger values of elastic modulus than static measurements obtained from the elastic portion of tensile stress-strain curve. Further, the static values may depend on whether the measurements are made in tension or compression [163]. The anomaly is due to the presence of thermal residual stresses caused by the difference in coefficient of thermal expansion of the matrix and the reinforcement.

In hybrid composites, containing a soft reinforcement such as graphite particles or carbon short fibres and a hard particle like $\text{SiC}_{(p)}$, the modulus values obtained are between that of unreinforced alloy and hard particle reinforced monocomposite. Song and Han [126] observed that the elastic modulus of Al- Al_2O_3 composite is greater by 27% than that of unreinforced alloy, whereas that of Al- Al_2O_3 -C hybrid systems is improved only by about 15-20%. However, these hybrid composites are synthesised mainly for better wear characteristics. It is possible to enhance the modulus of particulate composites by hybridising with a low percentage of whiskers or fibres. In general, Young's modulus of composites with highly elastic fibres increase with increase in fibre volume fraction. Schroder and Kainer [141] observed significant increase in the Young's modulus of 77 GPa in Mg-10 vol% Al_2O_3 (saffil fibres)-15vol% $\text{SiC}_{(p)}$ hybrid composite compared to 45 GPa of unreinforced magnesium. Similarly, introduction of SiC particles to Al-SiC fibre composites fabricated by squeeze casting has enhanced stiffness from 144 to 150 GPa [37].

2.5.2.2 Strength

The introduction of reinforcements to matrix alloy generally enhances both yield and ultimate tensile strengths. This increase in strength is dependent on volume fraction, type and morphology of the reinforcement. Continuous fibres offer higher strength compared to discontinuous ones. Whisker reinforcements compared to particles provide better strength with much higher yield strength under compression than in tension. In addition, the strength of discontinuously reinforced composites depends on the matrix alloy and its heat treatment conditions. The strength of

composite is also dependent on the fabrication methods. However, there are certain dispersoids such as graphite and flyash particles, which reduce the strength and are mainly used for improving wear resistance.

Both strengthening and stiffening of composites are dependent on the load transfer across the interface between the matrix and the reinforcement. A strong bond is usually formed with reaction between the matrix and reinforcement, the reaction product determining the nature of bond. A brittle reaction product at interface makes composite crack at lower strains. Even though the interface is free from reaction products, the tensile properties are dependent on the nature of bonding. In unidirectional reinforced composites, the longitudinal tensile strength and crack growth initiation resistance are found to be insensitive to the nature of the interface. However, a weak interface exhibits extensive debonding and reduces the transverse and torsional strength of the composite [164]. It is also observed that composite failure is associated with particle cracking and void formation within the cluster of particles [165-167]. The particle cracking observed in the composite containing coarser particles is due to the presence of fracture initiating defects. A high interfacial strength is required to minimize cracking along the interface and load the particles effectively.

In the case of hybrid composites, enhancement in the strength properties depends on the type of reinforcement added and also its function. The hardness and strength of Al-SiC_(p)-Gr_(p) hybrid composite is slightly lower than that of Al-SiC_(p) mono composite, but higher than Al-Gr_(p) monocomposite [106]. The addition of hard SiC to Al-Gr_(p) monocomposite enhances the strength and hardness of resulting composite. In continuous carbon fibre reinforced Al matrix monocomposites, the mechanical behaviour is greatly improved by hybridisation with a small percentage of SiC particle or whiskers. As discussed earlier, fracture of weak fibres propagates rapidly to adjacent fibres through direct fibre to fibre contact points resulting in a drastic failure. However, the presence of particulates or whiskers increases the interfibre spacing, the longitudinal and transverse flexural strengths by 50 % and the longitudinal tensile strength [38, 76]. Here, the function of particulates or whiskers in separating out the fibres is crucial in improving their strength. Similarly, SiC_(p) hybridisation in Al-SiC-Ti-C-O (Tyrrano) fibre reinforced composite enhances the

room and high temperature strengths of the composite. In $\text{Al}_2\text{O}_3(\text{sf})$ reinforced Mg alloy composite, the $\text{SiC}(\text{p})$ hybridisation has enhanced both hardness and strength of the composite.

2.5.2.3 Elongation

Incorporation of reinforcements in a matrix alloy reduces the ductility of composites rapidly, which is one of the major limitations of MMC. For example, Al(6061)(T6) has 12% elongation and incorporation of 15 vol% Al_2O_3 particle reduces it to 5.4%. This is because, the composite failure is associated with particle cracking and void formation in the matrix within the particle clusters. It is also noted that the matrix deformation between closely placed particles would be highly constrained. The percentage of elongation is dependent on the type, size and distribution of particles, matrix microstructure and nature of matrix-reinforcement interface. The larger particles tend to have higher probability of fracture initiating defects leading to early particle fracture. In case of non-uniform distribution of particles, intrinsic local stress triaxiality is generated in the clustered regions. A higher interfacial strength is required to minimise cracking along interface and load the reinforcement effectively. The matrix microstructure is also important since the fracture is ultimately controlled by the local matrix failure. In order to have maximum possible ductility, it is better to have fine and uniform particle size distribution, particle shape near to sphere, homogenous particle distribution in matrix and higher matrix ductility and interfacial strength. In the case of hybrid composites also, the addition of a second reinforcement could lead to further reduction in ductility.

2.5.2.4 Fatigue

The fatigue life of composites is significantly increased by the addition of reinforcements [168, 169]. The fatigue is related to the magnitude of the difference in stress intensity between the maximum and minimum loading (ΔK). The ΔK for Al-SiCp is around $2\text{-}4 \text{ MPa m}^{1/2}$ which is approximately twice that of unreinforced Al ($1\text{-}2 \text{ MPa m}^{1/2}$). The fatigue resistance of long fibre reinforced MMCs is superior to that

of unreinforced metal (fatigue limit increases by a factor of two) when loaded in tension along the fibre axis [170-172].

The proposed mechanisms for the enhancement in fatigue resistance are the crack deflection and a reduction in slip band formation due to the reinforcement. Increase in volume fraction of reinforcement increases the fatigue life under stress controlled conditions and could be attributed to decreased elastic and plastic strains that result from increasing modulus and apparent work hardening, both of which increase with increase in volume fraction. When the stress intensity at a crack is below K_{Ic} , immediate failure will not occur and the crack may grow. The fatigue loading is the major cause for sub-critical crack growth. Under constant strain amplitude conditions, the MMC is inferior in low cyclic regime, where plastic strain dominates, and in high cyclic regime, the composite is little different to unreinforced material. The enhancement observed in constant stress amplitude tests is due to the higher Young's modulus of the composites, the strain in the composite is lower than those in the unreinforced material at the same stress levels.

The fatigue strength of hybrid GrA-NiTM and A356-15% SiC monocomposite at the 10^5 cycle level is about 130 MPa. Overall low cycle fatigue properties of A356 alloy are slightly better than those of the MMC. The reason for the lower low cyclic fatigue life of both these MMC is mainly attributed to the constrained flow of ductile matrix due to the presence of reinforcements.

2.5.2.5 Toughness

Toughness is the energy absorbed in the process of fracture, and the resistance to crack propagation is termed as 'fracture toughness', K_{Ic} . The toughness of the composite depends on the type, size and orientation of reinforcement, matrix composition and microstructure and processing parameters. Fracture toughness of particulate composites generally decreases with increase in particle size at a given volume fraction and interparticle spacing. Fracture toughness decreases with increasing tensile strength for cast composites, whereas it increases by 70-100% for forged ones over that of cast ones. This increase in toughness with increasing amount of particulates is related to blunting of the original crack tip caused by the void

nucleated over the particles [173]. While the crack tip radius increases, the stress concentration at crack tip decreases resulting in a combined increase in fracture toughness values. In fact, pinning down of crack front by interparticle obstacles is shown to increase toughness, whereas in composites fracture toughness decreases due to the particle acting as void sites upto a certain volume percent and then increases with higher volume fraction due to blunting of cracks at the void formed over the particle matrix interface and absorption of the energy by voids [173].

Unidirectional fibre reinforcement can lead to easy crack initiation and propagation vis-à-vis the un-reinforced alloy matrix. Braiding of fibres can make the crack propagation toughness increases tremendously due to extensive matrix deformation, fibre bundle debonding, and pull out [174].

2.5.2.6 Creep

The creep resistance of Al 9Si 3Cu – 25 vol% Al₂O₃ composites at 400 °C is increased by 100% compared to that of unreinforced alloys [162]. The dependence of creep rate on both stress level and temperature is more in the composites compared to the matrix. The whisker-reinforced composites are more creep resistant than particulate composites. The addition of short fibre reinforcement enhances the creep strength, presumably because of effective load transfer to the fibres. Hence, it could be possible to enhance the creep behaviour of a particulate composite by hybridising it with whiskers or short fibres. Reports on creep studies of hybrid composites are limited.

2.5.3 Tribological Properties

The improved wear resistance of metal matrix composites enhances their potential as an engineering material. The improvement in wear resistance is dictated by shape, distribution and volume fraction of dispersoids used and matrix microstructure. The addition of hard dispersoids such as SiC and Al₂O₃ to aluminium improves the wear resistance in both dry and lubricated conditions [175-176]. Higher volume fraction and larger dispersoids size provides greater wear resistance. The addition of soft reinforcements such as graphite to aluminium alloys improve the

adhesive wear resistance. The tribological behaviour of graphite reinforced metal matrix composites has been reviewed [27]. The superior sliding wear performance is due to improved lubrication arising out of cleaving of the soft graphite located between the sliding surfaces and improved retention of an added lubricant in surface depressions left in the harder matrix. The mechanism of wear particle generations are (a) adhesion, deformation and fracture of asperities resulting from repeated single and multiasperity interaction during sliding, (b) ploughing by hard entrapped particles or hard asperities at the sliding surface, and (c) delamination caused by subsurface crack nucleation and propagation. The wear debris generated by this mechanism form loose particles, or sometimes go to the counter surface by mechanical interlocking or by adhesion on the counter surface.

The tribological behaviour of aluminium matrix composites with hybrid dispersoids is widely studied due to their enhanced wear resistance. The hybridisation of Al-SiC_(p) mono composite with soft reinforcements such as graphite particulates or fibres tends to increase the adhesive wear resistance of the composites. Further, the mild to severe wear transition load value has been shifted to very high value for Al-SiC_(p)-Gr_(p) HMMC compared to Al(356) alloy and Al(356)-SiC_(p) mono composites [Figure 2.4 (a) and (b)] [55]. Studies by Song *et al.* [75] have shown that wear behaviour of Al-Al₂O_{3(sf)}-C_(sf) composites has been improved 20-30% more than that of Al- Al₂O₃ composites. This is due to the presence of lubrication film formed by the addition of carbon fibres on the wear surface of hybrid composites.

Guo and Tsao [107] studying the tribological behaviour of hybrid Al(6061) - 10 vol% SiC_(p) -2/5/8 vol% graphite_(p) composites processed by powder densification method have observed that wear rate increases by increasing graphite content up to 5% Gr_(p) and drop to a lower value for 8% graphite. This can be explained based on two competing factors affecting wear rates of the composites. Firstly, the fracture toughness of the composite decreases as the amount of graphite addition increases, which means that the composites with graphite additions are easier to fracture during wear process, and therefore have higher wear rates. Secondly, as the amount of graphite addition have been increased, there is release of more graphite to the wear surface during the wear process serving as the solid lubricant to reduce the friction coefficient. Therefore, the composites with higher graphite additions would have

lower wear rates. The resultant of the two effects caused by the graphite addition is called the 'composite effect'.

2.5.4 Corrosion Resistance

The corrosion behaviour of MMC is also dependent on the type of matrix and reinforcement used as well as the fabrication route [29]. Both the enhancement and the reduction in the corrosion resistance are observed in MMC. Enhancement in corrosion resistance is generally observed due to unattacked reinforcement resulting in reduced surface area exposure. In the case of tungsten fibre reinforced uranium alloy, the fibres remain unattacked in salt solution with the matrix corroding at the same rate as unreinforced base alloy [177]. In some of the systems, localized corrosion behaviour due to galvanic effects arising from the potential difference between the matrix and reinforcement, crevice corrosion at interface of matrix and reinforcements or pitting corrosion at interfacial reaction product are observed. Microstructural contaminants and residuals of processing can also affect the corrosion.

Galvanic corrosion is observed in Al-Graphite, Al-B and Al-SiC systems with the former exhibiting the high corrosion rates in NaCl solution. Since graphite is a conductor and can serve as an inert electrode for proton and oxygen reduction, the high corrosion rates of Al-Gr were attributed to galvanic corrosion. Another cause of degradation in Al-Gr is the formation of Al_4C_3 by the reaction between aluminium and carbon. In wet environment, Al_4C_3 hydrolyses producing methane and aluminium hydroxide. The methods for improving the corrosion resistance are by eliminating galvanic corrosion by electrically decoupling the graphite fibre from the matrix by surface coatings and inhibiting oxygen reduction on graphite. Similar to Al-Gr, in Al-SiC system, the SiC can serve as inert electrode for proton and oxygen reduction and Al_4C_3 formation at Al-SiC interface can also aid. In Al- Al_2O_3 system, galvanic corrosion is unlikely to occur, since the resistivity of Al_2O_3 (99.7 % pure) is greater than about $10^{14} \Omega \text{ cm}$.

2.6 SOLIDIFICATION BEHAVIOUR OF MMC

Solidification process is a crucial step largely determining the pattern of particle distribution and microstructure of the solidified MMC, which in turn, influence the properties of MMC. The solidification behaviour of particle reinforced MMC is different from the base alloy matrix and depend on factors solely attributable to the presence of ceramic dispersoids in the melt, such as particle settling and floatation leading to local variations of particle volume fraction and thermo physical properties of the melt, as well as interaction between the particles and solidification front. The latter is mainly determined by the solidification rate and the morphology of solidification structure and may lead to particle capture by the front in some cases and to particle pushing to others. Both settling and particle front interaction during solidification may significantly influence the distribution pattern of the particles in the solidified MMC. The microstructure formation and the heat transfer characteristics during solidification process and effects of dispersoids on solidification curve are briefly discussed.

2.6.1 Solidification and Structure Formation

Direct transposition of rules developed for microstructural controls in the solidification of unreinforced metals are not possible with MMC because the reinforcements frequently modify the solidification of matrix. Nucleation and growth of matrix phases and their interaction with discontinuous reinforcements during solidification are dealt with.

2.6.1.1 Nucleation

The grain size of matrix is significantly affected by the homo- or heterogeneous nucleation of matrix phase on the reinforcements. In the case of aluminium and its alloys, the heterogeneous nucleation of primary phases in reinforcements seems to occur rarely, since grain sizes are far in excess than reinforcement diameter as frequently observed in aluminium reinforced silicon carbide [178-181], carbon [182] and alumina [61, 183, 184]. It is reported that TiC reinforced aluminium shows microstructural refinement [185]. The heterogeneous

nucleation of primary silicon phase on dispersoids have been observed in hypereutectic aluminium silicon alloy reinforced composite containing carbon, silicon carbide, SiO₂ and alumina [186, 187]. The number of primary silicon per unit volume is more in the composites compared with the unreinforced alloy. Freshly made aluminium oxide (i.e. not added externally but formed with in the melt by some reduction reaction) is generally an effective nucleant for aluminium [188]. Refinement of eutectic silicon was reported in Al-11.8Si alloy containing alumina particle [189]. Similarly, modification of Si in eutectic and hypoeutectic Al-Si alloys containing graphite particles is also observed. The extent of reduction in eutectic silicon size increases with increasing particle volume percent. The exact mechanism of eutectic silicon modification by graphite and alumina is not clear at present.

2.6.1.2 Growth of solid phase

The reinforcement can be either stationary or mobile during solidification as in infiltration technique and liquid metal stir casting respectively. When a moving solid/liquid interface approaches a mobile foreign particle suspended in liquid metal, the particle can either be captured or pushed away by the interface. If the growing solidification front captures the foreign particles, little redistribution of the reinforcements will occur during solidification, and hence the particle distribution in the solidified material will be as uniform as it was in the liquid state. On the other hand, if the particles are pushed by the solidification front, they will be redistributed and finally segregated in the last solidifying liquid matrix.

The first systematic study on particle pushing is due to Uhlmann *et al.*, [190] who mixed a number of different particles into various transparent organic matrix materials and have carried out horizontal directional solidification experiments under an optical microscope. They have found that the particles are not pushed at all in some particle matrix systems, whereas in others a critical velocity (V_c) have existed, below which the particles are pushed and above which they are captured by the interface. This critical velocity is dependent on the type of particle for a given matrix material and on the kind of matrix material for a given particle. The effect of particle size on V_c is not quite straightforward: when the particle size is large (hundreds of

micrometers in diameter), V_c decreases with increasing particle size, while for small particles (below 15 μm), it is virtually independent of the particle size.

2.6.2 Characteristics of Solidification Curve

Studies carried out on the effect of the presence of dispersoid on the cooling curve of composite melt presents contradicting results and explanations.

Studies by Hanumanth and Irons [191] have shown that the cooling rate of modified A356 alloy increases with the addition of particles. Jeng and Chen [192] have reported that the principal characteristics of the solidification curve of composites and the matrix are similar. Studies by Gowri and Samuel [193] have shown a marked difference in the characteristic thermal analysis parameters for reinforced and unreinforced materials at various cooling rates. Studies have also shown that the liquidus temperature of composite is lowered by the addition of particle. But, Kaufman *et al.* [194] comparing the cooling curves of A356 alloy and its composites containing 15 vol% SiC have shown that the liquidus temperature of composite is 5.5 °C higher than that of unreinforced A356 alloy. The addition of ceramic particles in the molten metal introduces more nucleation sites, and reduces the undercooling. Thus, the determined liquidus temperatures in composites is higher. But, as explained, the SiC does not act as a nucleating agent for the primary aluminium. In contrary, the thermal conductivity of the aluminium is much higher than those of SiC and alumina particles and the introduction of these particles decreases the thermal conductivity of the specimen and increases the temperature gradient within the specimen. Thus, the determined liquidus temperature in the composite is lower. Hence, it is necessary to look upon the effect of reinforcement on aluminium alloy matrix.

2.6.3 Casting/Mould Interfacial Heat transfer

The properties of cast metal matrix composites are largely dependent on the solidification behaviour which is dictated by the thermophysical properties of the melt and the mould, the rate of solidification and to a significant extent by the interfacial

heat transfer resistance at the boundary between mould and the metal. This resistance to heat flow at the casting/mould interface usually varies with time even if the cast metal remains in contact with the mould, due to the time dependence of plasticity of the freezing metal and oxide growth on the surface. In order to determine this thermal resistance, it is necessary to develop a mathematical model, which enables its calculation from measurable quantities such as the thermal histories at various thermocouple positions. The mathematical models adopted for assessing interfacial heat transfer by the analysis of experimental data are generally categorized as (1) purely analytical (2) semi-analytical and (3) numerical technique based on finite difference or finite element methods [195]. Analytical techniques developed by Clyne and Garcia [196] assume a constant interfacial heat transfer coefficient as in order to obtain an analytical solution for the Fourier equation of heat conduction, whereas the semi analytical or empirical technique involves solving of Fourier heat conduction using semi analytical formulae or curve fitting approach [197-200]. In the case of non linear situations, the interface conditions are the highly dynamic, for example, when the interface changes from a state of initial contact to a clearance gap, accompanied by a rapid drop in the interfacial heat transfer coefficient, numerical methods are more appropriate [200-204].

Various numerical techniques are adopted for the determination of transient metal-mould interfacial heat transfer for alloy systems [195, 205-207]. A number of investigations have been carried out on the effect of various solidification parameters on the microstructure and mechanical properties of the cast MMC [12-14, 18]. However, studies dealing with the effect of thermophysical properties of composite melt and different mould materials on the interfacial heat transfer at the metal/mould interface and their effect on solidification structure are limited.

2.7 INTERFACIAL CHARACTERISTICS OF MMC

The interface between the matrix and the reinforcement is the critical region in the composite system that is affected during the fabrication. If the interface is not tailored properly, it can lead to the degradation of the properties of the composites. The problems associated with the interfaces are the interfacial chemical reaction, degradation of the reinforcement, lack of wettability with the matrix, etc. These

interfacial problems are system specific. Hence, it is a difficult exercise to design optimized interfaces common and suitable for all the systems. Some of the methods to tailor desired interfaces with better properties are the modification of the matrix composition, coating of the reinforcement, specific treatments to the reinforcement and control of process parameters.

2.7.1 Wetting

Wetting of reinforcement by molten metal is an important aspect in MMC synthesis, which is favoured by the formation of strong chemical bonds at the interface. The presence of oxide films on the surface of molten metal and the adsorbed contaminant on the reinforcement surface generally leads to non-wetting of the reinforcement with molten metal. The wettability of a solid by a liquid is indicated by the contact angle as shown in Figure 2.6. The contact angle, θ , between solid, liquid and gas/vapour is related by the Young-Dupre's equation.

$$\gamma_{lv} \cos\theta = \gamma_{sv} - \gamma_{sl} \quad (2.4)$$

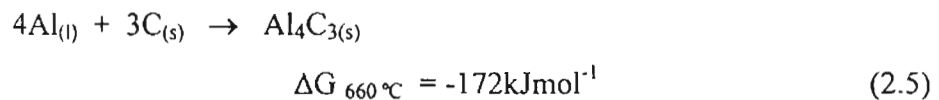
where, γ_{lv} is the surface tension of the liquid metal, γ_{sv} is the surface energy of the solid, and γ_{sl} is the solid/liquid interfacial energy. Based on the above equation, the contact angle, θ , can be decreased, by either increasing the surface energy of the solid, γ_{sv} , or decreasing the solid/liquid interfacial energy γ_{sl} , or by decreasing the surface tension of the liquid, γ_{lv} . The liquid is said to wet the solid when $\theta < 90^\circ$, that is, when $\gamma_{sv} > \gamma_{sl}$. Some of the techniques to improve metal-reinforcement wettability include metallic coatings on the reinforcements, addition of reactive elements such as magnesium, calcium or titanium to the melt and heat treatment of particles before addition.

2.7.2 Interfacial chemical reaction

During processing of metal matrix composites, a chemical reaction occurs at the interface between the matrix and the reinforcement in some systems. In such cases, it leads to the formation of an interface reaction product layer with properties

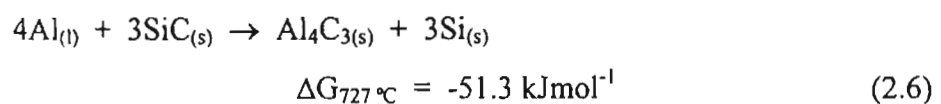
differing from those of either the matrix or the reinforcement. The extent of chemical reaction and the type of reaction products formed are dependent on the processing temperature, pressure and atmosphere, matrix composition and surface chemistry of reinforcements. Interfacial reaction can decrease the interfacial energy of the metal-reinforcement interface and improve adhesion through chemical bonding. The extent of the chemical reaction has a strong influence over the physical and mechanical properties of the composites. Further, the reaction products formed during processing may continue to form during service as well, thereby resulting in progressive improvement or degradation of the properties.

The following interfacial reaction is observed during the synthesis of carbon reinforced aluminium metal matrix composites, wherein the carbon can be either in the form of particulate or fibre based on graphite, pitch or PAN.



The reaction tendency of carbon fibre with molten aluminium alloy is observed to be severe when the melt temperature exceeds about 625 °C. The aluminium carbide formation degrades the fibres and decreases their strength. A discontinuous reaction product has been observed at the interface of the Aluminium-Graphite particle system when the melt temperature and contact time exceed 750 °C and 4h, respectively [208].

In silicon carbide-reinforced aluminium metal matrix composites, SiC is thermodynamically unstable in molten aluminium at temperatures exceeding 725 °C [209]. SiC reacts with molten aluminium [210, 211] to form Al₄C₃, rejecting metallic silicon according to the reaction



These reaction products have also been observed to cover SiC_(p) [212]. However, the above reaction can be suppressed by having a matrix alloy containing higher silicon content. Figure 2.7 shows the silicon level required in the matrix to prevent the formation of aluminium carbide as a function of the melt temperature [213].

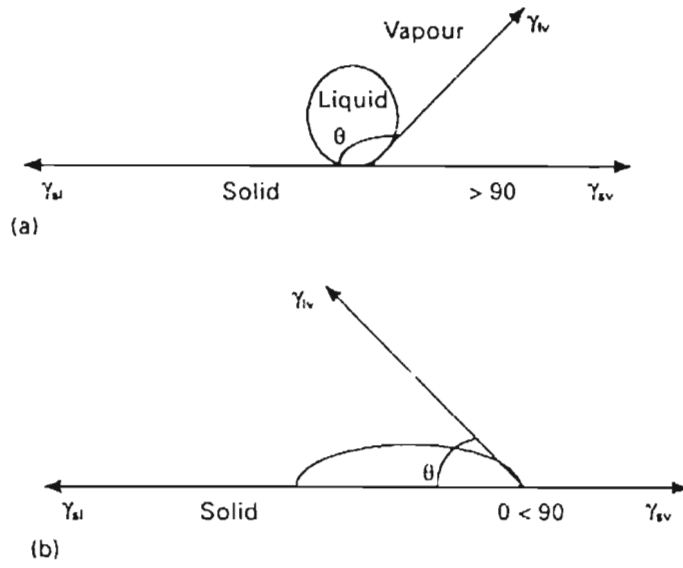


Figure 2.6: Schematic illustration of contact angle in a (a) non-wetting, and (b) wetting system.

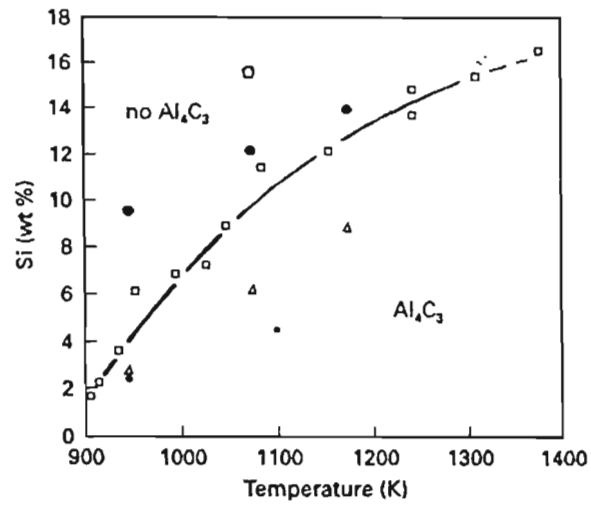
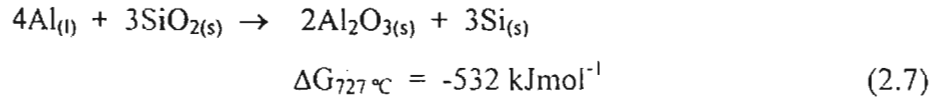
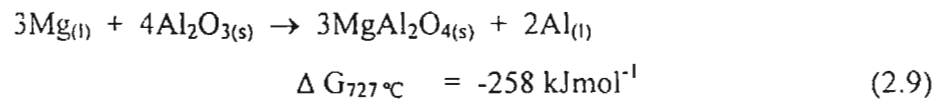
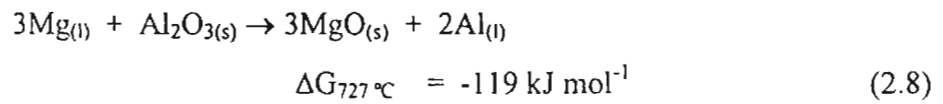


Figure 2.7: Silicon levels required in the matrix to prevent the formation of aluminum carbide as a function of melt temperature [Salvo et al. 213].

Low percent of carbon and SiO₂ present in Nicalon fibres (β-SiC) react with molten aluminium to form Al₄C₃ (Equation 2.5) and Al₂O₃ + Si (Equation 2.7), respectively



Alumina (Al₂O₃) is considered as an ideal dispersoid because of its good interfacial compatibility and non-degrading surface with liquid aluminium. However, most of the aluminium alloys of interest contain magnesium as an alloying element, which reacts with alumina according to



MgO may form at high magnesium levels (>1.5wt% Mg) and low processing temperatures, while spinel forms at low magnesium levels (<1.5 wt% Mg). Table 2.2 gives the possible reaction products and precipitates at the interface in various aluminium alloy matrices and reinforcement combinations [214-221].

Table 2.2: Possible reaction products and precipitates at the interface in various aluminium alloy matrix and reinforcement combinations

Matrix	Reinforcement	Reaction Products and Precipitates	References
Al	C	Al ₄ C ₃	205
Al	SiC	Al ₄ C ₃ , Si	214, 215
Al-Mg	SiC	Al ₄ C ₃ , MgO, Mg ₂ Si, MgAl ₂ O ₄	216
Al-Cu-Mg	SiC	CuMgAl ₂ , MgO	217, 218
Al-Mg	Al ₂ O ₃	MgAl ₂ O ₄	219
Al-Cu	Al ₂ O ₃	CuAl ₂ O ₄	220
Al-Li	Al ₂ O ₃	α-LiAlO ₂ , LiAl ₅ O ₈	220, 221

2.7.3 Interfaces and Composite properties

Most of the mechanical and physical properties of the metal matrix composites such as strength, stiffness, ductility, toughness, fatigue, creep, coefficient of thermal expansion, thermal conductivity and damping characteristics are dependent on the interfacial behaviour.

The interface plays a crucial role in transferring the load efficiently from the matrix to the reinforcement. The strengthening and stiffening of composites are dependent on the load transfer across the interface. A high bond strength is required at the interface for effective load transfer. A strong bond is usually formed with the reaction between the matrix and the reinforcement, the reaction product determining the nature of the bond. A brittle reaction product at the interface makes the composite crack at lower strains. The presence of coarse intermetallic precipitates at the interface, as in the case of Al-Cu-Mg/SiC_(p) composite, is also detrimental to mechanical properties. Studies on Al/SiC_(p), Al/B₄C_(p), Al/TiC_(p) and Al/TiB_{2(p)} composites show that Al/TiC_(p) has the highest yield and ultimate tensile strengths [222]. This is due to the better bond integrity at the Al/TiC_(p) interface. In unidirectionally reinforced composites, the longitudinal tensile strength and crack growth initiation resistance are found to be insensitive to the nature of the interface. However, the weak interface exhibits extensive debonding and reduces the transverse and torsional strengths of the composite [223]. The ductility of the composite is also largely influenced by the interfaces [224, 225]. Al/TiC_(p) composites are more ductile compared to Al/Al₂O_{3(p)} and Cu/ Al₂O₃ due to the better interfacial bonding arising out of the metallic bond [224].

The toughness of the composite is influenced by crack deflection or fibre pull-out. In unidirectional composites, a weak interface is desirable for increased toughness when a crack propagates perpendicular to the fibre, whereas a strong interface is required to prevent low energy failure when a crack is parallel to the fibre. In particulate composites, when particles are more rigid than a matrix with a weak bond, the increased toughness is due to crack blunting effects and it appears that the same effect could be obtained by dispersion of voids [226]. When a bond is strong and the particles are less rigid than the matrix, an increase in toughness can be

obtained by increasing the amount of material undergoing substantial massive plastic deformation. High residual stresses are developed in composites, when they are cooled from the processing temperature to room temperature due the mismatch in the coefficient of thermal expansion (CTE) between the fibre and matrix. As a result, radial, circumferential and/or longitudinal cracks are observed at the fibre-matrix interface region of certain composite system [227-228]. In particulate composites, the strengthening is also attributed to the thermal mismatch strain present at the particle-matrix interface.

Fatigue properties of composites are also influenced by the interface. Investigations on Al/graphite composites show that the fatigue crack propagation rate (FCPR) is higher than in Al/zircon composites having better bond strength at the interface [229-230]. This reveals that a weaker interface enhances the FCPR. Studies on the Al/SiC composite having a high bond strength at the interface show that a fatigue crack cannot propagate across the SiC particle unless it changes direction significantly and the crack deflection greatly reduces the FCPR [231].

Creep resistance of a particulate composite is determined with respect to creep threshold stress which is the index of resistance to creep. The creep threshold stress depends on the load transfer at the matrix reinforcement interface, which is dictated by the interface bond integrity. Al/TiB₂ *in situ* composites show higher creep resistance compared to powder metallurgy (P/M) processed Al/TiB₂ owing to the stronger interface and fine particle size in the former [222].

Studies on Al-15% TiC_(p) composites with 0.7 and 4 μm particles have shown that composites with 0.7 μm particles exhibit lower CTE due to more interfacial area acting as a thermal barrier. The lattice distortion is observed close to the matrix reinforcement interfaces. Studies on Al/SiC_(p) composites with particle sizes from 0.7-28 μm show that thermal conductivity increases with increase in particle size [232]. Al(6090)-SiC_(p) composites with particles in the range 10-28 μm show a higher thermal conductivity than unreinforced alloy, probably due to an excellent bonding at the interface [233]. Interfaces with reaction products act as stronger barrier to thermal conductivity than cleaner ones. In Ti/SiC_(p) composites with 0.5μm

reaction layer of Ti_5Si_3 , thermal conductivity is similar to that of unreinforced matrix. A thick reactive layer ($1\mu m$) reduces the thermal conductivity markedly.

2.8 APPLICATIONS

Metal matrix composites have emerged as one of the advanced engineering materials having potential application in the areas of aerospace, automotive, defence, electronics, general engineering and other advanced structures. They can be tailored to have superior properties such as high specific strength and stiffness, increased wear resistance, enhanced high temperature performance, improved thermal conductivity, low coefficient of thermal expansion, high damping capacity and better thermal and mechanical fatigue and creep resistances than those of monolithic material. Similarly, hybrid metal matrix composites can also be tailored to obtain better physical, mechanical and tribological properties. HMMCs are developed depending upon the specific requirements of the components to be fabricated and also to enhance certain properties of the monocomposite products.

Discontinuous HMMC based on aluminium alloys are processed for automotive applications with better wear resistance, low density, high specific stiffness and better thermal conductivity. The GrA-NiTM HMMC consisting of an aluminium matrix with hybrid SiC and nickel coated graphite particles have been designed for high wear resistance applications as a replacement for grey cast iron components in automobile applications where lower part weight, high thermal conductivity and diffusivity are desired [101-104]. Cylinder liner [Figure. 2.8(a)], different types of brakes and brushings are some of the components developed using GrA-NiTM HMMC. Figure 2.8(b) and 2.8(c) show sand cast rotor and Disc Brake system respectively. Table 2.3, comparing indexed finished part cost for grey cast iron Vs GrA-NiTM cylinder liner reveals both reduction in cost and weight for the latter.

Similarly, engine blocks and cylinder liners have been developed using Al-1.5Cu-9.6 Si (ADC12)-12% $Al_2O_{3(s)}$ -9% $C_{(s)}$ HMMC by Hayashi *et al.* [123]. The properties compared in Figure 2.9 have shown that HMMC engine blocks are light in weight and have lower wear depth than conventional engine block. These engine

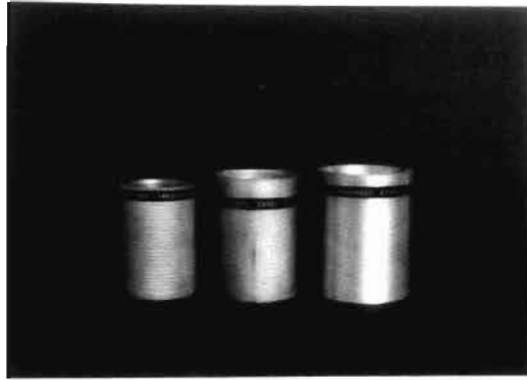
blocks can be efficiently mass produced through preform production and casting process.

Table 2.3: Comparison of indexed finished part cost for cylinder liner: Grey cast iron versus GrA-NiTM [102]

Details	Liner cost indexed to finished cast iron cylinder	
	Grey cast iron	Gr A-Ni TM
Material cost, %	20	55
Manufacturing cost, %	80	37
Finished part cost, %	100	92
Material Weight, g	2450	535 (Die Cast)
Finished Part Weight, g	1225	477

Reducing structural weight is one of the major ways to improve the performance of an aircraft. MMCs based on boron and carbon fibre reinforced aluminium alloys are used for aerospace applications. Al-60% C_(sf) MMC possessing low density, high axial stiffness, ultra low axial thermal expansion and good electrical conductivity have been used for boom /wave guide in space telescope. The SiC particle or whisker hybridisation in such composite could provide better mechanical performance than monocomposite with minimum volume fraction of fibre.

Hybrid composite based on smart materials can provide intelligent properties coupled with enhanced mechanical characteristics for structural applications. Functional gradient hybrid composites have been used in the fabrication of aluminium pistons, where hybrid dispersoids of alumina short fibres and aluminium titanate particles are locally reinforced as four graded layers of different volume fraction along the crown surface of the pistons [31].



(a)



(b)



(c)

Figure 2.8: *Photographs of GrA-NiTM HMMC components (a) cylindrical liners, (b) sand cast rotors and (c) DriscTM brake system. (Warner et al. [102])*

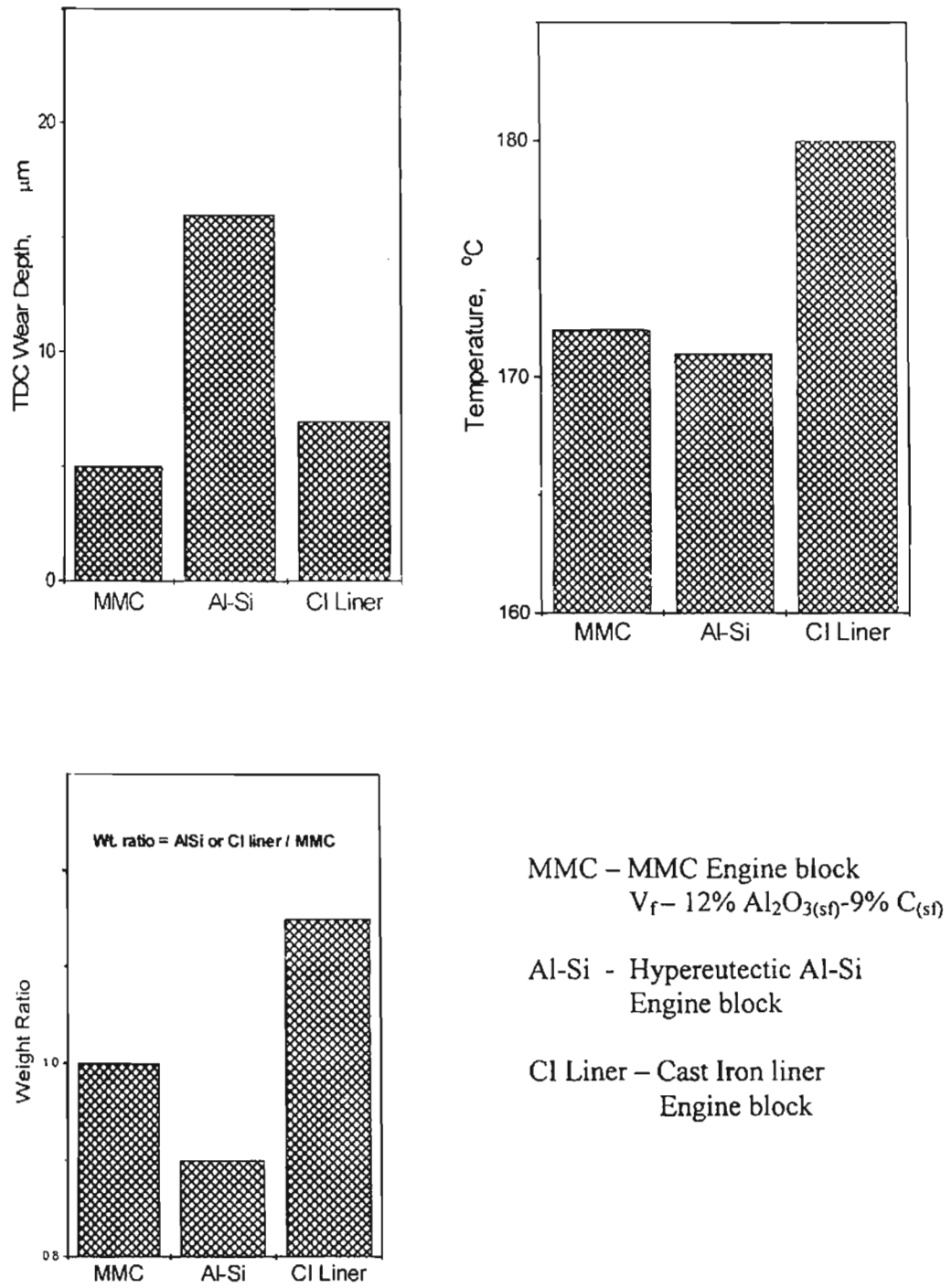


Figure 2.9: Properties comparison of Al-12% $\text{Al}_2\text{O}_{3(sf)}$ -9% $\text{C}_{(sf)}$ HMMC with ordinary engine block liners (Hayashi et al. [123])

2.9 GENERAL DISCUSSION

The review describes the processing, properties and applications of hybrid metal matrix composites along with a brief description on monocomposite processing and their properties. The concept of hybrid metal matrix composites emerges when more than one type of dispersoids are used in composite fabrication. Based on the type of reinforcement chosen, HMMCs are classified as continuous, discontinuous and continuous-discontinuous hybrid systems. Most of the investigations on HMMC are based on aluminium alloy matrix systems .

Most of the processing techniques used for monocomposites are suitable for HMMC with little change in processing parameters. The dispersion processes are widely used for making D-HMMC. The other methods are infiltration, spray deposition, powder metallurgy and *in-situ* techniques. For CD-HMMC and C-HMMC, the infiltration process is the appropriate one. The hybridisation of continuous fibre reinforced system with particles or whiskers improves the wetting and infiltration behaviour and also reduces the costly fibre volume fraction. The infiltration techniques are also used for making components with selective reinforcements thereby fabricating a functionally gradient component. HMMCs are also processed by coupling two processing methods. For example, a slurry of mono particle / whisker reinforced composite prepared by dispersion can be infiltrated through a fibre preform to make hybrid composite. Similarly, the fibre coating given over the surface of fibre, either as a interfacial reaction barrier or wetting promoter, reacts with the matrix elements to form a second *in-situ* dispersoid. Hence, the *in-situ* method is coupled with either infiltration or dispersion process. A combination of *in-situ* reaction synthesis and powder metallurgy process is also used.

Various studies mentioned above have shown that hybrid composites exhibit enhanced structural, physical, mechanical and tribological characteristics than conventional MMCs. However, the enhancement of a particular property depends on the type of reinforcements and matrix alloy used. While developing a hybrid composite system or a component, the choice of reinforcements and matrix alloy should be made after due consideration of the properties requirements. The studies have also shown that the hybridisation of hard and soft discontinuous

dispersoids has helped in (i) improving both abrasive and adhesive wear resistances, (ii) enhancing thermal conductivity and heat diffusivity and (iii) balancing the strength and stiffness requirements. Similarly, incorporation of particles or whiskers in continuous fibre system can result in enormous increase in tensile strength, longitudinal and transverse flexural strength and bending strength due to reduction in fibre to fibre contact failures. The hybrid composites with smart or intelligent characteristics can be fabricated either by incorporating a shape memory alloy or smart material to a metal matrix or by reinforcing ceramics reinforcements in a smart alloy matrix system. Hybrid composite systems also help in fabricating components with functional gradient properties.

HMMC appears to be a potential candidate for various applications due to its improved and tailorable properties not possible with monolithic alloys and monocomposites. Since the studies on HMMCs are started recently and only limited systems have been investigated, the real potential of this system could be tapped only if detailed investigations are carried out.

2.10 FUTURE RESEARCH AVENUES

From the foregoing, it is clear that HMMCs including functionally gradient materials with their appealing combinations of properties arising out of the synergistic effect of the chosen reinforcements and the matrix for various applications are only in the early stage of development and hence there are ample scope for further research work. Some of the broad based research avenues include

- ◆ Probing into synthesis and characterisation of new potential HMMC systems.
- ◆ Utilisation of cheap reinforcements for the fabrication of composites, as the cost of reinforcement affects its commercialisation.
- ◆ Mathematical modelling to predict the synergistic effects of the components of HMMCs as an aid for their judicious selection.
- ◆ Use of nanophase materials as hybridising agent.
- ◆ Use of mechanical alloying for HMMC synthesis.
- ◆ Optimising the best processing routes for different types of HMMCs and systems.

- ◆ Evaluation of various properties and characterisation of microstructure and interface in HMMCs to facilitate creation of a data bank on all the engineering properties.
- ◆ Development of smart and functionally gradient hybrid composites.
- ◆ Product identification and HMMC development with specific property requirements.

2.11 SUMMARY

Metal matrix composites with discontinuous dispersoids have become one of the most important advanced engineering materials used in the areas of automotive, aerospace, defence and general engineering. Among the various matrix materials available, aluminium and its alloys are widely used in composite fabrication. Most of the studies are concentrated on SiC, carbon and alumina reinforcements. Various other cost effective and potential reinforcements are to be investigated. Since the interfacial characteristics of MMC play a critical role in determining the composite properties, evaluation of interfacial behaviour is important. Similarly, solidification process is a crucial step largely determining the pattern of particle distribution and microstructure of the cast MMC, which in turn influences the properties of MMC.

Hybrid metal matrix composites are considered as the second generation metal matrix composites, where in more than one type, shape or size of reinforcements are used to obtain synergistic properties of both reinforcement and matrix chosen. Investigations on processing, characterisation of properties and product evaluation of HMMC have started recently and the outcome shows their potentiality as a futuristic material. The classification of HMMC is made on the basis of the type of reinforcements used as continuous, discontinuous and continuous-discontinuous hybrid systems. Depending on the functional behaviour, few systems are categorised as smart and functionally gradient hybrid systems. The conventional MMC processing techniques such as stir casting, infiltration, spray deposition, in-situ synthesis, powder metallurgy and diffusion bonding can be extended for fabricating HMMCs with minor changes in the processing parameters. The choice of processing method depends on the type of hybrid composites to be fabricated. Hybridisation of

monocomposites can enhance their structural, physical, mechanical and tribological behaviours depending on the type of reinforcement used. The choice of reinforcements and matrix alloy is dictated by the properties requirements of hybrid composite system or product to be fabricated. To tap the real potential of HMMC systems, extensive R &D work needs to be carried out by exploring new systems combining different reinforcements and characterising the resulting HMMCs with respect to all the engineering properties.

2.12 SCOPE OF THE INVESTIGATION

Aluminium matrix composites dispersed with discontinuous dispersoids have gained wide acceptance as an important engineering material in the areas of aerospace automotive, defence and general engineering. This is because of their better properties and performance over the monolithic alloys. Various studies have been carried out on the processing, structure–property correlations, interfacial and tribological behaviour of the composites [6-29]. Some of the barriers to their wider exploitation include cost (which is, of course, inter-related with global and specific usage levels) and shortage of property data and design guidelines. The use of simple processing techniques, standardization of processing parameters and utilization of low density and cheaper reinforcements could make their wider application possible. The interface between the matrix and the reinforcements also plays an important role in determining their properties. Hence, proper tailoring and control of interface are required for obtaining better properties. Similarly, MMC with better property combinations could be achieved by resorting to the development of new hybrid systems.

Among the various processing techniques available, the liquid metal stir casting is the simplest one for synthesising discontinuously reinforced aluminium matrix composites. This process offers the possibility of producing MMCs in large quantities at low cost. Very limited studies are carried out on the processing and characterisation of discontinuously reinforced aluminium HMMC using stir casting technique. The review of literature has revealed that most of the investigations are on fibre reinforced composites fabricated by infiltration techniques. Studies also show that addition of soft and hard reinforcements improves the adhesive and abrasive wear of composites compared to the matrix alloy and their mono composites. However, the

problems associated with mixing of hybrid reinforcements, effects of processing parameters and the presence of hybrid reinforcements on microstructural, interfacial, solidification, physical and mechanical characteristics are not fully understood. Hence, a detailed investigation is warranted.

The main objectives of the present investigation are the processing and characterisation of mono and hybrid composites based on cast Al-7Si-0.35Mg [Al(356)] matrix alloy and reinforcements with different morphology, namely particulates of silicon carbide, graphite and fly ash and short fibres of carbon and aluminosilicate. The composites fabricated are evaluated with respect to their structural, interfacial, solidification, physical and mechanical characteristics and correlated with the various processing parameters. Further, the utilization of the indigenously available low cost aluminosilicate fibres and the fine spherical flyash particles as reinforcements for the fabrication of aluminium matrix composites is explored.

CHAPTER 3

MATERIALS AND EXPERIMENTAL METHODS

3.1 MATERIALS

3.1.1 Matrix

The aluminium silicon-magnesium (356/LM25) alloy is chosen as the matrix alloy. The composition of the alloy is given in Table 3.1. The 356-aluminium alloy is one of the commonly used age-hardenable cast alloy for various applications. The alloy can be cast in permanent or sand mould and possesses excellent castability, good corrosion resistance and pressure tightness and better machining and welding characteristics. It has also proven as a potential matrix alloy in the fabrication of cast aluminium matrix composites. The thermophysical properties of matrix alloy are given in Table 3.2.

Table 3.1: Chemical composition of the matrix alloy

Alloy	Si	Mg	Cu	Fe	Zn	Al
356	7.5	0.35	0.2	0.2	0.1	Balance

3.1.2 Reinforcements

The different types of discontinuous reinforcements used for the present investigation are silicon carbide, graphite (synthetic and natural), and fly ash particles as well as short carbon and aluminosilicate fibres (standard and zirconia grade). The properties of these dispersoids are given in Table 3.3.

Table 3.2: Thermophysical properties of the matrix

Property	Al(356) alloy
Density (g/cc)	2.68
Thermal conductivity (W/m °C)	159 (solid) 121 (liquid)
Specific heat capacity (J/kg °C)	1084 (solid) 963 (liquid)
Latent heat (L) (kJkg ⁻¹)	389

(i) Silicon Carbide:

Among the various discontinuous dispersoids available for the synthesis of MMC, the silicon carbide particulates have attained the prime position. This is due to the fact that introduction of SiC to the aluminium matrix substantially enhances the strength, the modulus, the abrasive wear resistance and the thermal stability. The density of SiC is nearer to that of aluminium alloys (2.8-3.2 g/cm³). Further, SiC_(p) is easily available and cost effective and has good wettability with aluminium alloys. For the present investigation the green variety SiC_(p) of 23 μm average particle size (APS) is used.

(ii) Graphite:

Graphite particles are one of the low density dispersoids used in the fabrication of MMC and its addition to aluminium alloys improves the wear resistance and reduces the coefficient of friction. In the present study, synthetic graphite particles of 60 μm average particle size are used. Natural flaky graphite of 60 μm APS is also used for selected studies. (The word graphite particle means the synthetic graphite unless mentioned as natural graphite.)

Table 3.3: Thermophysical properties of the reinforcements chosen

Property	SiC Particle	Graphite particle		Carbon short fibre	Alumminosilicate short fibre		Fly ash Particles
		Synthetic	Natural		Standard Grade	Zirconia Grade	
Density (g/cc)	3.2	1.4	1.8	1.8	2.56	2.56	2.486
Average particle / Fibre size (μm)	23	60	60	7 (dia) 100 (length)	1.5 – 3 with assorted length	1.5 – 3 with assorted length	13
Thermal conductivity $\text{W/m}^\circ\text{C}$	20 (polycrystal)	355 (parallel to c-axis) 89 (normal to c-axis)	355 (parallel to c-axis) 89 (normal to c-axis)	355	0.140	0.13	0.06-016
Specific heat capacity $\text{J/kg}^\circ\text{C}$	1300	710	710	-	1.07	1.07	-

(iii) Carbon fibre

The pitch base chopped carbon fibres (M/s Courtaulds Grafil, UK) of 1mm length and 0.7 μm diameter are used.

(iv) Aluminosilicate fibre

Two grades of chopped aluminosilicate fibres namely standard grade and zirconia-toughened grade obtained from M/s Murugappa Morgan Thermal Ceramics Ltd., Chennai have been used. These fibres synthesized by melt-spin method are of assorted lengths and diameter with an average diameter of 1.5 – 3 μm containing small amounts of shots of varying sizes as well. The chemical compositions of the fibres are given in Tables 3.4.

Table 3.4: Composition of aluminosilicate fibres

Constituents	Amount, %	
	Standard Grade	Zirconia Grade
Al_2O_3	43-47	32-36
SiO_2	53-57	44-48
ZrO_2	-	16.5-19.5
Fe_2O_3	0.02-0.08	-
MgO	0.01-0.04	-
CaO	0.05-0.4	-
Others	Traces	Traces

(v) Fly ash:

The fly ash particles used for the studies are spherical in shape and are of assorted size with an average particle size of 13 μm . The spherical fly ash particles contained both solid spheres (precipitators) and hollow spheres (cenosphere). The density of fly ash particle measured by helium pycnometer is 2.486 g/cc. The major chemical constituents of fly ash are given in Table 3.5.

Table 3.5: Chemical composition of fly ash particles

Constituents	Amount, %
SiO ₂	59.46
Al ₂ O ₃	26.05
Fe ₂ O ₃	6.41
Na ₂ O	1.21
CaO	0.5
ZnO	0.1

3.2 COMPOSITE PROCESSING

The composites are fabricated mainly by liquid metal stir casting techniques. The aluminium alloy is melted in a clay graphite crucible using resistance-heated furnaces. The composite synthesis is carried out in both 500 g and 10 Kg level melts in different capacity furnaces. The schematic of composite synthesis equipment is depicted in Figure 3.1. The alloy melt is mechanically stirred using an impeller driven by an electrical motor. The stirring speed is controlled by a dynamometer. The preheated particles are added to the melt with a known feed rate, stirring speed and melt temperature. The detailed processing parameters used for various systems are given under methodology in respective chapters. The shaping of the composites is made by gravity and squeeze casting methods. The typical permanent mould castings made from 500 g and 10 Kg level are shown in Figure 3.2(a) and 3.2(b) respectively.

The compocasting and modified compocasting techniques have been used for processing Al-Fly ash composite systems and the details of those are given in Chapter 7. In the liquid metal stir casting, the incorporation of fly ash particle into the melt and pouring of composite melt into the mould are carried out in a fully liquid state condition (ie. above liquidus temperature of the matrix alloy). In the case of compocasting process, both the above steps are carried out in a semisolid state (a temperature between the solidus and liquidus temperatures). However, in the case of modified compocasting process, the addition of particle is carried out in a semisolid state and the casting above the liquidus temperature.

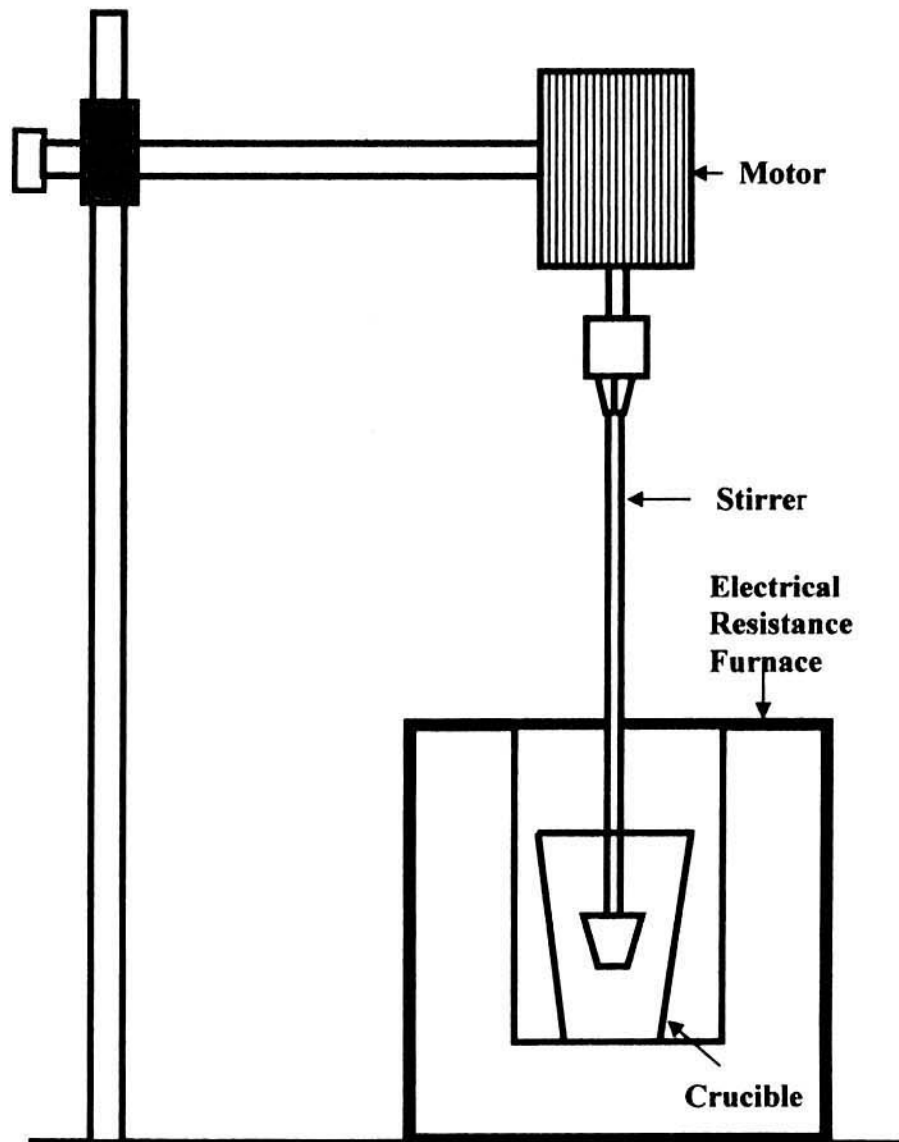
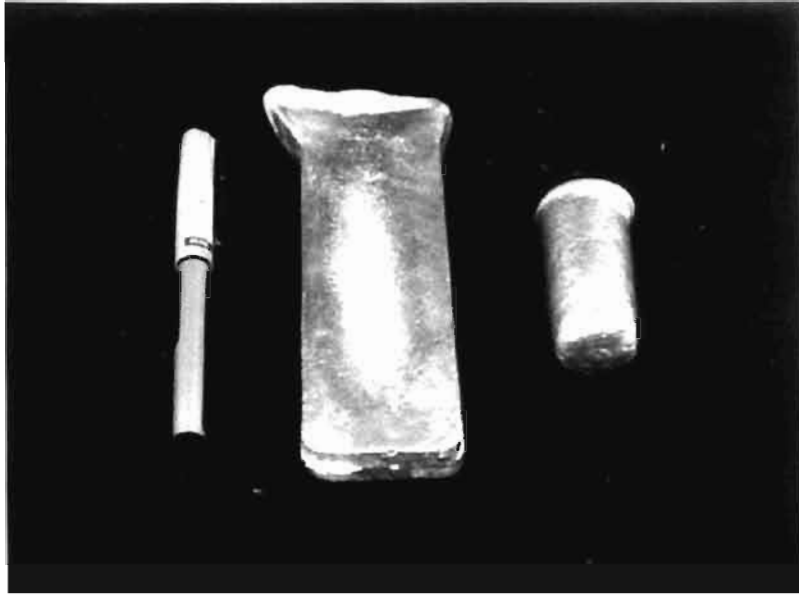


Figure 3.1: *Schematic diagram of composite fabrication setup for liquid metal stir casting.*



(a)



(b)

Figure 3.2: Typical permanent mould composite castings made with (a) 500 g and (b) 10 Kg level melt

3.3 SOLIDIFICATION STUDIES

The solidification studies have been carried out using a computer aided cooling curve analysis method to evaluate the effect of different reinforcements and moulds of varying cooling rates on the solidification curve. The studies also correlate the microstructural variation with respect to the changes in cooling curve. The study is also extended to determine the effect of the thermophysical properties of melt and mould on the metal/mould interface heat transfer during solidification of aluminium silicon alloy and its composites.

Three different types of moulds having varying heat extracting capacity viz., metal, graphite and sand of similar dimension were used for the solidification of alloy / composite melt. The thermophysical properties and dimensions of the cylindrical mould with thermocouple positions are given in Table 3.6 and Figure 3.3 respectively. Figure 3.4 shows the experimental set up of computer-aided data acquisition system connected to the moulds.

Table 3.6: Thermo physical properties of the mould materials

Property	Steel	Graphite	Sand
Thermal conductivity (K), (W/m°C)	42	147	0.52
Density, (ρ) (kg/m ³)	7860	2200	1600
Specific heat capacity (Cp) (J/kg°C)	580	1515	1170

3.4 HEAT TREATMENT STUDIES

Al-7Si-0.3Mg (356) is a precipitation hardening alloy. The common heat treatment procedure applied is T6 condition, ie. solution treatment followed by precipitation or age hardening. The prescribed solution treatment is 12 hrs at 525-545°C and age hardening at 155-175 °C for 8-12 hrs.

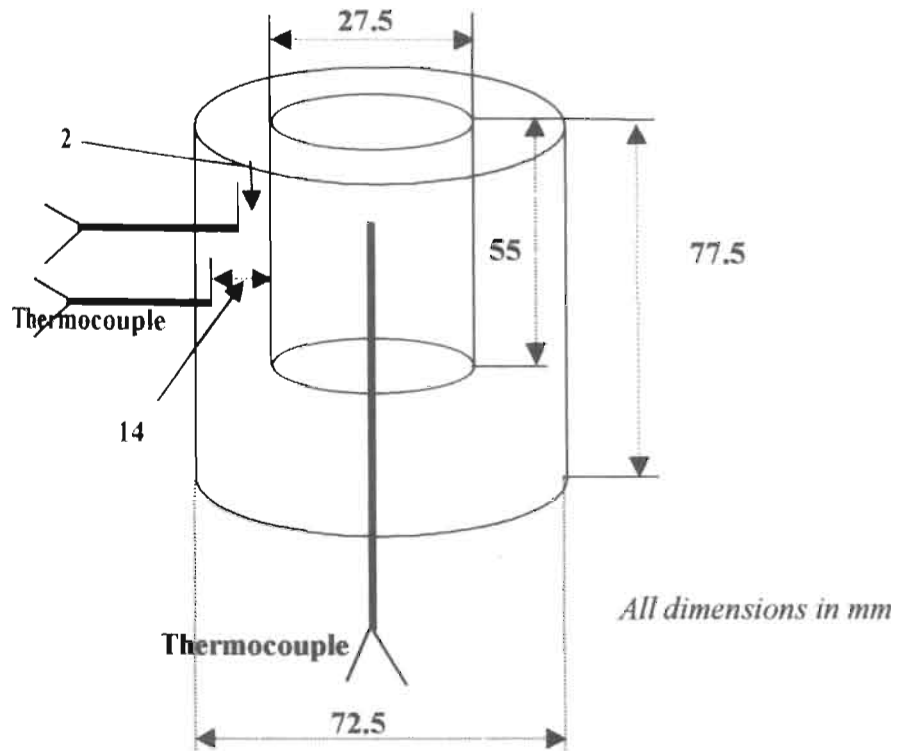


Figure 3.3: *Dimensions of cylindrical mould and thermocouple positions*

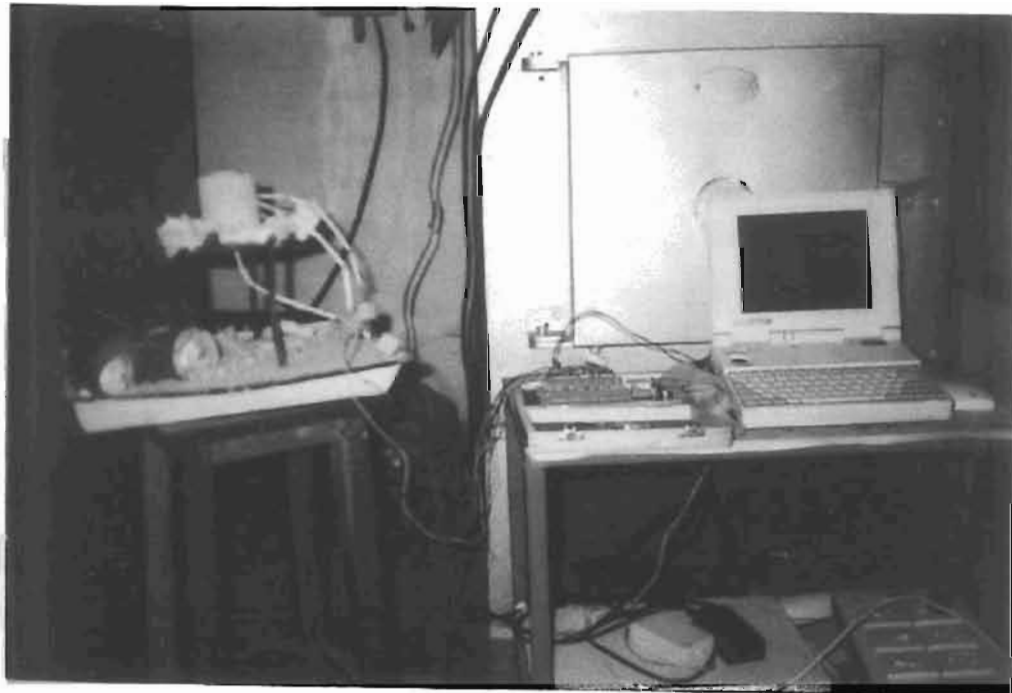


Figure 3.4: *Experimental setup of computer-aided data acquisition system.*

In case of metal matrix composites, the presence of dispersoids affects the heat treatment characteristics. Hence to obtain the optimum properties, the age hardening behaviour of composites has been evaluated. The solution treatment of the alloy and the composites are carried out at 535°C for 12 hrs. The samples are naturally age hardened for 12 hrs prior to artificial ageing. The samples are precipitation hardened at 165°C for varying time of 2, 4, 6, 7, 8, 9, 10 and 12 hrs. The heat treatment response of the above specimens is evaluated by hardness measurements using Brinell hardness tester.

3.5 STRUCTURAL STUDIES

The structural features of the alloy and composites have been characterised using optical microscopy (OM), Image Analyser, Scanning Electron Microscopy (SEM), Energy dispersive X-ray spectroscopy (EDX) and Atomic Force Microscope (AFM).

3.5.1 Optical Microscopy

The metallographic specimens are cut from the castings using both band saw and Leco-CM15 cut off machine with carborandum and diamond tip coated wheels. The specimens are polished using silicon carbide emery paper of sizes varying from 80, 200, 400 and 600 grit sizes. The specimens are washed thoroughly using liquid soap and water while going to next paper size and the orientation of polishing surfaces was changed by 90°. After completion of the paper polishing the specimens was polished using diamond paste. For alloy, the specimens are polished using “Silvo” and final polishing was done using 0.25 µm diamond paste in a rotating wheel (around 500 rpm) with a gentle applied pressure. In case of composite specimens, the polishing has been carried out using diamond paste of varying size ranging from 6.3, 1 and 0.25 µm. The specimens are washed very well using liquid soap solution. The specimens have been observed and analysed both in as polished and etched (using dilute hydrofluoric acid solution) conditions. The microstructural features of alloy and composite specimens are observed using Leitz Optical Microscope at different locations with varying magnifications.

3.5.2 Image Analysis

The quantitative microstructural analysis of the alloy and composites have been carried out using 'Clemex-Vision' Image Analyser for the determination of grain size, dendritic arm spacing (DAS) or dendritic cell size (DCS), reinforcement distribution and their volume fraction measurements. The metallographic specimens for image analysis are observed through an 'Olympus' optical microscope. The images are captured using a video camera and transmitted to the computer for analysis using 'Clemex-vision image analysis' software. Both manual and automatic image analysis have been carried out.

3.5.3 Scanning Electron Microscopy (SEM)

Scanning electron microscopy is performed in as-received and treated reinforcements, alloy and composites specimens. The alloy and composites samples are either deep etched using hydrofluoric acid or fractured samples are used. The reinforcements and selected composite specimens have been gold coated to make a conducting surface for SEM observations. A 'JEOL' scanning electron microscope is used for the analysis.

3.5.4 Energy Dispersive X-ray Spectroscopy (EDS)

The EDS is used for chemical analysis of the different phases and precipitates appearing in the matrixes, interfaces and surface of the reinforcements. Only selected composite samples are subjected to EDS. The 'EDAX' and 'OXFORD' EDS attached to SEM were used for the studies.

3.5.5 Atomic Force Microscope (AFM)

AFM is used to obtain images up to atomic resolution on conductors and insulators. AFM have been used to observe the interfacial behaviour of the composites.

3.6 PHYSICAL CHARACTERISTICS

3.6.1 Density Measurement

The densities (ρ) of the samples are measured using the application of Archimedes' principle. The expression is given as

$$\rho = (W_a \rho_l - W_l \rho_a) / (W_a - W_l) \quad (3.1)$$

where W is the weight, ρ is the density and the subscripts 'a' and 'l' referred to air and liquid medium. In the present study water is used as the liquid medium.

3.6.2 Electrical Conductivity Measurement

The electrical conductivities of the alloy and composites are measured using eddy current testing machine, the 'TECHNOFOUR' conductivity meter type 901. The measurement could be used to determine the homogeneity of particle distribution in the composites.

Conductivity meter works on the principle of eddy currents. A probe induces eddy currents at a fixed frequency in the test part. The currents affect the electrical impedance of the test probe. The change in impedance is proportional to the electrical conductivity of the test part. Thus, conductivity measurement is possible by measuring the corresponding change in probe impedance. Direct reading in %IACS is obtained from the instrument. Both as cast and polished specimens are used for electrical conductivity measurements. The presence of reinforcements in the composites affects the electrical conductivity of the specimen.

3.7 MECHANICAL CHARACTERISTICS

3.7.1 Hardness Measurement

Hardness measurements of alloy and composites are determined using Brinell hardness testing machine. Brinell hardness number (BHN) is calculated using the formula

$$\text{BHN} = \frac{2P}{[\pi D(D - (D^2 - d^2)^{1/2})]} \quad (3.2)$$

Where P – applied load (kgf)

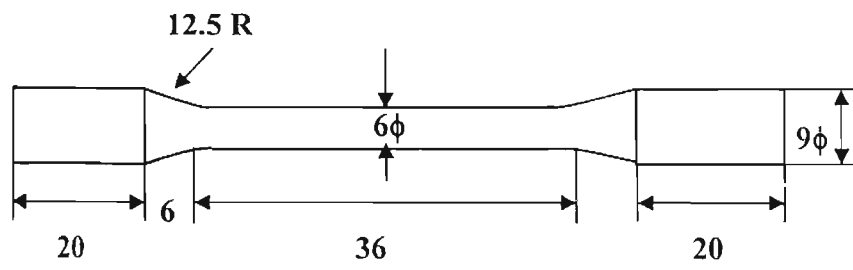
D – diameter of the indenter ball (mm)

d – diameter of the impression (mm)

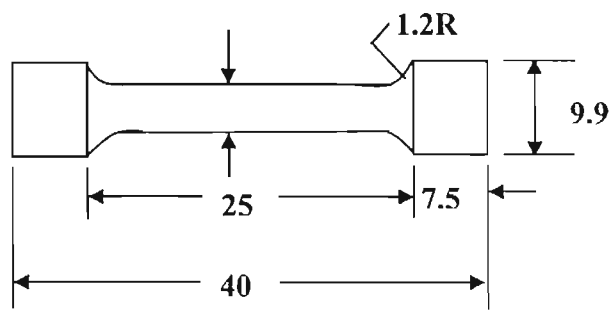
The diameter of the indenter ball is 2.5 mm and a load of 612.5 kgf for twenty seconds was applied. The surface of the specimens on which the impression is made have been machined and polished to 400 grit size. The distance between the centres of indentation from the edge of specimen or edge of another indentation is maintained at least half the diameter of the indentation. By knowing the indentation diameter, the hardness values are obtained from a standard table for a particular applied load and indentation ball diameter.

3.7.3 Mechanical Testing

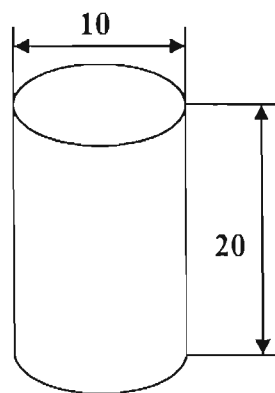
The tensile and compression testing of alloy and composites are tested in Instron Universal Testing Machine No: 1195 and 8801. The tensile specimens are fabricated according to the ASTM standards B557M and have been tested according to the ASTM standards E-8. The dimensions of tensile and compression specimens are given in Figure 3.5. An average of minimum three to five specimens is used for testing particular condition.



(a)



(b)



(c)

All dimensions in mm

Figure 3.5: Dimensions of specimens used for mechanical testing (a) Standard tensile specimen (b) Hounsfield Tensometer specimen and (c) Compression testing specimen. (All dimensions in mm)

CHAPTER 4

Al (356) - SiC - GRAPHITE MONO AND HYBRID COMPOSITES

4.1 INTRODUCTION

Aluminium matrix composites reinforced with discontinuous dispersoids such as SiC and graphite have received considerable attention as an important advanced material for the application in the areas of automobile, aerospace, defence and general engineering. These discontinuous composites with isotropic properties are more attractive due to their better physical, mechanical and tribological properties compared to the conventional alloys, the possibility of near-net shape manufacturing of components using conventional metal processing techniques, cost effectiveness compared to fibre or whisker reinforced metal matrix composites and their easy adaptability to current design practice.

Investigations have shown that the presence of soft carbon fibres in Al-Al₂O₃-C (short fibre) hybrid composites improves the wear resistance by 20-30% more than that of Al-Al₂O_{3(s)} composite [75]. MMCs with hybrid fibre comprising of alumina and carbon short fibres have shown better sliding wear properties compared to various short fibre reinforced composites [126]. With the aim of producing cheaper hybrid composites, studies have been made on processing particulate hybrid composite systems [35, 103-107]. Aluminium-SiC particulate composite hybridized with nickel coated graphite particles has shown higher wear resistance, seizure resistance and load bearing capacities at elevated temperature than non-graphitic composite [35]. The lower contact temperatures obtained in graphite containing hybrid composites has promoted mild wear while the formation of tribolayers has increased the transition from mild wear to severe wear and seizure. Most of the above studies have made use of nickel-coated graphite to improve the wettability. These hybrid composites represent the merging philosophies in tribological materials design: hard particle reinforcement and soft particle lubrication [35].

Few studies carried out on Al-SiC-graphite hybrid composites mainly highlight on the wear resistance enhancement of these composites. However, studies are limited on the effect of processing parameters on the structure and properties as well as the effect of hybridization on structural, solidification, physical and mechanical characteristics of the composite.

A number of investigations have been carried out on the effect of various solidification parameters on the microstructure and mechanical properties of the cast MMC [12, 13, 18]. However, studies dealing with the effect of thermophysical properties of composite melt and different mould materials on the interfacial heat transfer at the metal/mould interface and their effect on solidification structure are limited. Further, investigations carried out on the effect of the presence of dispersoid on the cooling curve of composite melt present contradicting results and explanations. Hence, a detailed study on this aspect is required.

The aims of the present investigation are to (i) fabricate mono and hybrid aluminium composites containing SiC and graphite particles and (ii) evaluate the effects of (a) processing parameters on the structure and properties of these composites and (b) hybridization of SiC and graphite on solidification, structural, physical and mechanical behaviour of the composites.

4.2 METHODOLOGY

The aluminium-silicon-magnesium (356) alloy is used as the matrix alloy. The chemical composition and properties of the matrix alloy are given in Table 3.1 and 3.2 respectively. The reinforcement materials used are green α -silicon carbide particles of 23 μm APS and synthetic and natural graphite particles of 60 μm APS. The thermophysical properties of the reinforcements are described in section 3.3.

The composites are fabricated by liquid metal stir casting techniques. The aluminium alloy is melted in a clay graphite crucible using a resistance-heated furnace. The composite syntheses are carried out both in 500 g and 10 Kg level melts in different capacity furnaces. The preheated particles are added to the melt with

controlled feed rate, stirring speed and melt temperature. The stirring speed is in the range of 700-750 rpm and the processing temperature is 720-740 °C. The SiC particles are preheated at 750 °C for 2 hrs to remove the volatile contaminants on the particle surface and to artificially oxidise the surface to obtain a layer of SiO₂ which could promote better wetting. The graphite particles are preheated at 400 °C for 2 hrs.

Both gravity and squeeze casting methods are used for casting the composites. Most of the castings are carried out in permanent moulds. Squeeze casting is carried out using 150T hydraulic press with a pressure of 150 MPa. The liquid metal is poured into the preheated die (300 °C) and pressed using the ram. The specimens for structural analysis are prepared from the as cast billets.

In the case of hybrid composites synthesis, different modes of particle addition are attempted and evaluated.

- ◆ Mode A: SiC_(p) addition followed by graphite,
- ◆ Mode B: Graphite addition followed by SiC_(p) and
- ◆ Mode C: Mixed mode of addition, i.e. prior mixing of particles prior to preheating.

Since the mixed mode has resulted in better distribution of dispersoid, further processing is carried out with mixed mode. In mixed mode, initially the SiC_(p) is heated to 750 °C for 2 hrs and then cooled and mixed with graphite particles and again preheated at 400 °C for 2 hrs prior to introduction into the melt. After the completion of particle addition, melt is stirred for 15 minutes and held for 5 minutes prior to the gravity die casting. Graphite and sand moulds are used in the case of solidification studies.

The structural, solidification, physical and mechanical characteristics of the matrix alloy and composites fabricated are evaluated using different methods described in Chapter 3. The solidification of mono and hybrid composites are studied in detail for different heat extraction rates with respect to the cooling curve parameters and the microstructures.

4.2.1 Estimation of Heat Flux

The non-linear estimation technique of Beck [234, 235] is adopted to analyze the transient heat transfer at the metal mould interface. The one dimensional heat conduction equation,

$$\rho C_p \frac{\delta T}{\delta t} = \frac{K}{r} \frac{\delta}{\delta r} \left(r \frac{\delta T}{\delta r} \right) \quad (4.1)$$

where T – temperature and t – time.

is solved inversely. In this inverse technique, the surface heat flux density is estimated from the knowledge of the measured temperature inside a heat-conducting solid. This is done by minimizing the function at regular finite different intervals.

$$q = \sum_{i=1}^{Ms} (T_{n+1} - Y_{n+i})^2 \quad (4.2)$$

where q = heat flux, $M = \frac{\Delta \theta}{\Delta t}$ and s = a small integer

T_n and Y_n are calculated and measured temperatures respectively at a location close to the metal mould interface. $\Delta \theta$ and Δt are the time steps for the estimation of heat flux and temperatures respectively.

Applying the condition for minimization, the correction for heat flux (δq) at each iteration step is estimated. This procedure is continued until the ratio ($\delta q/a$) is less, simultaneously yielding the mould surface temperature in contact with the casting and the interfacial heat flux.

4.3 RESULTS

4.3.1 Structural Characteristics

Figure 4.1 shows the SEM photomicrographs of the reinforcements used in the as received condition. The angular shape and assorted sizes of 23 μm average particle

size SiC particulates are revealed in Figure 4.1(a). The natural graphite [(Figure 4.1(b)] is more flaky in nature than synthetic graphite [Figure 4.1(c)]. The X-ray diffraction patterns of graphite particles (natural and synthetic) are given in Figure 4.2. The intensity of characteristic crystalline carbon peak is high in natural graphite [Figure 4.2(a)] and low in synthetic graphite [Figure 4.2(b)]. This may be attributed to the partial graphitisation of carbon in the latter.

4.3.1.1 Optical Microstructures and Image Analysis

The optical microstructures of 356-aluminium alloy cast by gravity and squeeze casting method are depicted in Figure 4.3. The image analysis results showing the variation in structural morphology of primary aluminium and eutectic silicon phases in the matrices of base alloy and different composite systems are given in Table 4.1. The addition of particles to the matrix alloy has decreased the size of primary aluminium phase. Similarly, the size of eutectic silicon is also reduced by the addition of particles. The squeeze casting has reduced the size of primary aluminium to a greater extent compared to the gravity casting. The size of eutectic silicon is very small so that the exact measurement could not be made by image analyser.

Figure 4.4 shows the optical photomicrographs of gravity cast Al (356)-15% SiC_(p) composite. There is no evidence for the SiC particles acting as nuclei for α -Al dendrites and the particles are pushed to the last solidifying eutectic region. In few places, clustering of SiC particles has occurred during solidification and porosities are observed. Figure 4.5 shows the microstructures of gravity cast Al (356)-5% graphite mono composite. The synthetic graphite particles [Figure 4.5(b)] become finer and results in better dispersion and distribution than natural graphite [Figure 4.5(a)] in the composite.

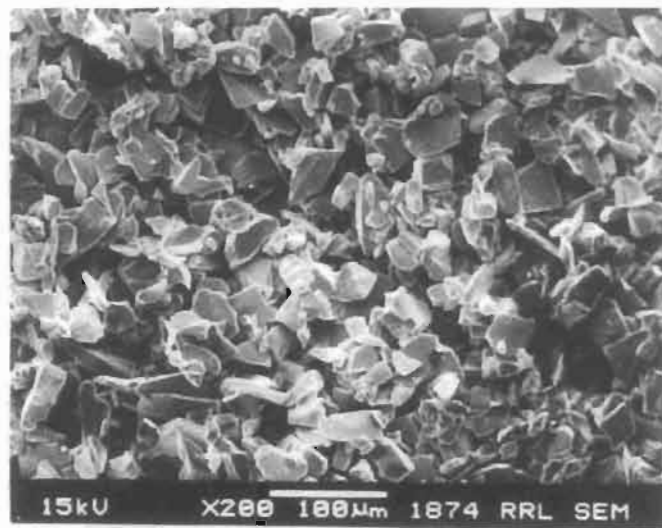
The typical microstructures of the hybrid composites containing 10% SiC and 3% graphite prepared with different modes of addition and cast in permanent mould are shown in Figure 4.6. The Al (356)-10% SiC_(p)-3% Graphite_(p) hybrid composites synthesised by the mixed mode of particle addition has resulted in better distribution than other two modes of addition. The mode 'A' (SiC_(p) followed by graphite

addition) has yielded only better distribution of SiC with agglomerated graphite, which is due to the higher stirring time experienced by the SiC and its contact with fresh matrix alloy. Whereas in the case of mode 'B' graphite addition followed by SiC addition, the former gets distributed well and the latter tends to agglomerate.

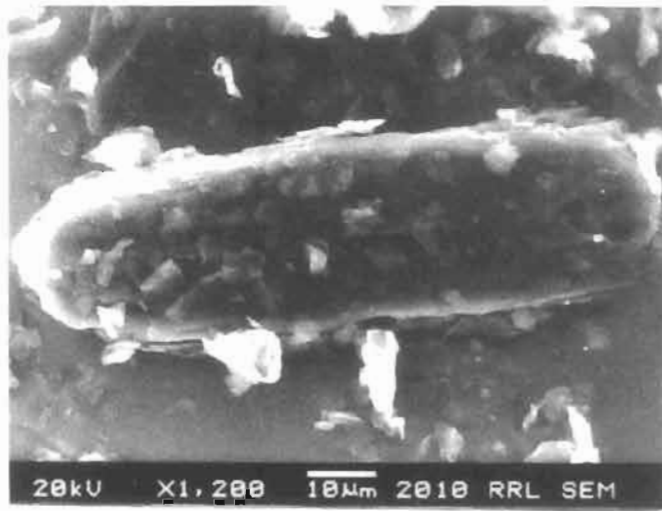
The optical photomicrograph of gravity cast Al (356)-15% SiC_(p)-5% natural graphite hybrid composite is shown in Figure 4.7(a). Like mono Al-SiC_(p) composite, both SiC_(p) and graphite in hybrid composite do not act as nuclei for α -aluminium and both the particulates tend to segregate in the eutectic region of the matrix. The microstructure shows both coarse and fine graphite particles in the matrix. With coarser graphite particles, the SiC particles form a ring around them. Similarly, very fine graphite particles also have a tendency to encircle around the SiC particles.

Figure 4.7(b) shows the photomicrograph of gravity cast Al (356)-15% SiC_(p)-5% synthetic graphite hybrid composite. The general microstructural features observed with synthetic graphite hybrid systems are similar to those observed with natural graphite hybrid composites. But, the size of the synthetic graphite particles becomes finer due to fragmentation during synthesis compared to natural graphite particles. The encircling of large graphite particle by SiC particle as well as SiC_(p) by finer graphite particle is observed in both natural and synthetic graphite containing hybrid composites [Figure 4.8].

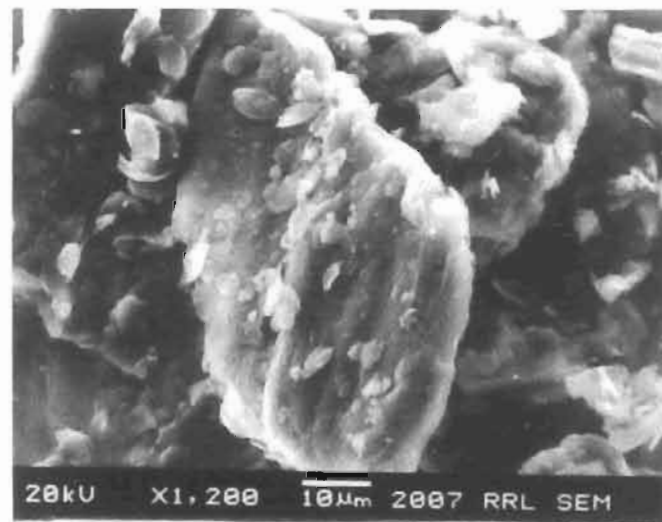
The optical micrograph of squeeze cast Al(356)-15% SiC_(p) monocomposite is shown in Figure 4.9. The primary α -phase in squeeze cast ingot gets refined compared to the gravity cast microstructure [Figure 4.4]. Further, the eutectic silicon also gets modified and the porosity content is less in squeeze cast ingot. The particle distribution is improved by fine α -phase formation in squeeze cast composite due to the application of pressure. Similar to squeeze cast mono SiC_(p) reinforced composite, the primary phase and eutectic phase are finer in squeeze cast hybrid composite than in gravity cast composite leading to better distribution. However, few clusters of SiC and graphite particles are observed in hybrid composites [Figure 4.10(a) and (b)], as observed in the case of mono composites.



(a)

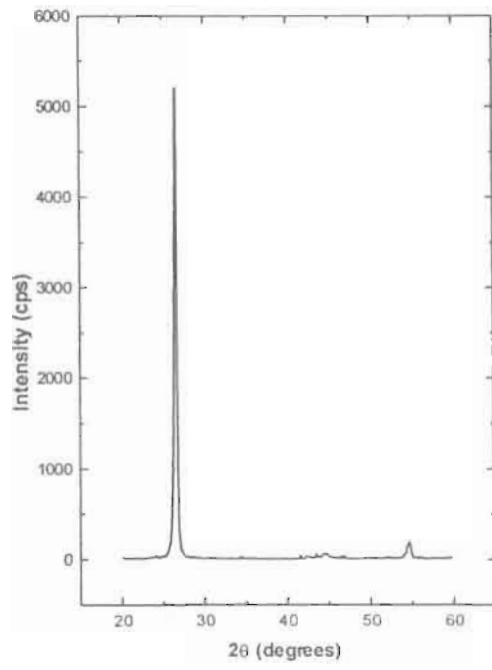


(b)

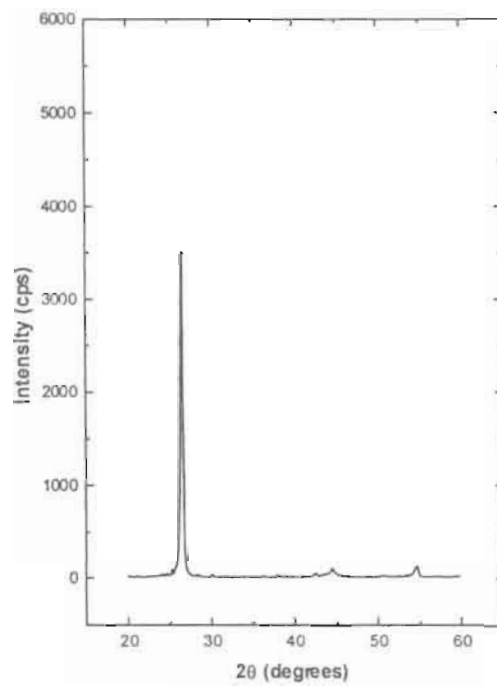


(c)

Figure 4.1: *Scanning electron micrograph of various reinforcements used for composite fabrication. (a) Silicon carbide, (b) Natural graphite and (c) Synthetic graphite particles.*

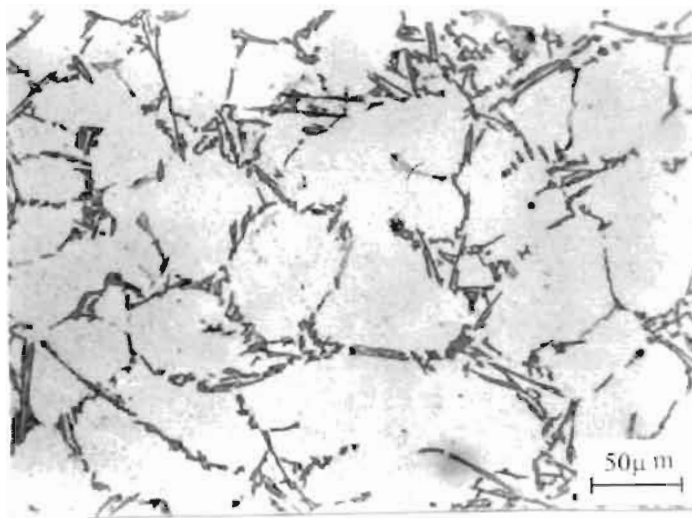


(a)

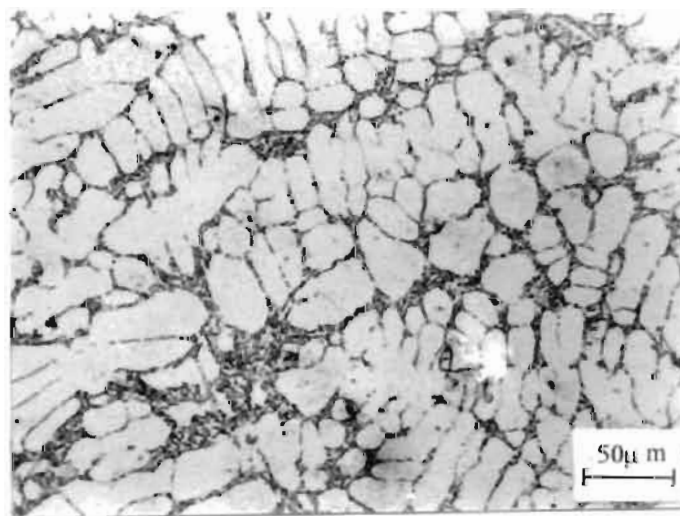


(b)

Figure 4.2: XRD pattern of two different types of carbon used as reinforcements (a) Natural graphite and (b) Synthetic graphite



(a)



(b)

Figure 4.3: *Microstructures of 356 aluminium silicon alloy
(a) Gravity cast and (b) Squeeze cast.*

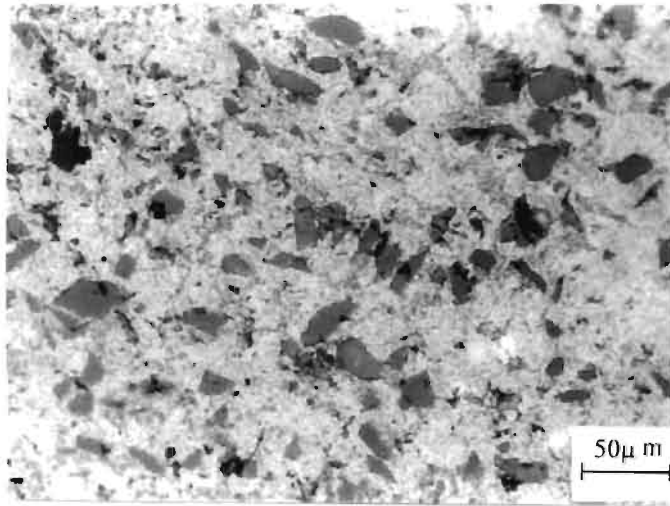


Figure 4.4: *Microstructure of gravity cast Al(356) – 15% SiC_(p) mono composite*

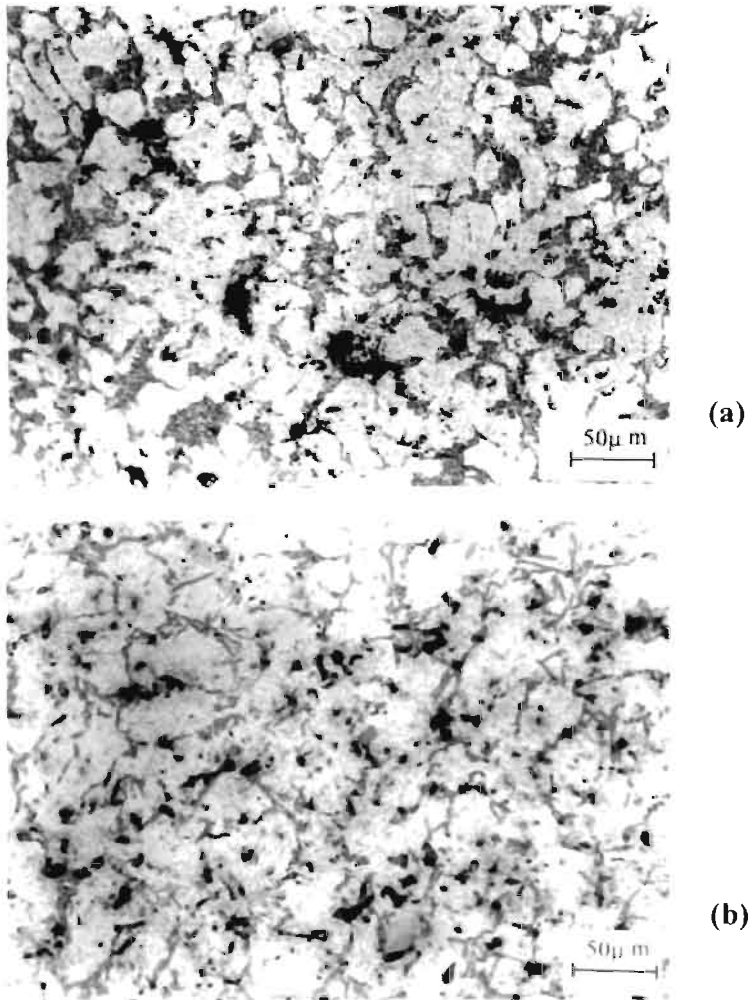


Figure 4.5: *Microstructures of gravity cast Al(356) – 5% Graphite mono composite. (a) Natural and (b) Synthetic*

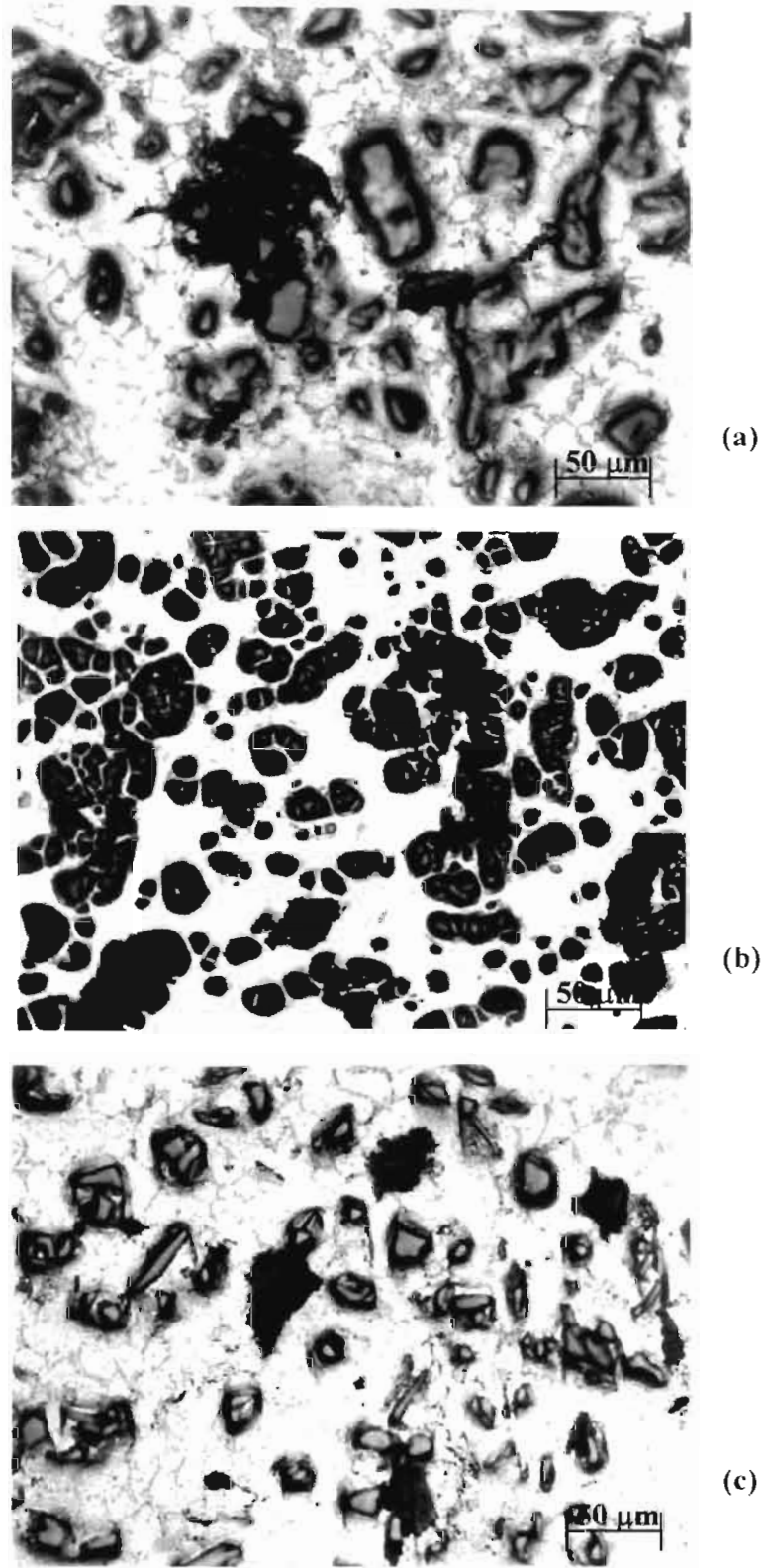


Figure 4.6: *Photomicrographs of gravity cast Al(356)-15% SiC_(p) - 3% graphite (natural) hybrid composites (a) SiC_(p) followed by graphite addition (b) Graphite followed by SiC_(p) addition and (c) Mixed mode of addition.*

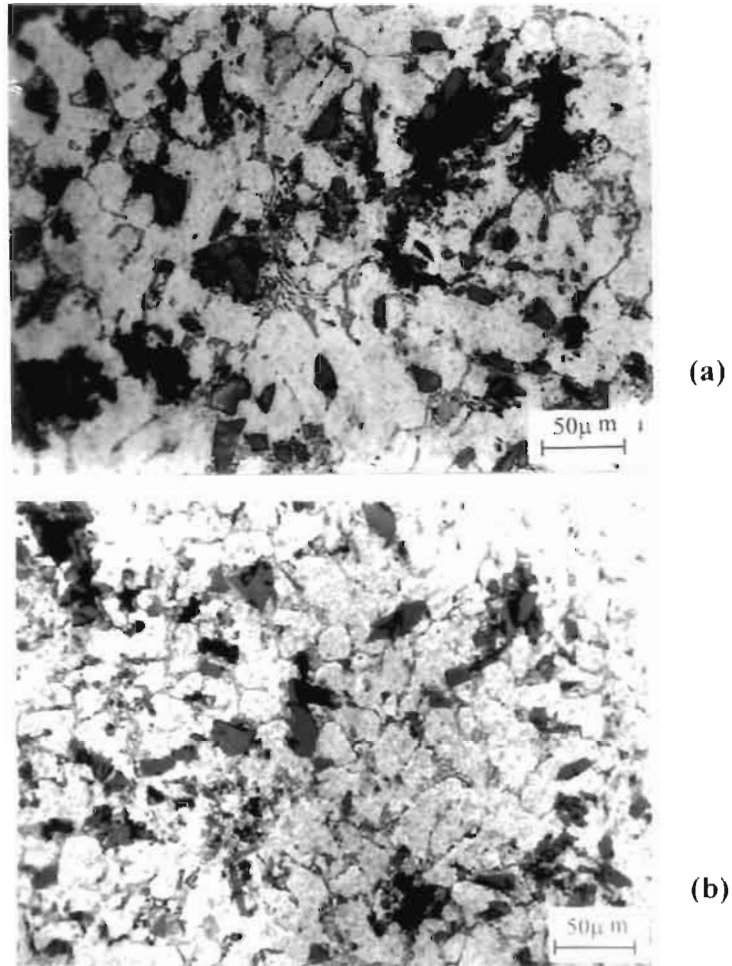


Figure 4.7: *Microstructures of gravity cast Al(356) – 15% SiC_(p) - 5% graphite hybrid composites (a) natural graphite and (b) synthetic graphite*

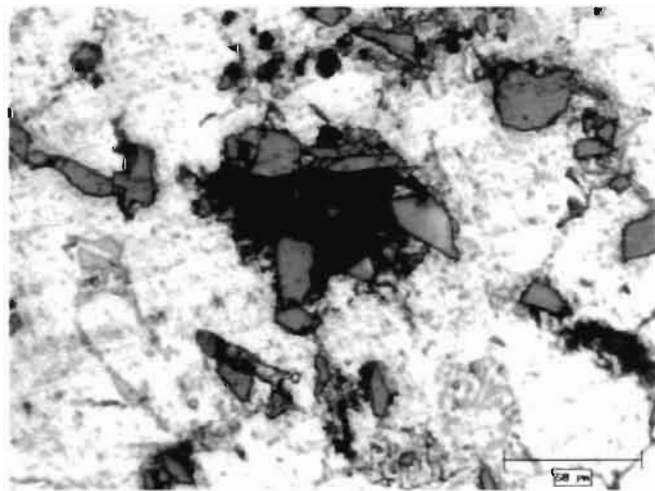


Figure 4.8: *Microstructure showing encircling of graphite by SiC particles in gravity cast Al(356) – 15% SiC_(p) - 5% graphite hybrid composites*

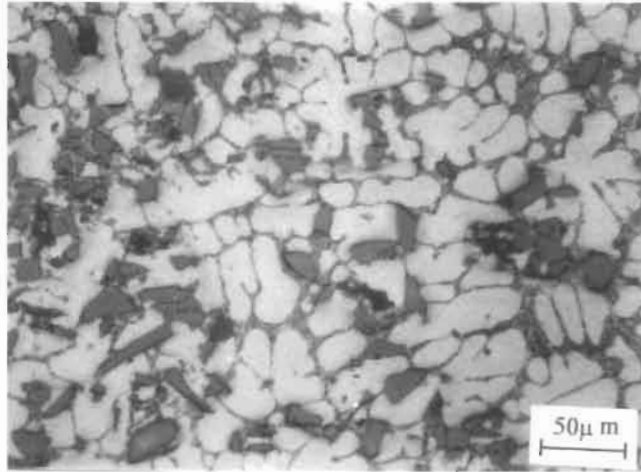


Figure 4.9: *Photomicrograph of squeeze cast Al(356)-15% SiC_(p) mono composite*

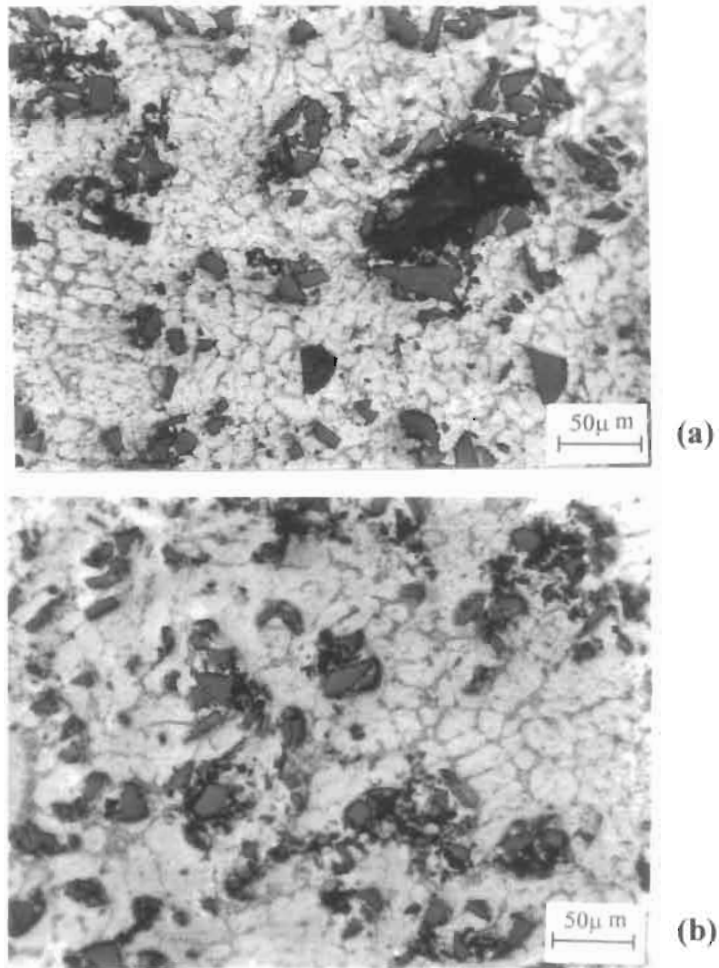


Figure 4.10: *Microstructures of Al(356) - 15% SiC_(p) - 5% graphite hybrid composites solidified by squeeze casting (a) natural graphite and (b) synthetic graphite*

Table 4.1: Variation in structural morphology of primary aluminium and eutectic silicon phases in the matrices of base alloy and different composite systems.

Alloy/ composite system	Primary aluminium		Eutectic Silicon		
	Area μm^2	Perimeter μm	Length μm	Area μm^2	Aspect Ratio
Gravity Casting (Permanent mould)					
Al(356)	2959	233	18.43	41.91	9.17
Al(356)-15% SiC	837	119	4.14	4.84	4
Al(356)-5%Gr(N)	575	97	4.63	6.5	3.79
Al(356)-5%Gr(S)	900	129	4.47	5.79	4
Al(356)-15% SiC- 5% Gr(N)	1113	139	6.44	14.10	3.53
Al(356)- 15% SiC-5% Gr(S)	1025	133	-	-	-
Squeeze casting					
Al(356)	710	104	5.19	8.27	3.48
Al(356)-15% SiC	347	78	-	-	-
Al(356)-15% SiC- 5% Gr(N)	253	67	-	-	-
Al(356)-15% SiC- 5% Gr(S)	284	70	-	-	-

4.3.1.1 SEM microstructures and EDS analysis

SEM photomicrographs of squeeze cast Al (356)-15% SiC_(p) monocomposite are shown in Figure 4.11. The SiC particles distributed in the matrix with sharp edges [Figure 4.11 (a)] reveal that there is no remarkable interfacial reaction between the particles and the matrix. Further, there is good bonding between the matrix and reinforcement. The presence of eutectic phase and fibrous needle shaped Fe bearing intermetallics adjacent to SiC particle are observed [Figure 4.11(b)]. The fibrous needles are the β -iron intermetallic phases. The eutectic silicon is observed to nucleate in the surface of iron intermetallic phase [Figure 4.11(c)]. The elemental X-ray mapping of Al (356)-15% SiC_(p) obtained from energy dispersive X-ray spectroscopy is given in Figure 4.12. The Figure 4.12(a) is the SEM image of the composite and b,c,d,e and f are the elemental X-ray mapping of Al, Mg, Si, O and C respectively. The Al elemental mapping shows the high intensity of Al in the matrix region. Similarly, the intensity of Mg is also high in the matrix region in general and near to the SiC particles in particular. However, the intensity of Si is high in the SiC particle region as expected and few in the matrix region, which is due to the eutectic silicon

present in the matrix. The intensity of oxygen is high in the matrix region due to the oxides and spinel phases present. The carbon shows a high intensity in the SiC regions.

The Figure 4.13 shows the SEM micrograph of Al (356)-15% SiC_(p)-5% graphite_(p) hybrid composite. The Figures 4.14 and 4.15 show the tensile and compression fractographs respectively of Al(356) base alloy and Al(356)-15% SiC_(p) mono composite. Both brittle and ductile type of fracture is observed.

4.3.2 Solidification Characteristics

4.3.2.1 Cooling curve analysis

The typical thermal analysis parameters of 356-aluminum alloy are shown in Figure 4.16. Introduction of an alloying element or a second phase particles in the form of dispersoid into the matrix alloy usually affects the various time and temperature parameters of the solidification curve. The nature of cooling curve always has an impact on the microstructure and mechanical behaviour of the material. Figure 4.17 shows the cooling curve of Al(356) base alloy cast in different moulds. Figures 4.18-4.21 depict the effects of the addition of magnesium and various reinforcements on the cooling curve of the 356 alloy. Figure 4.22 shows the cooling curve of Al(356) base alloy and composites determined using Aluminium Meltlab data logger system.

Figure 4.17 shows the cooling curves of 356-aluminium silicon alloy solidified in steel, graphite and sand moulds. As the thermal conductivity of graphite is higher (i.e., 147 W/m°C) than steel (42 W/m°C) and sand (0.52 W/m°C), the alloy melt poured in the graphite mould is subjected to higher cooling rate than those poured in other two moulds. But, the poor wetting between solidifying metal and the surface of the graphite mould leads to a reduction in its cooling rate. However, the estimated cooling rate of 7.76 °C /s for graphite is still higher compared to 5 and 1.04 °C /s for metal and sand moulds respectively. When the wetting promoter Mg is added to the alloy, the cooling rate of graphite mould has increased to 9.66 °C /s [Figure 4.18]. This shows the improved contact at the casting/mould interface due to the presence of Mg. The role of Mg as a wetting promoter for ceramic particles in

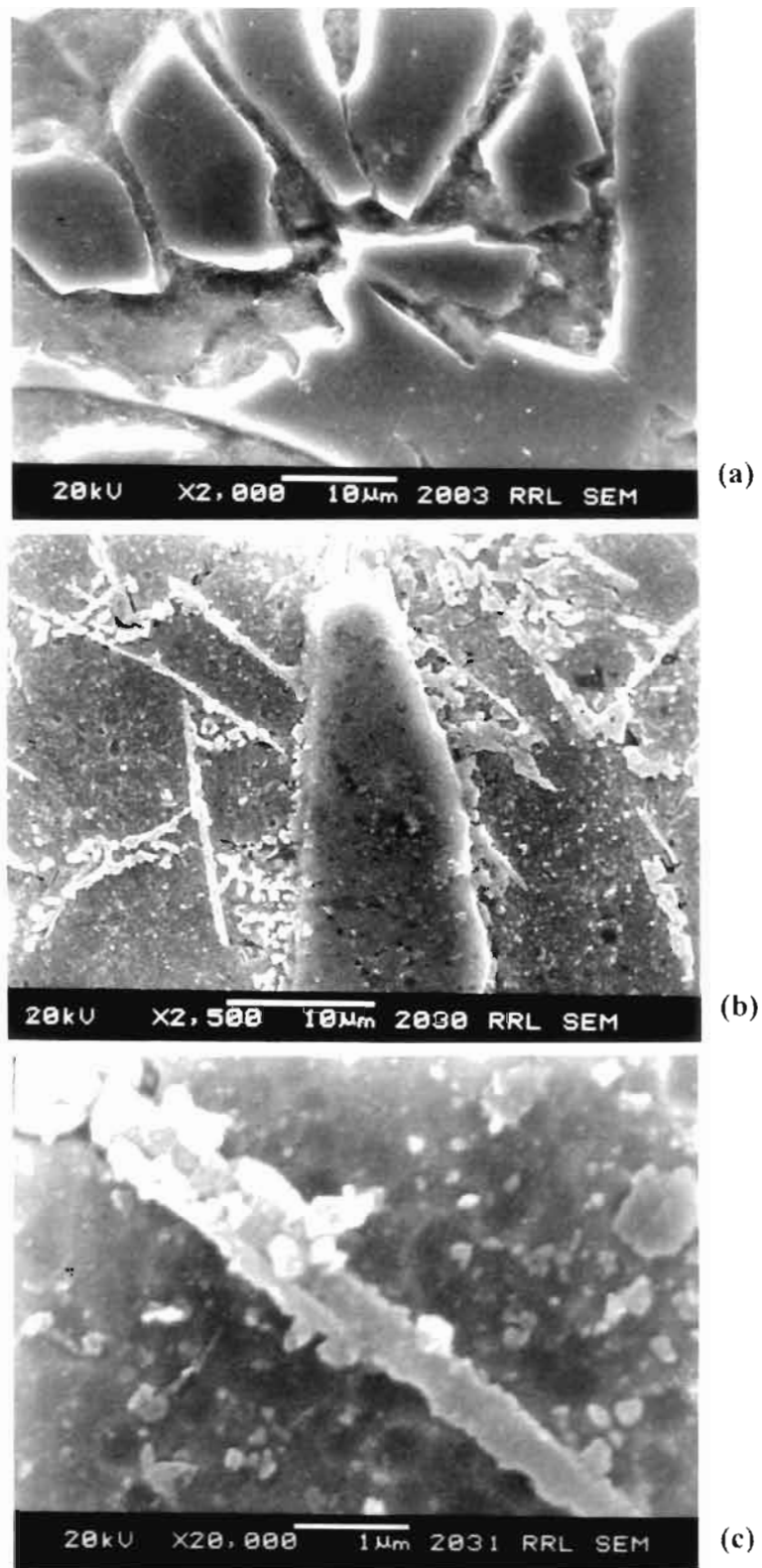


Figure 4.11: Scanning electron micrograph of Al(356)-15%SiC_(p) mono composites.
 (a) SiC particles in the matrix.
 (b) Single SiC particle in the matrix and fibrous iron intermetallics.
 (c) An iron intermetallic phase with eutectic phase surrounding it.

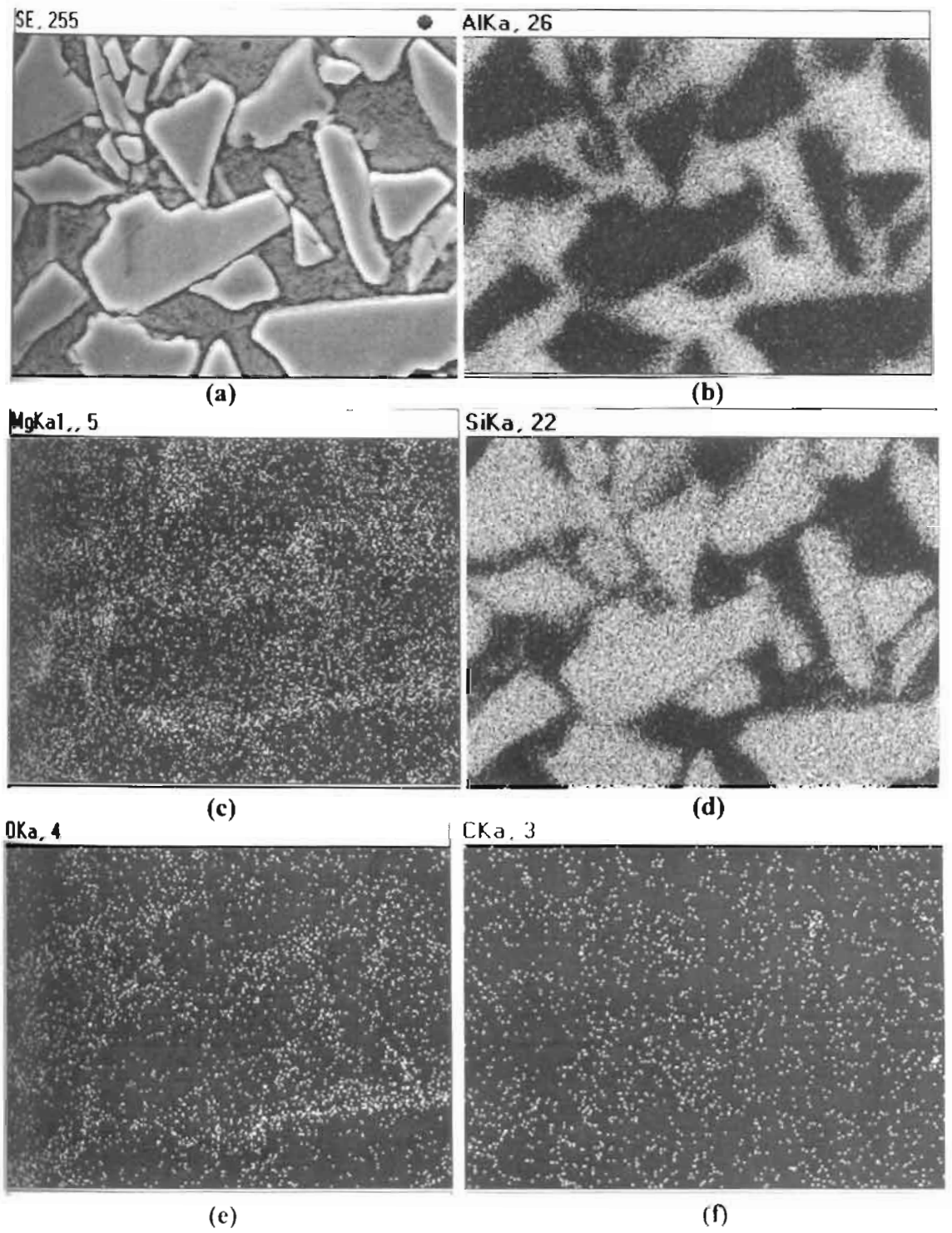


Figure 4.12: EDS elemental X-ray mapping of Al(356)-15% SiC_(p) mono composite.

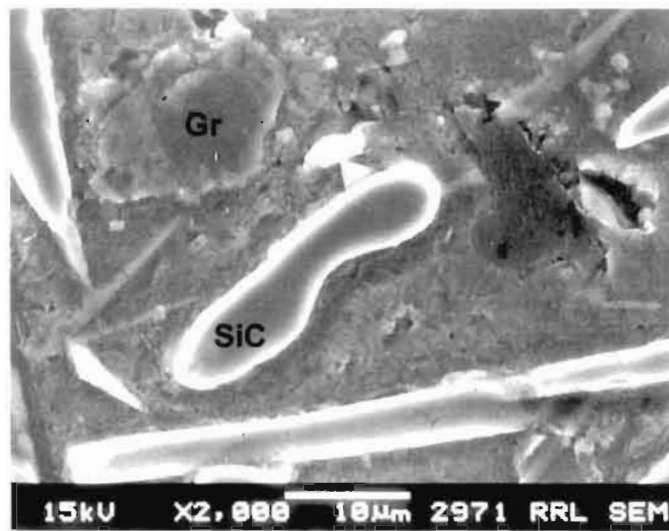


Figure 4.13: SEM micrograph of Al(356)-15% SiC_(p) - 5% graphite hybrid composites

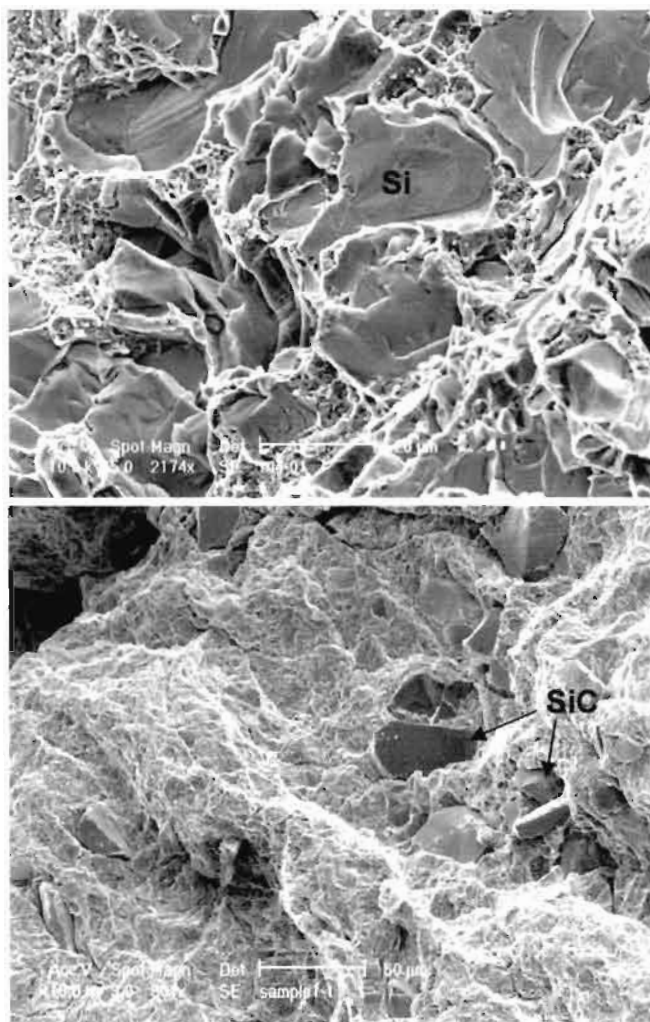


Figure 4.14: Tensile fractograph of (a) Al(356) base alloy and (b) Al(356)-15% SiC_(p) composite.

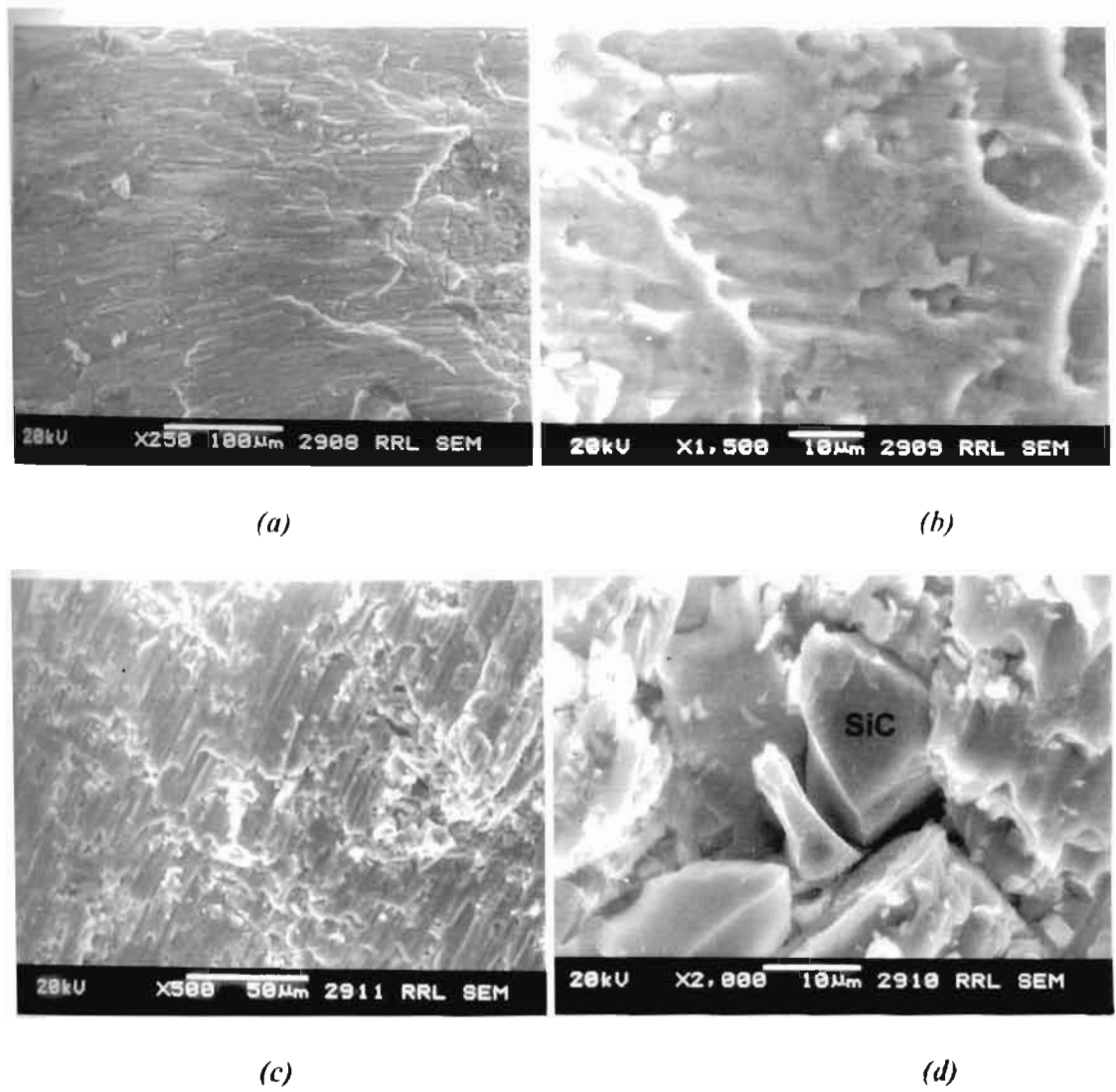


Figure 4.15: Compression fractograph of (a) and (b) Al(356) base alloy and (c) and (d) Al(356)-15%SiC_(p) composite

aluminium alloy system by scavenging the oxide layer and promoting interfacial reaction is well established. As expected, the sand mould shows a very low cooling rate, i.e., around 1 °C /s for both the alloy and composite systems. It is also observed that an increase in cooling rate suppresses the liquidus arrest temperature. In graphite mould, the liquid arrest temperature corresponding to the nucleation and growth of primary aluminium is lower than that of sand mould.

In the composites, the liquidus temperature of the matrix alloy is lowered with the introduction of particles compared to the unreinforced alloy [Figure 4.19-4.22]. Figure 4.23 shows the variation in liquidus temperature with the increasing SiC weight fraction. The eutectic temperature of composites is also lowered with the addition of particles.

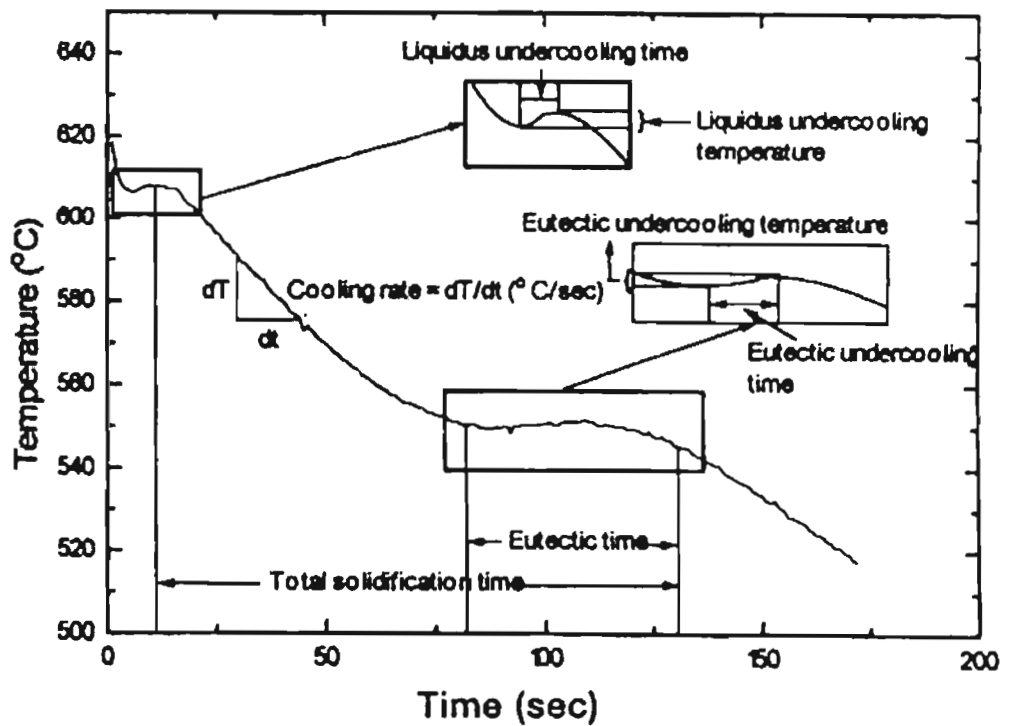


Figure 4.16: Thermal analysis parameter of 356 aluminium silicon alloy

The total solidification time is defined as the time interval between the start of primary aluminium phase solidification and the end of eutectic phase solidification and the eutectic solidification time is the interval between the start and the end of eutectic phase solidification. Figures 4.24 and 4.25 show the variation of total

solidification time and cooling rate with increasing SiC weight percentages respectively. Introduction of SiC_(p) decreases the total solidification time and this decrease is more in sand mould compared to graphite and metal moulds, which have shown an increasing trend in total solidification time after 20% SiC_(p). Similar trend is also observed in the case of eutectic solidification time.

Figures 4.26(a) and (b) show the variation of the total heat content and the thermal conductivity of composite respectively in molten (l) (727 °C) and solidified (s) (25 °C) conditions with increasing vol.% of SiC_(p). In general, the thermal conductivity (λ_c) of the composite lies between those of the individual components (λ_m) matrix alloy and (λ_r) reinforcement. Hashin and Strikman [236], Rosen and Hashin [237] and Taylor [238] have discussed about the upper and lower bound values for thermal conductivity of composites. The upper bound is given by ROM,

$$\lambda_c = V_r \lambda_r + (1 - V_r) \lambda_m \quad (4.3)$$

(V_r is the volume fraction of the reinforcement)

and the lower bound, is given by the following equation first derived by Maxwell [19]

$$\lambda_c = \lambda_m \left(\frac{\lambda_r + 2\lambda_m - 2V_r(\lambda_m - \lambda_r)}{\lambda_r + 2\lambda_m + V_r(\lambda_m - \lambda_r)} \right) \quad (4.4)$$

The upper bound values fits well mainly for the continuous fibre reinforced composites along the fibre axis. For particulate composite, the conductivity values would be near to the lower bound. The percentage reduction in thermal conductivity of the composites with 10, 20 and 30-vol% of SiC_(p) in solid state are 13.5, 26 and 37.7 % respectively.

The formation of iron intermetallic is reflected in the cooling curves for the castings solidified in low cooling sand mould, which is similar to the observation made by Mackay *et al.* [239]. The undercooling and temperature of solidification corresponding to the iron intermetallic formation are observed in between the liquidus and solidus temperature [Figure 4.18]. Iron being the common contaminant during the

processing of these composites, its intermetallic compounds such as Al_5FeSi (β) and $\text{FeMg}_3\text{Si}_6\text{Al}_8$ (π) could form.

4.3.2.2 Interfacial heat transfer analysis

Estimated values of heat flux for unreinforced and reinforced alloys cast in the steel, graphite and sand moulds are shown in Figures 4.27-4.31. It can be observed that higher peak heat flux (q_{\max}) values are associated with graphite mould followed by metal and sand mould irrespective of the melt cast. The addition of 1% Mg to the aluminium-silicon alloy has increased the peak heat flux values at the casting/mould interface in all the three moulds, i.e. 153 to 188.5 kWm^{-2} , 852.3 to 900 kWm^{-2} and 25.5 to 56 kWm^{-2} for steel, graphite and sand moulds respectively. This shows that the interfacial contact between the casting and mould is improved because of the enhanced wetting between the mould and aluminium alloy melt containing additional Mg. The estimated heat flux values at the interface are maximum shortly after pouring and dropped off rapidly in the case of all the melt/mould combinations. In the case of sand mould, two peaks are obtained for the alloy systems. Introduction of particles to the matrix alloy affect the heat transfer behaviour of the melt. The estimated q_{\max} values for the composites are lower than the alloy melts solidified under similar conditions. When $\text{SiC}_{(p)}$ are added to the alloy, the q_{\max} values get reduced with increasing weight percent of particles.

The estimated casting / mould interface temperatures for the matrix alloy and composite systems cast in steel and sand moulds depicted in Figures 4.32(a-b) show that incorporation of additional 1% Mg increases the interface temperature due to the better casting / mould interface contact than the Al(356) base alloy. Further, the addition of graphite particles to the matrix alloy improved the thermal conductivity of the system, thereby increasing the interfacial temperatures in steel and sand moulds.

4.3.3 Heat Treatment Characteristics

The heat treatment behaviour of Al(356) alloy, Al-15% $\text{SiC}_{(p)}$ and Al-15% $\text{SiC}_{(p)}$ -5% $\text{Gr}_{(p)}$ composite are evaluated by hardness measurements and the results are

depicted in Figure 4.33. The composites exhibit an accelerated ageing behaviour at the early stage of aging process. The time for peak ageing of unreinforced alloy at 165 °C is 8 hours, whereas the composites attain the peak hardening at 7 hrs. The peak hardness value of Al(356) –15% SiC_(p) is higher than the unreinforced alloy. After peak ageing and holding for two hours, the hardness of composite tends to decrease with increase in ageing time.

4.3.4 Physical Properties

The density and electrical conductivity of the alloys and the composites are evaluated.

4.3.4.1 Density measurement

The Figure 4.34 shows the density of the base alloy and the gravity and squeeze cast composites along with the theoretical values (standard handbook value for alloy and rule of mixtures values for composites) for comparison. The density of gravity and squeeze cast alloy and composites are lower than theoretical value due the porosity present in the composites. The gravity cast Al(356)-15% SiC_(p) shows higher values compared to other systems. The introduction of graphite particles has lowered the composite density. The application of pressure during solidification reduces the porosity to a considerable level and hence the densities of squeeze cast alloys and composites are very closer to the respective theoretical value.

4.3.4.2. Electrical conductivity measurement

Figure 4.35 (a) shows the variation in electrical conductivity of Al(356)- SiC_(p) composites with different weight fraction. Increase in SiC weight fraction has reduced the electrical conductivity. Figure 4.35(b) shows the variation of electrical conductivity of Al(356)-SiC composites with varying weight fraction at different locations from bottom to top of the casting. The bottom and top portion of the casting show slightly higher value than the middle portion.

Figure 4.36 shows the electrical conductivity of Al(356)-SiC_(p) composites with varying weight fraction and particle size. The composites containing coarser SiC_(p) (118 μm APS) gives higher conductivity than that containing finer 23 μm SiC particle. Observation has shown that variation in cooling rate, porosity levels and surface characteristics of test specimen affects the measured values.

4.3.5 Mechanical Properties

4.3.5.1 Hardness

The hardness values of the alloys and composites in as cast and heat treated conditions are shown in Figure 4.37. The incorporation of 15% SiC particles has increased the hardness of the matrix alloy both in as cast and peak aged conditions. However, the 5% graphite addition to Al (356)-15% SiC_(p) system has lowered the hardness values both in as cast and peak aged conditions.

4.3.5.2 Tensile and compressive strengths

The tensile and compressive strength of the base alloy, the mono and the hybrid composites are evaluated. The Figures 4.38 and 4.39 show the ultimate tensile strength and compressive strength of the base alloy and the composites. The presence of porosity has lead to the lower tensile strength in composite, whereas the compressive strength has increased. Higher compressive strength is obtained in Al-15% SiC_(p)-5% Gr_(p)(Nat) hybrid composite. However, hybridisation of synthetic graphite has reduced the compressive strength than the Al(356)-15% SiC_(p) monocomposite.

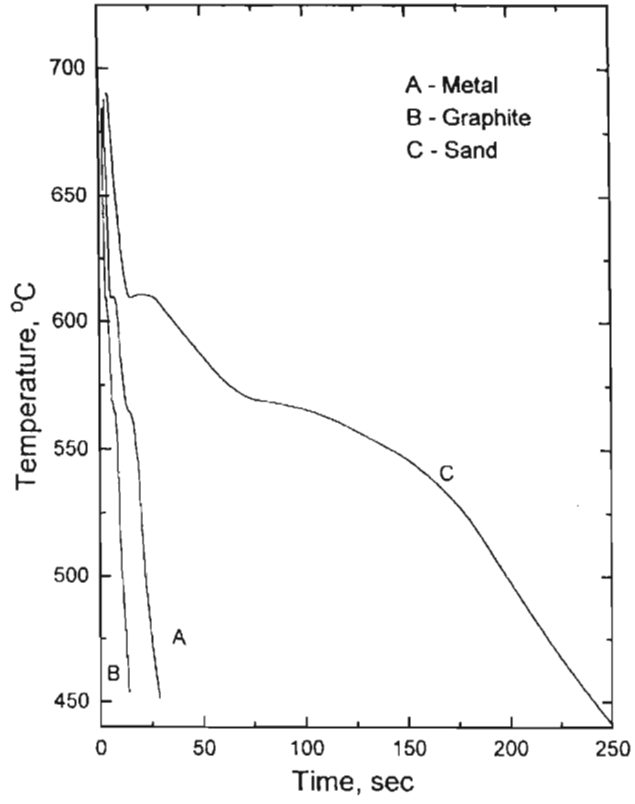


Figure 4.17: *Cooling curve of 356 Al alloy solidified in metal, graphite and sand moulds*

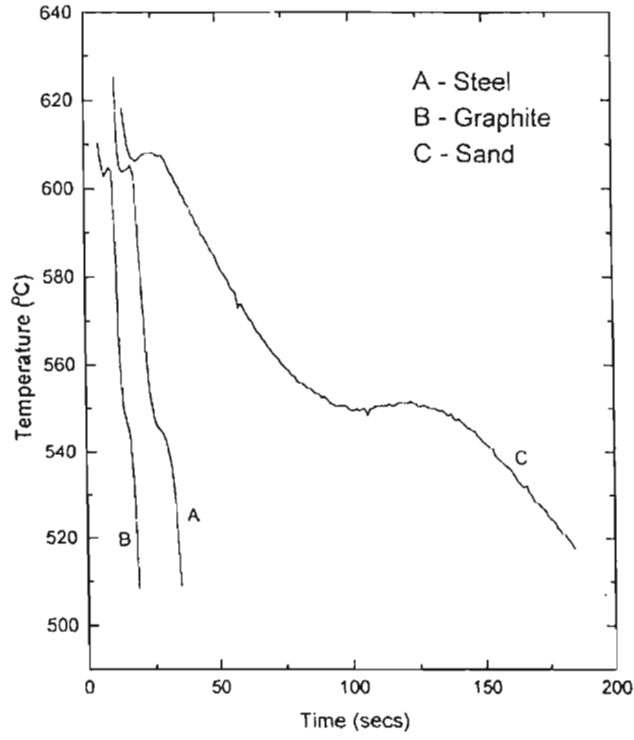


Figure 4.18: *Cooling curve of 356 Al alloy-1% Mg solidified in metal, graphite and sand moulds*

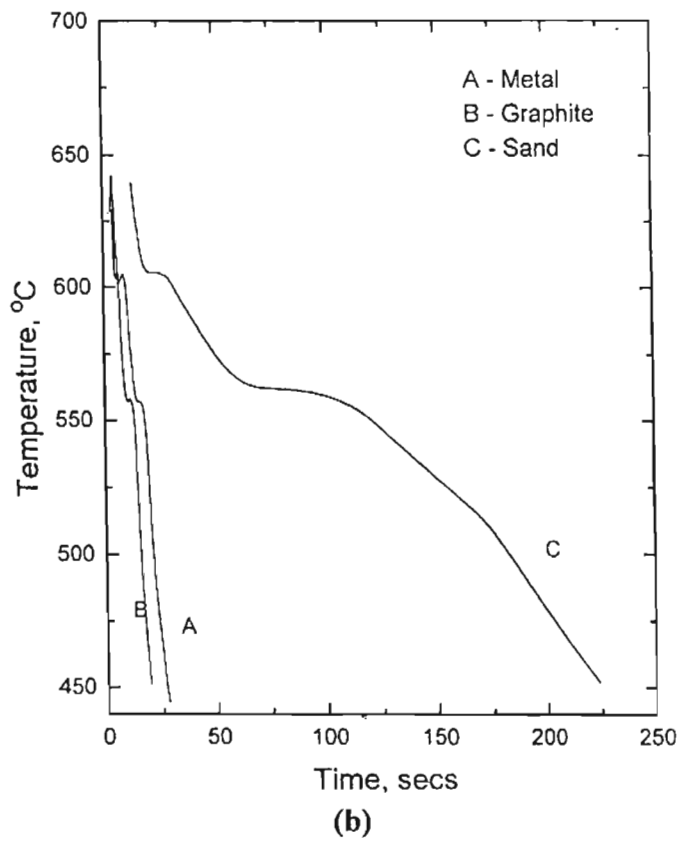
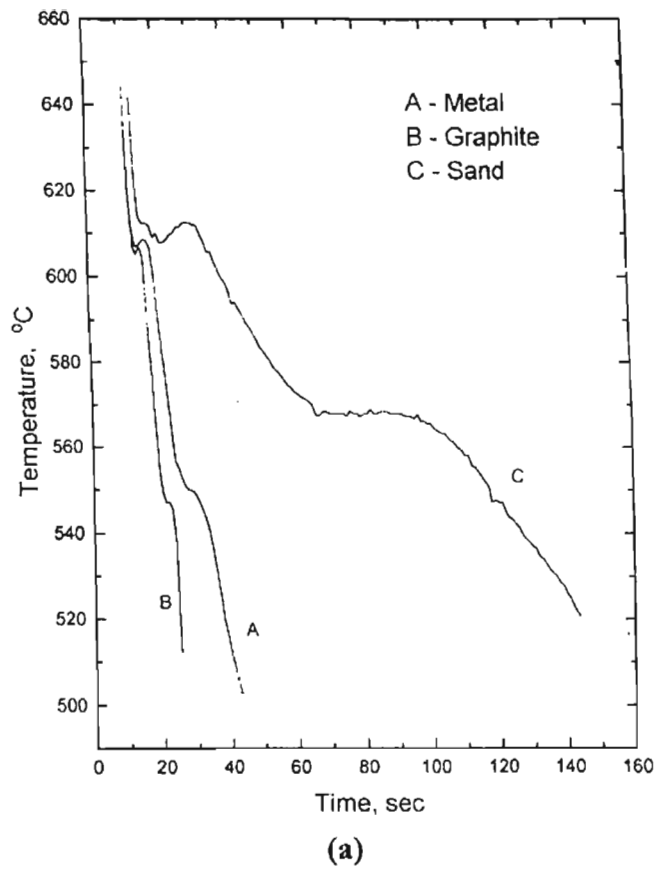


Figure 4.19: *Cooling curve of Al (356)-SiC composites with varying weight percentages (a) 10% and (b) 20 % solidified in metal, graphite and sand moulds*

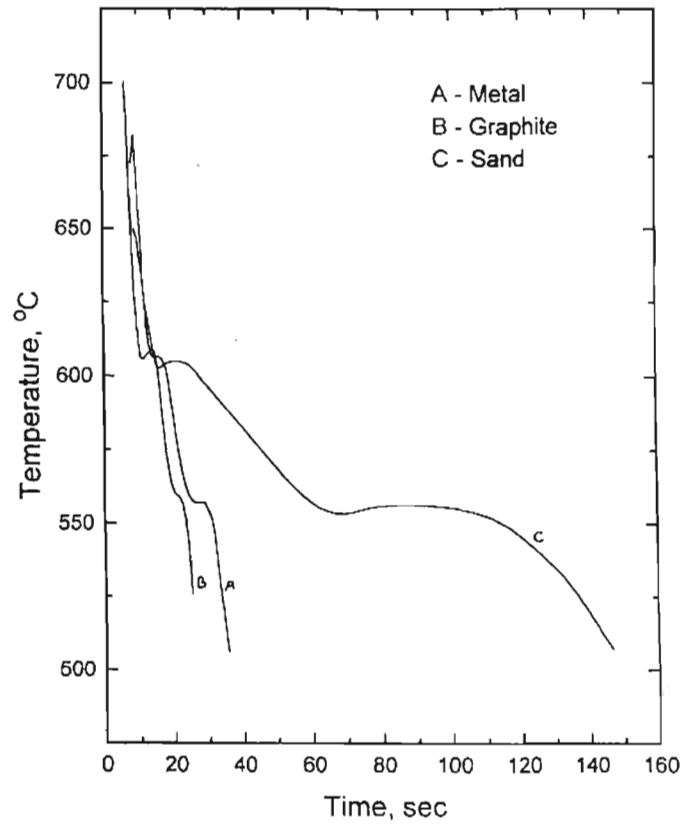


Figure 4.20: Cooling curve of Al(356)-5% Graphite particle reinforced composite solidified in metal, graphite and sand moulds

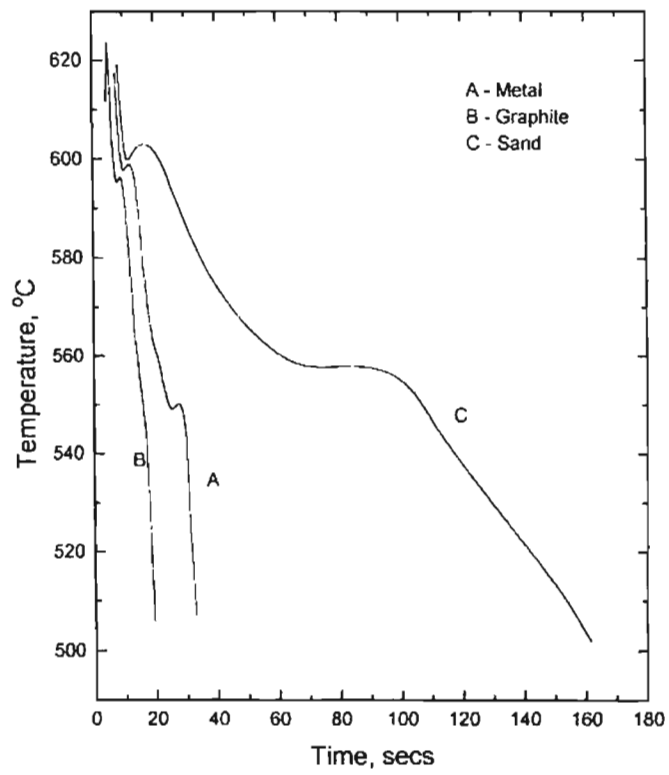


Figure 4.21: Cooling curve of Al(356)-15% SiC_(p)-5% graphite hybrid composite solidified in metal, graphite and sand moulds

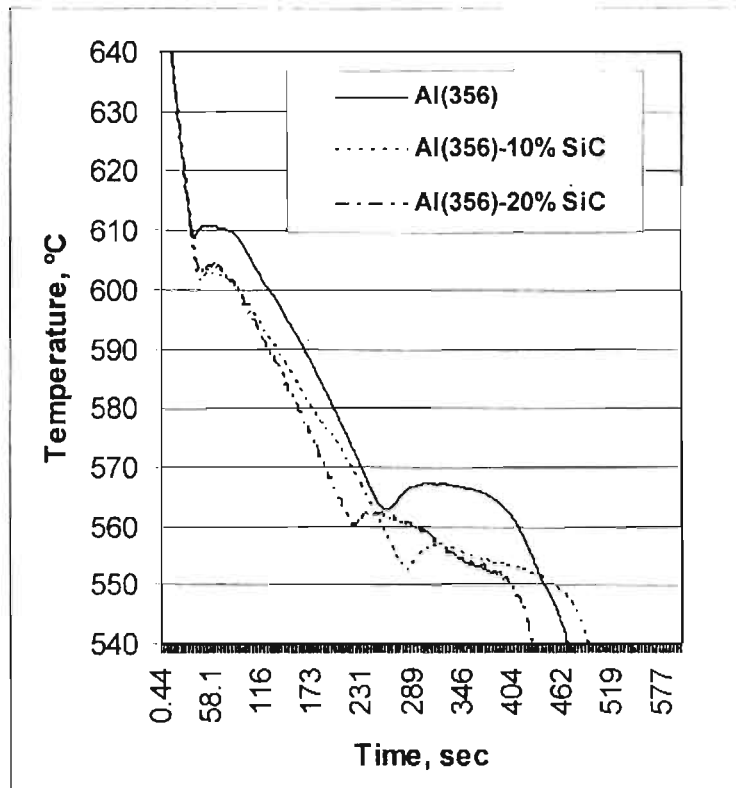


Figure 4.22: Cooling curves of base alloy, 10 and 20 % $\text{SiC}_{(p)}$ reinforced 356 aluminum matrix composites determined using Aluminium Meltlab data logger system using the standard steel cup.

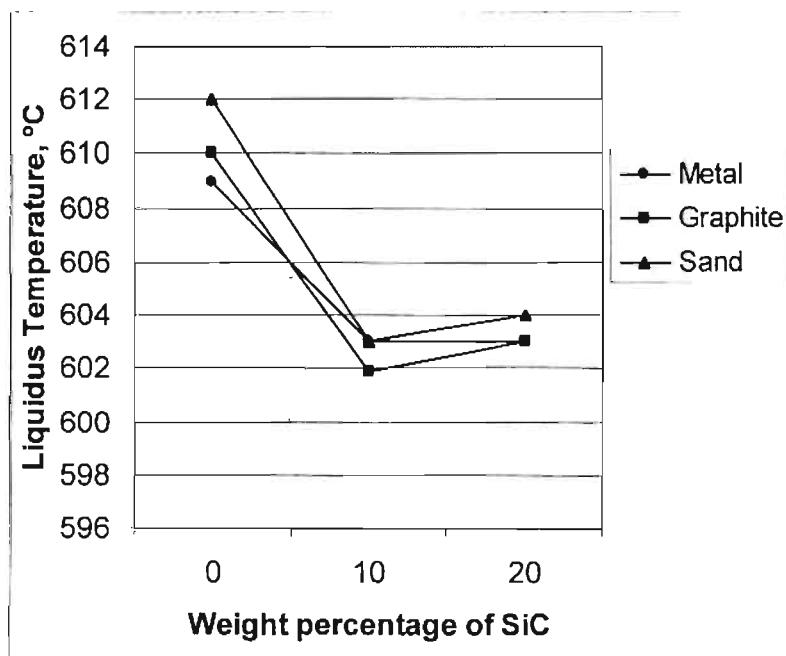


Figure 4.23: Variation in liquidus temperature with the increase in $\text{SiC}_{(p)}$ weight fraction.

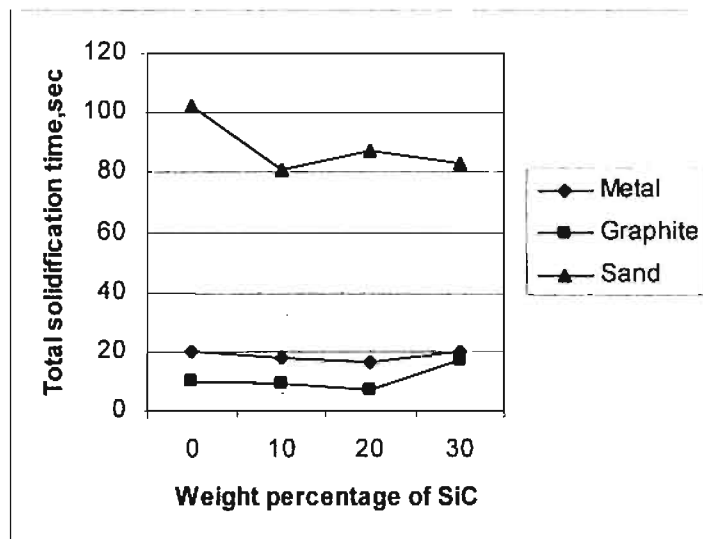


Figure 4.24: Variation in total solidification time with increase in $SiC_{(p)}$ weight fraction.

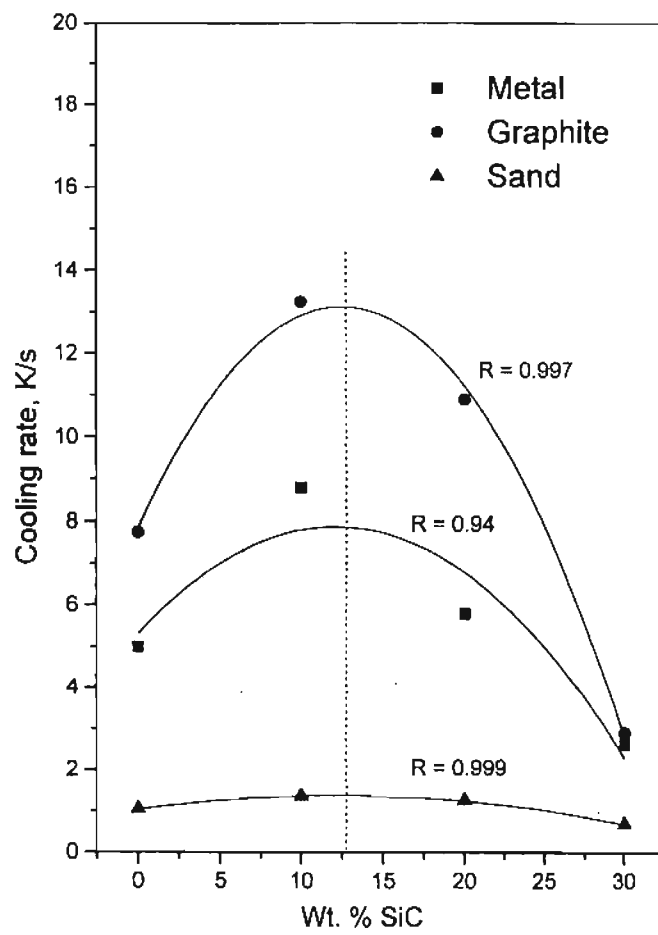
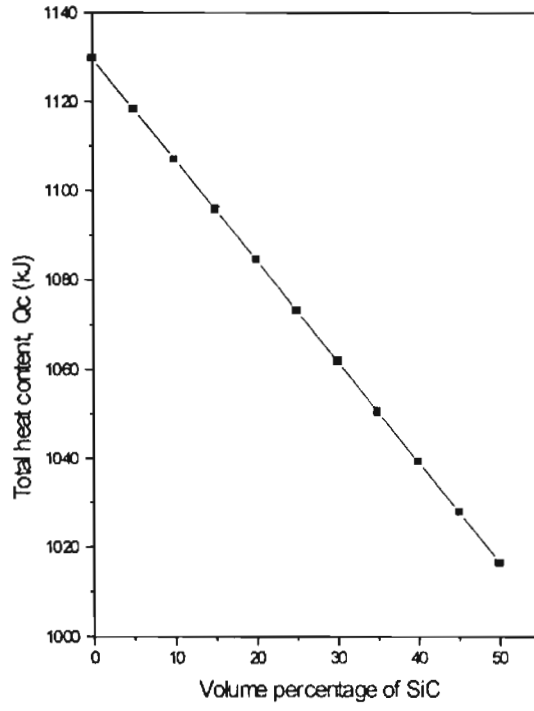
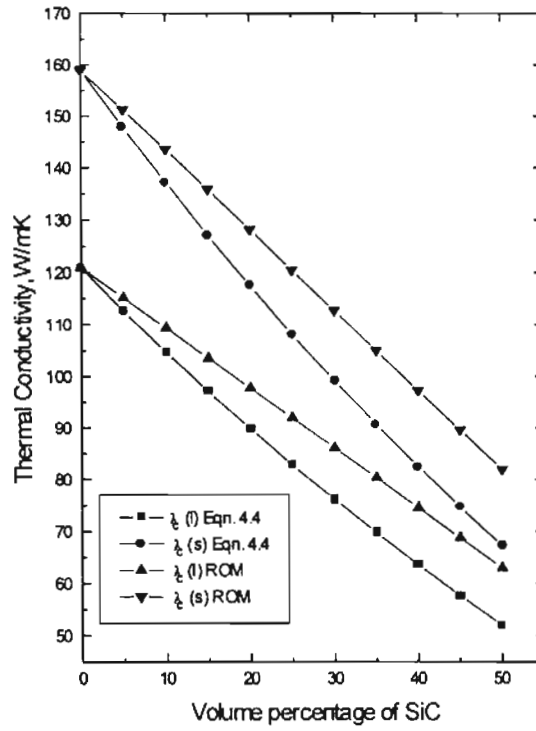


Figure 4.25: Variation in cooling rate with increase in $SiC_{(p)}$ percentage in metal, graphite and sand mould



(a)



(b)

Figure 4.26: Variation of (a) total heat content of the composite and (b) thermal conductivity of composite in molten (l) (727 °C) and solidified (s) (25 °C) conditions with increase in vol% of $SiC_{(p)}$.

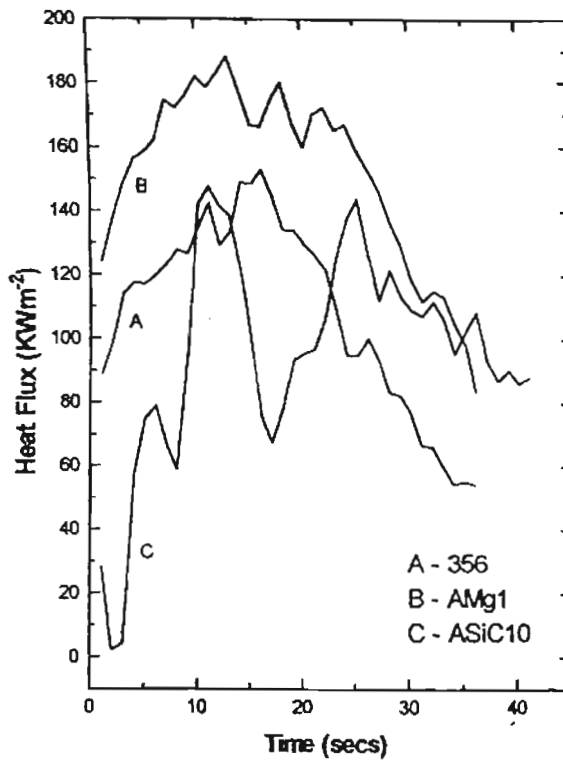


Figure 4.27: Variation in interfacial heat flux with time for 356 alloys with and without 1% Mg and 10% SiC_(p) reinforced composite cast in steel mould

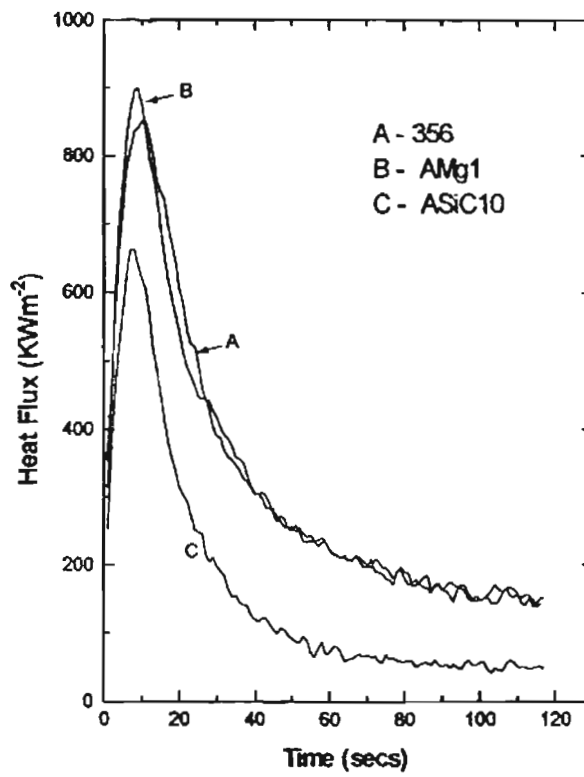


Figure 4.28: Variation in interfacial heat flux with time for 356 alloy with and without 1% Mg and 10% SiC_(p) reinforced composite cast in graphite mould

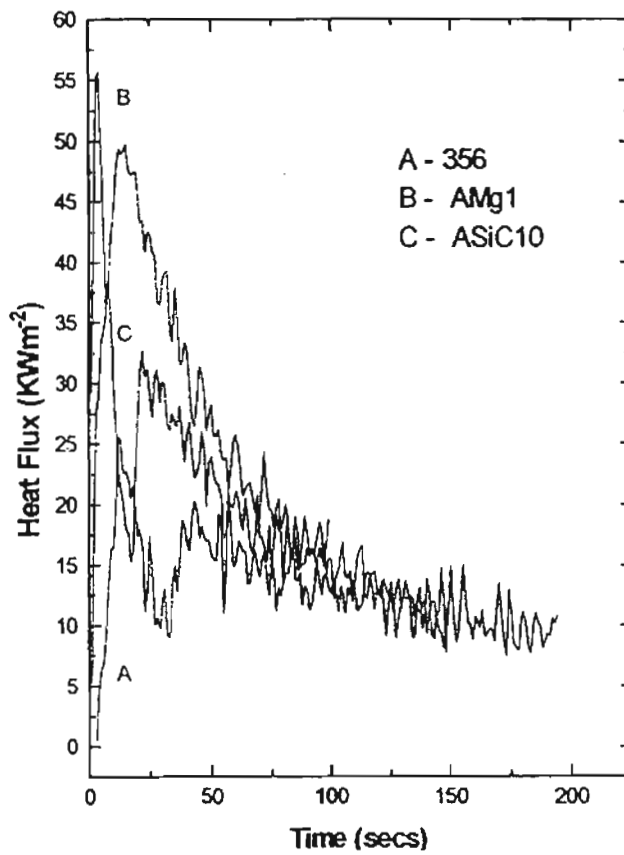


Figure 4.29: Variation in interfacial heat flux with time for 356 alloy with and without 1% Mg and 10% SiC_(p) reinforced composite cast in sand mould

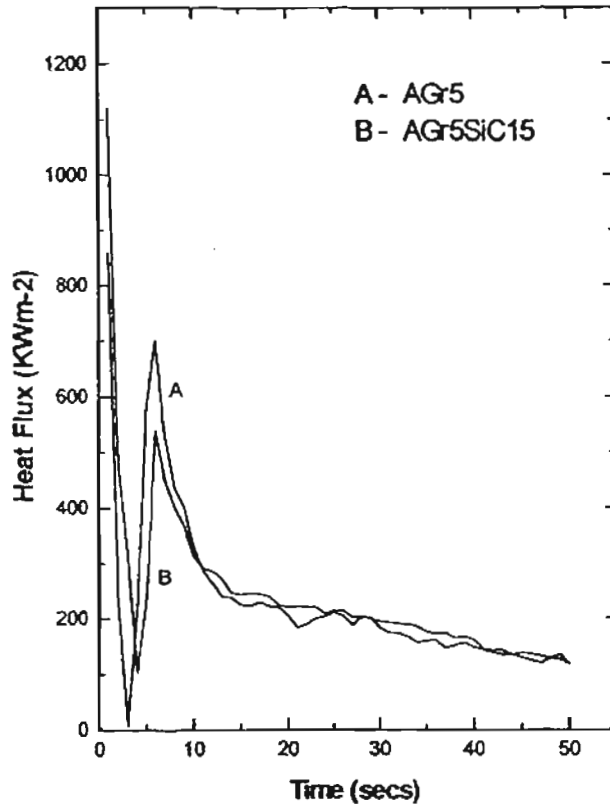


Figure 4.30: Variation in interfacial heat flux with time for 356 alloy reinforced with 5% Gr and 15% SiC_(p)-5% Gr composites cast in steel mould

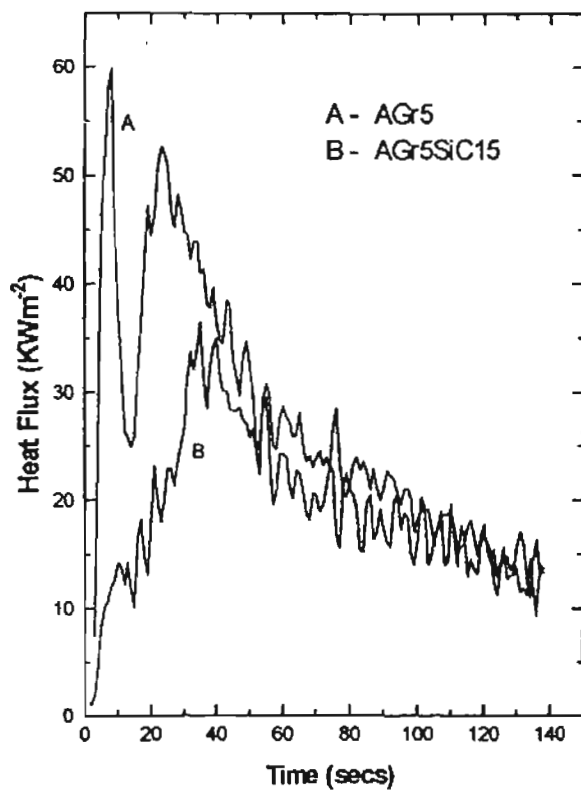
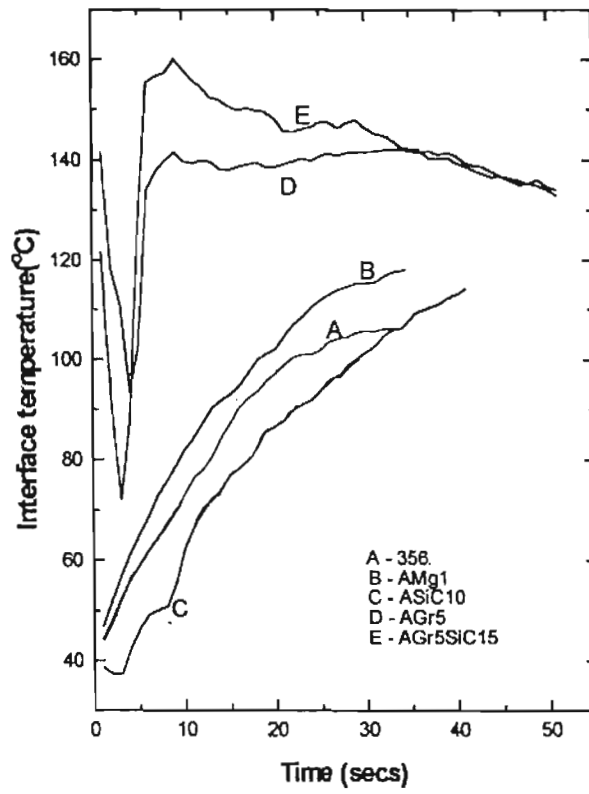
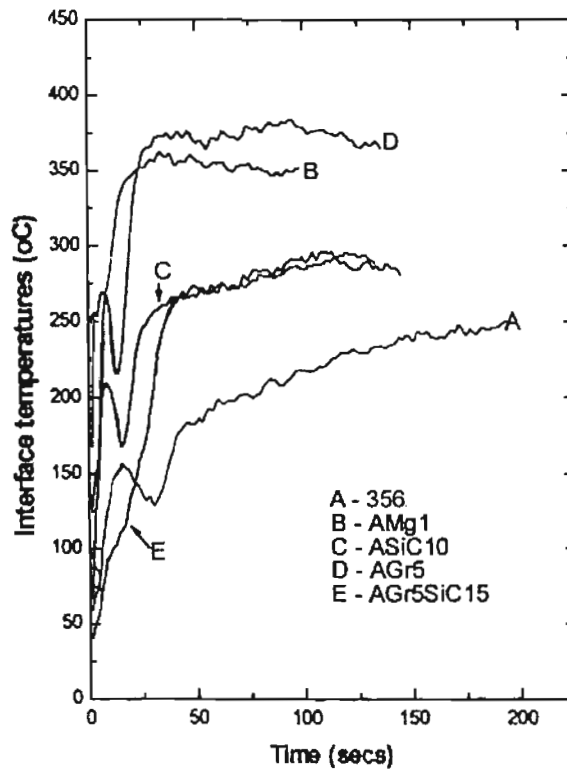


Figure 4.31: Variation in interfacial heat flux with time for 356 alloy reinforced with 5% Gr and 15% SiC_(p)-5% Gr composites cast in sand mould



(a)



(b)

Figure 4.32: Estimated casting/ mould interface temperatures during solidification of various alloys and composites, (a) Steel and (b) Sand mould

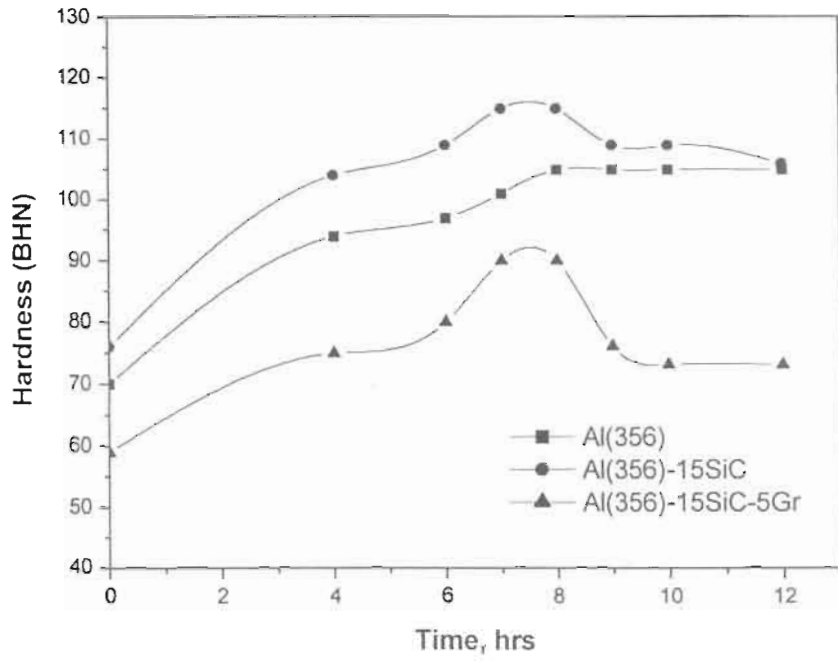


Figure 4.33: Ageing characteristics of 356 aluminum alloy and Al (356)-15% SiC_(p) mono and Al (356)-15% SiC_(p)-5%graphite hybrid composites

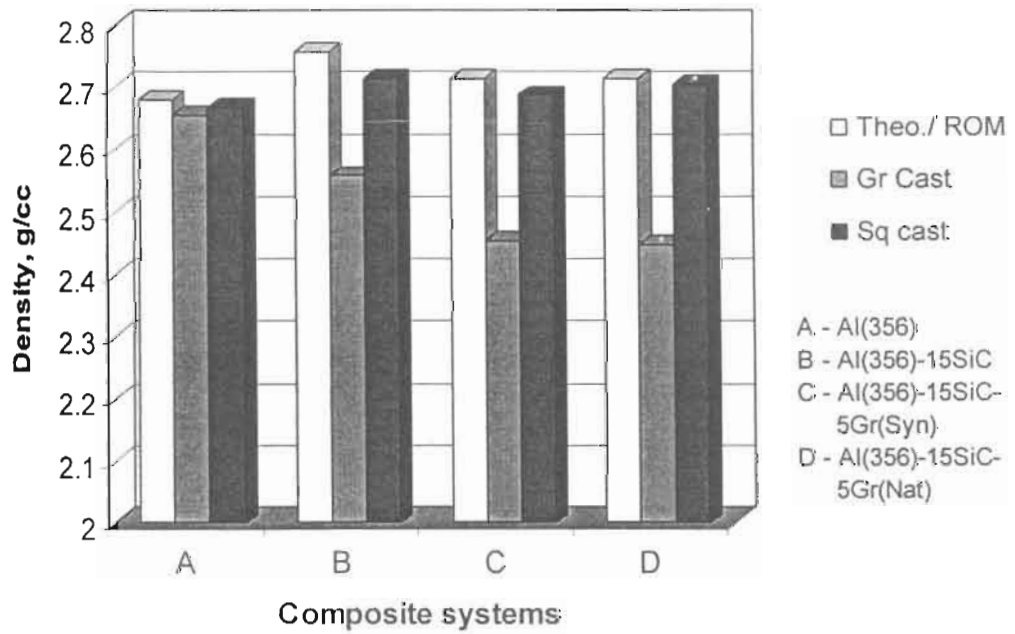
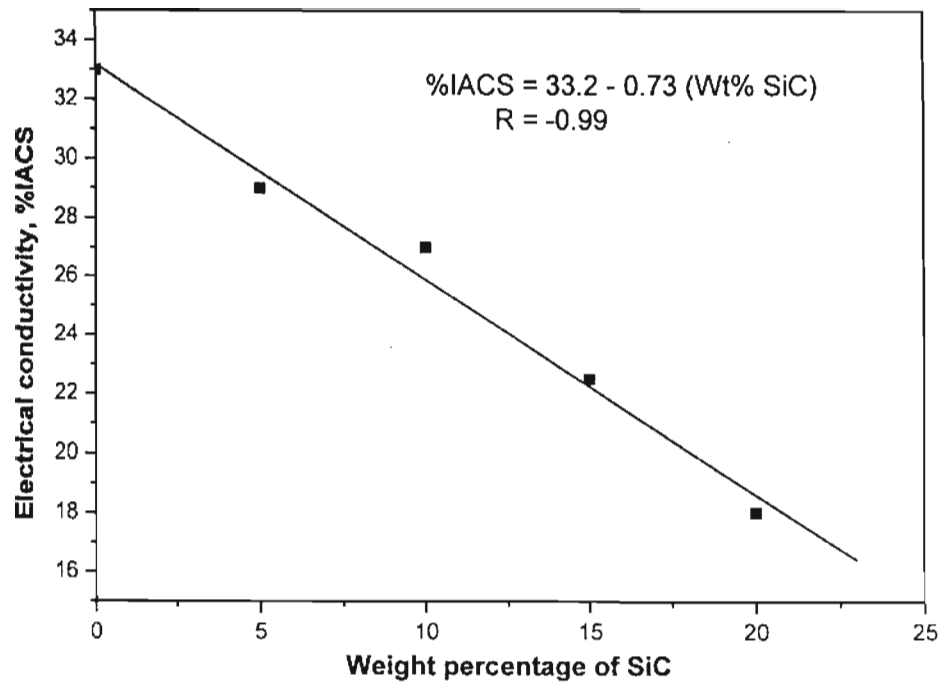
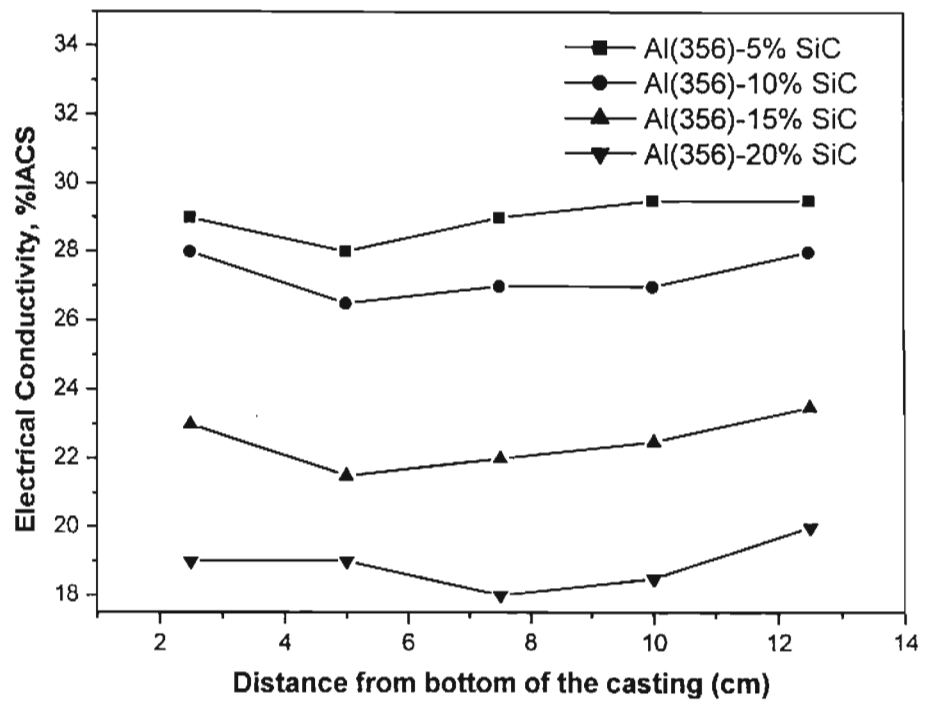


Figure 4.34: Variations in densities of base alloy and composites solidified under gravity and squeeze cast conditions



(a)



(b)

Variation in electrical conductivity of Al(356)-SiC_(p) composite with varying (a) weight fraction and (b) at different positions of the casting

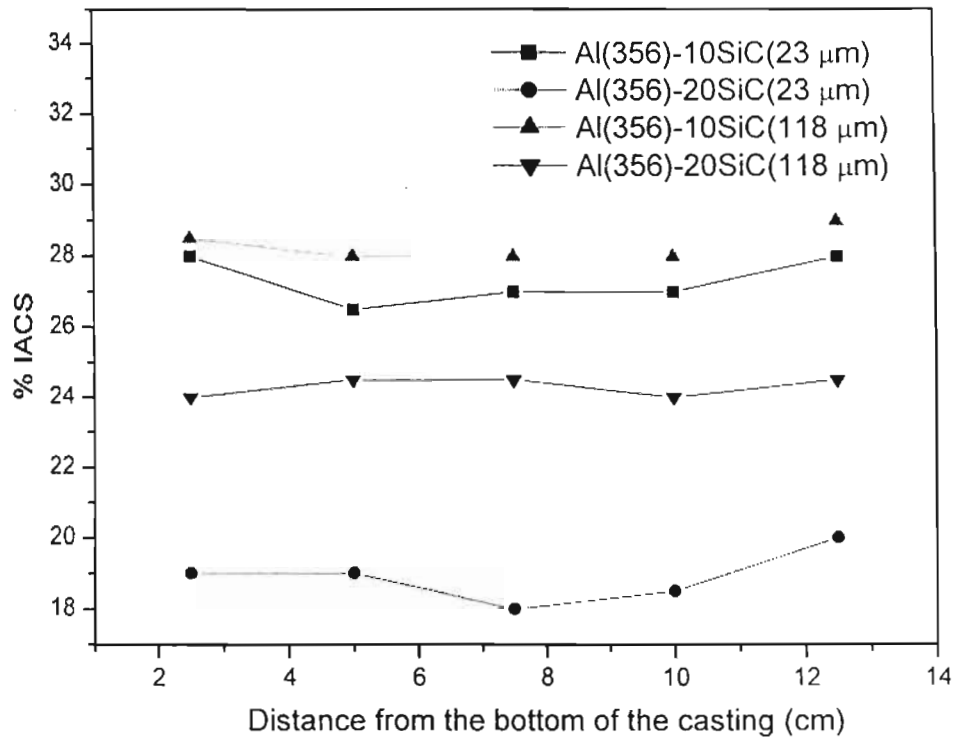


Figure 4.36: Variation in electrical conductivity of Al(356)-SiC_(p) composite with varying weight fraction and particle size of SiC

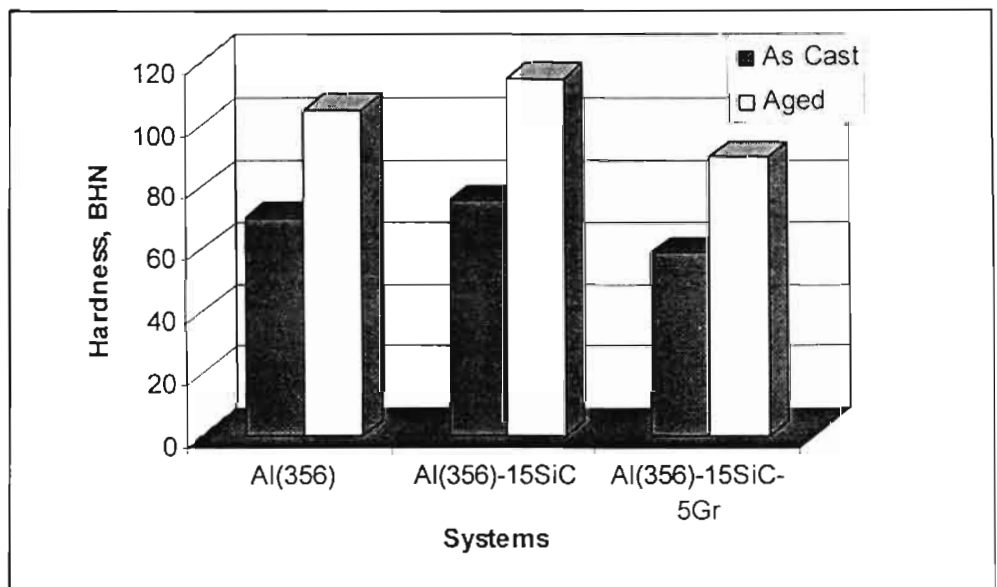


Figure 4.37: Hardness values of base alloy and composite systems in as cast and aged conditions

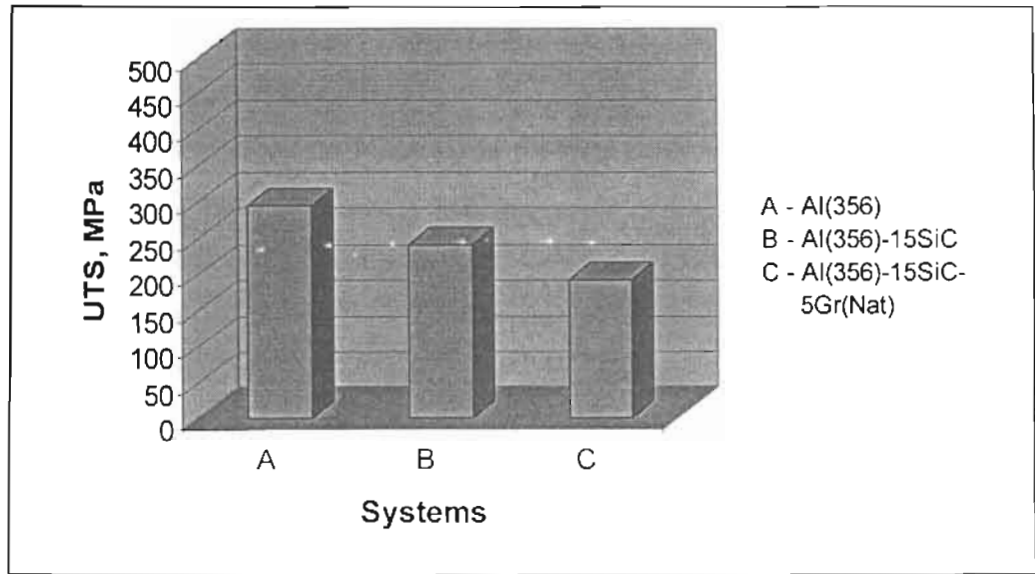


Figure 4.38: Ultimate tensile strength of the base alloy and the composite systems

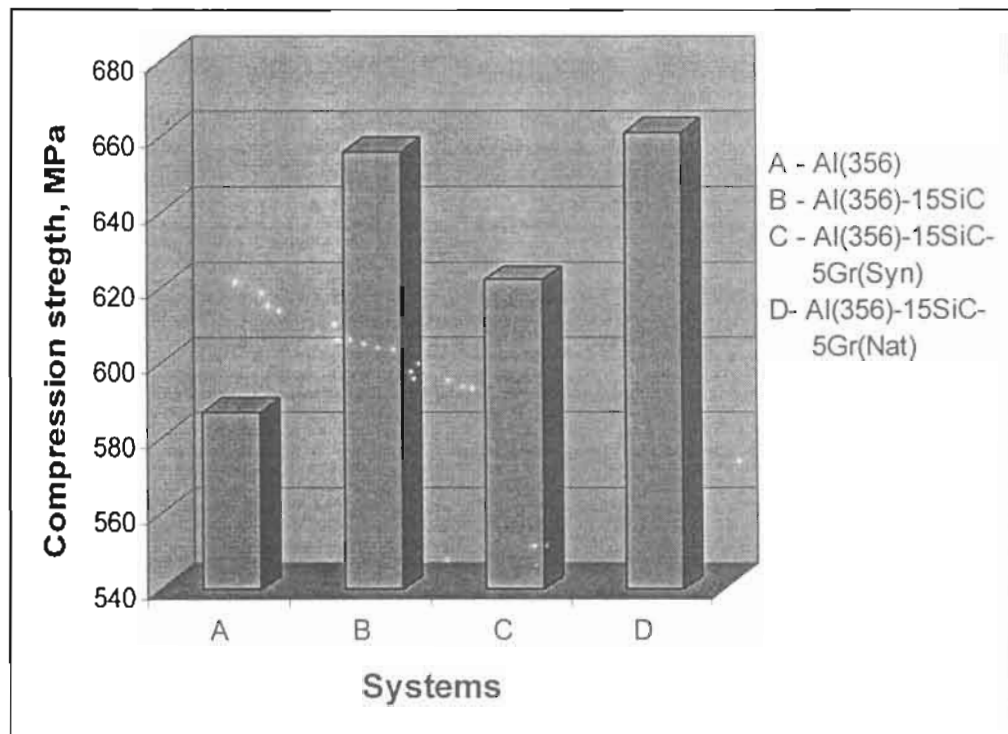


Figure 4.39: Compression strength of the base alloy and the composite systems

4.4 DISCUSSION

4.4.1 Processing and Microstructural Evolution

The microstructure evolved in cast composites depends on the characteristics of the constituent materials (matrix and reinforcement) and various processing and solidification parameters. The criteria for the selection of constituent material rely on the type and nature of composite to be fabricated. The choice of Al(356) matrix alloy is due to its better properties and popularity as the most commonly used cast aluminium alloy. In the case of Al (356)-SiC_(p) composites, the presence of silicon in the matrix could control the interfacial reaction between SiC_(p) and Al melt. In the case of reinforcements, the hard SiC particle could provide increase in specific strength and stiffness and abrasive wear resistance and the soft graphite particle could improve the adhesive wear resistance and reduce the density of the composite.

The important steps involved in composite synthesis by liquid metal stir casting are (i) the pre-treatment of reinforcements, (ii) melting of matrix alloy and addition of wetting promoters and other alloying elements, (iii) introduction, mixing of reinforcements and (iv) solidification of the composite melt. The variations in the processing parameters of the above steps affect the final solidification structure and properties of the composite.

The pre-treatment of SiC and graphite particles is carried out to improve their wetting with the liquid aluminium alloy. The pre-treatment of SiC at 750 °C for 2 hrs removes the volatile contaminants from the particle surface and forms a layer of SiO₂ on the particle surface by artificial oxidation. The presence of SiO₂ on the particle surface helps in improving the wetting of SiC particle with Al-7Si-0.35Mg matrix alloy. The pre-treatment of synthetic and natural graphite particles is carried out at 400 °C for 2 hrs to remove the volatile contaminant. In the case of synthetic graphite particles, there is 20-25 % weight loss due to the burning of carbon. The XRD studies have shown that the synthetic graphite contains more partially graphitised carbon compared to natural graphite. Hence, the natural graphite is more stable at high temperature.

During hybrid composite synthesis, the SiC and graphite particles are premixed before their addition. The other two modes of addition are also evaluated.

but the premixed particles provide better dispersion of particles with lower addition time, ie, higher feeding rate. In the case of premixed particle addition, the SiC_(p) is first preheated at 750 °C for 2 hrs, mixed with graphite particles, again heated at 400 °C for 2 hrs and then introduced to the matrix melt.

The density, wetting behaviour and mechanism of SiC and graphite particles are different. The SiC_(p) with higher density (3.2 g/cc) than the matrix alloy (2.68 g/cc) tends to settle and the graphite particle with lower density (1.8 g/cc) tends to float. However, these particles experience hindered settling phenomena, which could improve their distribution. But, the dispersion of particles is mainly dependent on their wetting with the matrix alloy. The SiC tends to wet liquid Al quickly than the graphite particles.

The wettability of a solid by liquid is indicated by the contact angle between them or by the work of adhesion. The contact angle between the solid SiC/graphite particle, liquid aluminium matrix and gas/vapour could be related by the Young's Dupre's equation.

$$\gamma_{lv} \cos \theta = \gamma_{sv} - \gamma_{sl} \quad (4.5)$$

Where γ_{lv} is the surface tension of the liquid aluminium matrix, γ_{sv} is the surface energy of the reinforcement and γ_{sl} is the interfacial energy between the liquid aluminium and the solid particle. The increase in wettability is obtained by lowering the contact angle, θ . The contact angle can be decreased by (i) increasing the surface energy of the solid reinforcement, γ_{sv} (ii) decreasing the reinforcement/matrix interfacial energy and (iii) decreasing the surface tension of the liquid metal, γ_{lv} .

In the case of Al (356)-SiC_(p) system, (i) the pre-heat treatment of SiC particle tends to increase the surface energy of the reinforcement, (ii) the addition of Mg to the matrix alloy tends to decrease the surface tension of the liquid matrix alloy and (iii) the MgAl₂O₄ spinel phase formed due to the interaction of surface oxidised SiC with the liquid Al matrix tends to decrease the reinforcement/matrix interfacial energy.

Hence, all these factors help in improving the wetting of SiC particle with the matrix Al.

In case of Al (356)-15% SiC_(p)-5% graphite HMMC, the mixed mode of addition has resulted in better dispersion of the particles. The variation in the densities of the particles leads to opposing behaviour, i.e. denser SiC_(p) tends to settle, while lighter graphite tends to float causing hindered settling effect. The hindered settling phenomenon improves distribution of the particle in the composites.

The microstructural refinement observed in the squeeze cast Al(356) alloy and Al(356)-15% SiC_(p) monocomposite is due to the increased cooling rate experienced by the melt in the squeeze casting than the gravity casting. This is caused by the applied pressure resulting in more intimate contact between the melt and the die consequently increasing the melt/die heat transfer coefficient. The lower porosity observed in squeeze cast alloy is due to the high-applied pressure resulting in better feeding of solidification shrinkage. Since the few particles clusters found in Al(356)-15% SiC_(p) monocomposite are individually separated in the matrix, the clustering might have occurred during solidification and not due to insufficient wetting or stirring before casting. The clusters might have occurred due to flow of the interdendritic liquid towards the solidification shrinkage areas and prevention of particle movement by already solidified phase. The presence of oxide films can also lead to particle clustering. In both gravity and squeeze cast structures, the SiC particle does not facilitate the nucleation of primary phase due to the higher thermal gradient experienced at the interface between SiC and liquid metal during solidification. The formation of iron intermetallics can be due to the presence of excess iron in the base alloy or iron picked up during processing. Since the base alloy structure does not show the presence of iron intermetallics, the second reason is more possible.

In both gravity and squeeze cast Al (356)-15% SiC_(p)-5% graphite system (both natural and synthetic graphite) the reinforcements get segregated in the eutectic region revealing that both SiC and graphite do not act as a heterogeneous nucleus for α -phase. Nucleation of primary phase over a particle requires certain amount of under cooling. Therefore, when the particle temperature remains higher than the matrix melt

temperature, nucleation is not likely to occur on the particle surface. The particle pushing phenomena varies with respect to particle type, size, density and shape. The lighter and smaller graphite particles tend to have higher particle mobility. The dispersed particle clustering similar to squeeze cast $\text{SiC}_{(p)}$ monocomposite is observed in hybrid composite where the clusters contain both SiC and graphite.

The encircling of large graphite particle by SiC particle as well as $\text{SiC}_{(p)}$ by finer graphite particle is observed in both natural and synthetic graphite containing hybrid composites. This might have occurred either during processing or solidification. It is suggested that bridging between two different particles could be due to the layer of adsorbed gases present over the graphite particles [240]. Alternatively, the MgO formed at the graphite surface by scavenging of oxygen by Mg [24] can also lead to the formation of MgAl_2O_4 spinel that in turn can wet SiCp surface and act as a bridge between the graphite and the SiC particles. A detailed interfacial analysis needs to be carried out to understand the nature of bonding between different particles.

4.4.2 Solidification Behaviour

In composites, the liquidus temperature of the matrix alloy is lowered with the introduction of particles compared to the unreinforced alloy. This can be attributed to the presence of reinforcement, which is considered as an impurity and the unfavourable primary aluminium nucleation condition prevailing at the reinforcement surface. Studies by Gowri and Samuel [193] have also shown that addition of particles has lowered the liquidus temperature by about 10 °C.

In general, the introduction of $\text{SiC}_{(p)}$ decreases the total solidification time and this decrease is more in sand mould compared to graphite and metal moulds, showing an increasing trend in total solidification time after 20% $\text{SiC}_{(p)}$ addition. Similar trend is also observed in the case of eutectic solidification time. During solidification, two phenomena can occur in the composite melt compared to the un-reinforced alloy. The first one is the reduction in the amount of latent heat to be extracted corresponding to the weight percentage of solid silicon carbide particle in the liquid metal, leading to a

decrease in solidification time (phenomenon I). The total heat content of the composite decreases with increase in the SiC particle volume percent [Figure 4.26(a)].

The second is the low conducting dispersoids can hinder the heat transfer during solidification and increase the solidification time (phenomenon II). Figure 4.26(b) has shown a decrease in thermal conductivity of the Al(356)-SiC_(p) composite with the varying volume fraction of SiC in both the liquid (above liquidus temperature of the matrix alloy – 613 °C) and the solidified state.

However, the first phenomenon dominates at lower weight fraction, while the second phenomenon at higher weight fraction (there by increasing the solidification time than lower weight fraction composites). This is also evidenced from the variation of cooling rate with wt% of particle [Figure 4.25]. The cooling rate of composite increases with increasing amount of SiC_(p), reaches a maximum around 12.5 wt% of SiC_(p) and then decreases with further increase in SiC_(p) for all the three moulds studied. It may be noted that the rate of increase as well as decrease in cooling rate with increasing weight percentage of SiC_(p) are dependent on the heat extracting capability of the mould material, i.e. higher for the fast heat extracting moulds, viz., graphite and metal than sand mould.

4.4.2.1 Casting / Mould interfacial heat transfer

It can be observed that higher peak heat flux (q_{max}) values are associated with graphite mould followed by metal and sand moulds irrespective of the melt cast. This is due to the higher thermal conductivity of graphite compared to the other two mould materials. The addition of 1% Mg to the aluminium silicon alloy has increased the peak heat flux values at the casting/mould interface in all the three moulds, i.e. 153 to 188.5 kWm⁻² for steel, 852.3 to 900 kWm⁻² for graphite and 25.5 to 56 kWm⁻² for sand mould. This shows that the interfacial contact between the casting and mould is improved because of the enhanced wetting between the mould and aluminium alloy melt containing additional Mg. It has been proven that addition of Mg improves the wetting between ceramic particles and Al alloy melt [24]. The present study brings out another important and very useful contribution of Mg addition in enhancing the

interfacial heat transfer at the metal-mould interface in all the three moulds chosen. Hence, Mg addition in Al composites results in multifunctional benefits.

The estimated heat flux values at the interface is maximum shortly after pouring and dropped off rapidly in the case of all the casting/mould combinations. The initial increase in the heat flux values is due to the good contact between the liquid metal and the mould surface. As the casting starts solidifying, the metal/mould interfacial contact becomes less because of air gap formation resulting in the reduction of heat flux values across the interface. In the case of sand mould, two peaks are obtained for the alloy systems. The first peak corresponds to the better interfacial contact of liquid metal with the mould, and then due to imperfect contact of the solidified metal, heat flux falls rapidly. The second peak corresponds to the heat transfer through the solidified metal and the casting/mould interface after gap formation and also due to the latent heat released during solidification.

Introduction of particles to the matrix alloy affects the heat transfer behaviour of the melt. The estimated q_{\max} values for the composites are lower than the alloy melts solidified under similar conditions. When $\text{SiC}_{(p)}$ is added to the alloy, the q_{\max} values get reduced with increasing weight percent of particles. The thermal conductivity and diffusivity of the composite melts are generally lower than the unreinforced melts due to the presence of low conducting dispersoid namely, silicon carbide.

As explained earlier, the presence of reinforcements affects the solidification rate of the composite system in two ways. When 5% graphite is introduced, the q_{\max} value is increased in sand mould [Figure 4.30 and 4.31], wherein not only the phenomenon I exists but also the higher thermal conductivity of graphite aids in increasing the peak heat flux values. The peak metal/mould interfacial temperature [Figure 4.32(a) and (b)] also reveals this. But in the case of 10% SiC reinforced composites, the q_{\max} value is lower than that of the alloy cast in all the three moulds, where in although both the phenomena are operative, but the phenomenon II is dominant.

Addition of 1% Mg to the base alloy increases the interface temperature due to the better casting/mould interface contact than the Al(356) base alloy [Figures 32(a-b)]. The addition of graphite particles to the matrix alloy improved the thermal conductivity of the system, thereby increasing the interfacial temperatures in steel and sand moulds.

4.4.3 Heat Treatment Characteristics

The evaluation of heat treatment characteristics by hardness measurement has shown that the composites exhibit an accelerated ageing. This phenomenon is due to the increase in dislocation density in the vicinity of the particles generated during the thermal stress (caused by the mismatch in the coefficient of thermal expansion between the matrix and reinforcement) and an elastic residual stresses field in the matrix around the reinforcement as a result of quenching, thereby resulting in more rapid and finer precipitation. In Al(356) alloy, Mg_2Si is the precipitation hardening phase formed. The higher dislocation density in the composites could also increase the solute diffusivity. This enhanced diffusivity of Mg atoms has been suggested [241] as the reason for the higher growth rate of Mg_2Si precipitates. Since dislocations are the favourable sites for the nucleation of the precipitates [241], finer precipitates are expected in the composites having a high dislocation density in the matrix. Furthermore, ageing is a process in which precipitate nucleates, grows and ripens simultaneously. The decrease in hardness after peak aging with increase in time is due to the precipitate coarsening.

4.4.4 Physical Properties

The deviation in the density values of the gravity and squeeze cast alloys and the composites compared to the theoretical values is due to the variation in the microstructure especially the porosity. One of the major problems associated with the stir casting process is the entrapment of air during the addition of particles. The air entrapment leads to the porosity formation reducing the density and other properties of the composites.

The structural variations of alloys and composites have a strong impact on the electrical conductivity. The increase in weight fraction of low conducting dispersoids reduces the electrical conductivity of the composites. The lower conductivity is exhibited by the composites having finer particles (23 μm APS) than coarser particles (118 μm APS). This is attributed to the increased surface area of the former leading to more scattering of electrons and hence more disturbance to the conductivity.

4.4.5 Mechanical Properties

The hardness values of both the alloys and composites have shown sharp increase on heat treatment due to precipitation hardening. The introduction of hard SiC particle has enhanced the hardness of the composites compared to the base alloy. However, the hybridization with soft graphite particle has reduced. The presence of porosity in the composite lowers the tensile strength. The compression strength of mono and hybrid composite are higher than those of the alloy. The synthetic graphite hybridization has resulted in lower compression strength than natural graphite due to its enhanced interfacial reaction. The synthetic graphite is partially graphitised compared to natural graphite as evidenced from the XRD structure.

4.5 SUMMARY

1. The mixed mode of particle addition during hybrid composite synthesis provides better dispersion of particles.
2. The natural graphite is more stable than synthetic graphite during heat treatment. The synthetic graphite becomes finer during mixing than natural graphite.
3. There is no remarkable interfacial reaction at the $\text{SiC}_{(p)}$ – matrix interface, except the formation of MgAl_2O_4 spinel due to the presence of SiO_2 layer over $\text{SiC}_{(p)}$.
4. Addition of both the SiC and graphite particles to the matrix has reduced the size of primary aluminum and eutectic silicon phases compared to the base alloy.
5. Fine dendritic cell size obtained in squeeze cast composite ingots aids in better distribution of particles in the matrix than gravity casting. However, few particle clusters are observed in both mono and hybrid composites.

6. The hindered settling phenomena experienced in hybrid composites due to the presence of low-density graphite and high density $\text{SiC}_{(p)}$ leads to improved distribution of reinforcements.
7. Introduction of both the silicon carbide and the graphite reinforcements into the Al(356) matrix alloy reduces the liquidus temperature.
8. Addition of ceramic reinforcement to alloy reduces the total solidification time and eutectic solidification time of the composite cast in sand, steel and graphite moulds at lower weight fraction and increases at higher weight fraction.
9. Cooling rate of Al(356) alloy increases with the introduction of $\text{SiC}_{(p)}$ and reaches a maximum at 12.5 wt% $\text{SiC}_{(p)}$ and then decreases with further increase in $\text{SiC}_{(p)}$.
10. The graphite mould shows a higher peak heat flux value than steel and sand moulds due to the higher thermal conductivity of graphite.
11. Incorporation of additional Mg to the composite melt has multifunction. Apart from its well-known function as a wetting promoter of ceramic particle with the aluminium alloy matrix, it results in better contact at the metal/mould interface, thereby by enhancing heat transfer rate.
12. The addition of graphite particles to the alloy matrix enhances the effective thermal conductivity of the composite system, whereas silicon carbide particles reduces it.
13. Accelerated ageing is observed in both mono and hybrid composites.
14. The addition of particles lowered the electrical conductivity of composites, the coarser particles provide higher electrical conductivity than finer particles.
15. The hardness of composite increases with the introduction of SiC particles and decreases with graphite particle hybridization.
16. The compressive strengths of mono and hybrid composite are higher than that of the matrix alloy. The synthetic graphite hybridization provides lower compression strength than natural graphite.

CHAPTER 5

Al(356)-SiC_(p)-C_(sf) MONO AND HYBRID COMPOSITES

5.1 INTRODUCTION

Metal matrix composites reinforced with short fibres have been used for industrial applications mainly as a structural material owing to their ease of fabrication, relatively low cost and better isotropic properties than continuous fibre reinforced composites. The short fibre reinforced composites have the advantages of both continuous fibre and particulate reinforced composites namely of superior mechanical properties of fibre composite and easier fabricability of particulate composite. The carbon short fibre reinforced metal matrix composites are used for making various components for automotive, aerospace and electronic applications.

Carbon fibres are low density reinforcements existing in both crystalline and amorphous forms. Carbon fibres of extremely high modulus are made by carbonisation of organic precursor fibre followed by graphitisation at high temperature. The organic precursor fibres are generally textile polymeric fibres, which can be carbonised without melting. The commonly used precursor fibres are polyacrylonitrile (PAN), rayon and other fibres made from pitches, polyvinyl chloride, polyimides and phenolics. Pitch based fibres are used in the present study. Pitch based carbon fibres are attractive because of the cheap raw material, high yield of carbon and a highly oriented carbon that is obtained from mesophase pitch precursor fibre. The common sources of pitch are poly vinyl chloride, petroleum asphalt and coal tar.

The objectives of the present study are to synthesise Al-C_(sf) mono and Al-SiC_(p)-C_(sf) hybrid composites and evaluate the effect of processing parameters on the structure and properties of the composites.

5.2 METHODOLOGY

The matrix alloy used is cast aluminium-silicon-magnesium (356) alloy. The chemical composition and properties of the matrix alloy are given in Table 3.1 and 3.2 respectively. The reinforcement materials used are silicon carbide particles of 23 μm APS and pitch based chopped carbon short fibres of 1mm length and 0.7 μm diameter. The thermophysical properties of the reinforcements are described in Section 3.3.

The pre-treatment of $\text{SiC}_{(p)}$ is described in section 4.2. In the case of carbon short fibre, various treatments such as pre-heat treatment at different temperatures, treating the fibre in aqueous media, acetone media and sodium silicate solution with controlled pH in the range of 4-5 are attempted to separate the fibres from the bunches. After these treatments, settling studies have been carried out to assess the efficiency of separation by observing the fibres in the dried condition. The fibres dispersed in different media such as acetone, water and 0.02% sodium silicate aqueous solution maintained at pH 4-5 using ultrasonic vibration and poured into a measuring jar and the height of the fibre column is measured at different settling times.

The details of composites fabrication by liquid metal stir casting technique is described in Section 4.2. In the present studies, the stirring speed is kept in the range of 700-750 rpm during SiC addition and around 650 rpm during carbon fibre addition. The SiC is added first and followed by the carbon fibre addition. The premixing of fibre and particulates before its introduction leads to agglomeration. The gravity casting in permanent mould has been adopted for shaping. The specimens for structural analysis and mechanical characterisation are prepared from the as cast billets. The structural, solidification, physical and mechanical characteristics of the alloys and composites fabricated are evaluated using different testing methods described in Chapter 3.

The composite systems fabricated are Al (356)-15% SiC_(p) and Al(356)-3% C_(sf) mono composites and Al (356)-15% SiC_(p)-3% C_(sf) hybrid composite. The details on various aspects of Al (356)-15% SiC_(p) mono composite are discussed in Chapter 4.

5.3 RESULTS

Figure 5.1 shows the SEM photomicrographs of as received and surface treated carbon short fibres. The as-received carbon short fibres are in agglomerated bunches. In order to disperse these carbon short fibres into aluminium alloy matrix, they require deflocculation. The fibres are at first preheated at 400°C for 15 minutes to remove the polymeric coating over their surface applied during sizing. The preheated fibres are washed in acetone coupled with ultrasonic vibration to remove stains of the polymeric coating and other foreign particles sticking to the surface. The fibres are then treated with sodium silicate solution coupled with ultrasonic vibration and then dried in an oven. The surface treated fibres are well deflocculated and cleaned [Figure 5.1 (c) and (d)]. Figure 5.2 shows the relation between the settling time versus the volume of the fibre column. The fibres dispersed in acetone settle quickly while those in sodium silicate take longer time for settling. This shows that the sodium silicate deflocculates the fibres very well than both in acetone and water.

The X-ray diffraction pattern of the carbon fibres given in Figure 5.3 shows that the carbon fibres are in the amorphous state.

5.3.1 Optical Microstructures and Image Analysis

Figure 5.4 shows the optical photomicrographs of Al(356)-3% C_(sf) mono composite. The fibres are well dispersed in the metal matrix with random orientation and tend to break during mixing. The primary phase does not show any nucleation on the surface of the fibres. Fibres are seen in the eutectic region of the matrix. Fine eutectic silicon phases are observed near to the surface of the fibre. Iron intermetallics are observed in the matrix.

Optical microstructure of Al (356)-15% SiC_(p)-3% C_(sf) hybrid composite is shown in Figure 5.5. The silicon carbide and carbon fibre are well separated and distributed in the matrix. The dispersion of SiC_(p) and C_(sf) are better than their respective mono composites [Figure 4.4 and 5.4(a)]. However, the problems associated with the fibres are severe breakage due to the presence of SiC particles. Figures 5.6(a) and (b) show the optical photomicrographs of mono and hybrid composites which have been used for measuring the features using the image analyser. In the former, long and randomly oriented fibres are observed, whereas in the latter, the fibres are broken into fibres of smaller length as observed in Figure 5.6(b).

5.3.2 SEM Microstructures and EDS Analysis

Figures 5.7(a) and (b) show SEM photomicrographs of Al(356)-3% C_(sf) mono composite revealing the interface reaction. The precipitation of eutectic silicon and very fine reaction products on the surface of the carbon fibre are seen in Figure 5.7(b). Figures 5.8(a-c) show the SEM photomicrographs of Al(356)-15% SiC_(p)-3% C_(sf) hybrid composites. The distribution of angular shaped SiC particle and dark black circular shaped carbon short fibres oriented in the longitudinal direction of the polished surface are seen. The edges of the SiC particle reveal no remarkable reaction [Figure 5.8(b)] and the matrix-SiC interface is clean from any reaction product except the presence of large eutectic silicon phase near the interface. However, the matrix-carbon fibre interface [Figure 5.8 (c)] shows very fine reaction products arising out of the reaction of fibre with the matrix.

SEM photomicrographs of Al(356)-3% C_(sf) mono composite [Figure 5.9] show a single carbon fibre oriented in (a) lateral and (b) longitudinal direction of the ingot revealing presence of very fine white precipitates on the surface of the carbon fibre [Figure 5.9(a)]. The EDS analysis has shown that the white precipitates are mostly alumina and the elongated phase in Figure 5.9(b) is found to be eutectic silicon phase.

Figure 5.10 shows the EDS elemental X-ray mapping of Al(356)-3% C_(sf) monocomposite. The SEM image of a location in the composite and the elemental X-

Figure 5.10 (a)-(f) respectively. The elemental mapping of carbon shows its rich content in the area of the fibre [Figure 5.10(b)]. However, higher oxygen content is observed around the fibre as seen in oxygen elemental map [Figure 5.10(c)]. This assists oxide formation around the fibre. Magnesium is present uniformly through out [Figure 5.10(d)]. X-ray elemental mapping of aluminium shows that its intensity is very high in the primary aluminium phase region, lower in the eutectic silicon region and almost nil in the carbon fibre region [Figure 5.10(e)]. However, compared to the area of carbon fibre in the Figure 5.10(a), it is smaller in the Al elemental map [Figure 5.10(e)], showing the presence of Al on the edges of the fibre. This also supports the possibility of presence of the aluminium oxide on the edges of fibre. Silicon map [Figure 5.10(f)] shows that it is rich in eutectic region compared to the α -phase region.

EDS line scan of Al(356)-3% $C_{(sf)}$ mono composite is given in Figure 5.11. The two peaks with high intensity observed in carbon line scan correspond to the carbon fibre. The oxygen line scan shows that the fibre interface is rich in oxygen. Similarly, the intensity of Mg is high at the matrix area near to the fibre. The aluminium intensity is very low in the fibre region compared to the α -phase showing very high intensity. The intensity of silicon is very high at the eutectic silicon region.

Figure 5.12 shows the EDS elemental X-ray dot mapping of Al(356)-15% $SiC_{(p)}$ -3% $C_{(sf)}$ hybrid composites. Secondary electron image of hybrid composite is given in Figure 5.12(a) and the respective X-ray elemental mapping of carbon, oxygen, Mg, Al and silicon are given in Figure 5.12(b)-(f). The elemental X-ray mapping of carbon shows a high intensity in the carbon fibre region [Figure 5.12(b)]. In the case of oxygen mapping, its intensity is less in the reinforcement region whereas the carbon fibre-matrix interface region shows the high intensity [Figure 5.12(c)]. Magnesium mapping shows its presence through out the matrix with comparatively less amount in the reinforcement region [Figure 5.12(d)]. The elemental X-ray mapping of Al shows very high intensity in the α – phase region and low intensity in the eutectic region of the matrix [Figure 5.12(e)]. The interface region between carbon fibre and matrix also shows less intensity of Al. The regions where silicon carbide particle and carbon fibre are present are seen as dark region, which are

free from white X-ray spots corresponding to Al. However, the dark region corresponding to carbon fiber is smaller than the original area of carbon fiber in the Figure 5.12(a). This shows that the interface region of carbon fiber contains aluminium and also the Al has penetrated into the fibre region, probably due to the reaction. The elemental X-ray mapping of Si shows high intensity in the SiC particle region and eutectic silicon region.

The EDS line scan of Al(356)-15%SiC_(p)-3%C_(sf) hybrid composite is given in Figure 5.13. The line scan of carbon shows two high intensity peaks corresponding to the carbon fibre area. In the case of oxygen line scan, the intensity is high at the interface region of the carbon fibre and the matrix, which is similar to that observed in the elemental X-ray mapping of mono- and the hybrid-composite. Also two narrow peaks of oxygen corresponding to the two sides of the SiC_(p) – matrix interface are observed. The line scan of Mg shows few high intensity peaks in the matrix and interface region. The aluminium line scan gives high intensity peaks corresponding to the matrix region and no signals are observed in the SiC_(p) and C_(sf) area. The Si peaks are observed in the region of SiC, eutectic silicon and Mg₂Si precipitates. The above observations reveal the presence of alumina at the carbon fibre- matrix interface. Similarly, the presence of peaks corresponding to oxygen, magnesium and aluminium at the SiC_(p)-matrix interface show the existence of a fine layer of MgO or MgAl₂O₄.

Figure 5.14 shows the EDS spectra of Al(356)-15%SiC_(p)-3% C_(sf) composite showing (a) spectrum of over all microstructure constituting the matrix and reinforcement, (b) the spectrum of SiC particle and (c) the spectrum of carbon short fibre. The spectrum of overall structure gives peaks corresponding to Al, Si, Mg, C and O. The X-ray signal of the aluminium is mainly from the matrix and little contribution from alumina observed in the carbon fibre matrix interface and the MgAl₂O₄ spinel phase. The characteristic X-ray peak of silicon is contributed by the eutectic silicon phase present in the matrix, Si from the silicon carbide particle and of the Mg₂Si phase. The low intensity peak of Mg is contributed by the magnesium from the matrix and the phases like MgAl₂O₄ and Mg₂Si. The characteristic oxygen signal is contributed by the alumina and spinel phases formed due to the interfacial reactions. The spectra of carbon fibre shows very high intensity peak of carbon from

the fibre and very mild signal of Al, Mg and Si. Similarly, the spectrum taken from SiC particle shows characteristic peaks of high intensity Si and low intensity carbon.

The atomic force microscopic (AFM) structures of Al(356)-15% SiC_(p) -3% C_(sf) hybrid composite is shown in Figure 5.15. The AFM structure gives the surface morphology of the composite specimen with respect to the variation in the level of different phases on the surface under examination. The structure shows angular shaped light patches which correspond to the SiC particles. As the SiC particles are very hard and during specimen preparation the polishing leads to wear of matrix phase quickly leaving the SiC particles projecting outward from the matrix. The variation in the depth can be compared from the colour scale given. Similarly the carbon fibres are also observed on the surface as small spherical or oval shaped phases as these fibres are oriented horizontally to the polished surface. However, much detail on the interfacial behaviour could not be derived from the structures.

5.3.3 Ageing Behaviour

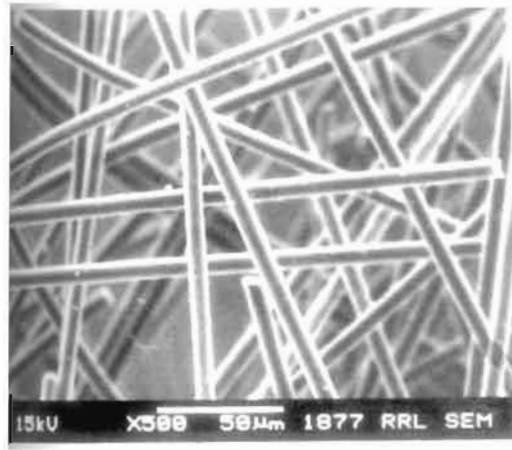
The Figure 5.16 shows the ageing curve of Al(356) base alloy, Al(356)-15% SiC mono composite and Al(356)-15% SiC_(p) -3% C_(sf) hybrid composite. The graph shows the variation in hardness with respect to the ageing time. The specimens are solutionised at 535 °C for 12 hrs, quenched in hot water and subjected to ageing studies. The peak age hardness of composites is higher than that of the base alloy due to the contribution from the reinforcements. The composites have shown accelerated ageing compared to the base alloy and the overaging starts early in composites. However, in hybrid composites, two steps of hardness increase is observed.

5.3.4 Density

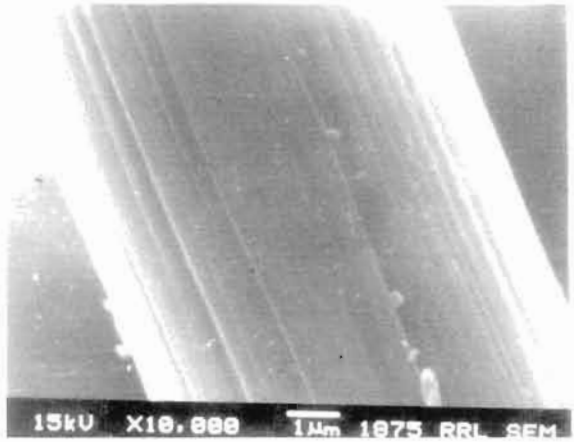
Figure 5.17 shows the theoretical (ROM) and measured densities of the base alloy, and the mono and the hybrid composites. In all the cases, the measured density values are lower than the theoretical values. This could be attributed to the presence of porosity formed during processing. In the case of composite, the variation in density is large because the additional porosity is formed due to the air entrapment during MMC synthesis involving stirring.

5.3.5 Mechanical Characteristics

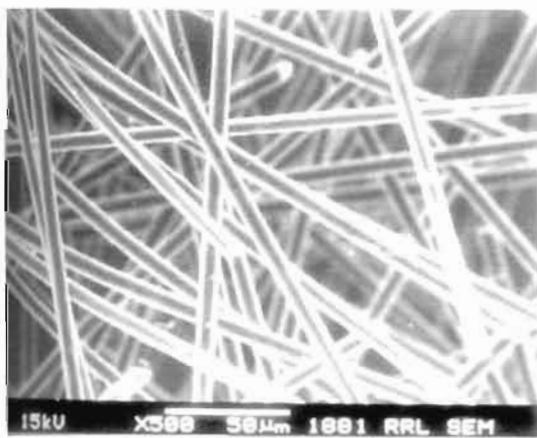
The Brinell hardness values of the as cast and peak aged base alloy, the mono and the hybrid composites are shown in Figure 5.18. The hybrid composite shows higher hardness values of 81 BHN (as cast) and 128 BHN (aged) compared to the mono composite and base alloy. The higher hardness is due to the effect of the $\text{SiC}_{(p)}$ reinforcement and the hard and brittle reaction products formed. The tensile strength of hybrid composite has shown lower values due to the presence of porosity, degradation of fibre due to the high interfacial reaction and the breakage of fibres. The compression strengths of the base alloy, the mono and the hybrid composites are shown in Figure 5.19. The compression strength of Al(356)-15% $\text{SiC}_{(p)}$ mono composite is higher than that of the base alloy, with hybrid composite exhibiting a value lower than that of the mono composite and closer to the base alloy.



(a)



(b)



(c)



(d)

Figure 5.1: SEM photomicrographs of (a) and (b) as received and (c) and (d) surface treated carbon fibres.

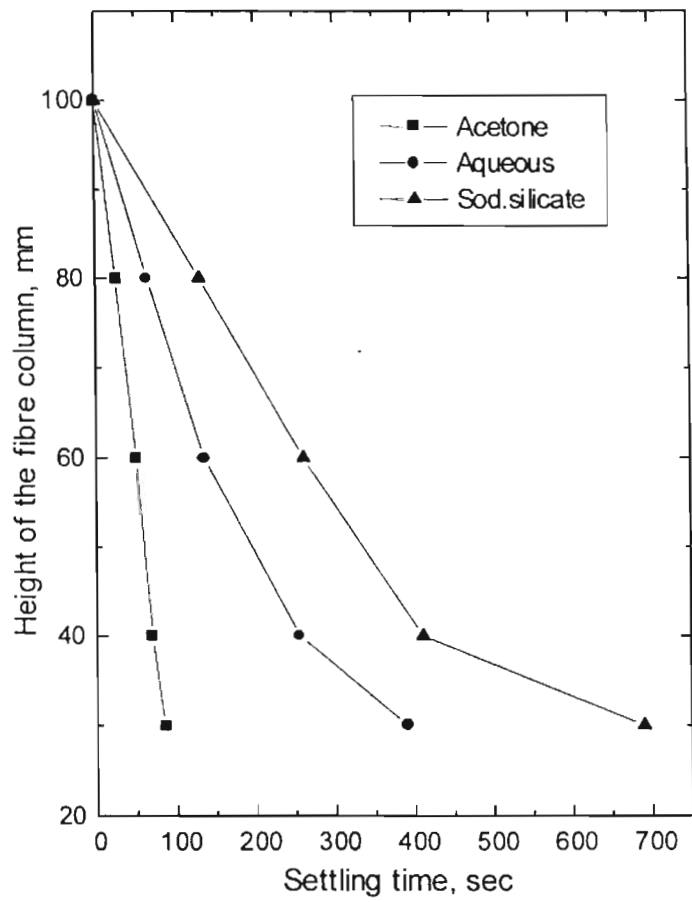


Figure 5.2: *Variation of the height of the carbon fibre column with settling time in different treatments.*

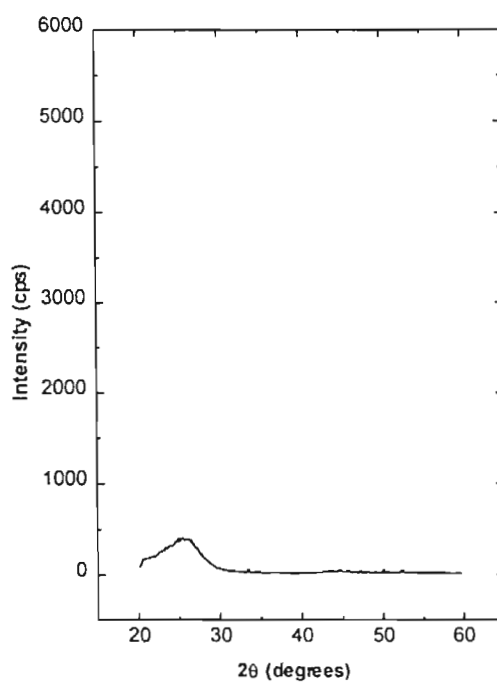


Figure 5.3: *X-ray diffraction pattern of carbon fibre.*

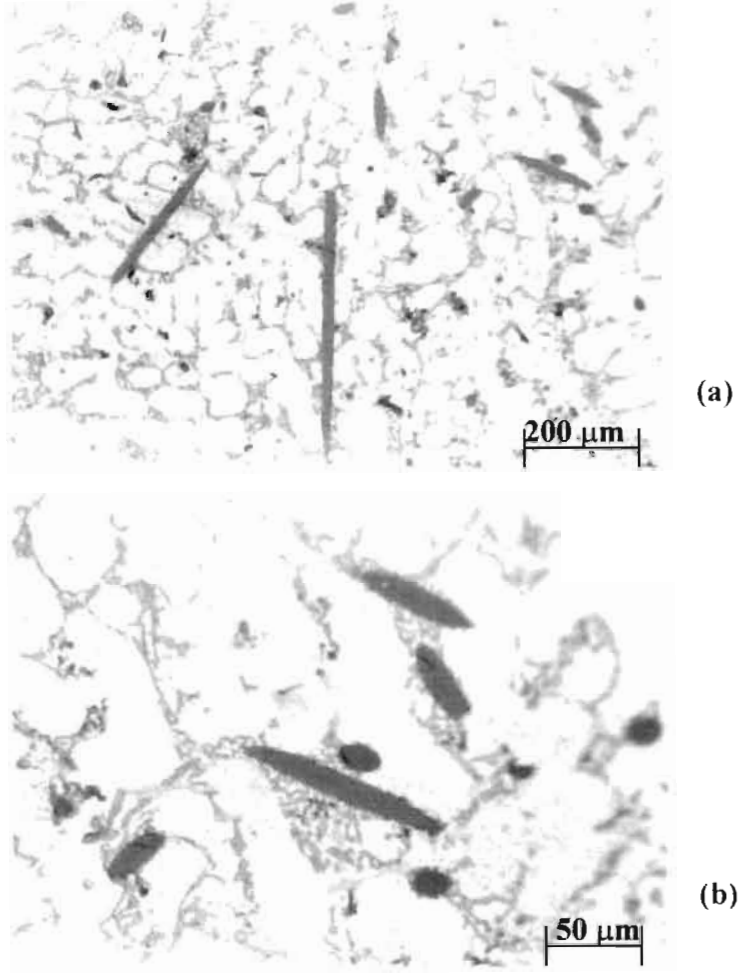


Figure 5.4: *Photomicrographs of Al(356)-3% C_(sf) mono composite*

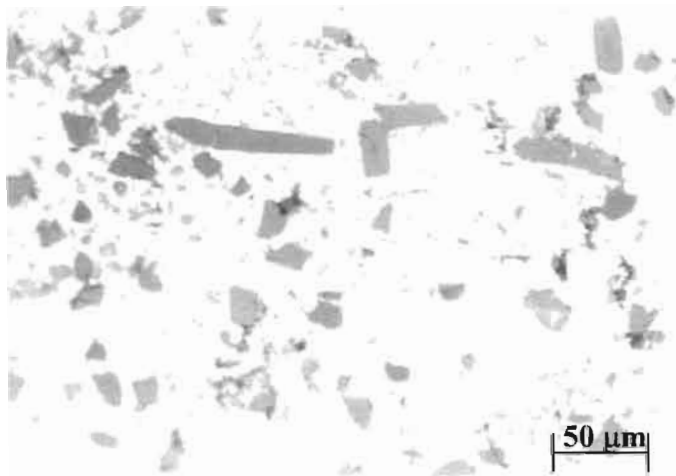
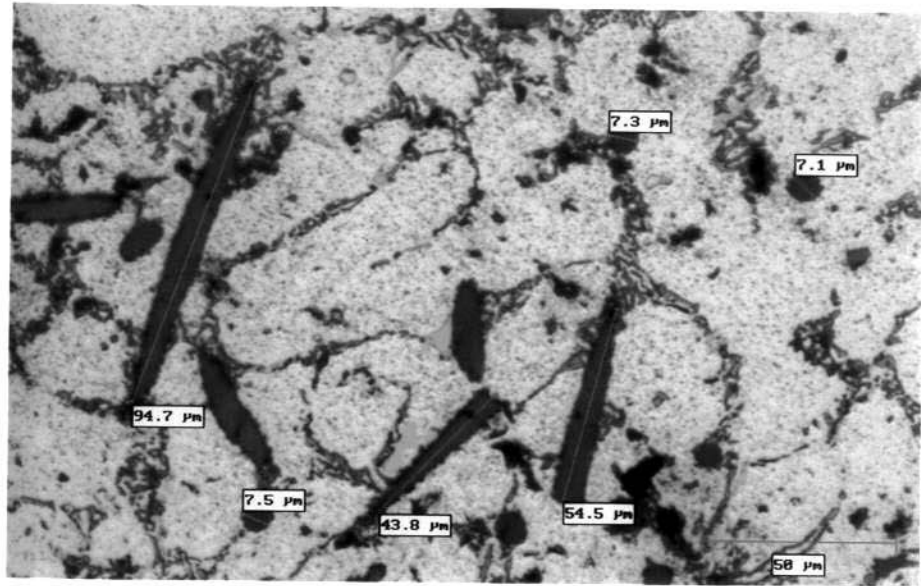
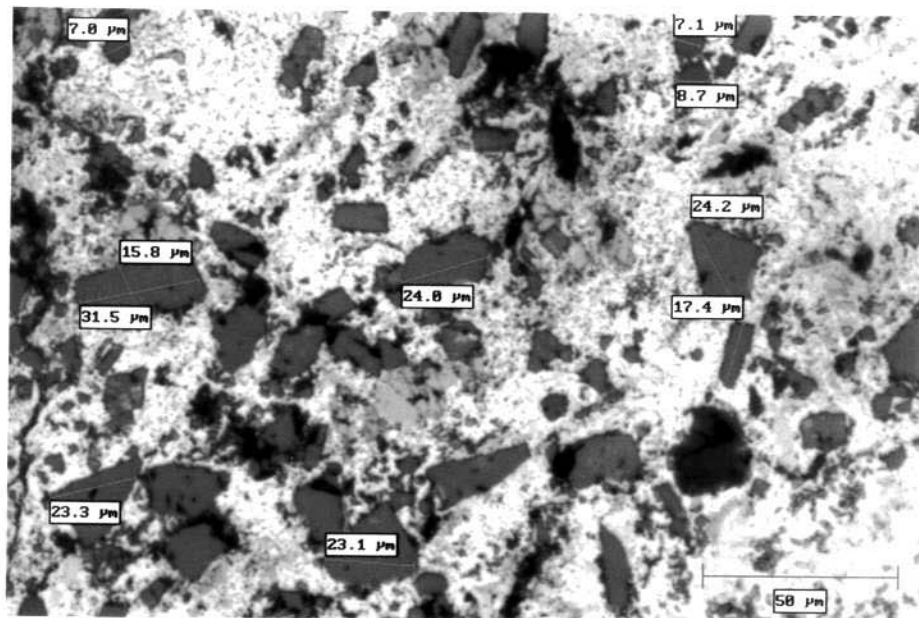


Figure 5.5: *Photomicrograph of Al(356)-15% SiC_(p)-3% C_(sf) hybrid composite*

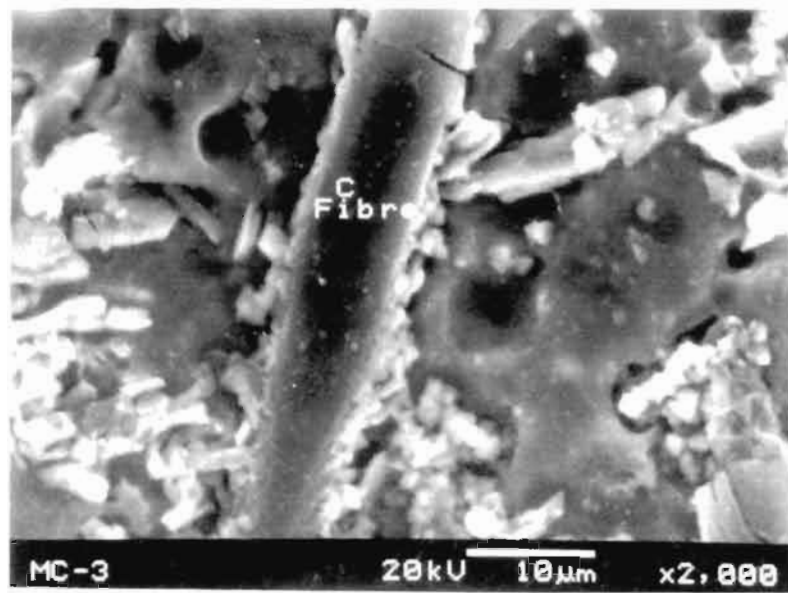


(a)

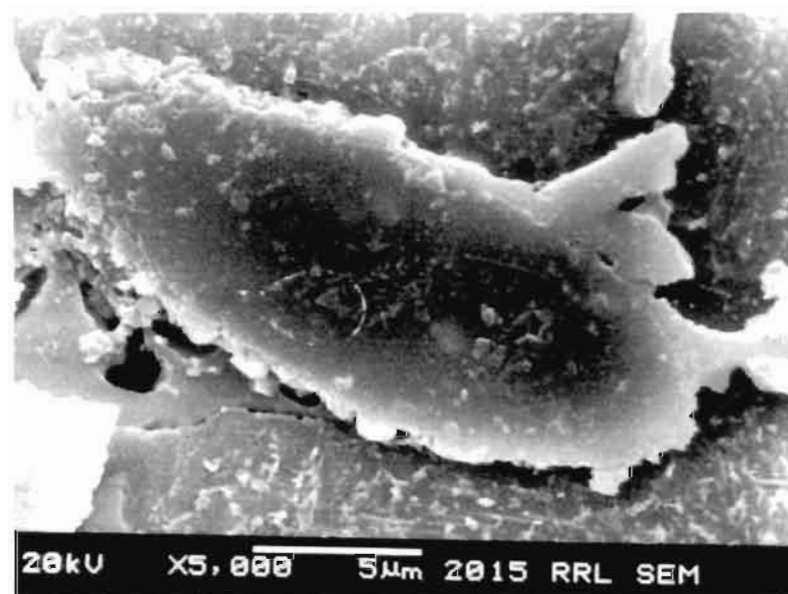


(b)

Figure 5.6: Photomicrographs of (a) Al(356)-3% $C_{(sf)}$ mono composite and (b) Al(356)-15% $SiC_{(p)}$ -3% $C_{(sf)}$ hybrid composite from image analyser.

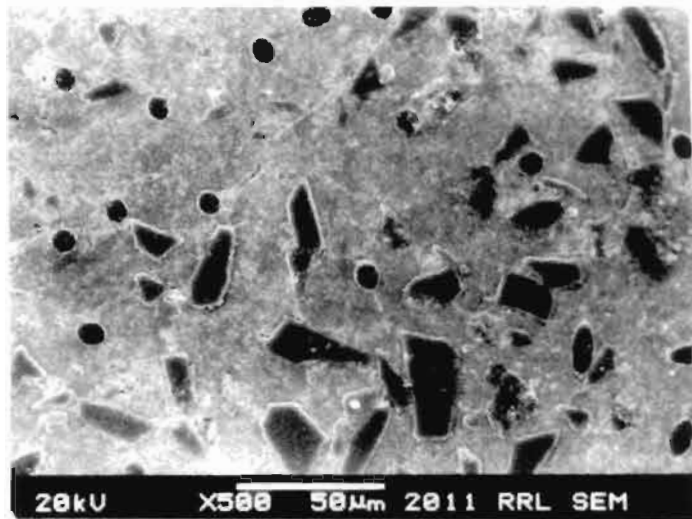


(a)

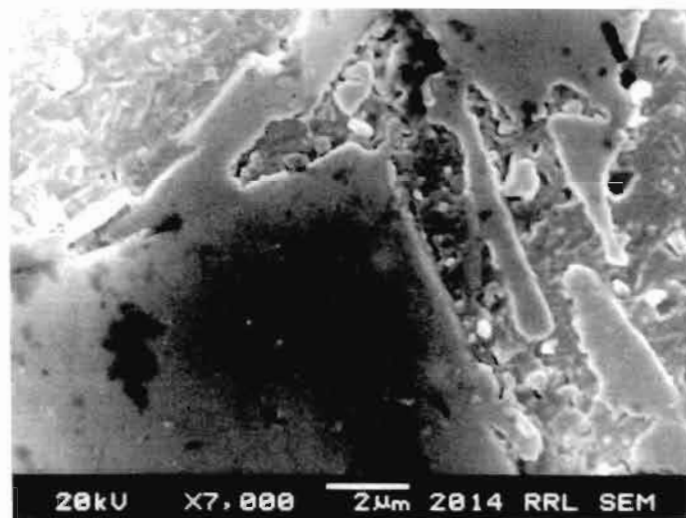


(b)

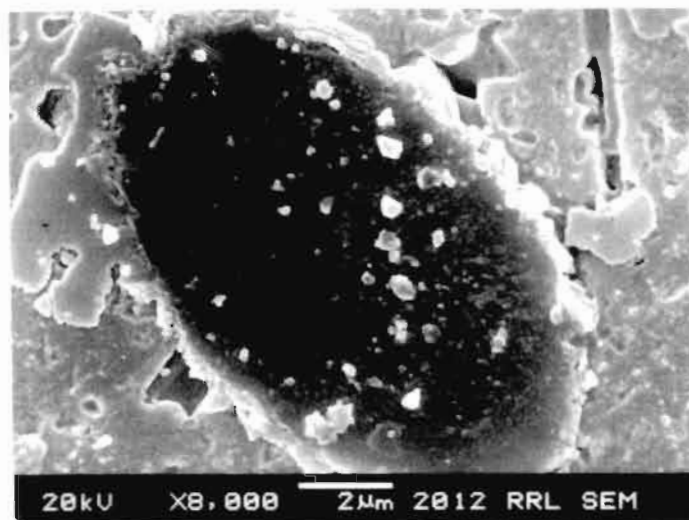
Figure 5.7: SEM photomicrographs of Al(356)-3% $C_{(sf)}$ mono composite



(a)

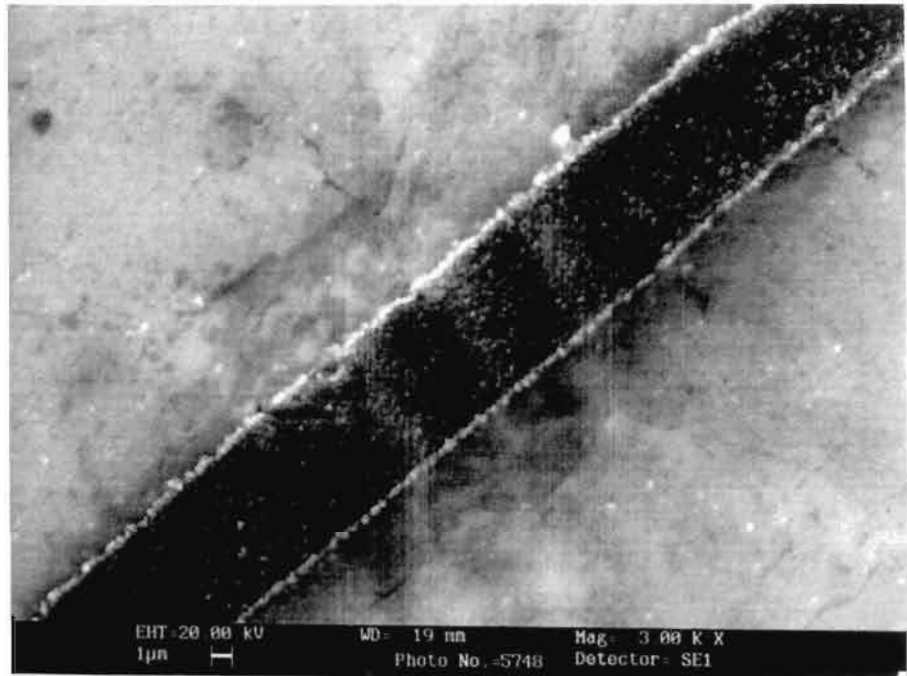


(b)

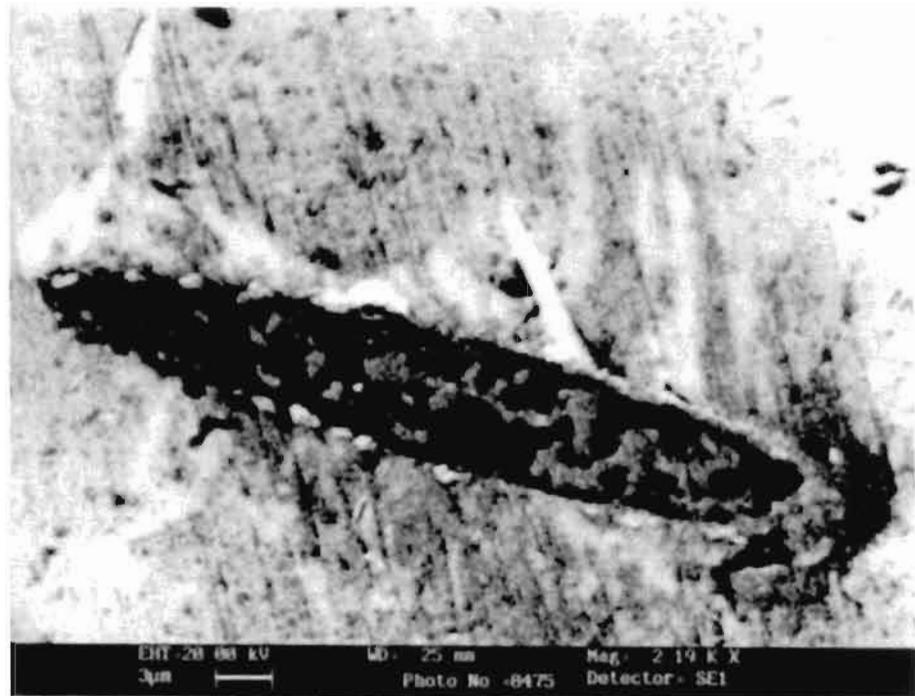


(c)

Figure 5.8: SEM photomicrographs of Al(356)-15% SiC_(p)-3% C_(sf) hybrid composite



(a)



(b)

Figure 5.9: SEM photomicrographs of Al(356)-3% C_(sf) mono composite showing a single carbon fibre oriented in (a) lateral and (b) longitudinal direction with respect to the ingot.

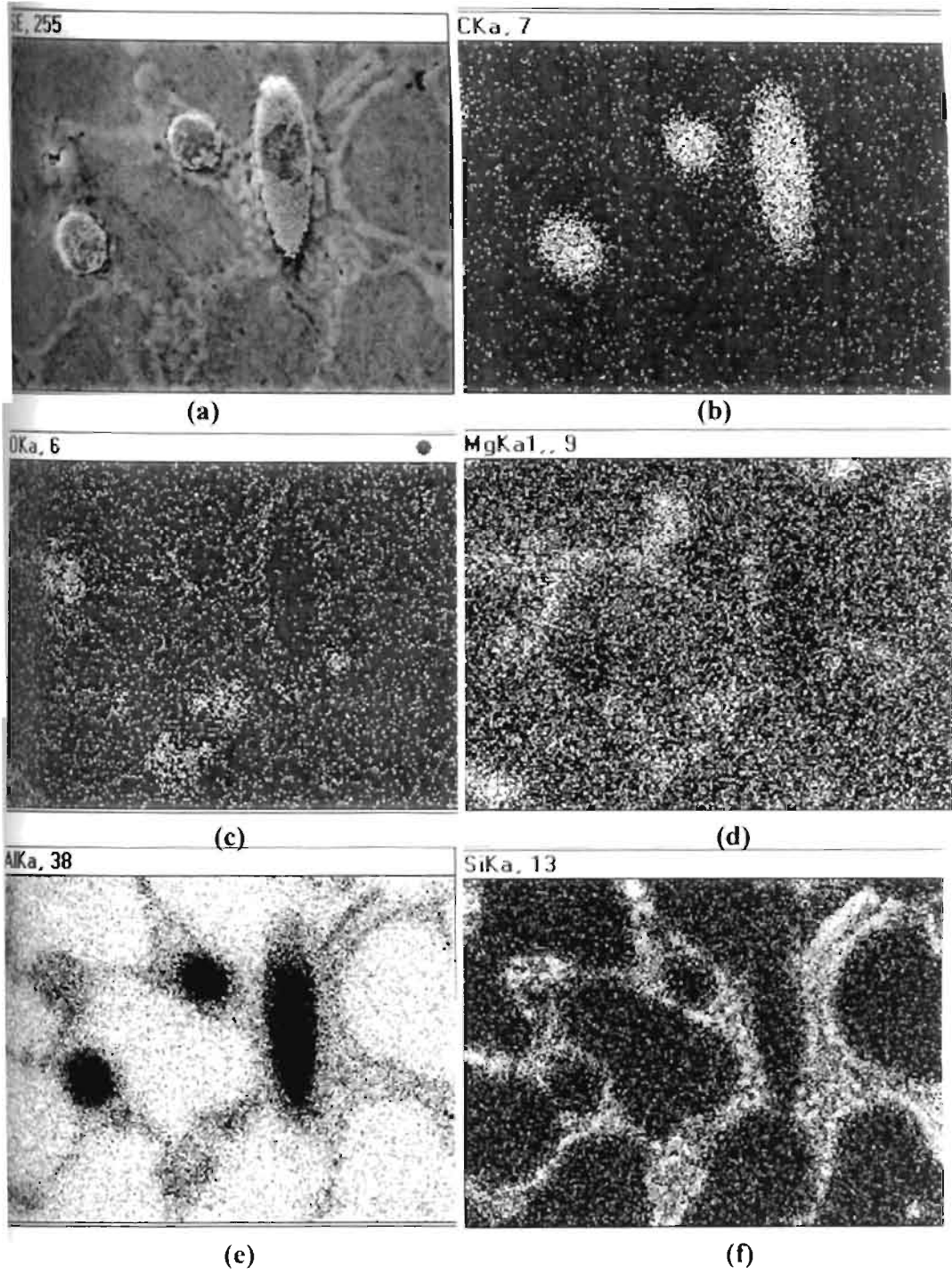


Figure 5.10: EDS X-ray elemental mapping of Al (356)-3% C_(sf) mono composite

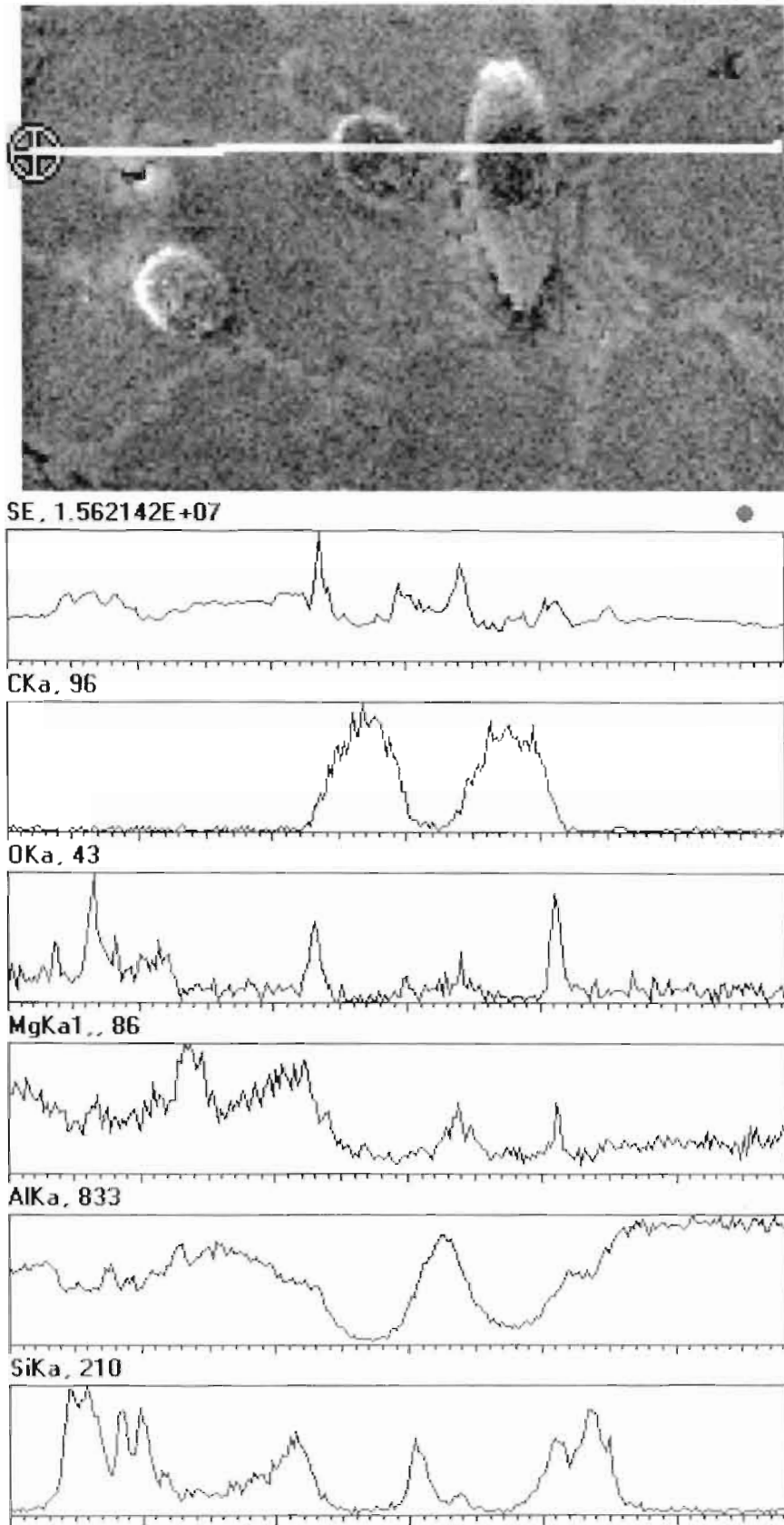


Figure 5.11: EDS line scan of Al(356)-3% C_(sf) mono composite

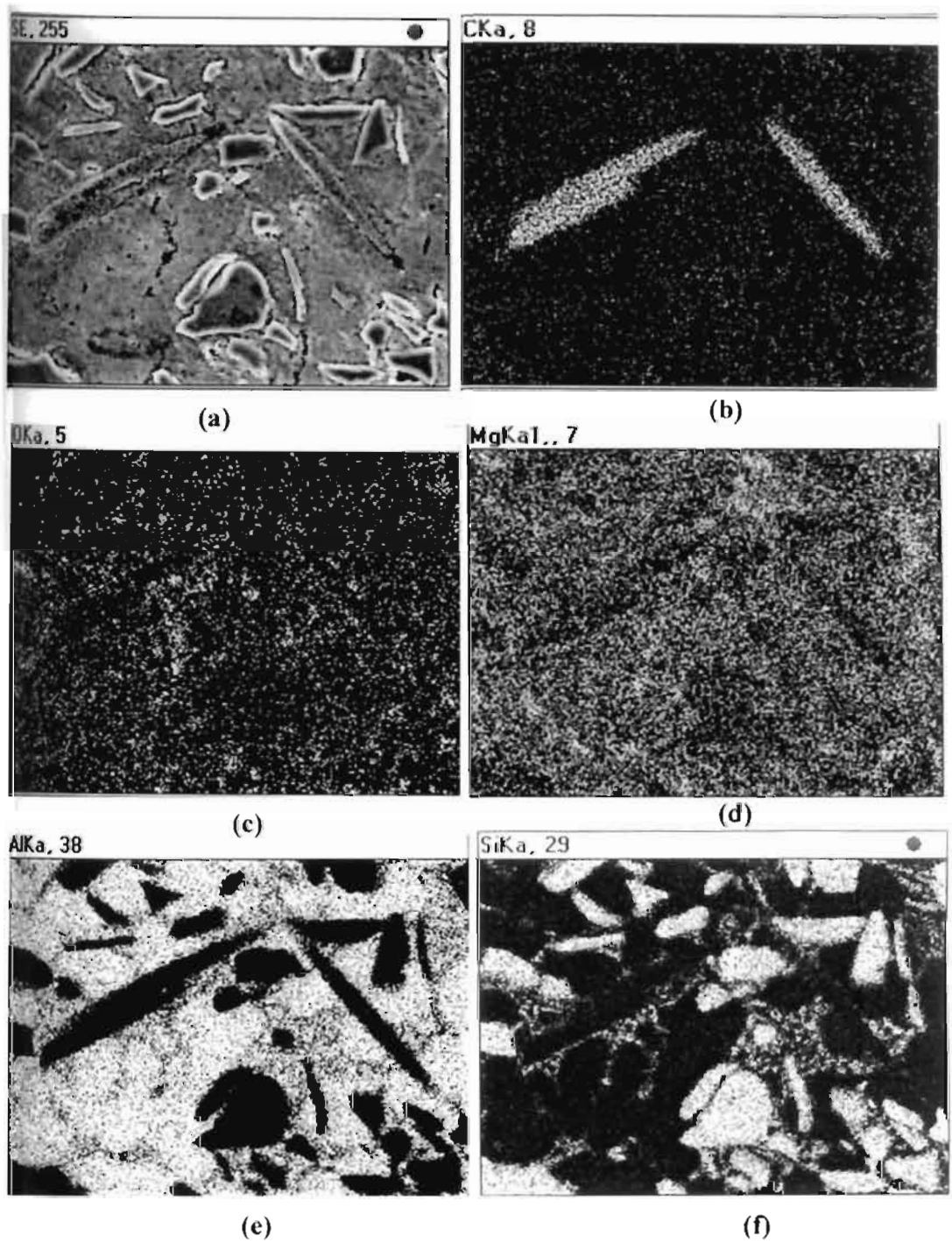


Figure 5.12: EDS elemental X-ray mapping of Al(356)-15% SiC_(p)-3% C_(sf) hybrid composite

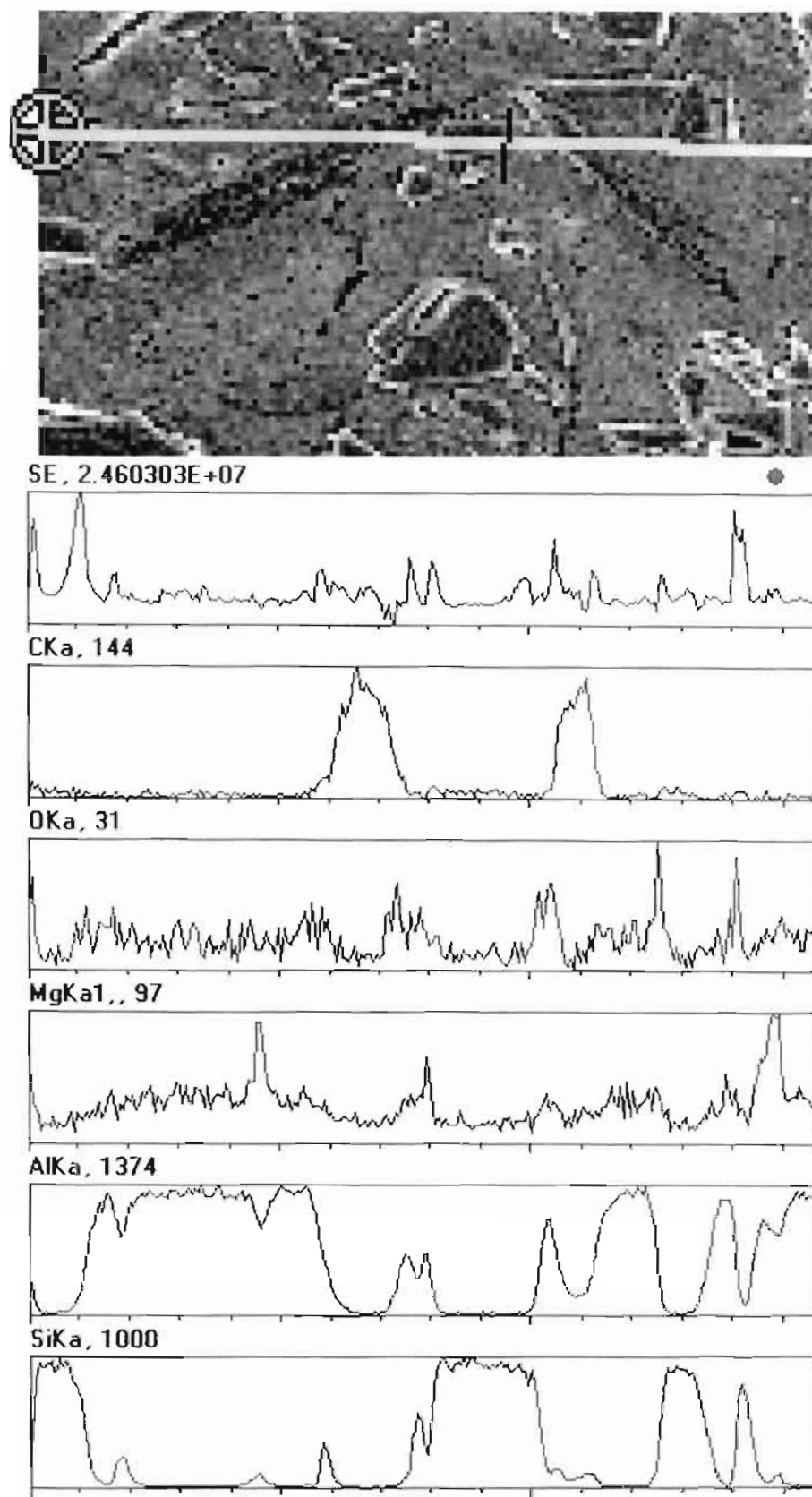
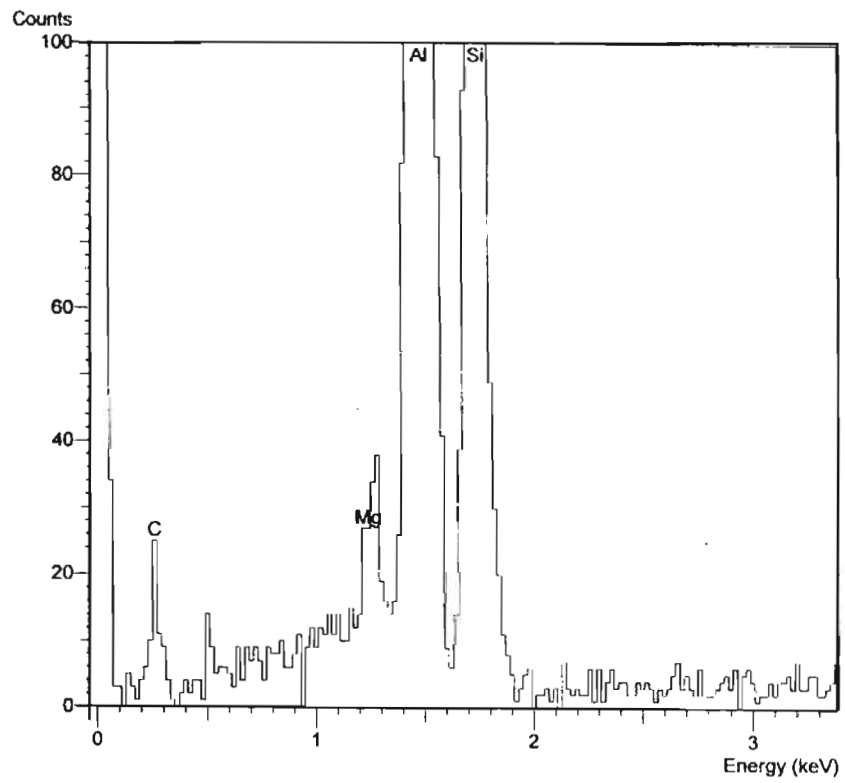
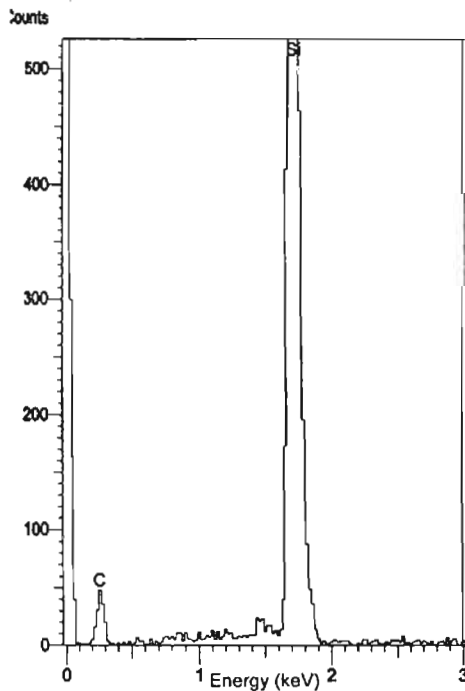


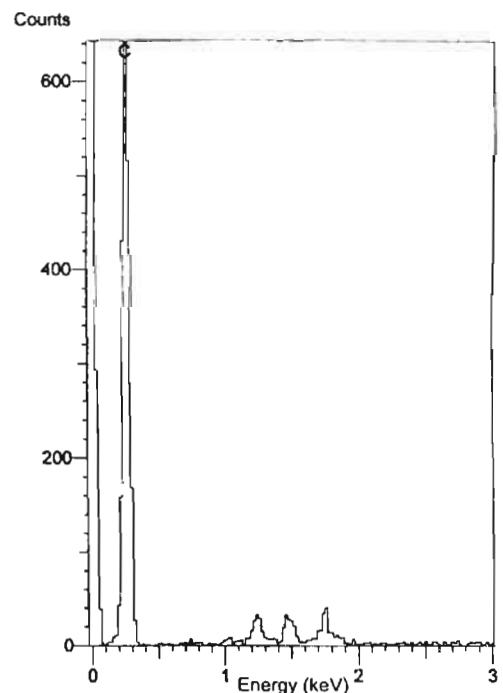
Figure 5.13: EDS line scan of Al(356)-15% SiC_(p)-3% C_(sf) hybrid composite



(a)

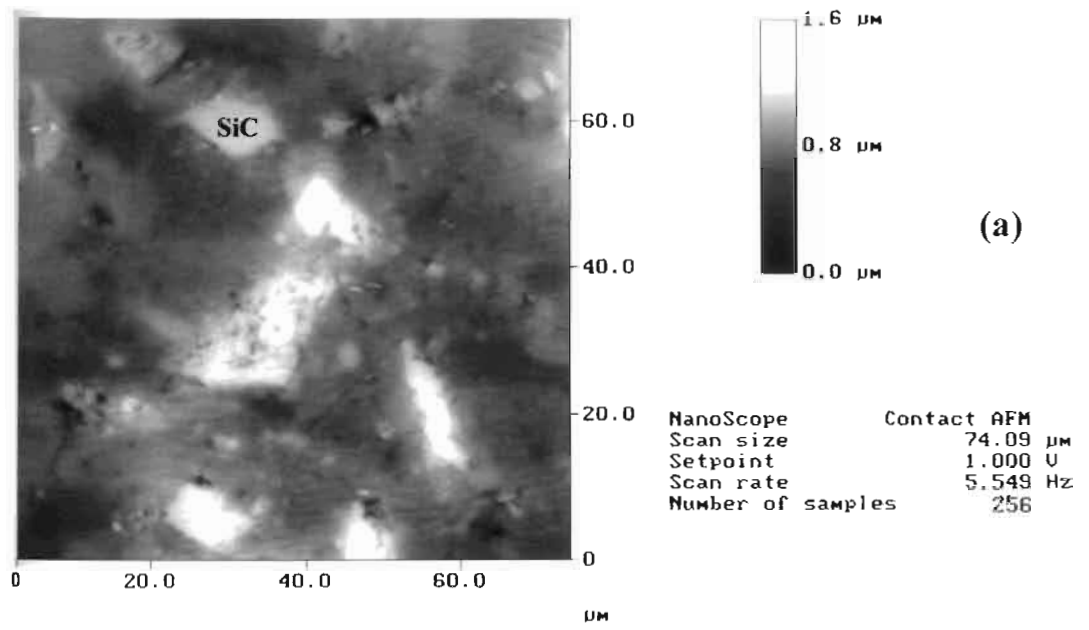


(b)



(c)

Figure 5.14: EDS spectra of Al(356)-15% SiC_(p)-3% C_(sf) hybrid composite (a) overall matrix, (b) SiC particle in the matrix and (c) carbon short fibre in the matrix.



rr13-01

Rr13-01a

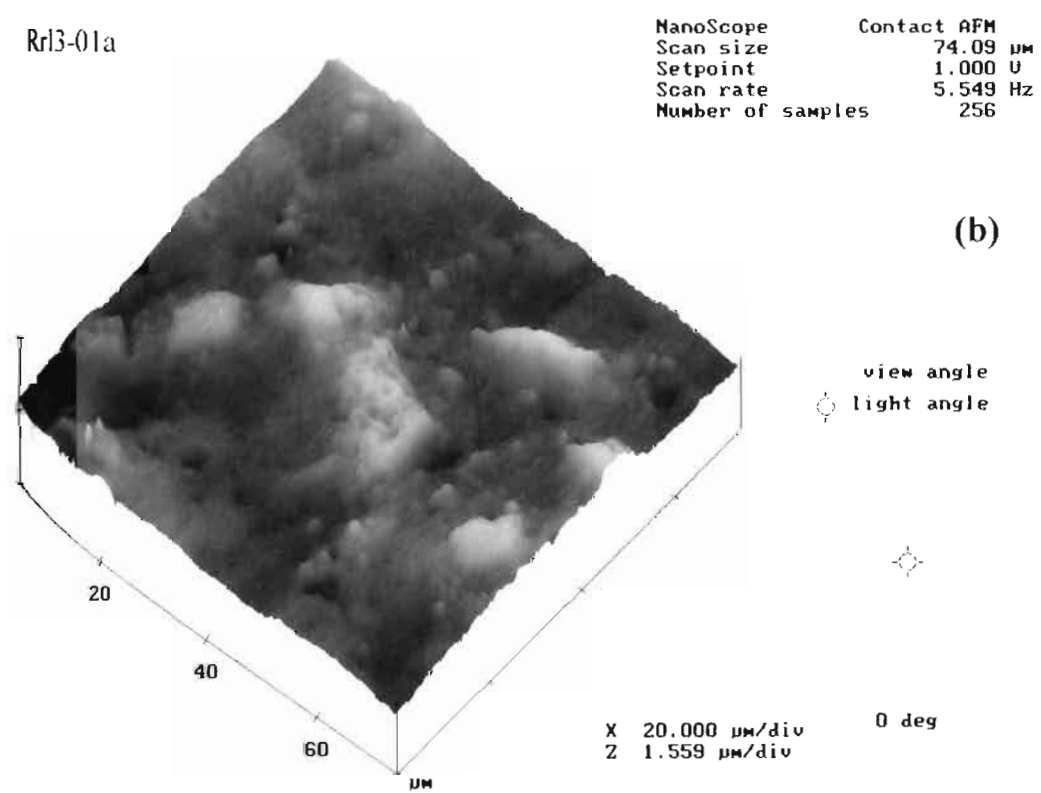


Figure 5.15: Atomic Force Microscopic structures of Al(356)-15% SiC_(p)-3% C_(sf) hybrid composite

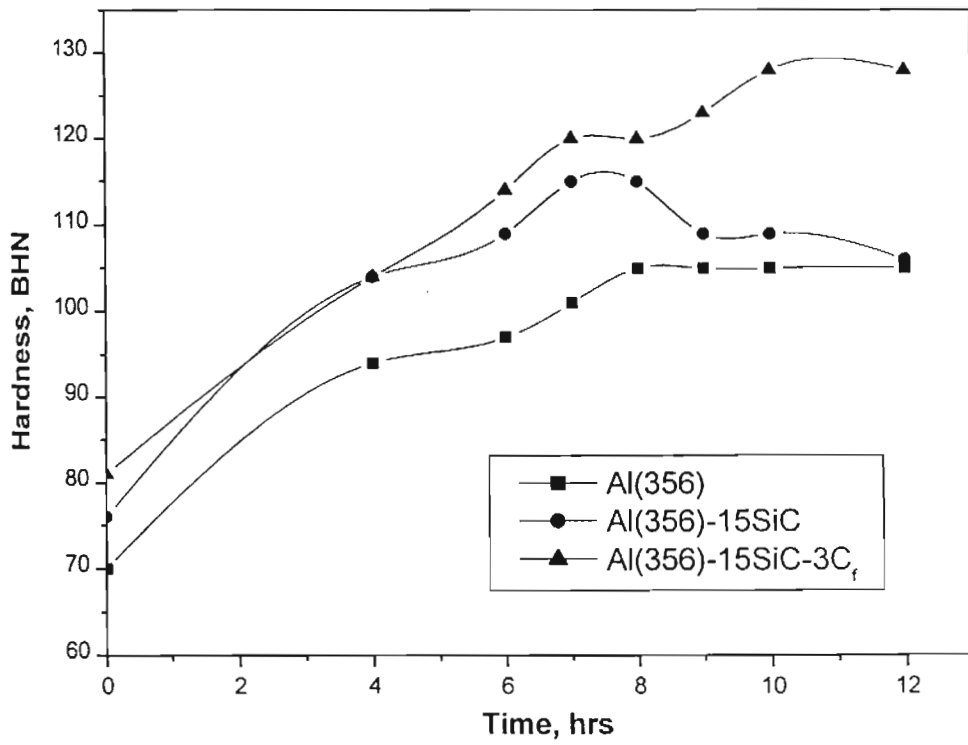


Figure 5.16: Ageing characteristics of alloy and composites with respect to hardness measurements.

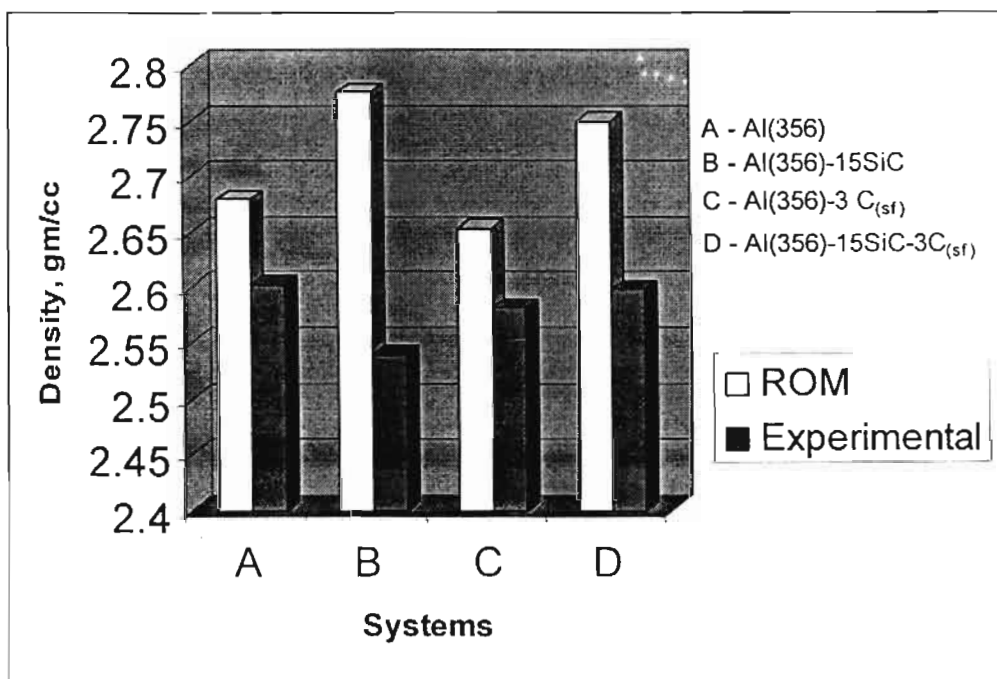


Figure 5.17: Density of base alloy and composite systems

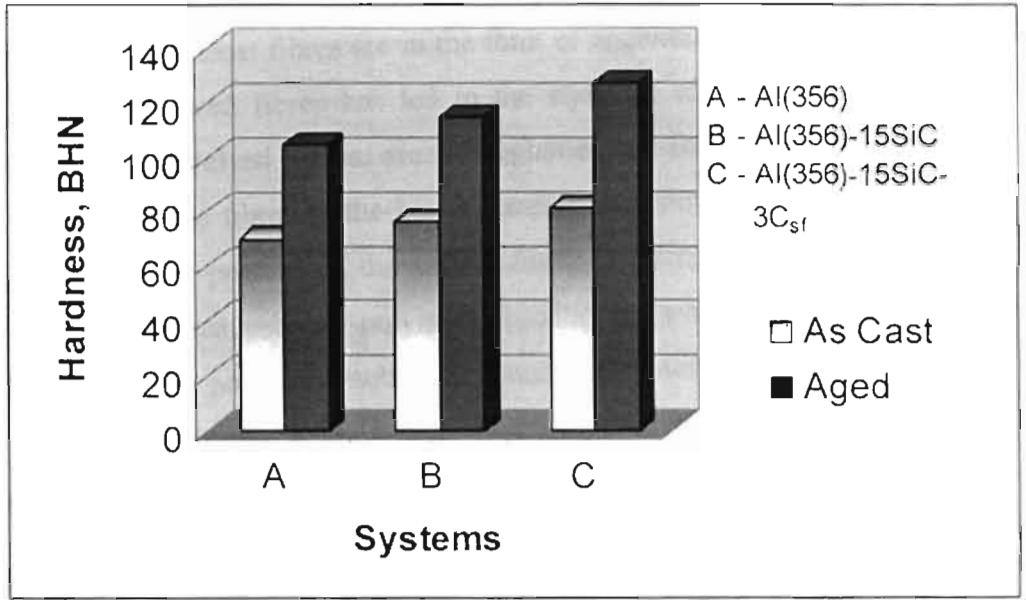


Figure 5.18: Hardness of base alloy and composite systems

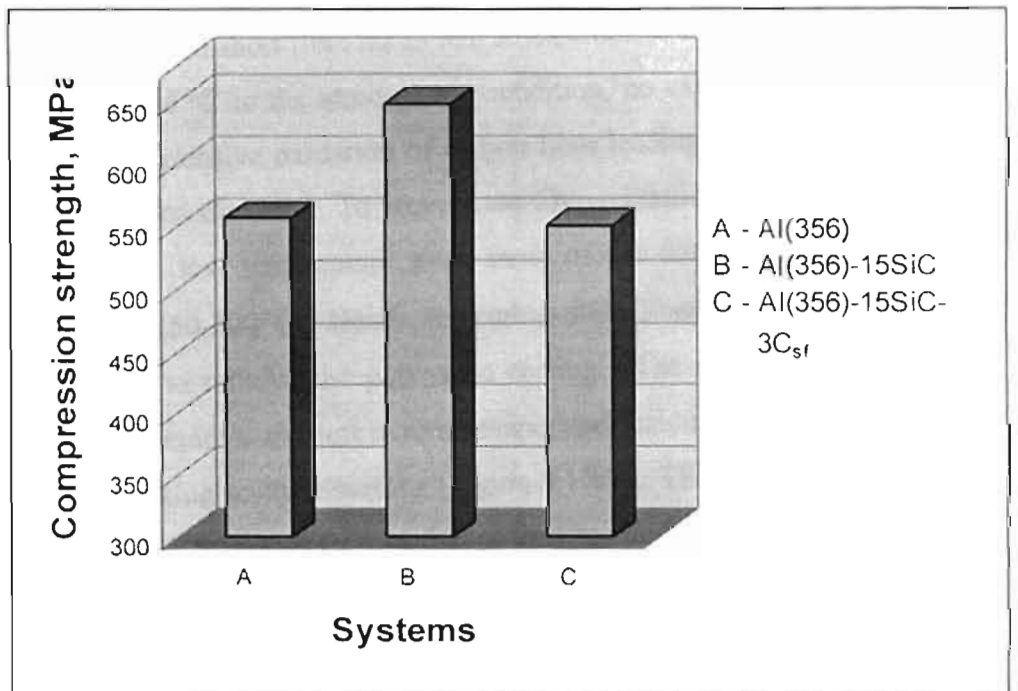


Figure 5.19: Compression strength of base alloy and composite systems

5.4 DISCUSSION

5.4.1 Fibre treatments

The as received carbon short fibres are in the form of agglomerated bunches. Introduction of these as received fibres has led to the rejection of fibres during processing. Since the as received fibres are in agglomerated form, the liquid aluminium does not wet all the fibres in the bunch, causing rejection of the fibres. Further, during manufacturing process of the carbon fibres, a sizing and finishing treatment is given to the fibres using a polymeric coating for avoiding abrasive damage during handling. This polymeric substance usually becomes half burnt and sticks the fibres together affecting wetting with liquid aluminium. Hence, it is essential to remove the polymeric coating from the surface of the fibres and introduce deflocculated and surface cleaned carbon fibres into liquid aluminium. Since sufficient surface treatment studies are carried out on aluminosilicate fibres [Chapter 6], the inefficient surface treatment methods tried earlier are not attempted.

When a gram of carbon short fibre taken in a silica crucible is kept in an oven for about 20 minutes at 750 °C in the atmospheric condition, no carbon fibre is left over. This is due to the extensive oxidation of carbon fibre leading to formation of carbon monoxide and carbon dioxide. To prevent the fibre oxidation, it is preferred to heat treat the fibres at low temperature since most of the common polymeric coating get evaporated at 250-300°C. Hence, the carbon short fibres are heat treated at 400°C for 15 minutes to remove the polymeric coating. The carbon fibres are cleaned using acetone to remove any left over or evaporated residues of coating and also foreign particles sticking to their surface [Figure 5.1(b)]. The surface grooves seen in the fibres are the die markings formed during the fibre drawing process.

The separation of fibres can be carried out mechanically or chemically. The mechanical separation could lead to extensive fibre damage by rubbing. Hence, chemical separation coupled with ultrasonic vibration is selected. The settling experiment carried out on different media namely aqueous, acetone and sodium silicate solution has shown that the sodium silicate is very effective in deflocculation of fibres and keeps the fibres separated in dried condition. The acetone is efficient in

cleaning its surface since it is a good organic solvent. Application of ultrasonic pulses aids in deflocculating the interlocked fibres and also in removing the surface coating by better interaction of solvent with the fibre surface. However, the acetone treatment is not efficient in keeping the fibres well separated in dried condition even though it get separated in the acetone medium. Well separated fibres in dried condition are required for the free flow of fibres during their introduction during MMC synthesis by stir casting process. The sodium silicate treatment facilitates in keeping the fibres separated in dried condition. The overall steps involved in surface treatment of fibres are (1) heat treatment at 400°C for 15 minutes to burn off the polymeric coating (2) washing of the fibres in acetone medium coupled with ultrasonic agitation and (3) deflocculation of fibres in 0.02% sodium silicate solution at pH 4-5 range and drying it in the oven at 150°C for 2 hrs.

5.4.2 Structural and Interfacial Characteristics

5.4.2.1 Al(356)-3% C_(sf)

The microstructures of Al(356)-3% C_(sf) mono composite have shown good dispersion of carbon fibre in the matrix [Figure 5.4]. The dispersion of the reinforcement is generally controlled by the wetting of the reinforcement with the matrix and the mixing process. In the present composite system, the wettability of carbon fibre with the liquid aluminium alloy matrix is controlled by the surface characteristics of the carbon fibre, the constituents and the physical characteristics of liquid alloy matrix and the physical and chemical interaction between the carbon fibre and aluminium alloy matrix. The wettability of a solid by liquid is usually indicated by the contact angle between them or by work of adhesion. The contact angle between the solid carbon fibre, liquid aluminium matrix and gas/vapour could be related by the Young's Dupre's equation.

$$\gamma_{lv} \cos \theta = \gamma_{sv} - \gamma_{sl} \quad (5.1)$$

Where γ_{lv} is the surface tension of the liquid aluminium matrix, γ_{sv} is the surface energy of the carbon fibre and γ_{sl} is the interfacial energy between the liquid aluminium and solid carbon fibre. The increase in wettability is obtained by lowering

the contact angle, θ . The contact angle can be decreased by (i) increasing the surface energy of the carbon short fibre, γ_{sv} (ii) decreasing the reinforcement/matrix interfacial energy and (iii) decreasing the surface tension of the liquid metal, γ_{lv} .

The surface energy is the excess energy per unit area associated with the surface because of the unsatisfied bonds at the surface. In the present case, the removal of polymeric coating from the surface of carbon and the sodium silicate treatment lead to the enhancement in wetting due to the presence of active silica layer over carbon fibre which could chemically interact with 356 alloy matrix. The above treatments increase the surface energy of carbon fibre. The other major factor for the improved wetting of carbon with aluminium is the interfacial reaction leading to aluminium carbide formation with covalent metal-carbon bonds. However, for the reaction to take place, pure aluminium has to come into contact with the fibre surface. According to Eustathopoulous *et al.* [242], the alumina layer present in aluminium usually prevents the direct contact of aluminium with carbon. However, the addition of active alloying elements such as magnesium weakens the aluminium oxide film. The interfacial energy, γ_{sl} of the carbon fibre and matrix is decreased by the chemical interaction between them to form aluminium carbide.

The work of adhesion (W_a) is another concept, which measures the wettability at the composite interface and is given by

$$W_a = \gamma_{lv} (1 + \cos \theta) \quad (5.2)$$

A high work of adhesion indicates good wetting. The condition for wetting in this case is $W_a > \gamma_{lv}$. That is the liquid metal wets the solid reinforcement surface only if the energy of the bonds that are created across the interface exceeds the surface tension of the liquid. In Al-carbon fibre system, the liquid aluminium reacts with carbon to form aluminium carbide, thus contributing to the work of adhesion and there by promoting wetting between the matrix and the reinforcement.

In stir casting process, after introducing the fibre into the matrix, wetting of the fibre with the matrix is the first major phenomena to occur and the second being the mixing of the fibres with the matrix to provide good distribution. During the

mixing process, an optimum stirring speed is maintained to obtain fairly uniform distribution of fibres. The fibres are distributed randomly [Figure 5.4(a) and (b)]. The fibres are observed to get broken due to the abrasion of the fibre with the stirrer blade. The breaking of fibres cannot be fully avoided during stirring process except minimising the same by maintaining an optimum stirring speed.

In mono composite, the distribution of carbon short fibre [Figure 5.4(a)] is better than that of the graphite particle [Figure 4.5(a)] because of the formers comparatively lower tendency to float (higher aspect ratio), better wetting with the matrix alloy and effective suspension (high viscosity).

The solidification of composite melt is the crucial step in microstructure formation of the cast composite. In Al (356)-3% C_(sf) system also, the carbon fibre does not act as a heterogeneous nucleation site for primary α -phase and hence the phase nucleates away from the region and grow towards the fibres. Thus, the fibres are pushed to the last freezing region of the composite. According to Kim and Rohatgi [243], the reasons for the segregation of reinforcement into the interdendrite regions are (a) the absence of nucleation or remelting of primary α -phase on the reinforcement surface and (b) the rejection of the particles by solidifying interfaces, i.e. the reinforcement pushing phenomena. The dendrite morphology of primary aluminium (α -phase) is affected in the composite due to the hindrance imposed by the fibre for the growth of secondary dendrite arms. Further, the growth of primary phase is also affected by the limited solute diffusion due to the barrier effect of the reinforcement and the delayed growth from the melt will give additional time for the formation of more nuclei [19].

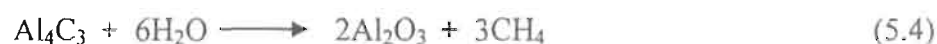
The eutectic silicon phase in the matrix has been observed to nucleate on the surface of carbon fibres with its refinement in the immediate vicinity of the fibre. The density measurement and microstructural observation have shown higher porosity content in Al(356)-3% C_(sf) composite than the base alloy. Increase in porosity content is due to the entrapment of gases as a result of high viscosity of the composite melt. The higher aspect ratio of the fibre ($l/d > 12$) compared to that of particulates

($l/d \sim 1$) showed sharp increase in the viscosity with even 3 wt% of the fibre introduction into the melt.

The SEM and EDS studies have shown that the carbon fibre is prone to interfacial reaction. The most commonly observed reaction is the formation of aluminium carbide according to the following reaction:



However, the observation at the interface by EDS has shown the presence of Al_2O_3 , which can form from the Al_4C_3 exposed to moisture according to the following reaction:



Since the SEM and EDS specimens are cut, polished and washed in moist environment, the aluminium carbide in the polished surface gets converted to Al_2O_3 appearing in the form of rod like structures [Figures 5.7, 5.8(c) and 5.9].

The mechanism for the chemical reaction of carbon with molten aluminium to form aluminium carbide involves diffusion of dissociated carbon atoms from the fibre surface through the interface containing oxides and carbide and reacting with molten Al yielding Al_4C_3 . In the initial stages of the reaction, oxygen is chemisorbed on an active surface site, followed by electron transfer from the carbon to the C-O pair bond and the desorption of the pair as CO [244-246]. The transferred electron strengthens the CO pair bond while weakening the bond between surface C atom and the underlying carbon, thus permitting the dissociation of surface C atoms and their diffusion across the interface. The aluminium carbide crystals nucleate heterogeneously on carbon and anisotropically as lath like particles into the Al matrix by ledge mechanism [246, 247]. Later during their coalescence, the carbide platelets grow into the fibres decreasing the tensile strength because of the random notches formed by the growth of platelets into the fibres.

5.4.2.2 Al(356)-15% SiC_(p)-3% C_(sf)

The optical and SEM photomicrographs of Al(356)-15% SiC_(p) -3% C_(sf) hybrid composite have shown good dispersion of SiC_(p) and carbon fibre in the matrix. However, the fibres in the hybrid composite are more damaged than the mono composite due to the abrasive of the SiC_(p) and the stirrer blade during stirring.

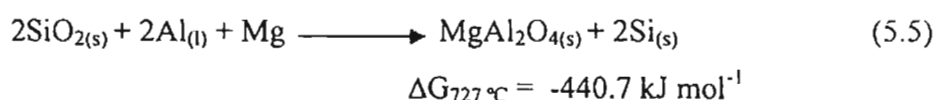
The mixed mode of addition of SiC_(p) and C_(sf) is not efficient for dispersing the reinforcements. The SiC_(p) is added first followed by the carbon fibre, since the wetting of carbon short fibre is better than the SiC_(p) particle due to the interfacial chemical reaction and also the fibre breaking is reduced. While prolonged stirring time of SiC_(p) could improve its wettability and dispersion in the matrix, lower stirring time reduces the higher interfacial reaction tendency of carbon fibre.

The wetting characteristics of SiC_(p) by liquid Al is different from that of carbon fibre. The wetting of pitch based carbon fibre is induced by the fibre heat treatment leading to the desorption of the absorbed gases, fibre surface treatment with sodium silicate solution and the interfacial chemical reaction with Al. In the case of SiC_(p), the wetting is promoted by the native SiO₂ present on the particle surface and the artificially formed SiO₂ by the surface oxidation using high temperature pre-heat treatment.

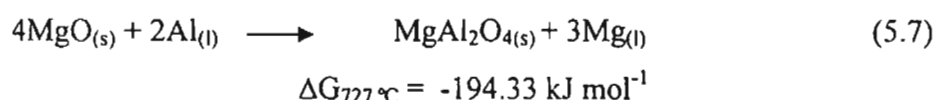
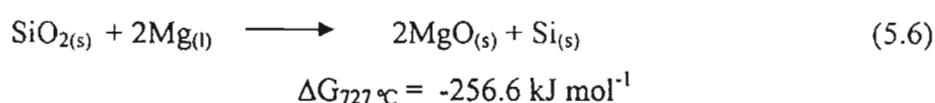
In general, a transition from non-wetting to wetting occurs at high temperatures because of dissociation of surface oxides. In the SiC-pure Al system, a reaction of aluminium with the surface oxide produces gaseous suboxide alumina which erodes the oxides and establishes direct physical contact between the SiC and the metal. With a native SiO₂ surface oxide film on SiC_(p), Al oxidation takes place and wetting is impaired by the generation of alumina. Since the above could occur before the attainment of equilibrium wetting, silica coatings may not be effective in promoting the wettability [248]. But in the present case, the presence of Mg in the matrix alloy (both added-1% Mg and present in matrix alloy -0.35% Mg) influences the wetting behaviour to a larger extent mainly with the formation of MgAl₂O₄ spinel.

SEM observation has shown that there are few gaps at the matrix –SiC_(p) interface which could have formed due to the non-wetting of the SiC_(p) surface and the presence of entrapped gas at the interface. The presence of non-uniformly oxidised SiC_(p) surface could also lead to non-uniform wetting. Like the mono composite, the hybrid composite also exhibits porosities at the interdendritic regions or at the particle matrix interface. Those porosities at the interface lead to dewetting of particles. The larger pores could cause segregations of the particles around them. Overall the porosities reduce the tensile strength of the composite.

The interfacial reaction in the hybrid composite is similar to that of monocomposite. However, the extent of the reaction depends on the reaction product formed and the nature of interaction between the reinforcements. The carbon fibre reacts with aluminium to form aluminium carbide. In the case of SiC_(p), the SiO₂ present in the surface reacts with Mg to form MgAl₂O₄ according to the reactions.



The mechanism of the above conversion of SiO₂ to MgAl₂O₄ is not a direct step. According to Le Petitcorps *et al.* [249] the sequence of conversion is SiO₂ → MgO → MgAl₂O₄, according to the reactions,



Apart from improving the wetting, the spinel could also prevent the formation of aluminium carbide. In Al-Si-Mg alloy matrix, the other phases likely to form are Al₂O₃, Al₂SiO₅ and Al₆Si₂O₁₃.

In the hybrid Al(356)-15% SiC_(p) -3% C_(sf) composite, the presence of SiO₂ layer on SiC_(p) causing the formation of MgAl₂O₄, the high silicon content (7 wt%) in the matrix alloy and the formation of aluminium carbide in carbon fibre could inhibit or retard the SiC_(p) reaction with Al to form Al₄C₃.

5.4.3 Ageing Characteristics

The ageing behaviour of Al(356)-15% SiC_(p) -3% C_(sf) composites has shown an accelerated ageing similar to the Al(356)-15% SiC. This is due to the high dislocation density caused by the mismatch in the coefficient of thermal expansion between the matrix and reinforcement. However, the hybrid composite has shown a two step increase in ageing time. This phenomenon could be due to the possible presence of any new precipitate which could harden the matrix. However a detailed probe is required to comment further on the same. The other major observation is the higher peak hardness observed in the hybrid composite (128 BHN) than in the mono composite (115 BHN), which could be due to the formation of brittle aluminium carbide precipitate which hardens the matrix. The fine aluminium carbide precipitates formed can get distributed in the matrix due to the dynamic interface caused by the motion of liquid metal due to stirring. A similar improved hardness has been reported by Lu [250] with Al-SiC_(p)-Graphite_(p) composite after heat treatment at 630 °C due to the interfacial reaction product aluminium carbide.

5.4.4 Physical and Mechanical Characteristics

The hybridisation of 3% C_(sf) with the Al(356)-15% SiC_(p) composite has influenced the physical and mechanical characteristics of the composite. The density of hybrid composite is lower than the SiC_(p) reinforced mono composite due to the introduction of low density carbon fibre. The measured densities of composites are lower than the theoretical densities due to the presence of porosities formed due to gas entrapment during synthesis.

The tensile strength of hybrid composite has shown lower values due to the presence of the degraded and broken fibres and the porosity. The compressive strength of Al(356)-15% SiC_(p) mono composite is higher than that of the base alloy,

but, the compressive strength of the hybrid composite is lower than and near to that of the mono composite and base alloy respectively. The possible reasons could be the presence of interfacial reaction and porosities.

5.5 SUMMARY

1. Addition of as received carbon short fibre to the matrix alloy leads to their agglomeration and rejection.
2. Among the various surface treatments attempted, sodium silicate treatment is effective in deflocculation of the fibres and maintaining the fluffiness for the free flow during the addition into the matrix.
3. The surface treated fibre provides better wetting and dispersion of fibre in the matrix.
4. The primary phase does not nucleate on the fibre surface whereas the eutectic silicon is observed to nucleate.
5. Interfacial reaction occurs at the carbon fibre – matrix interface with the formation of aluminium carbide providing better wetting, but it degrades the fibre surface.
6. Fibre breakage is observed in the composite due to the shearing experienced during synthesis, however in hybrid composite, SiC particle abrasion also leads to further breakage.
7. The hardness of the hybrid composite is increased when compared to the monocomposite.
8. Accelerated ageing is observed in both the mono and hybrid composites.
9. The density of the hybrid aluminium composite is lower than that of the Al-SiC monocomposite due to the addition of $C_{(sf)}$.
10. The tensile and compression strength of hybrid composite is lowered due to interfacial reaction and breakage of fibre.

CHAPTER 6

Al(356) – ALUMINOSILICATE SHORT FIBRE REINFORCED COMPOSITES

6.1 INTRODUCTION

Aluminium matrix composites reinforced with discontinuous reinforcements such as short fibres of carbon, silicon carbide and alumina are successfully fabricated [251-253] and used for different applications. The high costs of some of these short fibres have been overcome by resorting to the use of low cost aluminosilicate fibres with comparable performance. The aluminosilicate short fibres reinforced metal matrix composites (MMC), processed using techniques such as infiltration, squeeze casting, etc. have shown increased strength, wear resistance and fatigue life, lower thermal expansion coefficient, reduction in the component weight and lower product cost [254-258].

The enhancement in the strength and the modulus of the composite depends on the load transfer behaviour at the matrix/reinforcement interface. Hence, the interfacial characteristics of composites play an important role in determining the composites properties and performance. In the case of composites processed by liquid metallurgy technique, the reinforcement comes in contact with molten metal, leading to interfacial reactions. The alumina and aluminosilicate fibre reinforced aluminium alloy matrix composites have shown the tendency to interact with the matrix [259-263]. Most of the commonly used aluminium alloys contain Mg as an alloying element, which has the tendency to react with the Al_2O_3 or SiO_2 constituent of the dispersoids forming MgO or MgAl_2O_4 spinel [259-261]. Similarly, the mullite fibres having ZrO_2 have also been found to react with the aluminium alloys [262-263]. Most of the above studies are carried out on composites fabricated by infiltration techniques. Further, in liquid metal stir cast composites, the longer duration of contact of liquid metal with the dispersoids and the fluid flow could result in severe interfacial reactions.

In the present investigation, an attempt is made to (i) utilize an indigenous and cheaper variety of short aluminosilicate fibres as reinforcement in Al(356) alloy matrix through stir casting technique, (ii) study the microstructural, interfacial, solidification and heat treatment aspects and (iii) evaluate the physical and the mechanical properties of the resulting composites. The possible reactions, their mechanisms and the thermodynamics involved are also analysed. Further, the interfacial characteristics of the two different grades of aluminosilicate fibres used are compared.

6.2 METHODOLOGY

The matrix material used is Al-7Si-0.35Mg (356) aluminium alloy. Two grades of aluminosilicate fibres namely standard grade and zirconia-toughened grade obtained from M/s Murugappa Morgan Thermal Ceramics Ltd., Chennai, India have been used as dispersoid [264]. These fibres are synthesized using a melt-spin method and are of assorted lengths and diameter; an average diameter of 1.5 – 3 μm is obtained along with small amounts of shots (tiny spherical or oval shaped particles formed along with the fibres during synthesis) of varying sizes as well. The chemical composition and properties of the matrix alloy are given in Table 3.1 and 3.2 and those of fibres are given in Tables 3.4 and 3.3 respectively.

Since the as received fibres are in agglomerated bunch form with varying lengths, it is necessary to deflocculate these fibres prior to incorporation into the melt. In addition, the fibres having lengths more than 10 mm are to be removed from the bunch to prevent their agglomeration in the casting. Various types of fibre treatments are carried out in organic and aqueous media coupled with ultrasonic (Vibronics bath type – model VS 250) or mechanical stirring. The organic media used are distilled water, sodium silicate, ammonium acetate and acidic solutions of varying pH prepared using concentrated nitric acid. Since the as received fibres contain few longer ones even after 5 passes, they are also subjected to mechanical crushing prior to treatment. Both the standard and the zirconia grade fibres are subjected to the above treatments.

Fibres with some of the above selected treatments are used for composite synthesis. Microstructural characteristics of these composites are evaluated to find the best surface treatment. A detailed investigation on the interfacial behaviour of standard and zirconia grade fibres is carried out using SEM and EDS to evaluate the interfacial reactions. The heat treatment studies are carried out and its response is evaluated by the changes in the hardness. The MTDATA software (NPL, UK) [265] has been used for the thermodynamic calculations.

6.3 RESULTS

6.3.1 Fibre Treatments

Figure 6.1 (a) and (b) and 6.2 (a) and (b) show the SEM photomicrographs of as received standard and zirconia grade aluminosilicate fibres respectively. The introduction of as received standard grade and zirconia grade fibres, which are in the agglomerated form containing assorted lengths of fibres and shots of varying sizes, into the aluminium alloy leads to poor distribution of fibres, as well as rejection from the melt. Ultrasonic agitation of these fibres in alcoholic and acetone media results in better dispersion in the medium only, which after filtering and drying disappears, forming a thick mass. Hence, treatment of the fibres in these media has very little effect in deflocculation. On the other hand, mechanical stirring of fibres has resulted in breaking of fibre.

Ultrasonic treatment of fibres in an aqueous medium not only deflocculates the fibres but also allow settling of the shots at the bottom, which can be separated. Here again, the deflocculation and fluffy nature of the fibres achieved during the treatment is not retained after drying. The treatments of the fibres in sodium silicate and ammonium citrate solutions accompanied with ultrasonic agitation disperse the fibre well in the medium and the rate of settling of fibre after dispersion is reduced. The fluffy nature of the fibre is enhanced after drying (the volume increases by about 40% after the treatment). Treatment in acidic solution with varying pH coupled with ultrasonic vibration has shown that the 4-5 pH range is more effective in attaining better dispersion of fibres. This treatment has resulted in the best fluffy fibres after drying among the treatments attempted (approximately 75% increases in volume). Figures 6.1 (c) and (d) and Figure 6.2 (c) and (d) show the surface treated standard

and zirconia grade fibres respectively. The surface of as received fibres show peeled off layers both in standard [Figure 6.1(b)] and zirconia [Figure 6.2(b)] grades, the latter showing higher amount. The deflocculated fibres [Figures 6.1(d) and 6.2 (d)] show only a few peeled layers sticking to the surfaces of both the grades suggesting that deflocculation has separated the fibres and also cleanse them.

Visual examination of polished longitudinal cross section of the composite casting containing as received zirconia grade fibres has revealed not only the presence of agglomerated fibre bunches but also surface blackening of fibres. A few micro porosities are also observed in the casting [Figure 6.3(a)]. In the case of sodium silicate treated zirconia grade fibres dispersed composites, the casting has more micro porosities as seen in Figure 6.3(b). On the other hand, incorporation of zirconia grade fibres treated in acidic solution has resulted in better distribution of fibres with very few agglomerates as shown in Figure 6.3(c). Similarly, visual examination of the polished longitudinal cross section of composite castings dispersed with the standard grade fibres has shown that the acidic treatment [Figures 6.4 (b) and (c)] is the best compared to the as received fibre [Figure 6.4(a)] in terms of minimum macro pores and agglomerates. However, standard grade fibres unlike zirconia grade do not show any fibre surface blackening after incorporation in the aluminium alloy melt. Chopping of standard grade fibre prior to acidic treatments has resulted in further improvement in the distribution with minimum agglomerates [Figure 6.4(c)] than with acidic treatment [Figure 6.4(b)] alone.

6.3.2 Optical Microstructures

Figures 6.5 (a) and (b) show the typical microstructures of sodium silicate and acidic solution treated zirconia grade aluminosilicate fibre reinforced composites respectively from the bottom of the castings. The fibres and shots are reasonably well distributed in the matrix with the acidic treatment compared to the sodium silicate treatment, wherein a few fibre agglomerates are also observed. A similar distribution is also observed in both the middle and the top portions of a given composite casting. This reveals that fibres treated with an acidic solution of pH in the range of 4-5 result in better distribution [Figure 6.6]. The cracking of shots and the penetration of metal into the cracks during synthesis are observed in both the zirconia grade [Figure 6.5(b)]

and the standard grade fibres [Figure 6.6(b)]. The microstructures of Al(356)–15% SiC_(p) -5% aluminosilicate (standard) hybrid composite have shown that both the particles and the short fibres are in well separated and distributed form [Figure 6.7]. Figure 6.7(b) shows the cracked aluminosilicate shot in the matrix with infiltrated and solidified liquid metal as observed in the monocomposite. The microstructures of mono and hybrid composites show that the primary aluminium does not nucleate on the surface of the aluminosilicate fibres.

The XRD patterns of the as received [Figure 6.8(a)] and heat-treated (at 750 °C for 2h)[Figure 6.8(b)] zirconia grade fibre are almost similar with out any peaks. This indicates that the fibre is in the amorphous state and there is no remarkable reaction or structural change taking place during heating of fibres in the absence of liquid aluminium. On the other hand, the XRD pattern of blackened zirconia grade fibre extracted from the composite [Figure 6.8(c)] shows few peaks. The peaks at the 2θ values 38.5° and 44.8° correspond to pure aluminium of the matrix. The peak at 43° is of ZrAl₃. As this peak is not prominent, which may be due to the presence of a lesser quantity of reaction product than the detection level of the instrument (3%), it is not possible to confirm that the fibre surface blackening is due to ZrAl₃. Hence, a detailed study on interfacial behaviour is carried out.

6.3.3 SEM Microstructures and EDS Analysis

The EDS spectra of as received standard and zirconia grade fibres are given in Figures 6.9 (a) and (b). The standard grade fibre (Al₂O₃.SiO₂) shows the characteristic peaks of Al, O and Si corresponding to the Al₂O₃ and the SiO₂ present in the fibre [Figure 6.9(a)]. The zirconia grade fibre (Al₂O₃.SiO₂.ZrO₂) shows the characteristic peaks of Al, O, Si and Zr corresponding to the Al₂O₃, SiO₂ and ZrO₂ constituents present in the fibre [Figure 6.9(b)].

The surfaces of standard and zirconia grade aluminosilicate fibres incorporated in the composite [Figure 6.10 (a) and (b)] show the occurrence of interfacial reaction in both. However, the reaction is severe in zirconia grade fibre compared to standard grade fibre.

The SEM micrograph and the EDS spectra of the surface of standard aluminosilicate fibre and the nearby matrix of the composite are shown in [Figure 6.11(a-c)]. The intensity of X-ray peaks corresponding to Al, Mg and oxygen [Figure 6.11(b)] decreases in the same order and a very feeble peak corresponding to the presence of Si in the surface of the fibre is also seen. The EDS spectrum of the matrix [Figure 6.11(c)] adjacent to the fibre shows the presence of high intensity Al and low intensity Mg and Si peaks. The presence of eutectic silicon adjacent to the fibre as observed in Figure 6.12 reveals the possibility of its nucleation on the fibre surface.

The elemental X-ray maps of the composite matrix [Figure 6.13] show the eutectic silicon phase (dark black phase in Figure 6.13(a)) and an adjacent phase containing Al, Mg and oxygen (light white phases in Figure 6.13(a)). This light white phase is probably MgAl_2O_4 spinel, which has segregated around the eutectic silicon.

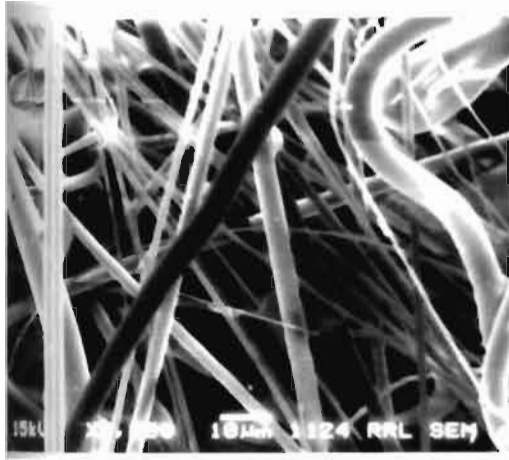
The analysis of the matrix has shown the presence of ZrAl_3 phase [Figure 6.14(a-c)]. Figure 6.14(a) shows the SEM photomicrograph of the ZrAl_3 phase (Al – 71.32 at% and Zr – 28.68 at%) present in the alloy matrix away from the fibre/matrix interface. The EDS spectra taken at the ZrAl_3 phase and the nearby matrix are also shown in Figure 6.14(b) and (c) respectively confirming the formation of ZrAl_3 phase. Apart from the binary compounds of Al-Zr, there could be possibilities of formation of Zr-Si binary compounds and Al-Si-Zr ternary compounds. Figure 6.15a shows the SEM photomicrograph of different compounds formed in zirconia grade aluminosilicate fibre reinforced composite. The EDS spectra [Figure 6.15(b)] of the white precipitate marked as '1' in Figure 6.15(a) shows the presence of aluminium (63.80 at. pct), silicon (12.44 at. pct) and zirconium (23.75 at. pct). The possible formula of the above compound is $\text{Al}_5\text{Zr}_2\text{Si}$. The EDS spectra in Figure 6.15c of the precipitate marked '2' in Figure 6.15a shows an intermetallic compound consisting of Al (53.63 at. pct.), Mg (16.81 at. pct.), Si (24.54 at. pct.) and Fe (5.03 at. pct.). This composition works out to be the most common Fe intermetallic compound observed in Al-Si-Mg alloys, namely π -phase ($\text{FeMg}_3\text{Si}_6\text{Al}_8$).

6.3.4 Heat Treatment

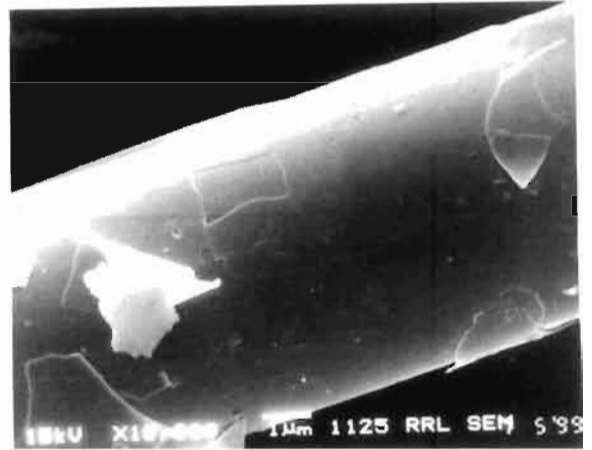
Figure 6.16 shows the aging time vs. hardness curves of Al (356) matrix alloy and Al (356) – 10% aluminosilicate fibre (standard) composite. The base alloy attains its peak hardness of 105 BHN in 8 hrs, which is the nominal hardness value of Al (356) alloy for T6 heat treatment. However, the composite has shown a very low hardness of about 85 BHN at peak-aged condition. On the other hand, the solution treated composite shows an average hardness of 71 BHN compared to 70 BHN of the base alloy.

6.3.5 Solidification Behaviour

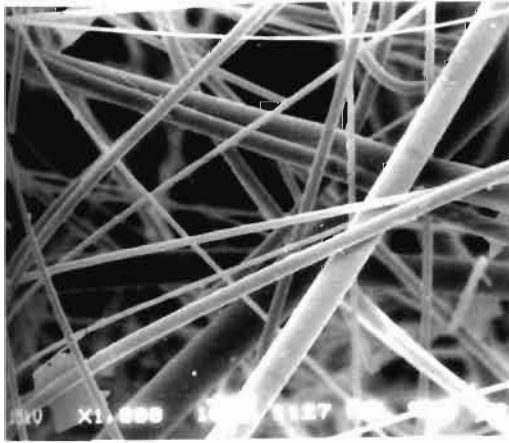
The solidification of metal matrix composites is different from the unreinforced matrix alloy because of the non-homogeneous and varied thermophysical properties of the composite melt. Studies on the effect of short ceramic fibres on the solidification behaviour of aluminium alloy are very scarce. Figures 6.17 (a) and (b) show the cooling curves of the composite melt cast in metal, graphite and sand moulds. It is observed that the liquidus temperature of the composite is lowered by about 8-12 °C compared to the unreinforced alloy [Figure 4.17]. The solidification curve of Al(356)-10%SiC-10% standard aluminosilicate fibre reinforced hybrid MMC solidified in graphite and sand mould is given in Figure 6.18. The casting/mould interfacial heat flux estimated by the numerical method (described in section 4.2.1) is given in Figures 6.19 (a) and (b). The peak heat flux values for the graphite mould is higher (600 kWm⁻²) followed by the metal (160 kWm⁻²) and the sand mould (50 kWm⁻²) for the ceramic fibre reinforced composites. Figures 6.20 (a-c) show the microstructures of Al(356)-10% aluminosilicate monocomposite cast in metal, graphite and sand mould containing iron based intermetallic compound formed. The iron intermetallics are formed during processing of composites. The morphology of iron intermetallics changes from acicular to plate like structure as the cooling rate is reduced from graphite, steel and sand moulds.



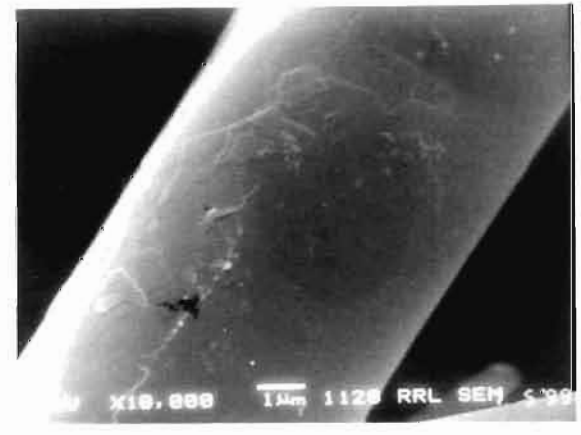
(a)



(b)

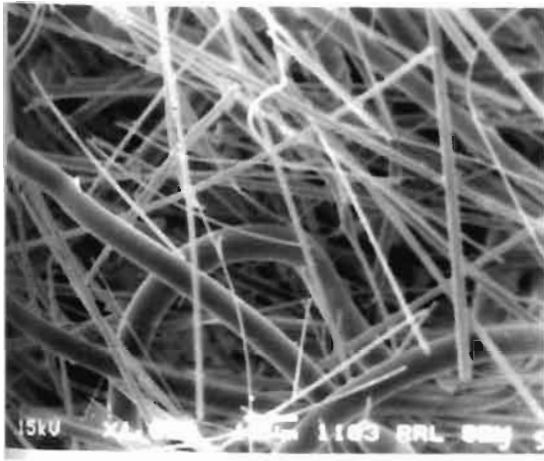


(c)

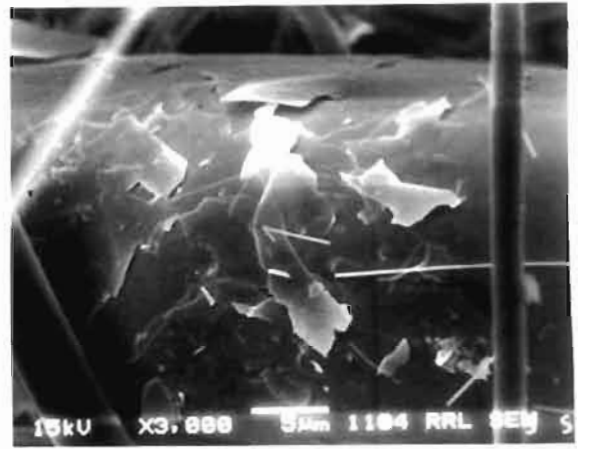


(d)

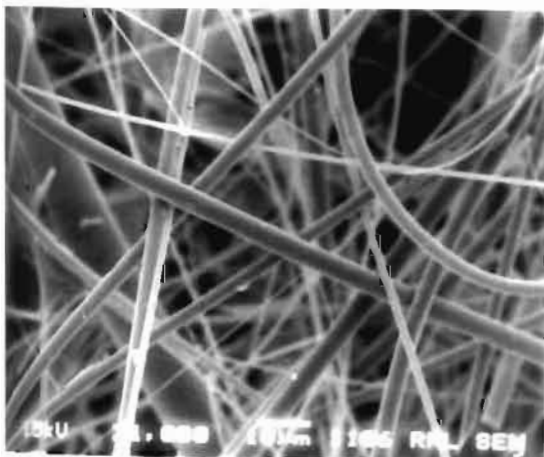
Figure 6.1: SEM photomicrographs of standard grade aluminosilicate fibre (a) and (b) as received fibre and (c) and (d) surface treated fibre.



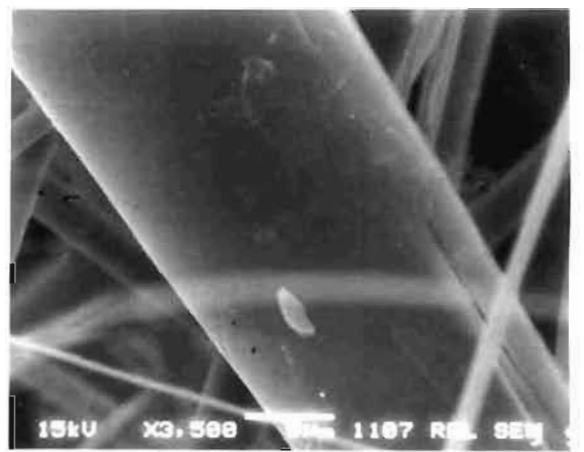
(a)



(b)



(c)



(d)

Figure 6.2: SEM photomicrographs of zirconia grade aluminosilicate fibre surface (a) and (b) as received fibre and (c) and (d) treated fibre.

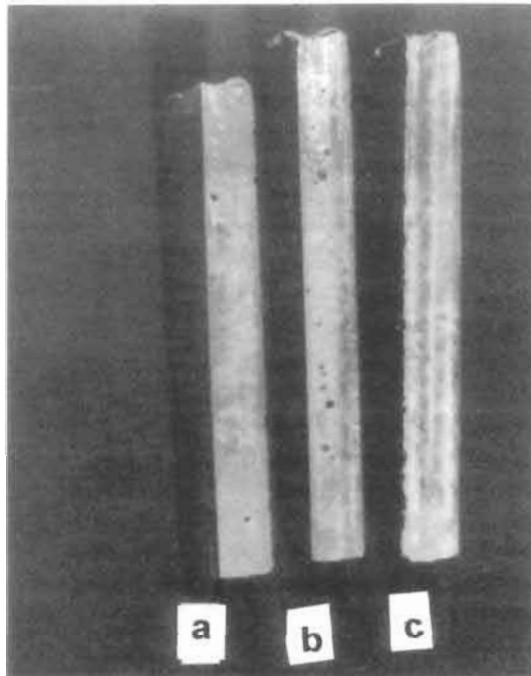


Figure 6.3: *Polished cross section of Al(356)-15% zirconia grade aluminosilicate fibre composites: (a) as received fibre, (b) ultrasonically dispersed in sodium silicate and (c) treated in acidic solution*

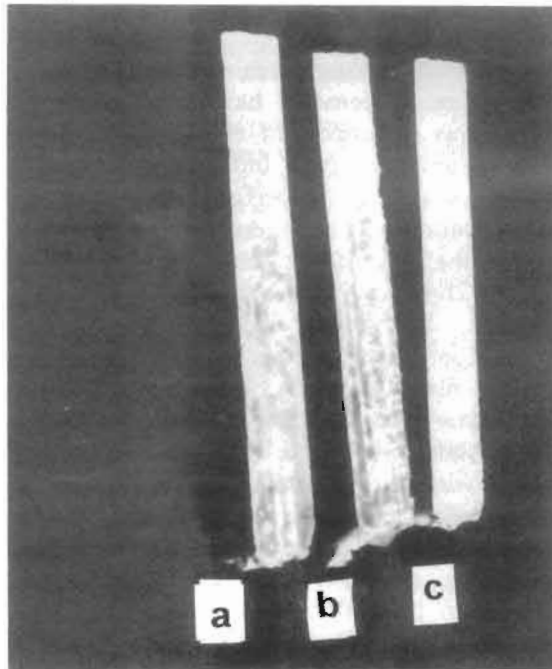
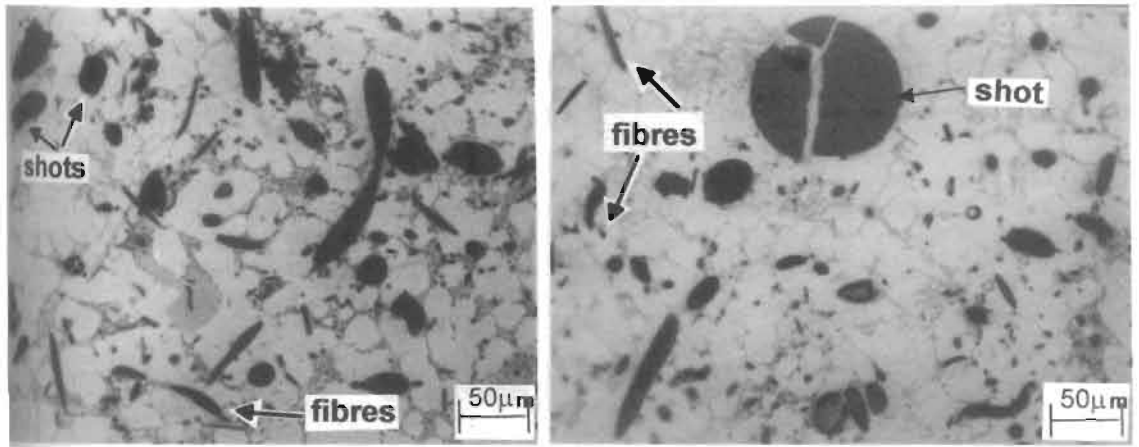


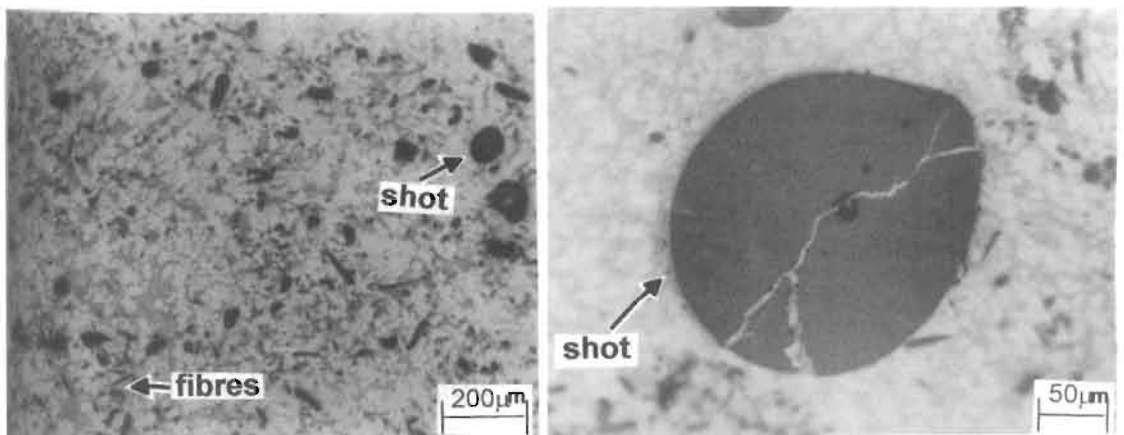
Figure 6.4: *Polished cross section of Al(356)-15% standard grade aluminosilicate fibre composites: (a) as received fibre, (b) acidic solution treated and (c) chopped and acidic solution treated*



(a)

(b)

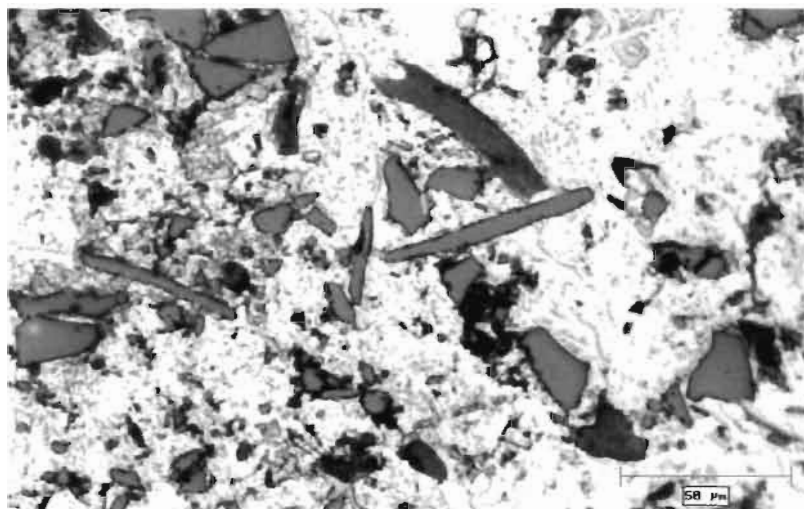
Figure 6.5: *Photomicrographs of Al(356)- zirconia grade aluminosilicate fibre reinforced composite (a) sodium silicate treated (b) acidic solution treated fibre.*



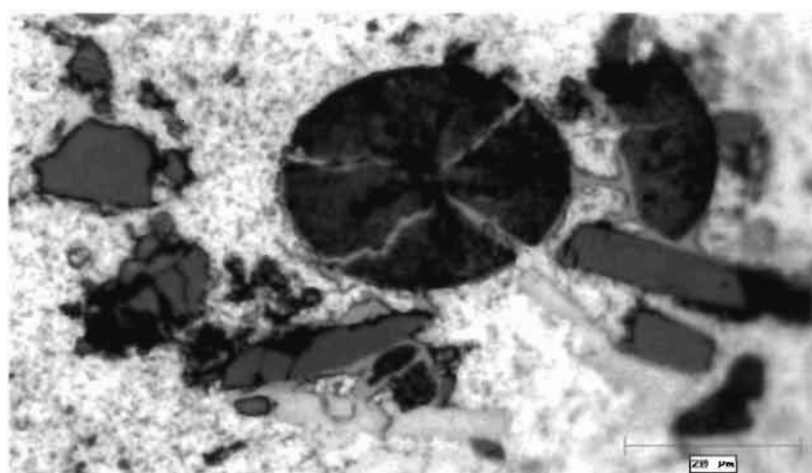
(a)

(b)

Figure 6.6: *Photomicrographs of Al(356)- acidic solution treated standard grade aluminosilicate fibre reinforced composite (a) distribution of fibres and shots (b) cracked aluminosilicate shot.*



(a)



(b)

Figure 6.7: (a) Microstructure of Al(356)-15% SiC_(p)-5% Al₂O₃.SiO₂ hybrid composite (b) Microstructure of Al(356)-15% SiC_(p)-5% Al₂O₃.SiO₂ hybrid composite showing a cracked shot in the matrix.

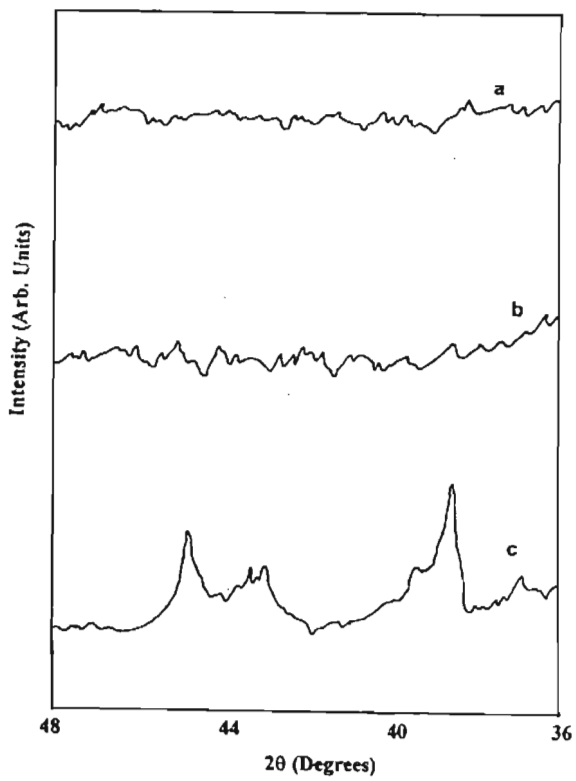


Figure 6.8: X-ray diffraction patterns of zirconia grade fibre in (a) as received, (b) heat treated (750 °C, 2 h), and (c) extracted from the composite (heated in Al alloy at 750 °C for 2 h).

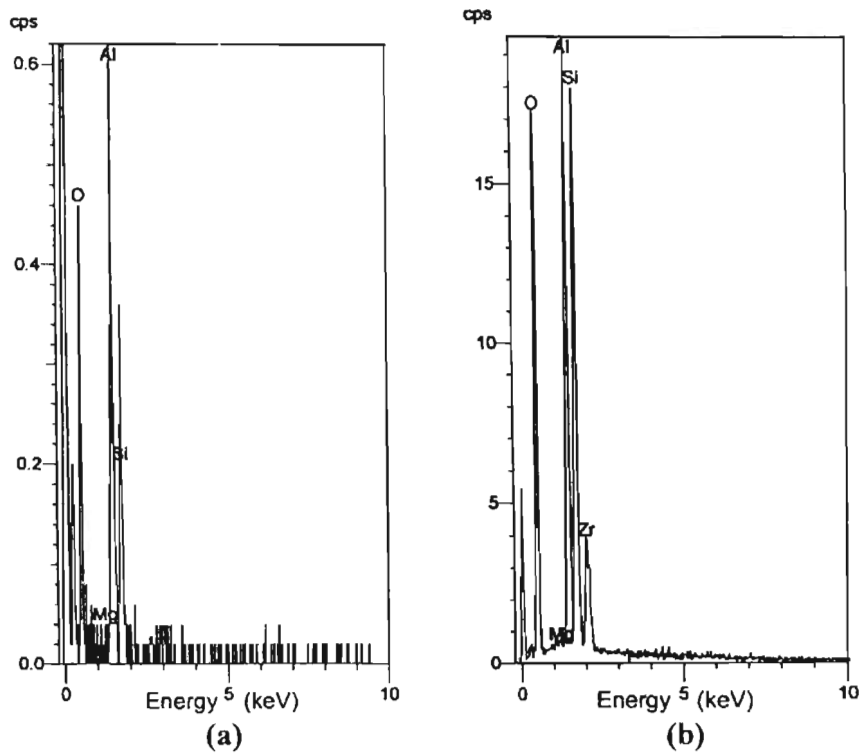
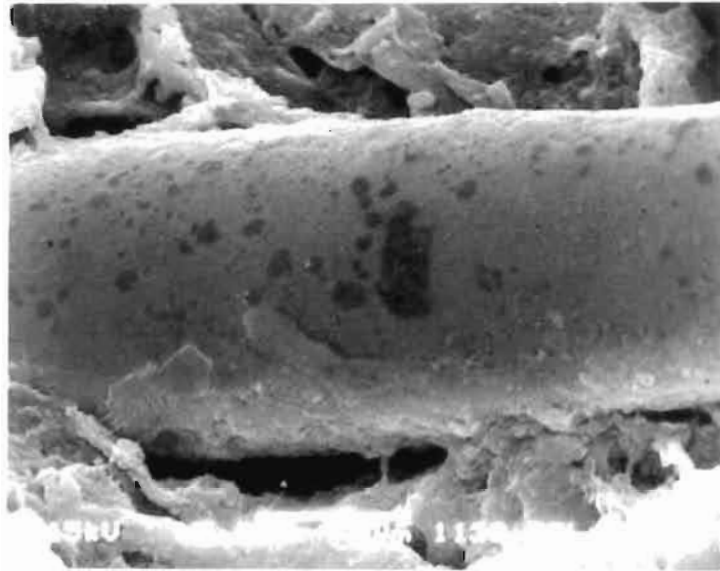
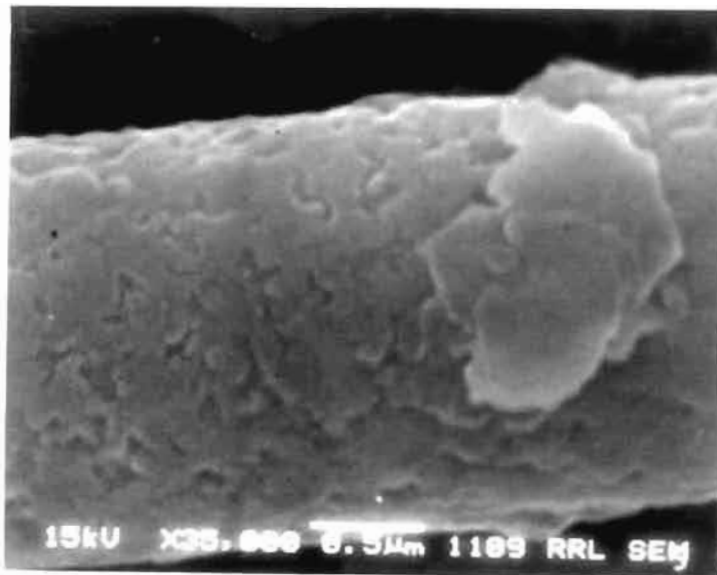


Figure 6.9: EDS spectra of as received (a) standard and (b) zirconia grade aluminosilicate fibre

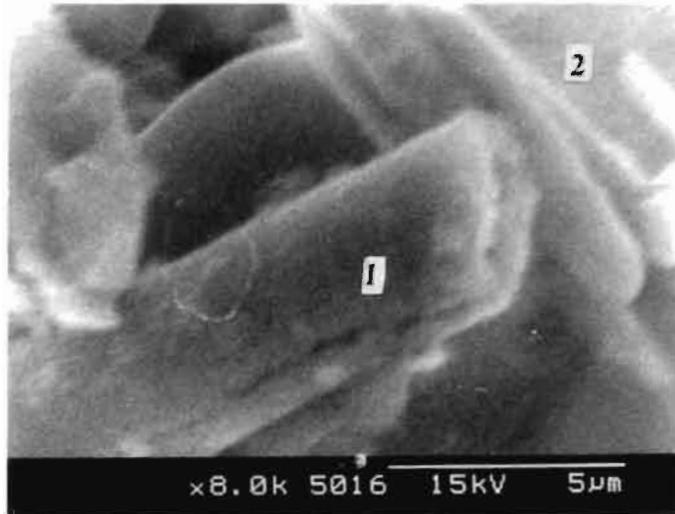


(a)

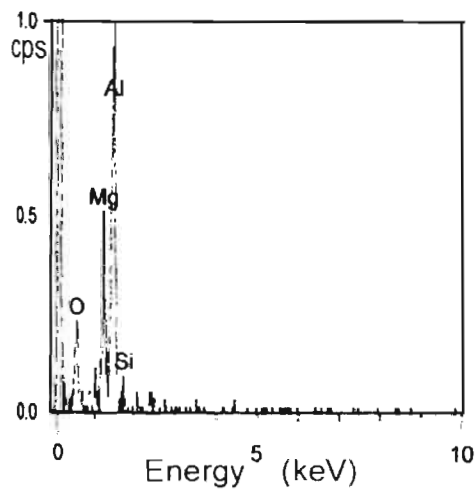


(b)

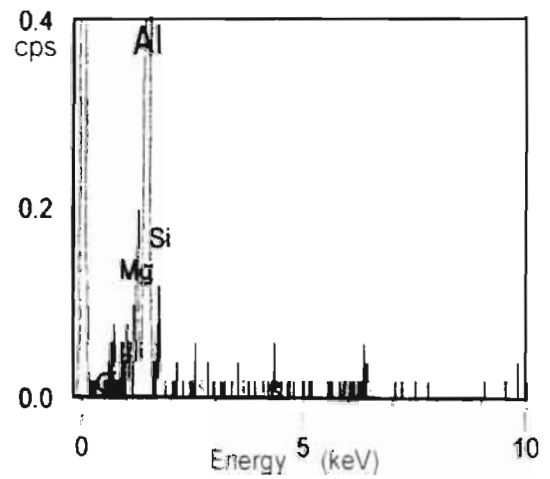
Figure 6.10: *SEM photomicrographs of the surface of the fibres observed in the composites (a) standard grade (b) zirconia grade.*



(a)



(b)



(c)

Figure 6.11: (a) SEM photomicrograph of standard aluminosilicate fibre in the composite, (b) EDS spectra showing the presence of $MgAl_2O_4$ on the fibre surface in the composite (position 1 in Fig 6.11a) and (c) EDS spectra of the matrix alloy (position 2 in Figure 6.11a)

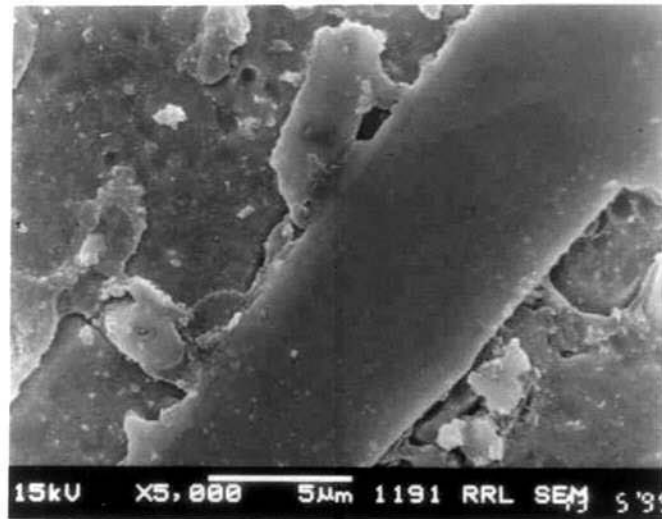


Figure 6.12: SEM photomicrograph of aluminosilicate fibre reinforced composites showing the presence of silicon over fibre surface.

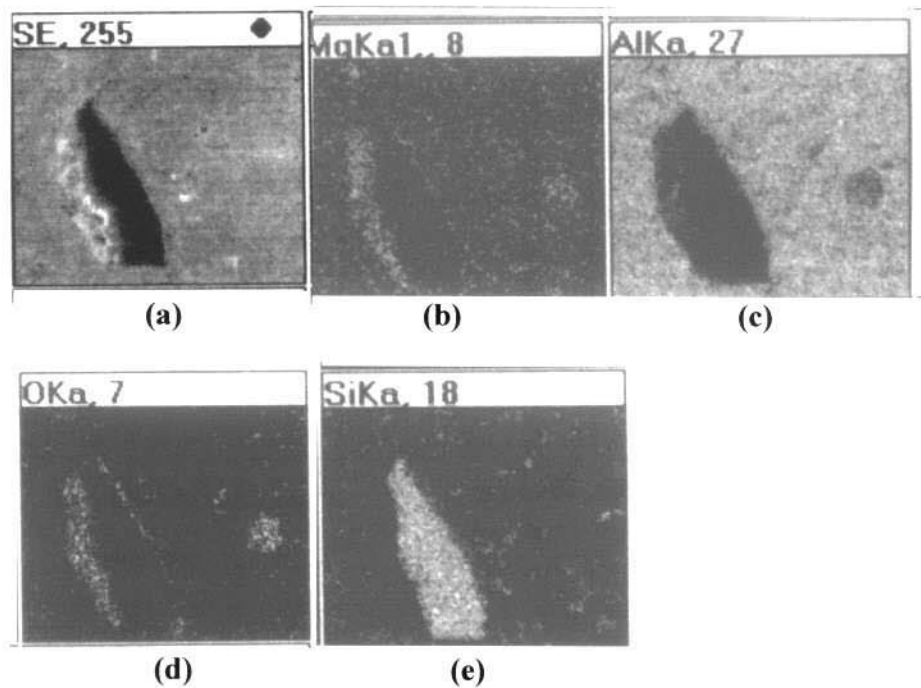
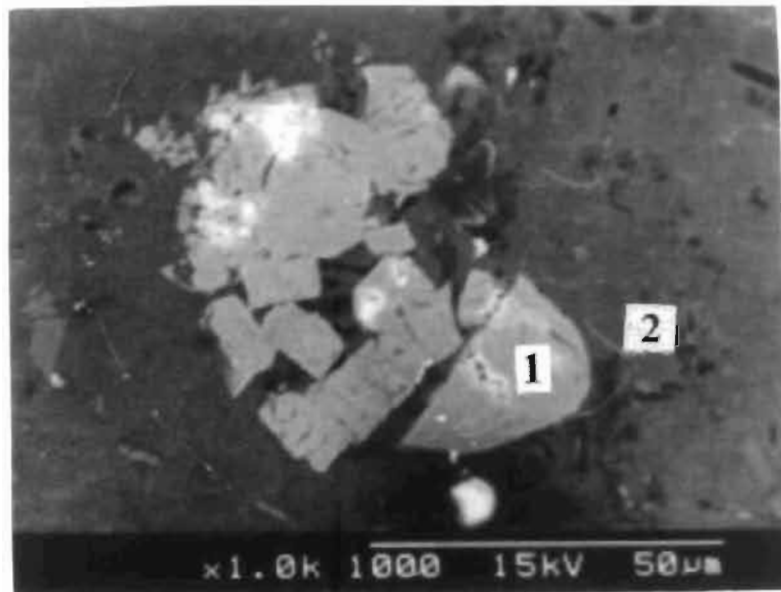
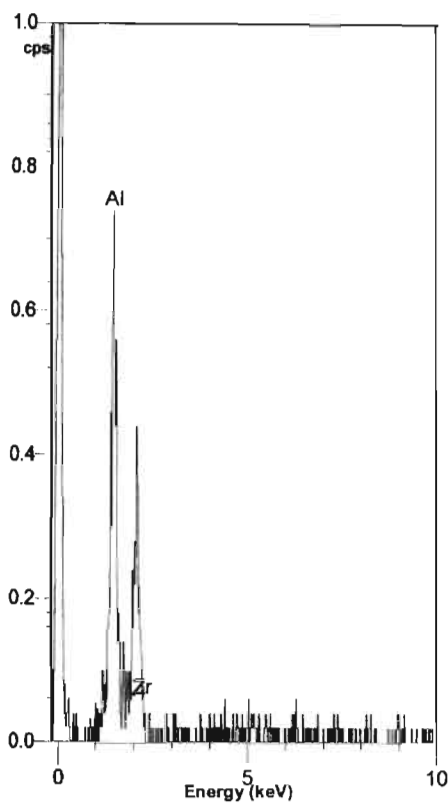


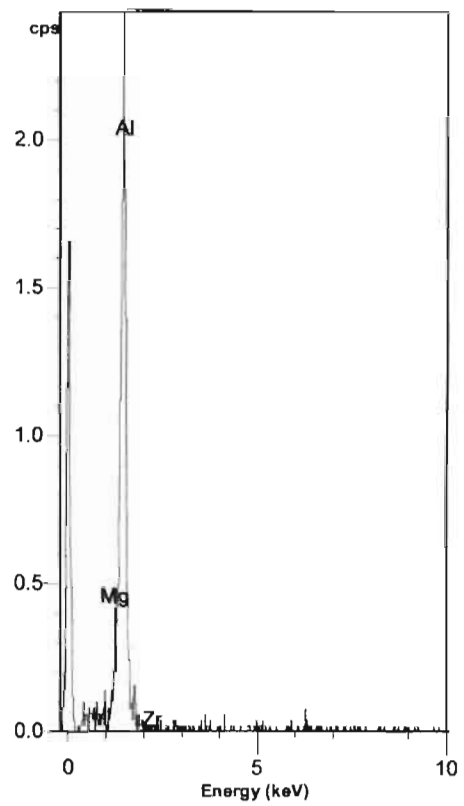
Figure 6.13: Elemental X-ray dot maps of standard aluminosilicate fibre dispersed composite showing the spinel formed segregating near to eutectic silicon region in the matrix.



(a)

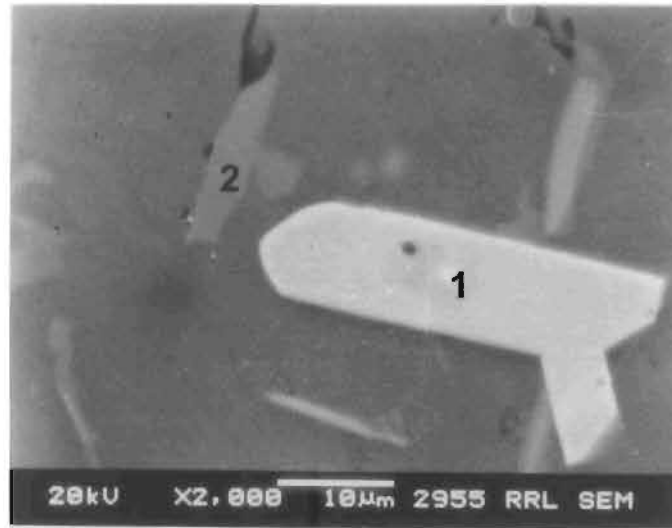


(b)

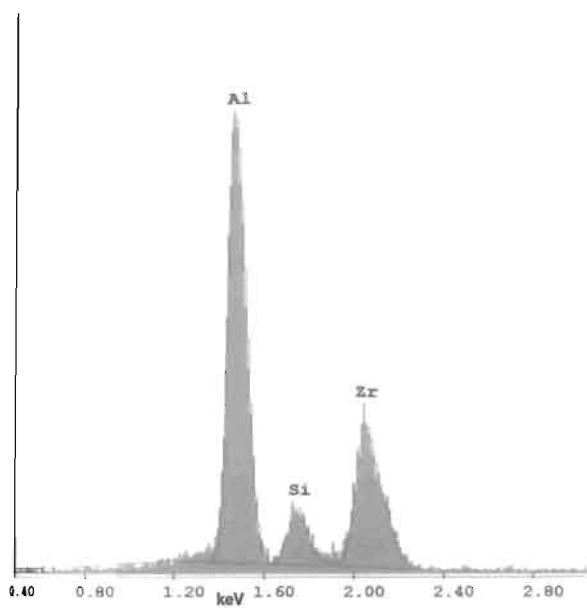


(c)

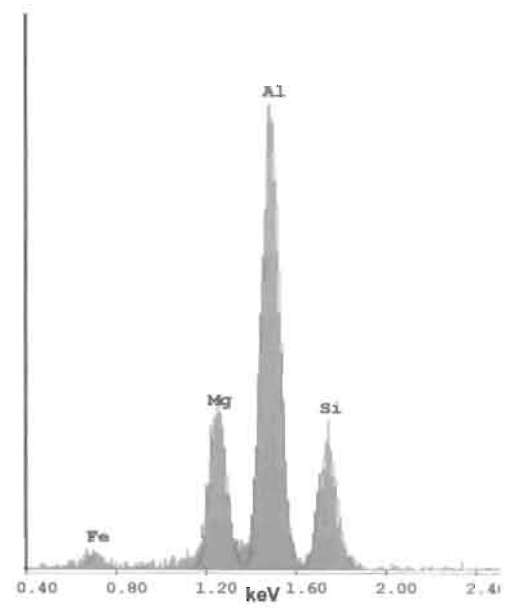
Figure 6.14: (a) SEM photomicrograph of $ZrAl_3$ phase formed by the reaction between the matrix and the reinforcement (b) the EDS spectra at position 1 in Figure 6.14a and (c) EDS spectra of position 2 in Figure 6.14a.



(a)



(b)



(c)

Figure 6.15: (a) SEM photomicrograph of the zirconia grade fibre reinforced aluminium matrix composite showing the presence of intermetallic compounds in the matrix, (b) the EDS spectra at position 1 in Figure 6.15a and (c) EDS spectra of position 2 in Figure 6.15a.

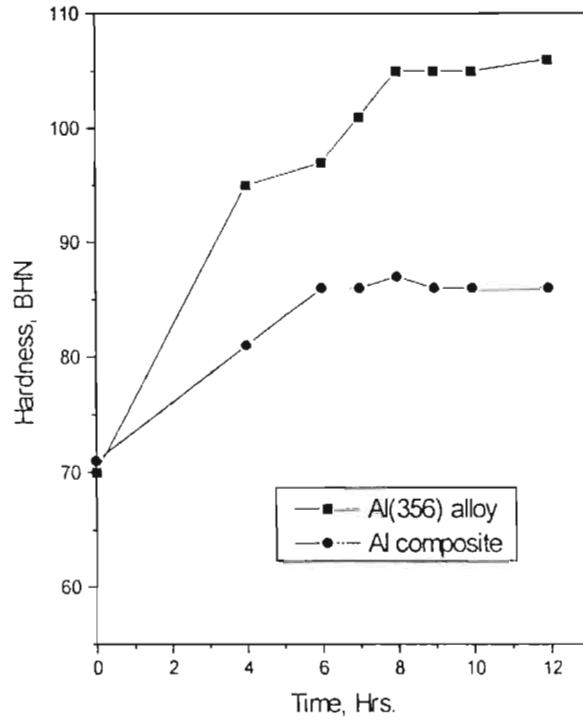


Figure 6.16: Aging curves for Al(356) base alloy and 10% standard aluminosilicate fibre reinforced composite.

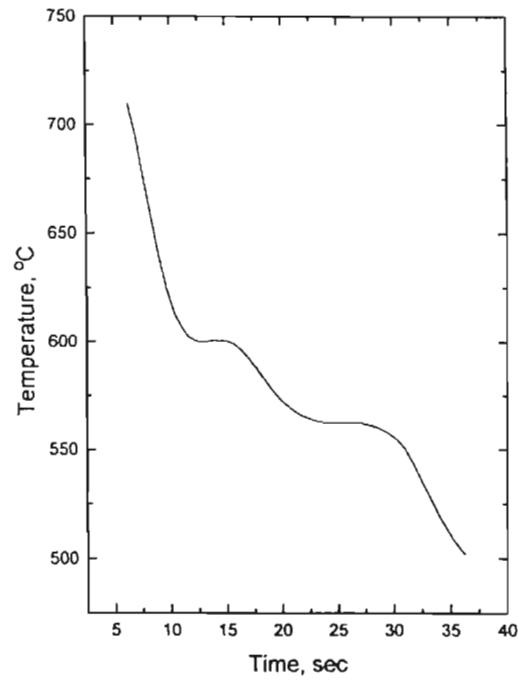


Figure 6.17(a): Solidification curve of Al(356)-10% standard aluminosilicate fibre mono composite cast in metal mould.

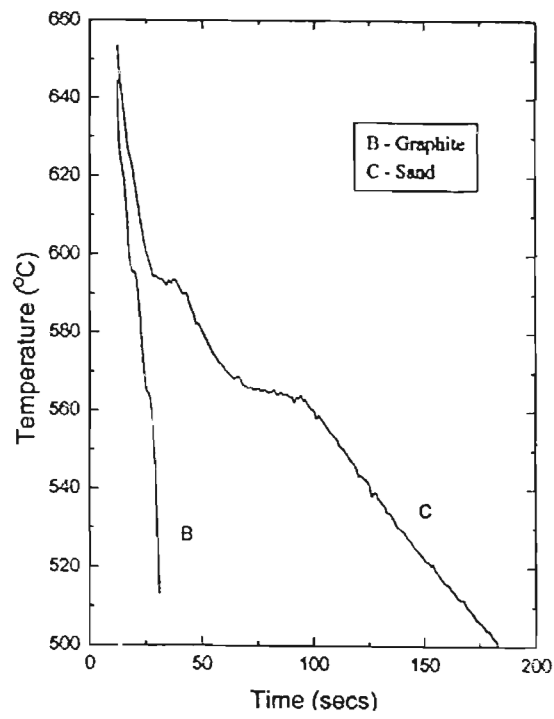


Figure 6.17(b): Solidification curve of Al(356)-10% standard aluminosilicate fibre mono composite cast in graphite and sand moulds.

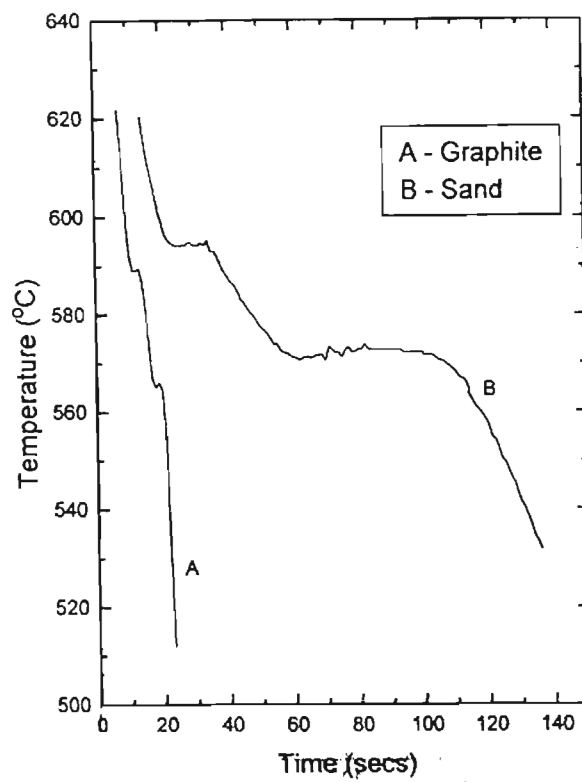
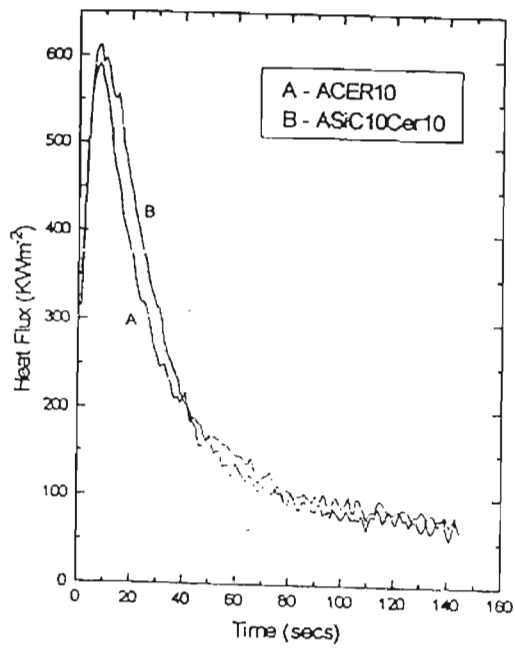
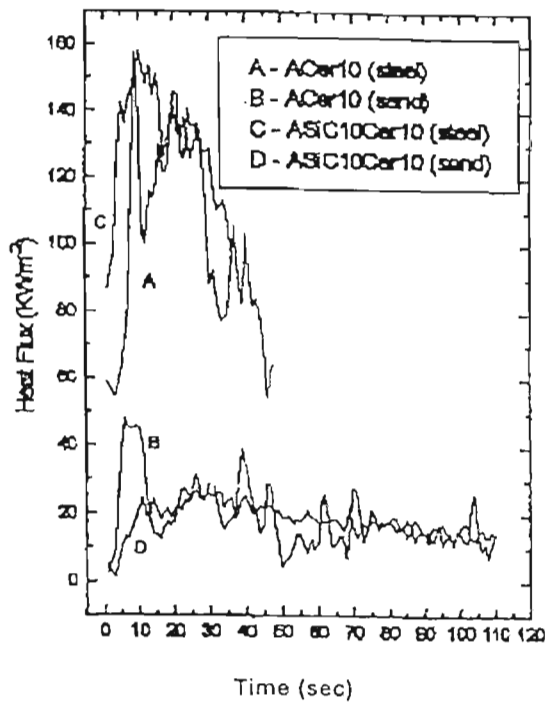


Figure 6.18: Solidification curve of Al(356)-10%SiC-10% standard aluminosilicate fibre hybrid composite cast in graphite and sand moulds

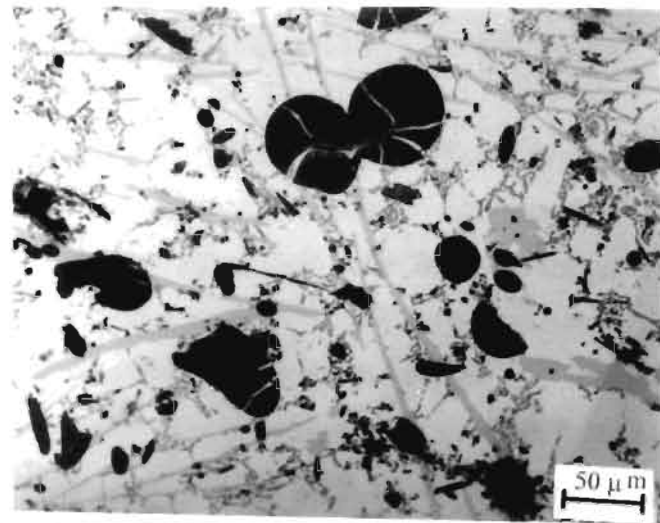


(a)

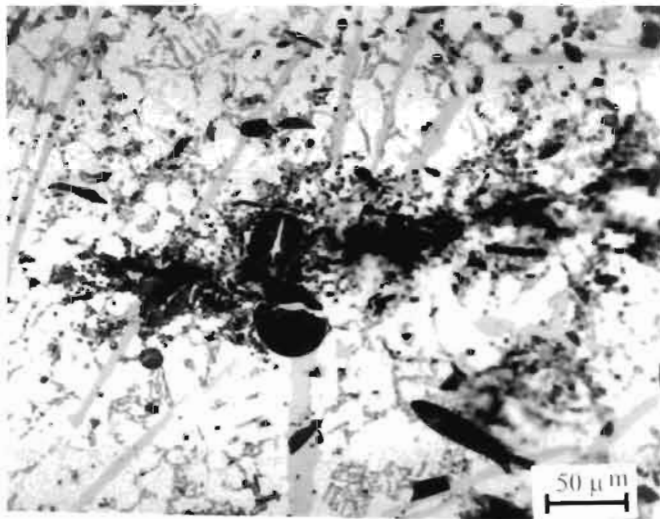


(b)

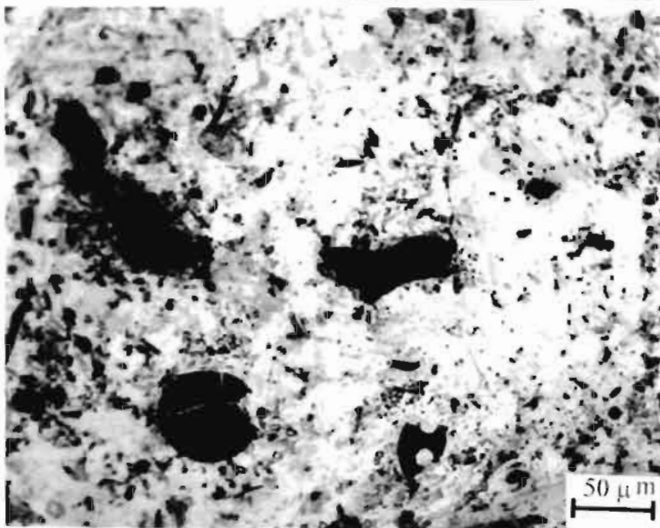
Figure 6. 19: Variation of interfacial heat flux with time for 356 alloy with ceramic fibre and its hybrid composite cast in (a) graphite and (b) steel and sand moulds.



(a)



(b)



(c)

Figure 6.20: Microstructures of Al(356)-10% standard aluminosilicate short fibre composite cast in (a) Metal (b) graphite and (c) sand moulds.

6.4 DISCUSSION

6.4.1 Fibre Treatments

The addition of as received aluminosilicate fibres into the aluminium alloy melt leads to poor dispersion and rejection of agglomerated fibres during processing. Hence, it is necessary to deflocculate these fibres before introducing into the molten metal. Mechanical stirring is not much effective as ultrasonic and leads to more fibre breakage. Therefore, chemical separation coupled with ultrasonic agitation has been observed to be a better process. The settling of shots faster than the fibres leads to their easy removal. However, still shots are present on the surface treated fibre. The treatment of fibres in acidic solution is comparatively the effective technique for the deflocculation of fibres as it retains the fluffy nature of fibres after drying.

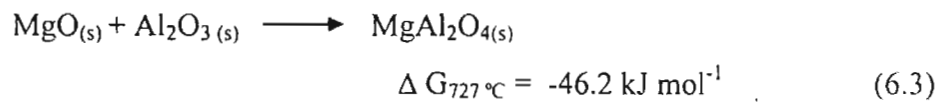
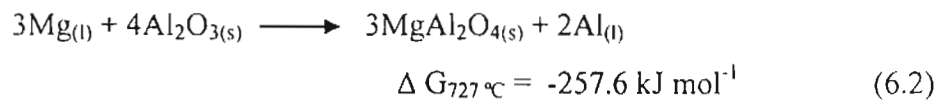
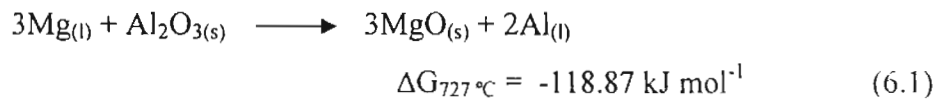
6.4.2 Microstructural Behaviour

The aluminosilicate fibres are well separated and distributed in the matrix due to the effective surface treatment of the fibres and the better bonding caused by the interfacial reaction between them. The thermal gradient at the matrix/reinforcement interface due to the large variation in the thermal conductivities of matrix alloy (121 W/m°C for liquid alloy) and reinforcement (0.140 W/m°C) prevents the primary aluminium nucleation on the aluminosilicate fibre surface.

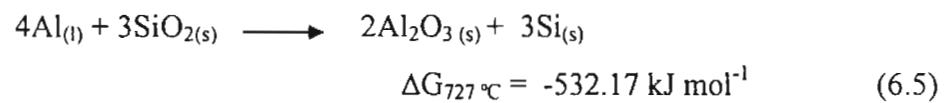
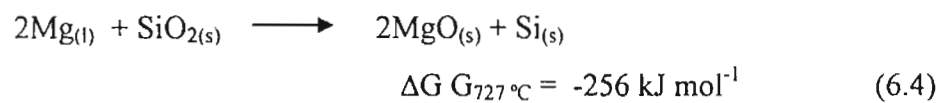
The cracking of shots and infiltration of metal into the cracks during synthesis are observed in both the zirconia grade [Figure 6.5(b)] and the standard grade fibres [Figure 6.6(b)]. Similar radial cracks in alumina particles have been reported [12] in aluminium- alumina particle composite containing Mg. It has been attributed to (i) the formation of large volumes of MgO on the outer layer of Al₂O₃, and the difference in thermal expansion leads to cracking of particle and (ii) to a limited extent to the thermal shock of the particle during its entry into the melt. The fact that penetration of the liquid melt through the fine crevices of aluminosilicate shots due to capillary effects has not left any visible porosity suggests that the cracking of shots has taken place during synthesis and not during solidification. There is also possibility for the cracking of fibres and shots during chopping operation.

6.4.3 Interfacial Behaviour

The results of interfacial studies show that both standard and zirconia grade fibre react with the matrix alloy. These interfacial reactions are detrimental to the properties of the composites. The possible reactions and various products formed are discussed below. The presence of high level of Mg at the surface of the fibre is due to the formation of the reaction products of the chemical interaction between the Mg from the matrix and the constituents of the reinforcement. The Mg can react with either Al_2O_3 or SiO_2 or both present in the fibre. The possible chemical reactions of Mg with Al_2O_3 are given below.



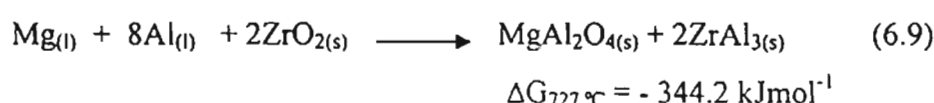
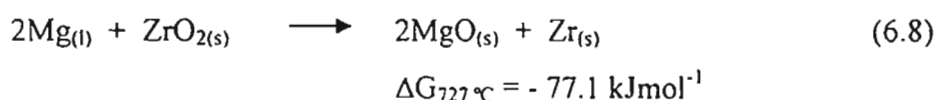
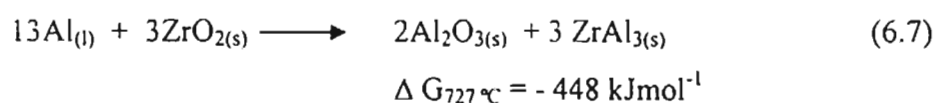
More over, Mg and Al can react with SiO_2 present in the fibre surface according to the reactions



In these three reactions, Si is rejected into the matrix. The poor solid solubility of Si in aluminium leads to its precipitation as silicon, which can possibly lead to the nucleation of the eutectic Si on the surface of aluminosilicate fibre [Figure 6.12].

Further, the higher concentration of Al, Mg and O over the aluminosilicate fibre and the presence of reaction products strongly suggest the formation and adhered layer of $MgAl_2O_4$ spinel over the surface of these fibres.

In the case of zirconia grade aluminosilicate fibres reinforced composites [Figure 6.10(b)], the interfacial reaction is more severe compared to standard grade fibre [Figure 10(a)]. In this case, in addition to the reactions (6.1) to (6.6), molten Mg and Al can react individually or together with ZrO_2 according to the following reactions.



The EDS spectra taken at the $ZrAl_3$ phase and the nearby matrix [Figures 6.14(a)-(c)] confirm the formation of $ZrAl_3$ phase. Comparing the free energy values, the reaction (6.7) could be the most probable one for $ZrAl_3$ formation.

According to an earlier study [266], ZrO_2 in crystalline form has not reacted with the molten Al or Mg and no reaction product has been detected at the particle matrix interface. In the present case, dissolution of both Al_2O_3 and SiO_2 , the major constituents of the fibre, exposes ZrO_2 to the molten Al or Mg. Since the ZrO_2 is in amorphous form, it reacts with Al or Mg more severely to form $ZrAl_3$ as one of the

reaction product, which gets distributed in the matrix due to the fluid flow experienced during composite synthesis.

In the standard aluminosilicate fibre reinforced composites, as per the free energy calculations, the reactions (6.1) to (6.6) can occur. The studies carried out on composites containing Mg as alloying element and Al_2O_3 as dispersoid have shown the formation of either MgO or MgAl_2O_4 . The thermodynamic stabilities of aluminium and magnesium oxides in Al-Mg alloys have been well studied [267]. Studies on the thermodynamic stabilities of MgO, MgAl_2O_4 and Al_2O_3 as a function of temperature and magnesium concentration have shown that Mg content above 0.02wt% in the melt could lead to the formation of MgAl_2O_4 by reacting with Al_2O_3 . The present alloy contains about 1% Mg. With this Mg content and a processing temperature of around 725 °C, the MgAl_2O_4 spinel phase is more stable than MgO. Hence, it can be concluded that the surface of fibre is enriched with Mg due to the formation of MgAl_2O_4 . Since the reaction (6.3) is a solid-state reaction, the reaction (6.2) is the most probable reaction among the reactions (6.1) to (6.3).

In the case of the reaction of Mg and Al individually with SiO_2 , since the free energy of formation of reaction (6.5) is higher than that of (6.4), the former reaction may be the most predominant one. The Al_2O_3 formed, being an impervious oxide, can prevent further penetration of liquid Al to react with SiO_2 . However, Al_2O_3 formed may not always stay at the interface leading to further reaction between the Al and the SiO_2 . Also, the Al_2O_3 formed may react with the Mg to form its oxide or spinel as per reactions (6.1) and (6.2). Hence, Mg can react with either Al_2O_3 present in the fibre or freshly formed Al_2O_3 due to the reaction (6.5). Once the Mg from the alloy is depleted to a very low level, further attack of Mg may not take place and the surface layer of fibre would have both the MgAl_2O_4 and the Al_2O_3 . This means, in the case of standard aluminosilicate fibre reinforced composite, multiple reactions can occur. The Al_2O_3 constituent is attacked by the Mg to form mainly the spinel, whereas, the SiO_2 constituent is attacked by both the Al and the Mg, the former being the more probable one. As per Figure 6.13, the presence of MgAl_2O_4 in matrix confirms that the spinel may not stay always at the interface and can go into the matrix as well. This is because of the renewal of interface between the matrix and the reinforcement occurring during the stirring process. The Mg loss in the matrix alloy

due to the interfacial reaction of the aluminosilicate fibres in the composites needs to be compensated for keeping the Mg level sufficient for precipitation hardening.

In the zirconia grade aluminosilicate fibre composite, the above said reactions and mechanisms of standard grade fibres are also possible. In addition, the ZrO_2 present in these fibres reacts with either Al or Mg as per the reactions (6.7) and (6.8) respectively. The aluminium forms an intermetallic compound $ZrAl_3$ with ZrO_2 . [Figure 6.14]. A Similar observation has been reported in the case of zirconia stabilized alumina fibre reinforced aluminium matrix composites fabricated by pressure infiltration process [262]. The Gibbs free energy of reaction (6.7) at 727 °C is a negative value ($\Delta G_{727\text{ °C}} = - 448 \text{ kJmol}^{-1}$) and hence the formation of $ZrAl_3$ is feasible. The phase diagrams of Al-Zr, Al-Zr-Mg and Al-Zr-Si show that $ZrAl_3$ is a stable phase in all these systems and it is the first intermetallic compound to form in equilibrium with the aluminium in the Al-Zr system [268]. Hence, the reaction between Al and ZrO_2 can be confirmed. But the reaction (6.8) between the Mg and the ZrO_2 could not be confirmed by experimental analysis since it doesn't form any stable intermetallic with Zr. Even though Zr is formed as per reaction (6.8), it may again combine with Al from the matrix or the free Al formed at the interface from the reaction (6.1) or (6.2) to form the intermetallic $ZrAl_3$. In general, the presence of large intermetallic phases such as $ZrAl_3$ and others can strengthen the matrix similar to that observed in particulate metal matrix composites. However, the severe reaction between the zirconia grade fibre and the Al matrix reduces the contribution of the $ZrAl_3$ towards strengthening. This means that the zirconia grade fibre is more vulnerable to interfacial reaction than the standard grade aluminosilicate fibre. Even though the zirconia contained fibres possess high temperature stability, their stability in Al-Si-Mg alloy is poorer compared to the standard aluminosilicate fibres as observed under SEM. This is due to the fact that zirconia grade fibres contain only about 32-36 wt% Al_2O_3 compared to 43-47 wt% in standard grade fibre. Since Al_2O_3 phase gives maximum resistance for the reaction in these fibres, zirconia grade fibres containing less amount of Al_2O_3 as well as 16.5-19.5 % ZrO_2 is highly reactive and thus becomes more susceptible for the reaction during composite synthesis.

As the composite is synthesized by stir casting technique, the reaction products formed due to interaction between matrix and reinforcement during the stirring process may not stay at the interface; instead part of this could enter into the matrix alloy. Thus in the present case a part of the spinel formed is segregated in the eutectic silicon region of the matrix [Figure 6.13].

6.4.4 Heat Treatment Response

The lower hardness of the aged composites can be attributed to the lower amounts of Mg_2Si precipitate formed in the matrix. This is because of the loss of Mg from the matrix as a result of the formation of $MgAl_2O_4$, the interfacial reaction product between the fibre and the matrix. According to Ribes *et al.* [269, 270], the formation of $MgAl_2O_4$ spinel at the interface in A356 aluminium alloy reinforced with oxidized SiC particles reduces the Mg content of the matrix. This reduction in Mg concentration has suppressed the age hardening behaviour owing to the precipitation of lesser amount of Mg_2Si . Similar loss of Mg caused by the interfacial reaction in Kaowool ($Al_2O_3 \cdot SiO_2$) fibre reinforced 339 aluminium matrix composite [261] has reduced the hardness of the composite proportional to the residual Mg concentration in the matrix. Hence, it can be concluded that the interfacial reaction depletes the Mg content in the matrix and thus lowers the extent of strengthening of the matrix.

6.4.5 Solidification Behaviour

The lowering of liquidus temperature of the composite compared to the base alloy can be due to the unfavourable conditions prevailing for nucleation of primary aluminium at the fibre surface. Similar phenomena is also observed in the cooling curve of SiC particulate reinforced Al(356) alloy melt [271].

Iron based intermetallic compound formation observed in the cooling curve of the sand mould [Figure 6.17b], similar to that by Mackey *et al* [271] could be either due to iron present in the alloy itself or picked up during processing. Iron being the common contaminant during the processing of these composites, iron intermetallic compounds would form.

Comparison of the peak heat flux values of different moulds show that the higher interfacial peak heat flux value observed for graphite mould is due to its high thermal conductivity than steel and sand moulds. Lower peak heat flux caused by lower heat transfer rate leads to longer solidification time as in the sand mould. The addition of 10% ceramic aluminosilicate fibre to the matrix alloy reduces the peak heat flux value from 852 to 600 kWm⁻². The lower thermal conductivity of the ceramic fibre reduces the overall thermal conductivity of composite system and hence the heat flux value. In addition, the total heat to be extracted from the composite system will be reduced by the presence of the fibre.

6.5 SUMMARY

1. The as received fibres are of assorted lengths in agglomerated bunches containing shots necessitating deflocculation of these fibres prior to incorporation into the melt.
2. Dispersion of these indigenous aluminosilicate short fibres into the aluminium alloy matrix is possible by liquid metal stir casting technique only after surface treatment.
3. Among the various surface treatments studied, the ultrasonic treatment of the fibre in acidic media (pH 4-5 range) has given better dispersion and less agglomeration and porosity in the composite castings.
4. The contact of aluminosilicate fibres with the liquid metal during the synthesis of composites leads to the excessive interfacial reaction. All the major constituents of the fibre such as Al₂O₃, SiO₂ and ZrO₂ react with the matrix elements.
5. MgAl₂O₄ spinel formation is observed in both the standard and the zirconia grade fibres. The formed spinel is observed both at the interface and in the eutectic region of the matrix.
6. The zirconia grade fibre reacts with aluminium leading to the formation of ZrAl₃ intermetallic as coarse precipitates in the matrix alloy.
7. The zirconia grade fibre is more affected by the interfacial reactions than the standard aluminosilicate fibre. This is probably due to the presence of lower amount of Al₂O₃, which normally offers better resistance to reaction during composite synthesis and also because of highly reactive ZrO₂ phase in the fibre.

8. The interfacial reaction depletes the Mg content in the matrix, thus reducing the amounts of Mg_2Si available during precipitation hardening and resulting in lower hardness for the composites during aging. Even though processing of short aluminosilicate fibre reinforced aluminium by liquid metal stir casting is possible, the reaction of fibres reduces the hardness and the tensile properties.
9. The addition of aluminosilicate fibre reduces the liquidus temperature of the matrix. Similarly, the peak heat flux values of ceramic fibre reinforced composite are lower than the matrix alloy due to the low thermal conductivity behaviour of the fibres.
10. The formation of iron intermetallic is reflected in the cooling curve recorded in the sand mould and also observed in the microstructures of the aluminosilicate fibre reinforced composite solidified in metal, graphite and sand mould. Iron intermetallics change their shape from acicular to plate like when solidified slowly in sand mould.

CHAPTER 7

Al(356) – FLY ASH COMPOSITES

7.1 INTRODUCTION

Among the various discontinuous dispersoids used, fly ash is one of the cheapest low-density reinforcement obtained in large quantities as a waste by-product during the combustion of coal in thermal power plants. Addition of fly ash particles improves the wear resistance, hardness and stiffness and reduces the density of the matrix material [272-277]. Compared to the commonly used reinforcements such as silicon carbide and alumina, fly ash is a very less expensive and low density dispersoid providing properties nearer to Al-SiC/Al₂O₃ systems. Liquid metal stir casting [273, 277, 278] and Infiltration techniques [279-281] are generally adopted for the synthesis of fly ash reinforced metal matrix composites. Aluminium and its alloys are commonly used as the matrix for the synthesis of fly ash, reinforced metal matrix composites. The fly ash reinforced aluminium matrix composites are also termed as 'Ash alloys' [272]. The aluminium- fly ash composites have potential applications as covers, pans, shrouds, casings, pulleys, manifolds, valve covers, brake rotors, and engine blocks in automotive, small engine and the electromechanical industry sectors [272]. There are two types of fly ash, namely, precipitator and cenosphere. The former is a solid fly ash with a density of 1.9-2.4 g/cc, and the later is a hollow fly ash with a density of 0.4 to 0.6 g/cc. Hence, cenosphere fly ash offers the best advantage of reducing the overall density of the composite. The major chemical constituents of fly ash are SiO₂, Al₂O₃, Fe₂O₃ and CaO. Mineralogically, the fly ash constitutes the aluminosilicate glasses containing quartz, mullite, hematite, magnetite, ferrite spinel, anhydride and alumina [272].

Earlier work [282] in the laboratory on the synthesis and characterisation of Al-12Si-fly ash (about 100 μm size) composite has revealed (i) the possibility of incorporating up to 10 wt% as received fly ash particle after heating in Al-12Si alloy

through liquid stir casting (ii) linear decrease in the density and the ultimate tensile strength and (iii) linear increase in the electrical resistivity of Al₁₂Si-fly ash composites with increasing dispersoid content. Further, microstructural analysis has shown tendency to (i) form increasing amount of needle shaped iron intermetallics (ii) nucleate primary silicon on the fly ash surface (iii) coarsen eutectic silicon around the fly ash particle and (iv) form agglomerates of fly ash with increasing content.

Various studies [272] carried out on the processing of fly ash composites have utilized larger particles of size greater than 50 μm . The addition of finer particles provides better properties and avoids segregation in the casting due to settling or floating. However, introduction of particles of size $< 20 \mu\text{m}$ leads to agglomeration of fine particles in the matrix thus giving poor properties. Hence, the utilization of fine fly ash particles for the synthesis of composites with uniform distribution and better properties poses a serious problem.

The present study aims at the utilization of fine fly ash particles of 13 μm average particle size for the synthesis of aluminium matrix composites and characterizing the resulting composites. The different processing techniques used are liquid metal stir casting, compocasting, modified compocasting and modified compocasting followed by squeeze casting.

7.2 METHODOLOGY

The matrix material used is Al-7Si-0.35Mg (356) cast aluminium alloy. The fly ash particles used as the dispersoid are of assorted size with an average particle size of 13 μm . The spherical fly ash contained both the solid sphere (precipitators) and the hollow sphere (cenosphere) particles. The density of fly ash measured by Helium pycnometer is 2.486 g/cc. The composites are fabricated using both the as received and the surface treated particles. The surface treatment is by ultrasonic vibration of the fly ash particles in 0.02% sodium silicate aqueous solution with a pH around 4. The surface treated particles are heat treated at 600 °C for 2 hrs prior to introduction into the melt. The composite processing is carried out in 0.5 kg level melt.

Liquid metal stir casting, compocasting and modified compocasting are used for the fabrication of fly ash composites. In the liquid metal stir casting, the incorporation of fly ash particles into the melt and pouring of composite melt into the mould are carried out in a fully liquid state (i.e. above liquidus temperature of the matrix alloy). In the case of compocasting process, both the above steps are carried out in a semisolid state (at a temperature in between the solidus and liquidus temperatures). However, in the case of modified compocasting process, the particle addition and the casting are carried out in the freezing range and above the liquidus temperature respectively.

The composites are shaped into 120 x 43 x 15 mm rectangular plates and 55 mm length x 27.5 mm diameter cylindrical castings by permanent moulds. In the case of modified compocasting, both the gravity and the squeeze casting methods are adopted. The squeeze casting is carried out using 150T hydraulic press and the ingot size is of 75 mm diameter x 50 mm long cylinder. Initially, composites with only 5 wt% flyash are synthesised to arrive at the best processing parameters. Later aluminium(356)-15 wt% fly ash composite is processed using modified compocasting followed by squeeze casting method.

Metallographic specimens are taken from the centre of composite cylinder, polished and observed under optical microscope. The composites are evaluated by image analysis, SEM, EDS, density measurement, eddy current testing and mechanical testing. The interparticle distance is determined using image analysis by taking the distance between two nearest particles.

7.3 RESULTS

SEM picture of the fly ash particles in as received condition [Figure 7.1(a)] shows that they are spherical in shape with assorted sizes and agglomerates of fine fly ash particles sticking to the surfaces of the larger ones. The surface treatment by deflocculation has cleaned the particle surface [Figure 7.1(b)] to some extent and also separated the finer ones. Figures 7.2 (a) and (b) show the SEM photomicrographs of

broken cenosphere particle containing smaller ones inside and non-spherical fly ash particle showing finer ones sticking to its surface respectively.

7.3.1 Optical Microstructures and Image Analysis

7.3.1.1 Liquid metal stir casting

The optical micrograph of Al(356)-5% fly ash composite [Figure 7.3(a)] shows that incorporation of as received (untreated) fly ash particles leads to porosity and large/chunky particle agglomerates in the interdendritic region. On the other hand, the surface-treated particles result in better dispersion of fly ash particle in the matrix by breaking large agglomerates and separating individual cenospheres [Figure 7.3(b)]. Further, it may be noticed that few agglomerates found in surface treated fly ash composites are not chunky. This can be attributed to the treatment, deflocculating and separating the particles. However, the pushing of fly ash particles to the interdendritic regions during solidification still takes place suggesting that the primary aluminium does not nucleate on the particle surface. Figure 7.4 shows a wide frequency distribution in interparticle distance from a minimum of 10 μ m to a maximum of 210 μ m in Al(356)-5% Fly ash (surface treated) composite synthesised by liquid metal stir casting and cast in metal mould. The average area of primary α -aluminium in these composites is $2.581 \times 10^3 \mu\text{m}^2$.

7.3.1.2 Compocasting

The microstructure of semisolid processed (compocast) Al(356)-surface treated 5% fly ash composite [Figure 7.5(a)] cast in metal mould has shown improved dispersion of fly ash particles compared to the one prepared by liquid metal stir casting. However, segregation of fly ash particles in the eutectic region i.e., in between the primary α -Al is also seen. In this case, the area of primary α varies between 0.5×10^3 to $25 \times 10^3 \mu\text{m}^2$ with a large number of α -phase having an average area of $3.5 \times 10^3 \mu\text{m}^2$. The composite solidified in the graphite mould has also shown similar distribution of fly ash particles [Figure 7.5(b)] like that cast in metal mould. The composite solidified in the crucible [Figure 7.5(c)] has exhibited similar dispersion of fly ash but with large primary α -aluminium with an average area of

about $12.95 \times 10^3 \mu\text{m}^2$ and a lower level of segregation of particles in the interdendritic regions. The frequency distribution in interparticle distance between the fly ash particles of composites cast in metal and graphite moulds as well as solidified in the crucible are plotted respectively in Figures 7.6(a-c). Figure 7.7 shows the microstructure of Al(356)-5% Fly ash composite processed by compocasting and cast in metal mould showing coarse primary phases.

7.3.1.3 Modified Compocasting Process

The composite synthesised by this process [Figure 7.8] shows a better distribution of the particles compared to the composites made by liquid metal [Figure 7.3] or by semisolid processed technique [Figure 7.5]. The average primary α -aluminium area is about $1.756 \times 10^3 \mu\text{m}^2$ [Table 7.1]. The interparticle distances are plotted in Figure 7.9(a) and most of the particles are in range of 30 to 70 μm apart. The interparticle distance in the 15% fly ash dispersed composite prepared by modified compocasting process followed by squeeze casting falls in between of 30 to 50 μm (Figure 7.9b). Figures 7.10(a and b) show the microstructures of Al(356)-15% Fly ash composite processed by modified compocasting followed by squeeze casting.

Table 7.1: Measured areas of primary α -aluminium phase in Al(356)-5% fly ash (treated particles) composites synthesised by different routes

Casting Process	Area of smallest size α -phase, $\times 10^3 (\mu\text{m}^2)$	Area of larger size α -phase, $\times 10^3 (\mu\text{m}^2)$	Weighted average area of α -phase, $\times 10^3 (\mu\text{m}^2)$
Liquid metal stir cast (metal mould)	0.5	10	2.581
Compocast (metal mould)	0.5	25	3.5
Compocast (graphite mould)	0.2	30	3.9
Compocast (solidified in crucible)	0.5	50	12.95
Modified compocasting (metal mould)	0.2	5	1.756

7.3.2 SEM Microstructures and EDS Analysis

The composite samples prepared for the optical metallographic examination have been deep etched and observed under SEM. Figure 7.11(a) is the typical cross section of a solid fly ash spherical particle. Eutectic Si is seen around the particle and in some places, Si seems to cover or originate from the surface of the particle. Figure 7.11(b) is the cross section of a hollow fly ash particle in the composite. Fine crystallites of fly ash particles are seen inside this particle. In this case, the amount of eutectic Si around the particle is less and the reaction between particles and the matrix is also minimum. In Figure 7.11(c), coming out of a fly ash particle from the matrix probably during polishing is seen suggesting its weak bonding with the matrix. Two gas holes are also seen with partial filling by the fine crystallites of spinel. These pictures clearly demonstrate the different levels of bonding possible between the fly ash and aluminium alloy matrix. Both 5% and 15% fly ash dispersed composites have shown similar bonding. Figure 7.12 shows the SEM micrograph of a broken cenospherical fly ash particle in aluminium matrix, wherein the liquid metal has infiltrated into the hollow space between the fine fly ash particles and solidified. This phenomenon of filling the hollow space of fly ash by matrix alloy increases the density of the composite.

Figure 7.13 shows the SEM photomicrographs of Al(356)-15% fly ash composites and their respective EDS spectra of different phases. The EDS spectra of position '1' in Figure 7.13(b) shows the peaks corresponding to Al(64.39 at %), Si (23.21 at %) and Fe (12.4 at %). The EDS spectra in Figure 7.13(e) of the phase 4 in the SEM photomicrograph also shows the peak corresponding to the iron intermetallic phase. This iron intermetallic phase has formed from the liquid matrix alloy that has infiltrated into the hollow sphere of cenospherical fly ash particle. This iron intermetallic phase had nucleated from the inner surface of the fly ash particle. The morphology of the phase reveals that it could be β -iron intermetallic phase (FeSiAl_5). The β - FeSiAl_5 is a brittle intermetallic compound having monoclinic structure and appears in the form of platelets. The SEM photomicrograph in Figure 7.13(a) shows two cenospherical fly ash particles into which the matrix phase has infiltrated and solidified. The EDS spectra in Figure 7.13(c) and (d) of phases marked as 2 and 3

inside the fly ash particle correspond to the eutectic silicon and primary aluminium phases respectively.

Figure 7.14(a) shows the SEM photomicrograph of Al(356)-15% fly ash composite showing solid fly ash particle around which eutectic silicon has nucleated. Figures 7.14(b) and (c) show the EDS spectra of eutectic silicon near and away from the matrix-reinforcement interface marked as 1 and 2.

The typical tensile fracture of the composites shows [Figure 7.15(a)] a mixed mode of ductile and brittle fracture. Generally, the hollow fly ash particles have shown fractured particles with good interfacial bonding [Figure 7.15(b)]. However, particle pull out is also seen [Figure 7.15 (c)] where interfacial gap between the particles and the matrix exists.

SEM fractographs of compression test specimens of Al(356) matrix alloy and Al(356)-15% fly ash particle composite are given in Figure 7.16(a) and (b) respectively. The base alloy shows long deformation bands with wide plateaus whereas the composites show very short deformation bands and plateaus. This is due to the lower ductility of composites than the base alloy. Hence, during compression loading, the base alloy deforms more than the composites. Further, the composite shows deep and wider deformation band, which is caused due to the ploughing action of particles during the compression loading. Observations at high magnification have shown the debonded and fractured fly ash particles in few places of the composites.

7.3.3 Physical Properties

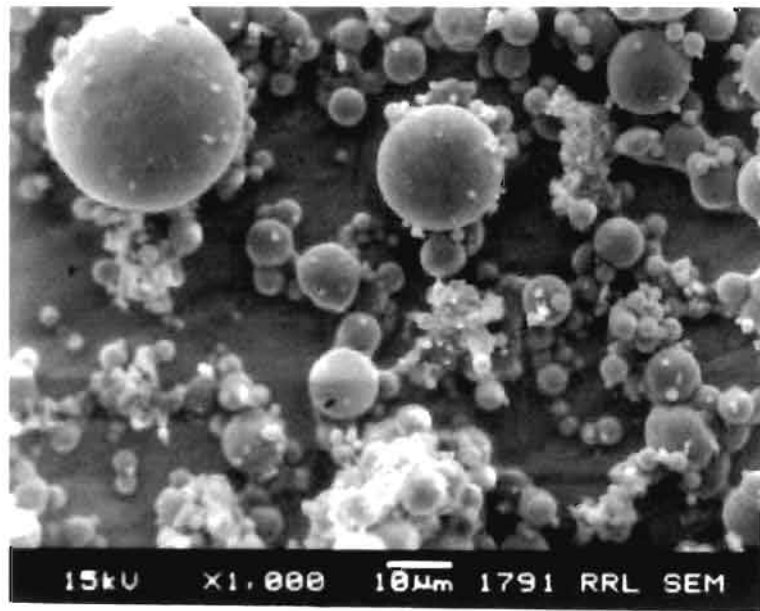
The measured densities of Al (356)-5% fly ash composites fabricated by different processing techniques and the calculated theoretical value by the rule of mixtures (ROM) are compared in Figure 7.17. The density of modified compocast composite is 2.65 g/cc, which is the highest among ones processed by different techniques in this investigation and closer to the theoretical value 2.67 g/cc. On the other hand, the liquid metal stir cast composite with as received particles shows the lowest value of 2.44 g/cc. This variation in density values is mainly due to varying porosity level and the order of particles separation and distribution. The composites

fabricated by compocasting gives a medium density values around 2.50 to 2.55 g/cc, the lowest being for the composite cast and solidified in crucible with very slow cooling rate.

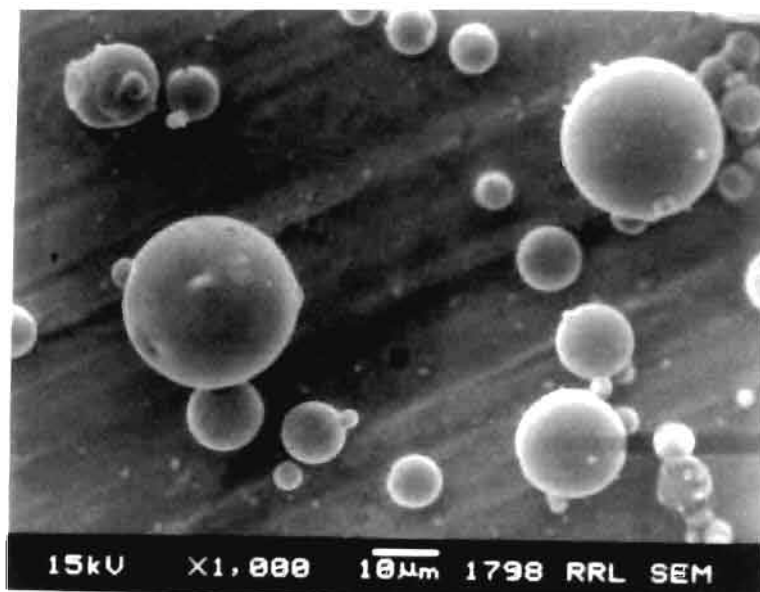
The electrical conductivities of Al (356) – 5% Fly ash composites fabricated by different techniques are compared in Figure 7.18. Similar to the density, the highest (30 %IACS), the lowest (18 %IACS) and the medium (26-28 %IACS) values of electrical conductivity have been obtained in the composites fabricated by the modified compocasting technique, liquid metal stir cast composite using as received particles and the compocasting respectively.

7.3.4 Mechanical Properties

The average tensile strength obtained in T6 condition for the 15% fly ash composite is 193 MPa, whereas the values for the squeeze and permanent mould cast alloy are 287 and 270 MPa respectively. The average compressive strength of 356-15% Fly ash composite in T6 condition is 623 MPa against 567 and 557 MPa for the matrix alloy cast by squeeze casting and permanent mould.

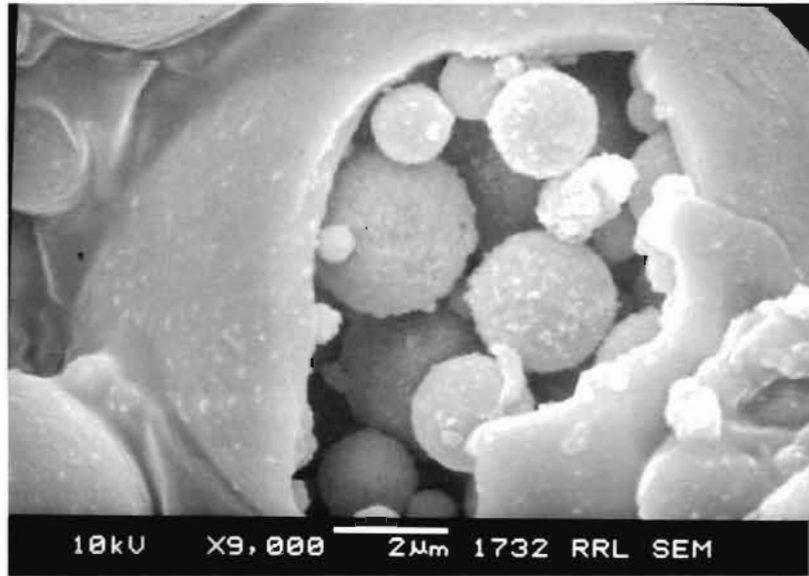


(a)



(b)

Figure 7.1: SEM photomicrographs of fly ash particles (a) as-received and (b) surface treated.



(a)



(b)

Figure 7.2: SEM photomicrographs of (a) broken cenosphere particle containing smaller particles inside and (b) non spherical fly ash particle with fine globular particles sticking.

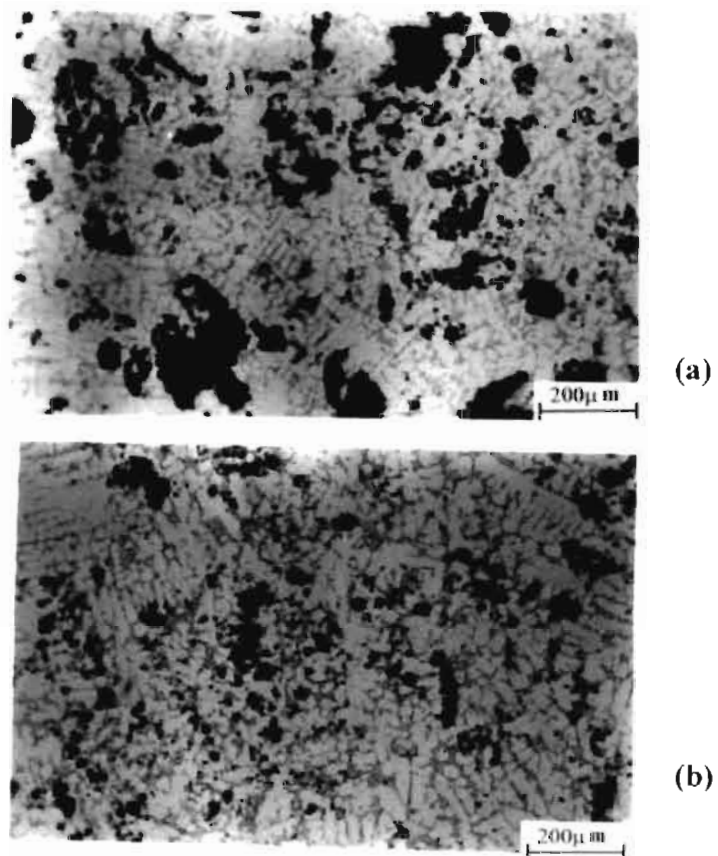


Figure 7.3: *Photomicrographs of Al(356)-5% (a) as-received and (b) surface treated fly ash composite synthesised by liquid metal stir casting and cast in metal mould.*

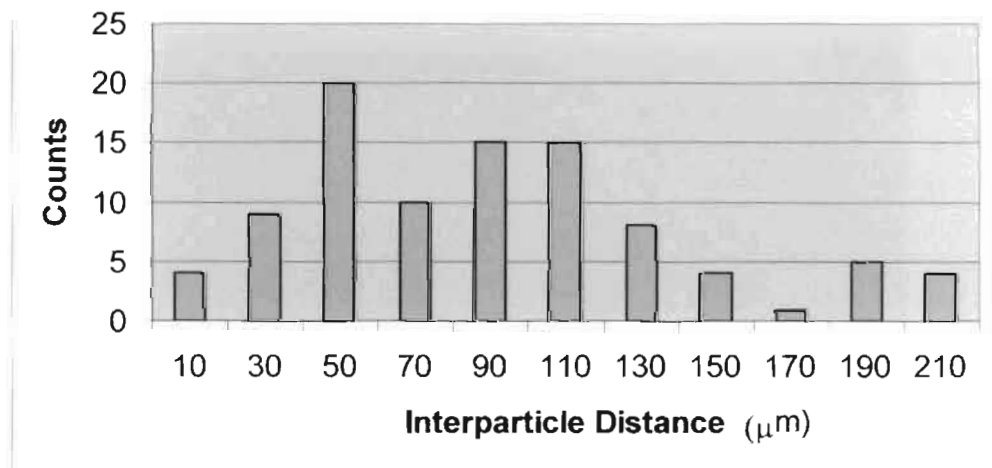
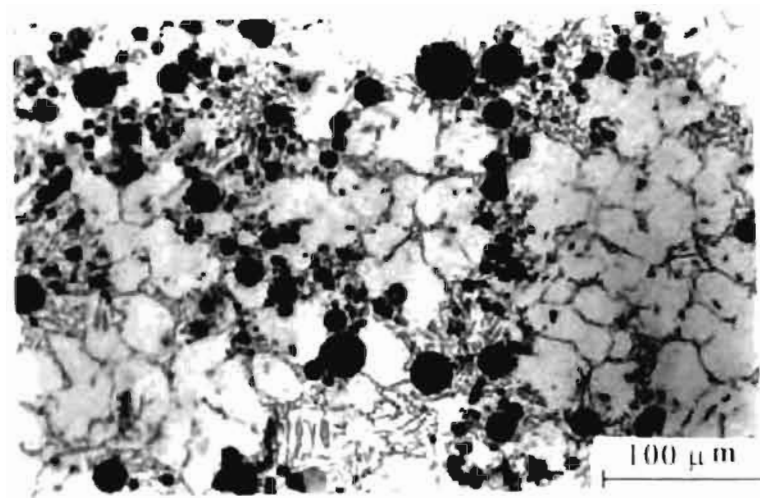
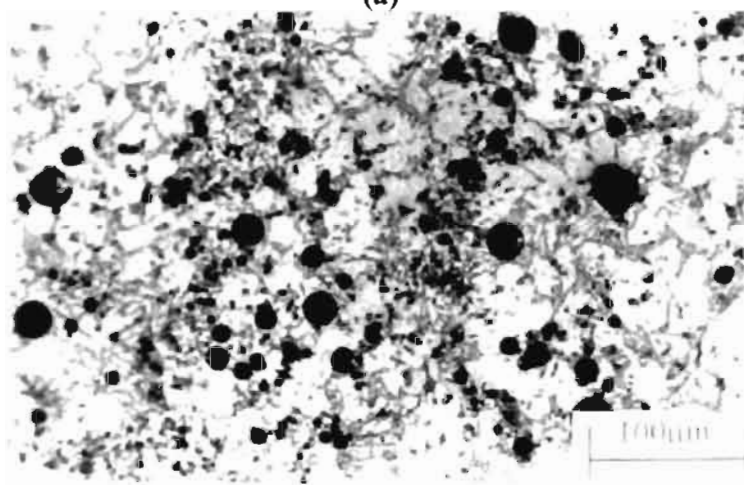


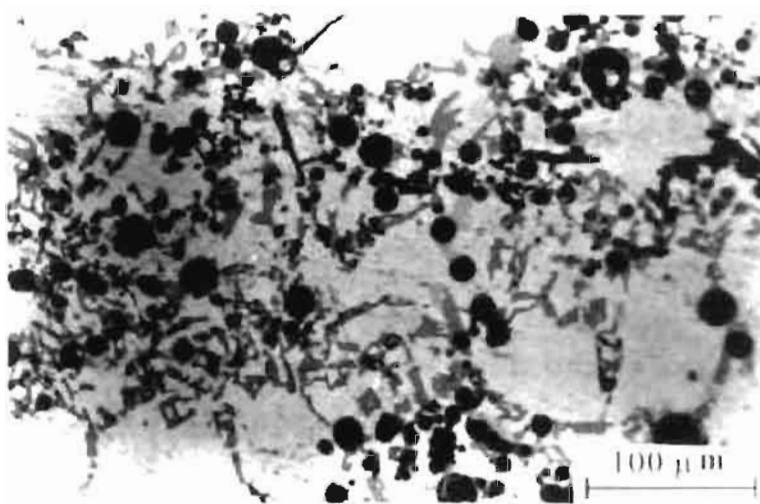
Figure 7.4: *Frequency distribution in the interparticle distance measured in Al(356)-5% fly ash (surface treated) composite synthesised by liquid metal stir casting and cast in metal mould.*



(a)

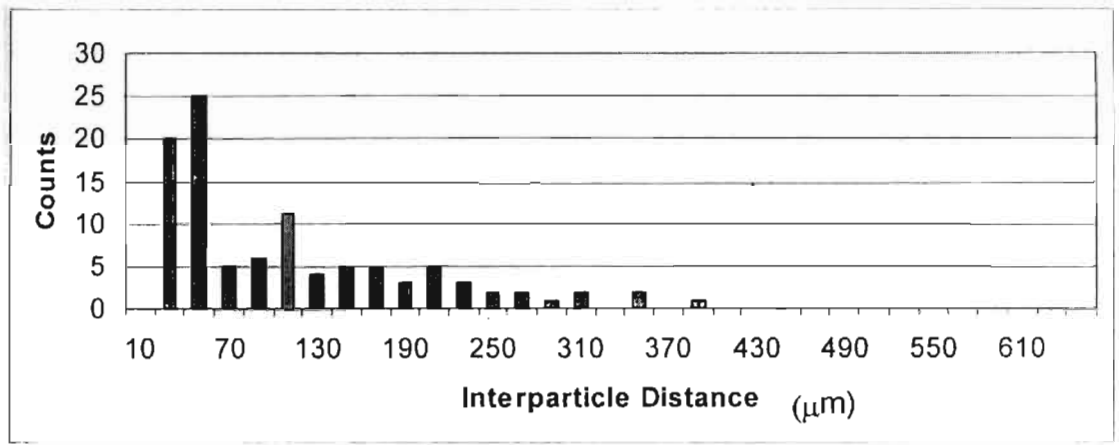


(b)

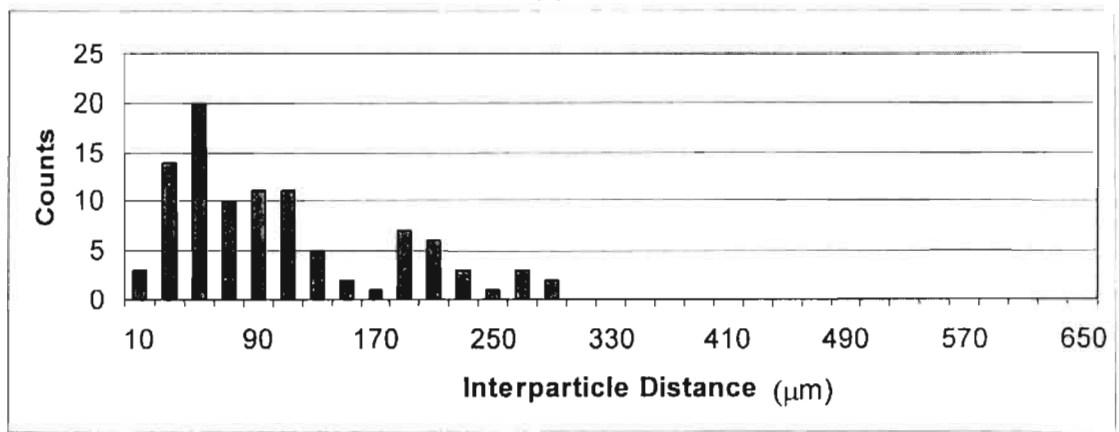


(c)

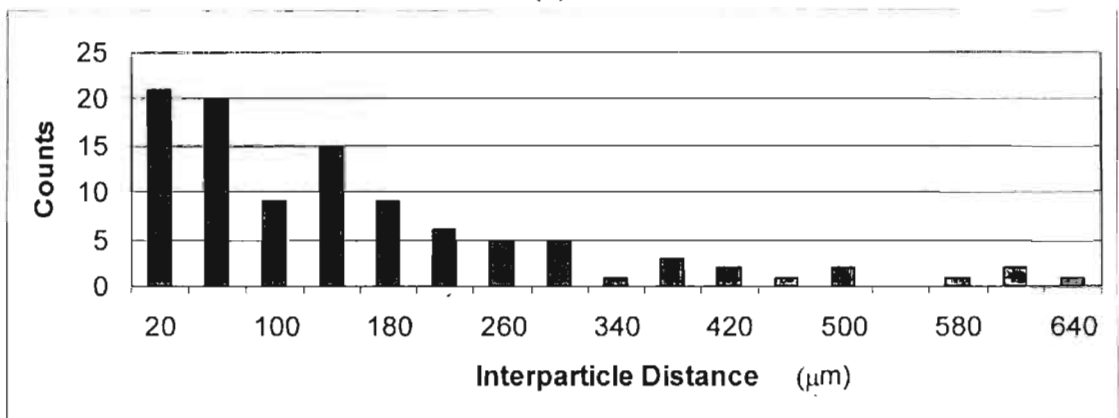
Figure 7.5: *Photomicrographs of Al(356)-5% fly ash (treated) composite processed by compocasting and cast in (a) metal mould, (b) graphite mould and (c) crucible*



(a)



(b)



(c)

Figure 7.6: Frequency distribution in the interparticle distance in Al(356)-5% fly ash (treated) composite processed by compocasting and solidified in (a) Metal mould, (b) Graphite mould and (c) Crucible

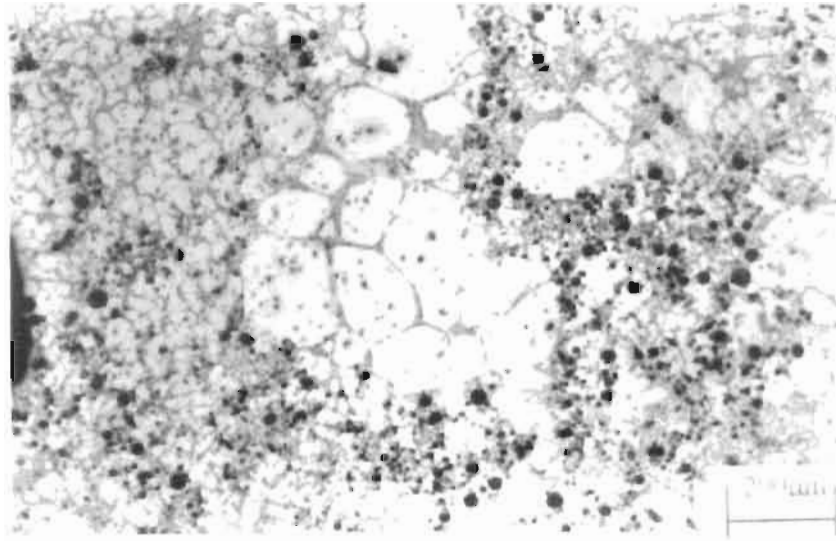


Figure 7.7: Photomicrograph of Al(356)-5% fly ash composite processed by compocasting and cast in metal mould showing coarse primary phases.

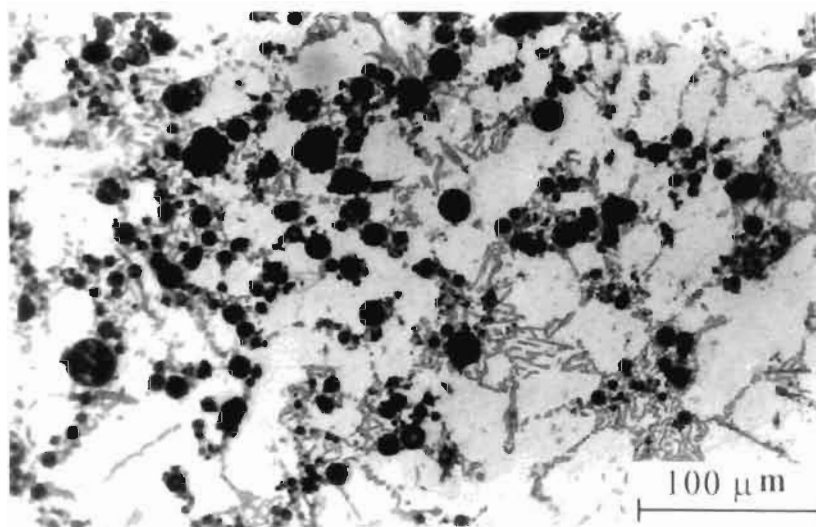
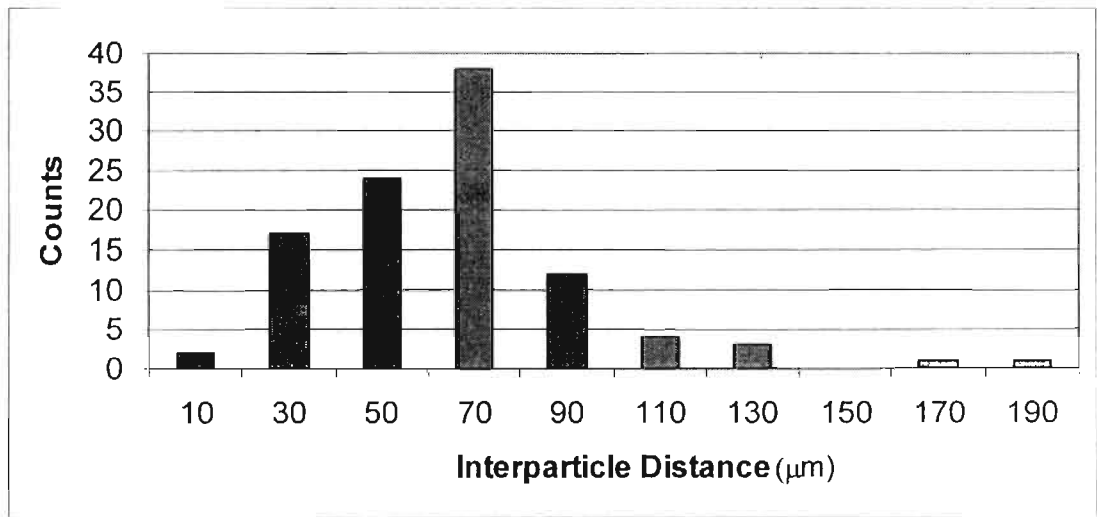
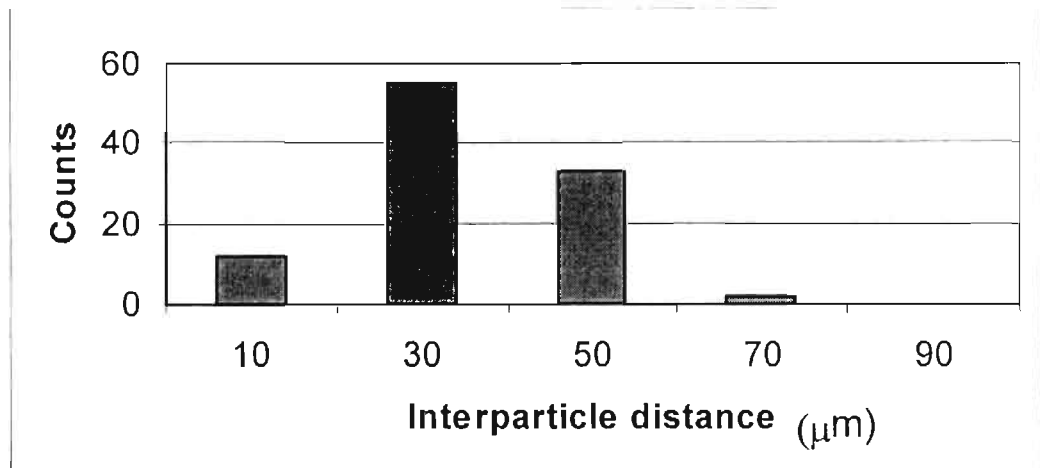


Figure 7.8: Photomicrographs of Al(356)-5% fly ash composite processed by modified compocasting and cast in metal mould.

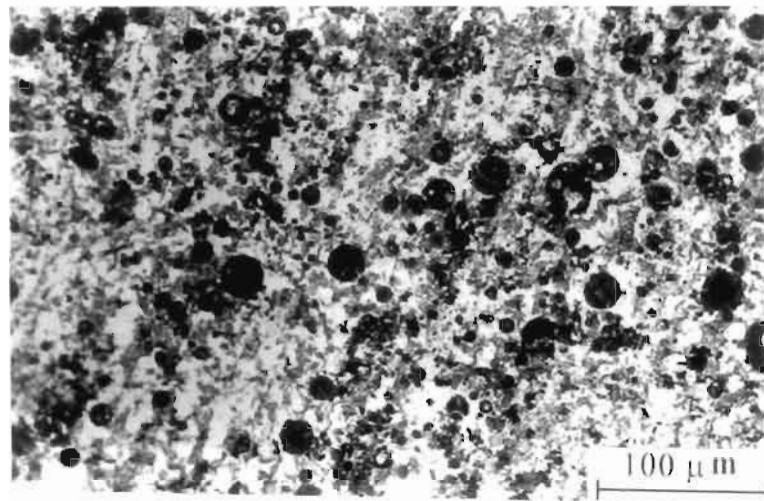


(a)

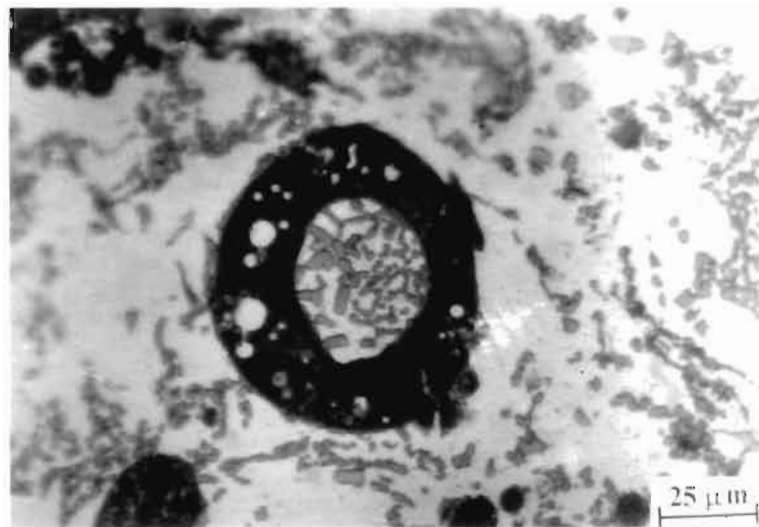


(b)

Figure 7.9: *Frequency distribution in the interparticle distance in (a) Al(356)-5% fly ash composite processed by modified compocasting and cast in metal mould and (b) Al(356)-15% fly ash composite processed by modified compocasting and cast by squeeze casting.*

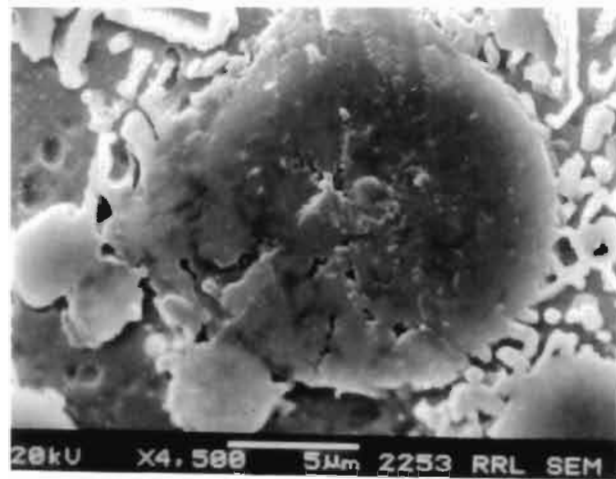


(a)

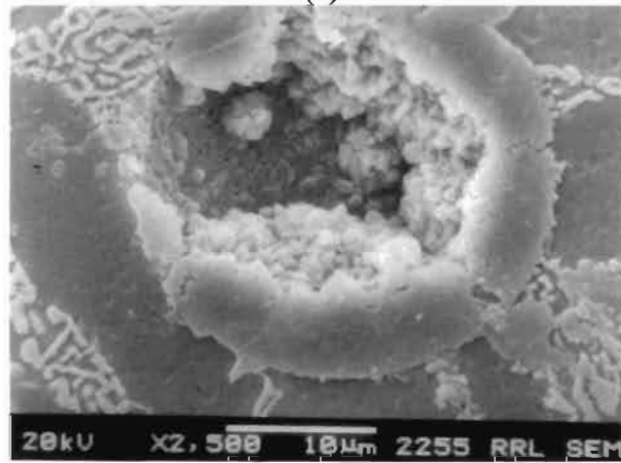


(b)

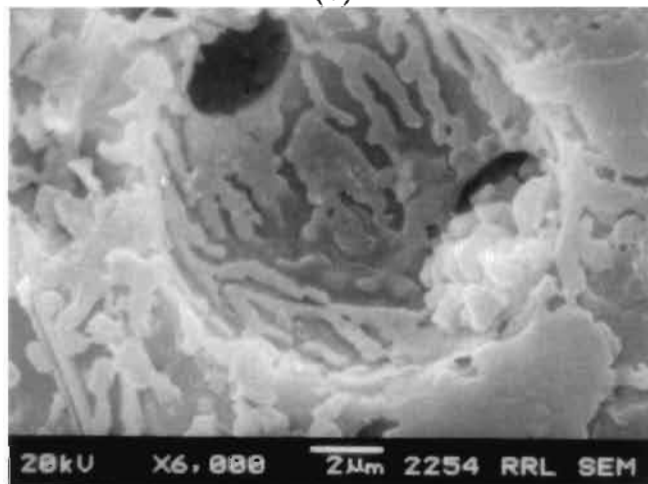
Figure 7.10: *Photomicrographs of Al(356)-15% fly ash composite processed by modified compocasting followed by squeeze casting. (a) Distribution of fly ash particle in the matrix and (b) hollow fly ash particle showing solidification of the matrix alloy in the cavity.*



(a)



(b)



(c)

Figure 7.11: SEM photomicrographs of Al(356)-15% fly ash composite processed by modified semisolid stir casting followed by squeeze casting. (a) solid fly ash particle, (b) hollow cenospherical fly ash particle and (c) Fly ash particle detached from the matrix showing $MgAl_2O_4$ phase and eutectic silicon.

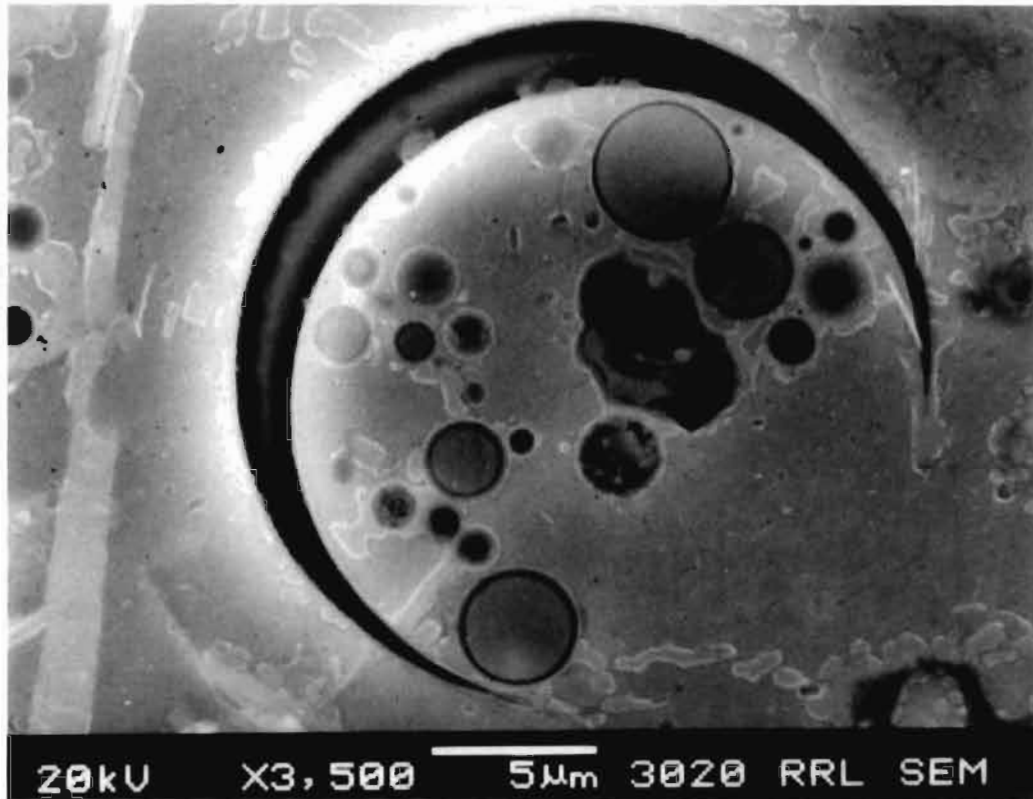


Figure 7.12: SEM photomicrographs of Al(356)-15% fly ash composite processed by modified semisolid stir casting followed by squeeze casting showing the solidification of infiltrated matrix alloy into a hollow space of broken cenospherical particle containing fine solid fly ash particle.



(a)

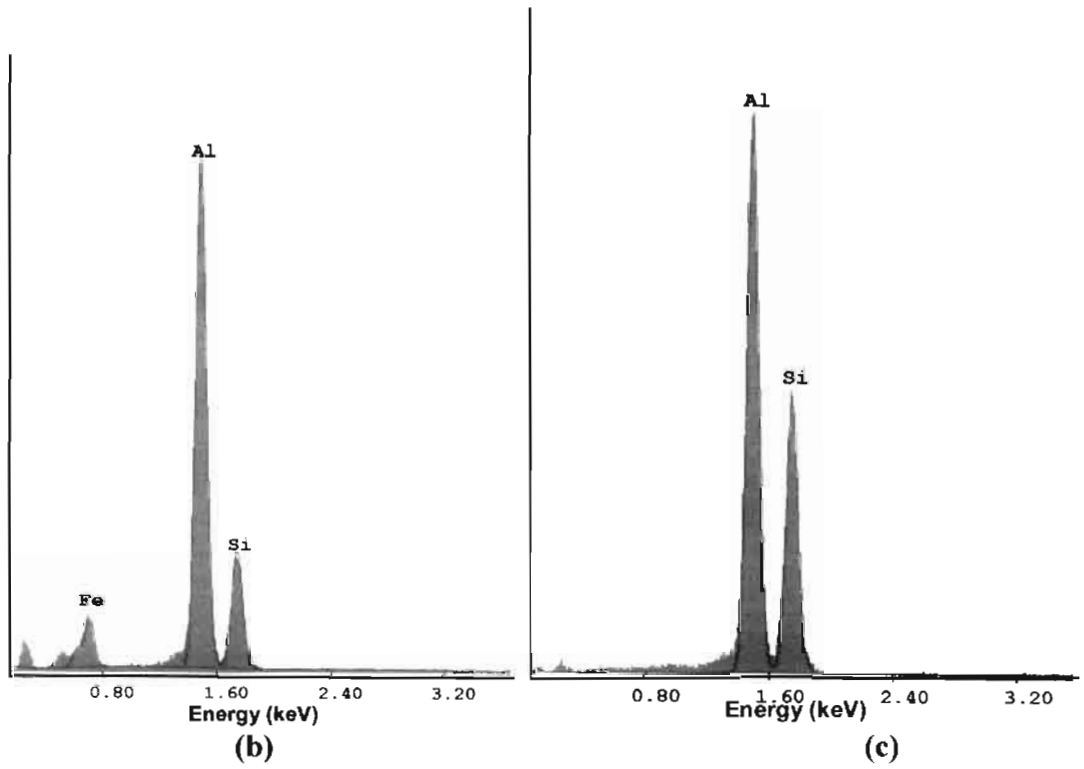


Figure 7.13: SEM photomicrograph (a) and EDS spectra of modified compocast Al(356)-15% fly ash composite of different phases marked as 1 - (b) and 2 - (c).

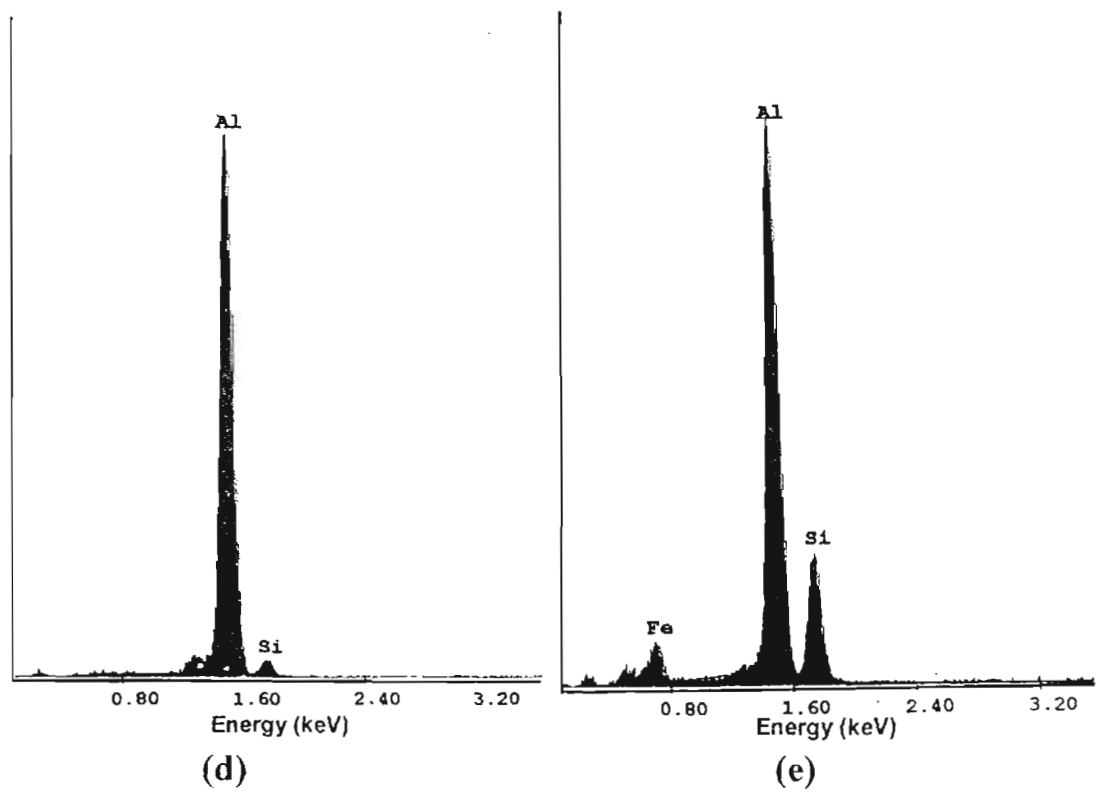
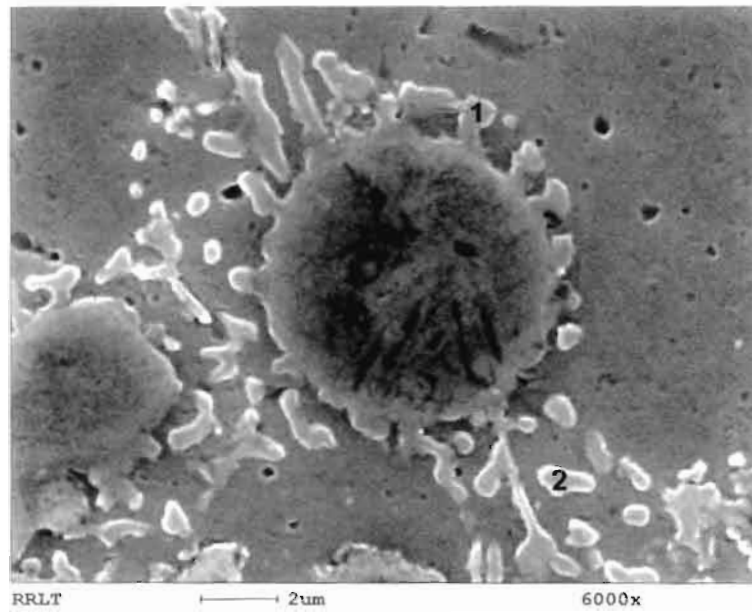


Figure 7.13: SEM photomicrograph (a) and EDS spectra of modified compocast Al(356)-15% fly ash composite of different phases marked as 3 - (d), and 4 - (e) in (a).



(a)

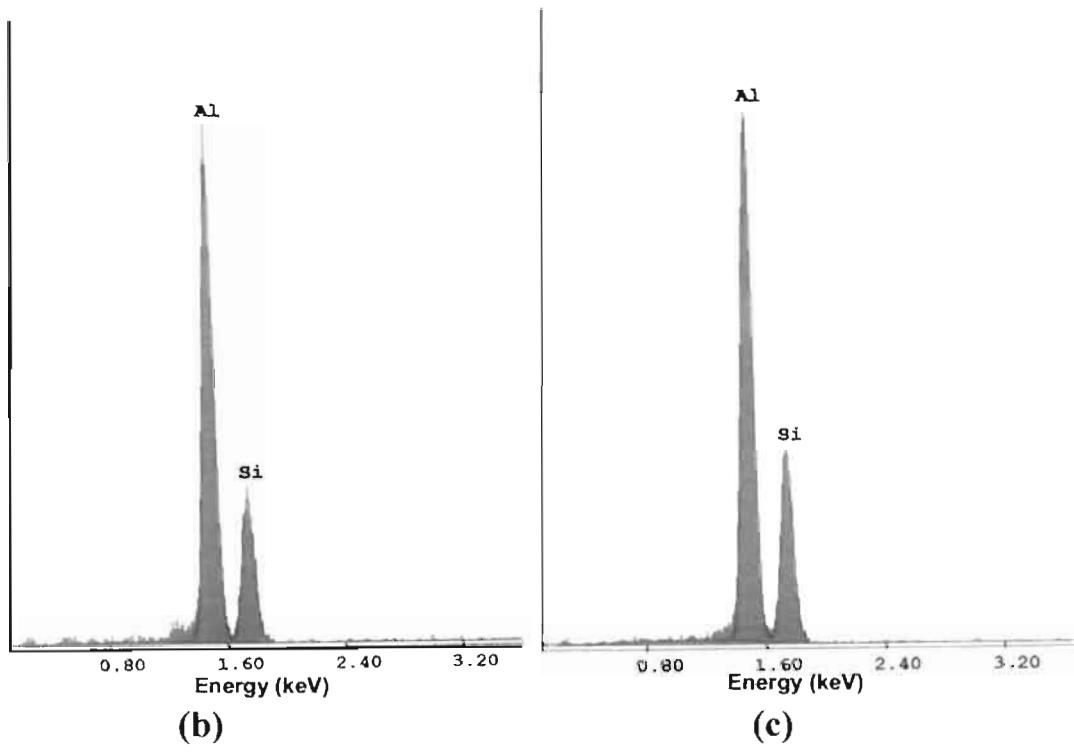


Figure 7.14: SEM photomicrograph (a) of modified compocast Al(356)-15% fly ash composites and EDS spectra of phases marked 1(b) and 2(c).

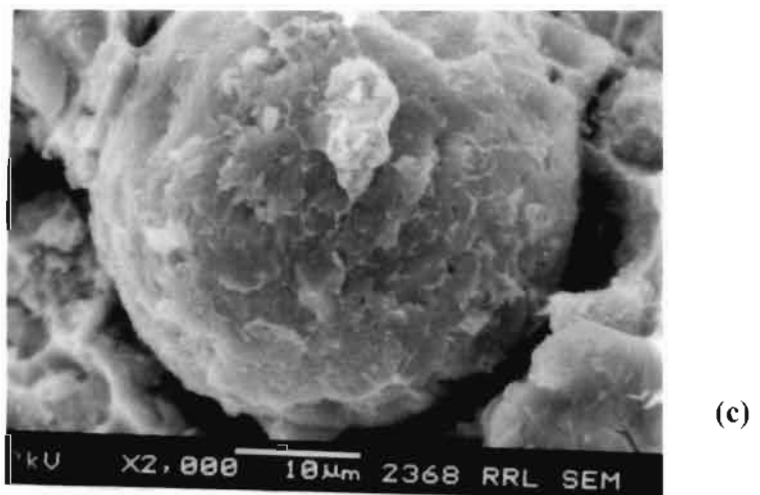
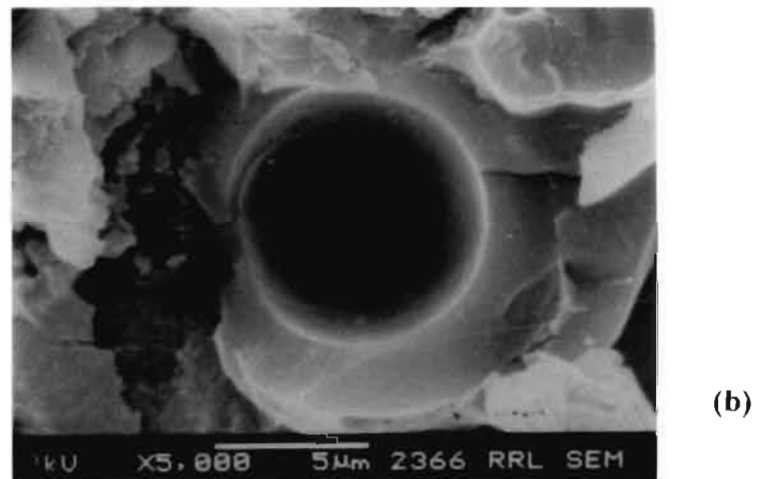
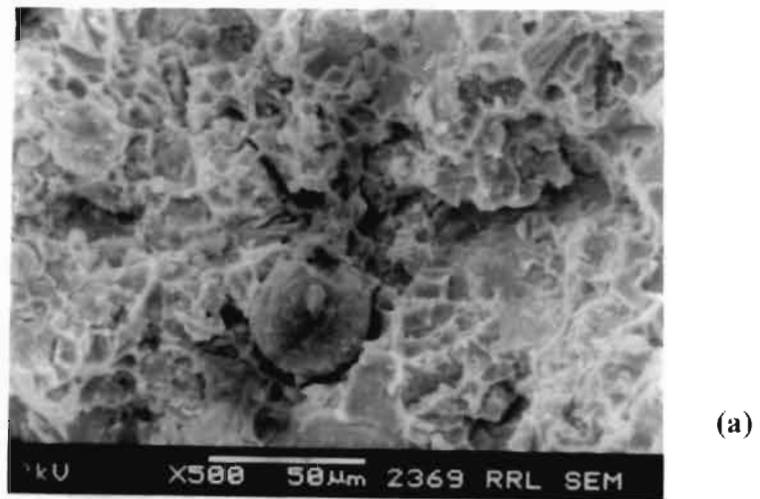
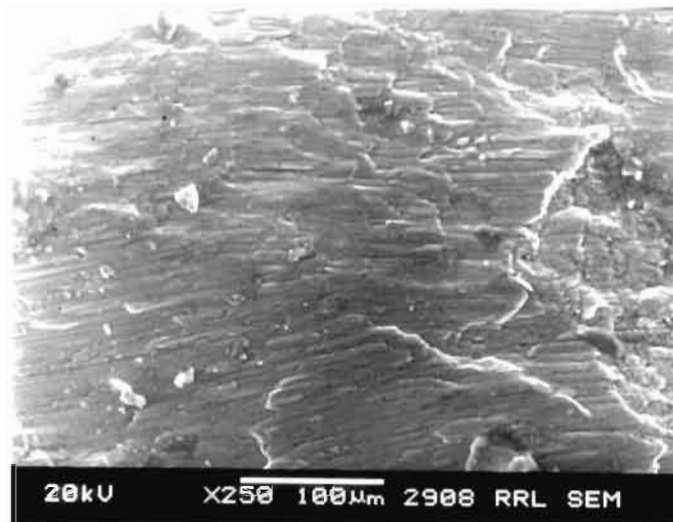
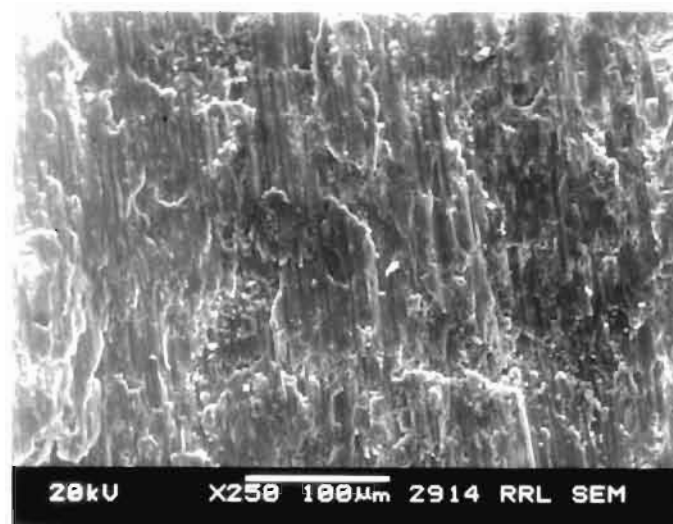


Figure 7.15: SEM photomicrographs of tensile fracture of Al(356)-15% fly ash composite processed by modified semisolid stir casting followed by squeeze casting. (a) Overall fractograph, (b) fracture showing cavity in cenospheric fly ash and (c) interfacial debonding of fly ash particle from the matrix.

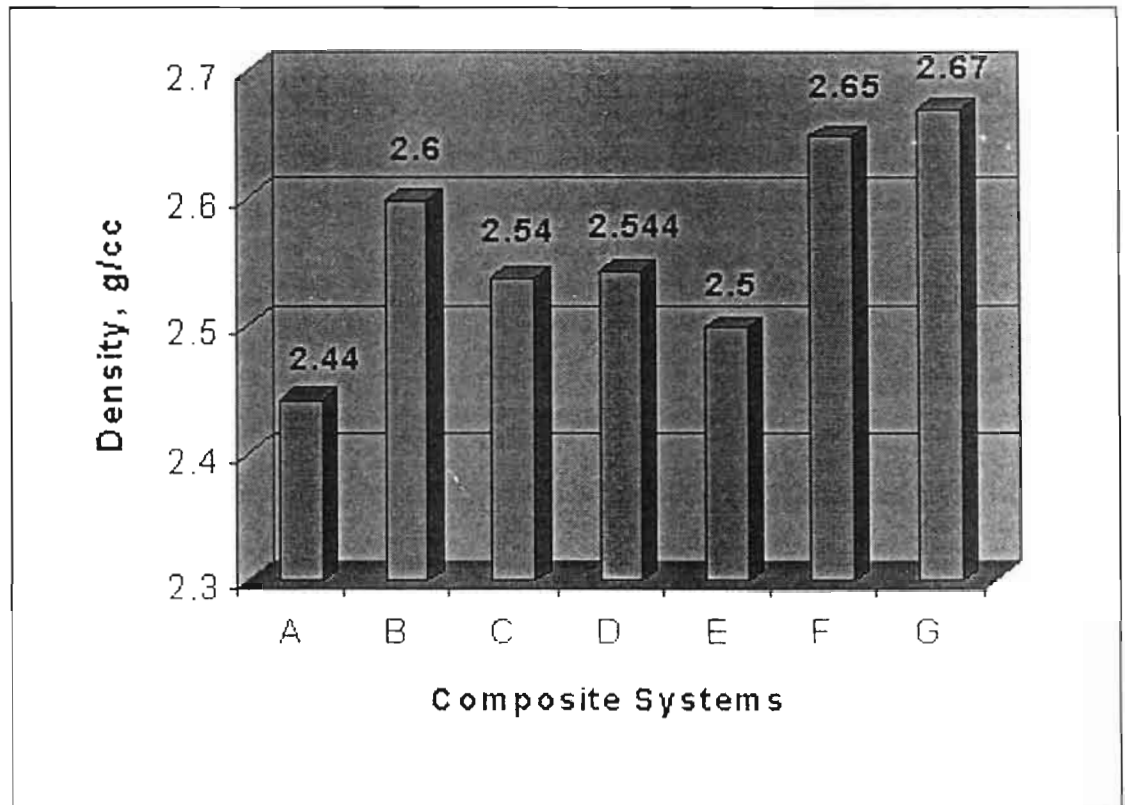


(a)



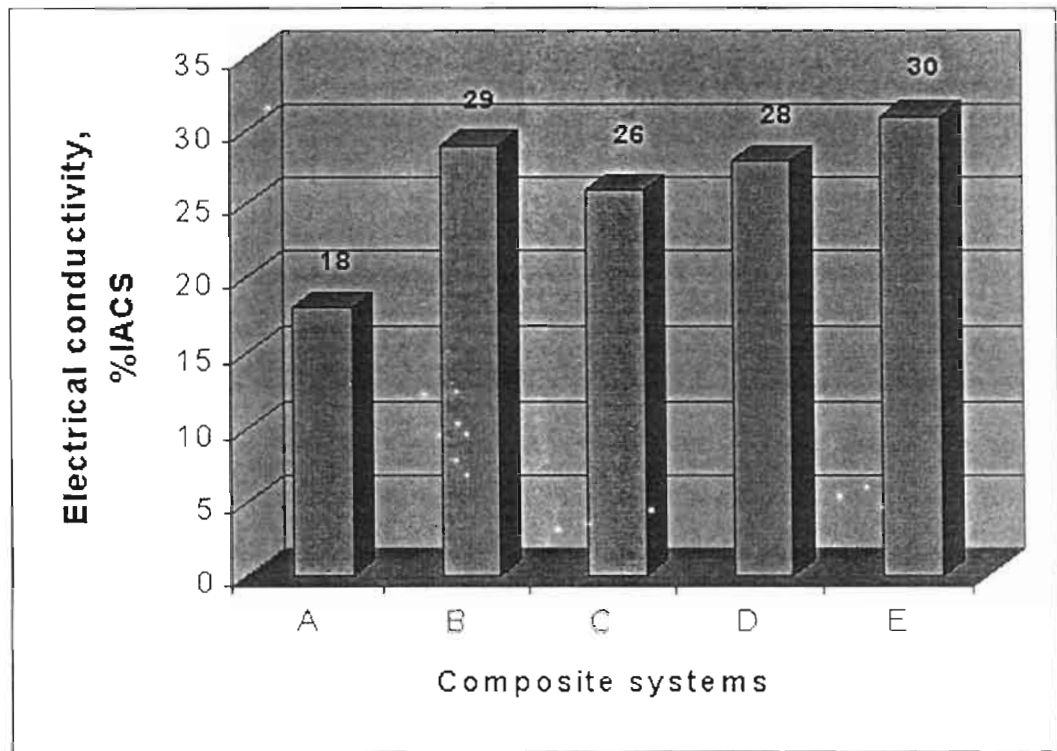
(b)

Figure 7.16: SEM photomicrographs of fractured compression specimens (a) Al(356) matrix alloy and (b) Al(356)-15% fly ash composite processed by modified semisolid stir casting followed by squeeze casting.



- A – As received particle, liquid metal stir casting, Metal mould (MM)*
- B – Surface treated (ST), liquid metal stir casting, MM*
- C – ST, semisolid stir casting, MM*
- D – ST, semisolid stir casting, Graphite mould*
- E – ST, semisolid stir casting, solidified in crucible*
- F – ST, modified semisolid stir casting, MM*
- G – Rule of Mixtures*

Figure 7.17: Densities of Al(356)-5% fly ash composites fabricated by different processing techniques.



- A – As received particle, liquid metal stir casting, Metal mould (MM)*
- B – Surface treated (ST), liquid metal stir casting, MM*
- C – ST, semisolid stir casting, MM*
- D – ST, semisolid stir casting, Graphite mould*
- E – ST, modified semisolid stir casting, MM*

Figure 7.18: *Electrical conductivities of Al(356)-5% Fly ash Composites fabricated by different techniques.*

7.4 DISCUSSION

The properties of the composites are strongly dependent on the uniformity of the distribution of the dispersoid in the matrix, the interfacial interaction between the matrix and the dispersoid in addition to the properties of the dispersoid. The processing method and their parameters play an influential role on the structure and properties of the composites.

7.4.1 Liquid Metal Stir Casting

The as received fly ash particles contain agglomerates with fine fly ash particles sticking to the surface of larger ones [Figure 7.1(a)]. When as-received fly ash particles are introduced into the molten metal, majority of them get agglomerated and remain in the interdendritic region with a few individual particles remaining in the matrix [Figure 7.3(a)]. These agglomerates generally aid porosity formation. Moreover, the addition of alloying element like Mg to the matrix as wetting promoter did not help much in improving the dispersibility.

The surface treatment deflocculates the fly ash particles and separates and removes the fine particles sticking to the surface of the larger ones [Figure 7.1(b)]. This reduces the number of agglomerates and leads to more number of individual fly ash particles in the composites. Further, by introducing the deflocculated fly ash particles, the gas porosity in the composite casting gets reduced from 8.61% to about 2.61%. This is also reflected by the increased electrical conductivity value of the composites from 18 to 29 %IACS [Figure 7.18].

The disadvantage with the liquid metal processing technique is the large scatter in the interparticle distance between the fly ash particles i.e., about 30-130 μm . Since the size of the composite castings is small in the present investigation and is made in the permanent moulds, the gravity-aided segregation has not been noticed prominently.

7.4.2 Compocasting

In this process, the higher viscosity of the alloy slurry imparts shear force over the agglomerates and aids in better separation of the dispersoids [283, 284]. The microstructure of the composite prepared by this technique has shown better dispersion of the fly ash particles with very less number of agglomerates [Figure 7.5(a)] compared to the liquid metal processed composite [Figure 7.3(b)]. Casting the composite slurry in metal or graphite mould [Figure 7.5(b)] has resulted in similar microstructure. The composite slurry solidified in the crucible has shown good dispersion of the fly ash [Figure 7.5(c)] but with coarser α -aluminium. The coarse α -phase is formed due to the Oswald's ripening process. Some fly ash particles are completely enveloped by the Si phase. The slower solidification rate of the composite slurry with lower thermal diffusivity of the fly ash brings the last solidifying eutectic Si rich liquid around the particle interface thus Si engulfing the particles. There is no evidence for the interfacial reaction between the matrix and the fly ash particles in the microstructure.

The compocast composites exhibit higher porosity levels of 4.72, 4.87 and 6.37% solidified in graphite mould, steel mould and in the crucible respectively compared to 2.6% in the liquid stir cast composite solidified in steel mould. This high level of gas porosity in the compocast composite castings is due to the higher viscosity of the composite slurry which does not facilitate the easy escape of the gases during mould filling and solidification. This leads to the poor mechanical properties of the composites. The compocast composite solidified in metal and graphite mould [Figure 7.6(a-c)] show similar frequency distribution of interparticle distance i.e., in the range of 30-50 μm , whereas crucible solidification gives segregation and wide range of distribution.

7.4.3 Modified Compocasting

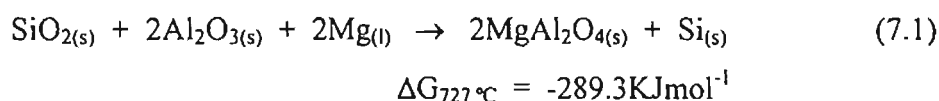
The advantages realized by reheating the composite slurry above the liquidus temperature and casting are the lower size of α -aluminium phase [Table 7.1], reduced rate of coarsening and segregation of the fly ash particles in the inter α -aluminium

region. The microstructure has shown the reduction in the number of agglomerates [Figure 7.8]. The interparticle distance measurements have shown that compared to compocasting here the interparticle distance has increased from 30-50 μm [Figure 7.6(a)] range to 50-90 μm and the scatter in the interparticle distance has also narrowed down very sharply. This is mainly due to reduction in the size of the α -phase. The increase in the wt% of particles from 5 to 15 naturally brings down the interparticle distance but the pattern of the frequency distribution is not appreciably affected [Figure 7.9].

Further, the sharp reduction in the porosity level to 0.75% and the increase in density to 2.65 g/cc [Figure 7.17] near to the ROM values of 2.67 g/cc of these composites clearly indicate that modified compocasting is the best synthesis route among the ones investigated.

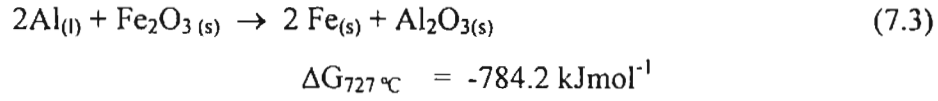
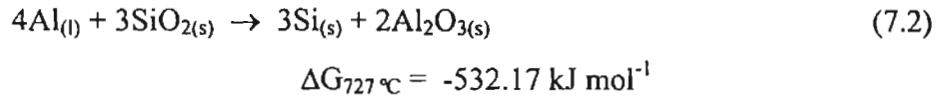
7.4.4 Interfacial Reaction

The major constituents of the fly ash are SiO_2 , Al_2O_3 and Fe_2O_3 and the minor ones are Na_2O , CaO and ZnO [Table 3.5]. All of these can react with the molten Al as well with the Mg present in the matrix alloy depending on the kinetics of the reaction. The possible combined reaction that can take place with SiO_2 and Al_2O_3 of the fly ash is



The MgAl_2O_4 spinel formed can be at the particle matrix interface or distributed in the matrix due to the fluid flow during synthesis and casting. The Si in the matrix alloy can retard the kinetics of above reaction (7.1) especially when the composites are synthesized by the compocasting technique since the liquid phase in the slurry is richer in Si with near eutectic composition.

Similarly, SiO_2 and Fe_2O_3 in the fly ash can react with the molten Al as per reactions (7.2) and (7.3) respectively.



The silicon formed as per reaction (7.2) will add to the eutectic silicon formed during solidification. The iron formed in the reaction (7.3) would diffuse away from the interface into the matrix alloy forming the iron intermetallics. Iron rich intermetallics are seen plenty in the composites prepared by liquid metal stir casting technique. But very few are observed in compocast composites due to its lower operating temperature. Similar observations have been made by Guo and Rohatgi on commercially pure Al alloy based fly ash composites [285].

The minor constituent of the fly ash Na_2O can also get reduced to metallic Na, which in turn helps in the modification of Si in the matrix alloy containing Si. The microstructures of these composites have shown modification of the Si, which can be due the presence of fly ash particles in the matrix as has been observed in graphite containing Al-MMC system [286].

The microstructure of the composite [Figure 7.11(a)] prepared by the modified compocasting technique followed by squeeze casting has shown that Si seems to be attached to the surface of solid fly ash particle as if Si is growing from the fly ash particle surface. According to the reaction (7.1), if Si is coming out as one of the reaction products being nascent in nature, it can also act as nucleating centre for the precipitate of Si from the matrix liquid when it solidifies. The cross section of a hollow fly ash particle [Figure 7.11(b)] does not show any surface reaction or reaction products with minimum precipitation of eutectic Si around the particle. There is no indication for the infiltration of liquid alloy into the fly ash but large numbers of MgAl_2O_4 spinel crystallites are seen inside it. Fly ash particles have been detached during polishing probably due to the poor interfacial bonding [Figure 7.11(c)]. The two small cavities seen are probably formed as the result of gas bubbles present over

the surface of the fly ash particles. The presence of Si phase inside the hollow depression clearly indicates that Si phase has surrounded the fly ash during solidification. The smooth appearance of these Si phase without any fracture clearly suggested that Si has not been attached or bonded to the surface of the fly ash particle. Hence, the interfacial reactivity and Si phase nucleation on the particle surface depend on the nature of fly ash particle.

The tensile fracture surface of the composites has shown a mixed mode of ductile and brittle fracture [Figure 7.15(a)]. The dimples come mainly due to the fracture of α -aluminium, whereas interfacial as well as eutectic Si regions exhibit brittle fracture. A hollow fly ash particle well bonded with the matrix has shown brittle fracture [Figure 7.15(b)], whereas a fly ash particle which has been partially bonded with the matrix show an interface gap resulting in debonding from the matrix [Figure 7.15(c)]. Since the particle surface is not clean like the as received particle surface, it is possible to have weak reaction as well as bonding between the particle and the matrix. This also suggests that the surface treatment given to the fly ash particles is not uniform in all fly ash particles.

These results clearly indicate that the surface treatment to the fly ash particles is required for deflocculation as well to cleanse their surface by which better contact between the particle surface and the matrix alloy can be achieved. Higher temperature of introduction i.e., by liquid metal processing can lead to more severe interfacial reaction. The reaction product is predominantly MgAl_2O_4 . The severity of the reaction between the particles and the matrix is of different extent leading to different types of fracture modes between the particles and the matrix.

7.5 SUMMARY

1. The incorporation of as received spherical fly ash particle of 13 μm APS in 356 Al alloy matrix by liquid metal stir casting process leads to agglomeration of particles in the composite with high porosity levels.
2. The surface treatment of particles in aqueous media containing sodium silicate deflocculates them.

3. Addition of treated fly ash improves the dispersion of individual particles in the composite reducing the porosity level in liquid metal stir cast composite. However, few agglomerates of particles and high interfacial reaction are observed.
4. By resorting to the semisolid processing / compocasting technique, improvements in the dispersion of the fly ash and low interfacial reaction are observed, however formation of coarse α -aluminum and segregation of the particle to the eutectic region takes place.
5. Further, improvements in the particle separation and distribution are achieved by modified semisolid processing / compocasting. i.e. by reheating the semisolid/compocast composite slurry just above the liquidus and then casting in the permanent mould or squeeze casting.
6. Interfacial reactions are more in liquid metal stir cast composites than in compocast composites.
7. The Al from the matrix would react with SiO_2 and Fe_2O_3 and Mg reacts with SiO_2 and Al_2O_3 constituents of the fly ash.
8. Fracture surface of composites showed mixed mode of ductile and brittle fracture. Both particle fracture and interfacial debonding are observed.
9. The interfacial reactivity and Si phase nucleation on the particle surface depend on the nature of fly ash particle.

CHAPTER 8

CONCLUSIONS

The present investigation has aimed at the synthesis and characterisation of both mono and hybrid aluminium metal matrix composites systems based on 356 alloy. The different reinforcements used are particles of silicon carbide, natural and synthetic graphite and fly ash as well as short fibres of carbon and aluminosilicate. The liquid metal stir casting technique is used for the composite processing except in fly ash particulate system where compocasting and modified compocasting technique have also been used. Both the gravity and the squeeze casting techniques are used for casting. Al metal matrix composites successfully synthesised include mono (Al-SiC, Al-Graphite, Al-carbon, Al-aluminosilicate and Al-Flyash) as well as hybrid metal matrix composites (Al-SiC-graphite, Al-SiC-carbon and Al-SiC-aluminosilicate) systems. Effect of dispersoid surface treatments and their mode of addition especially in the case of hybrid MMC preparation on the resulting composite quality are also studied. The composite synthesised are characterised with respect to their microstructure, electrical conductivity, interface, mechanical properties and solidification parameters. The major observations and conclusions drawn are given under each composite system studied.

1. Al(356)-SiC-graphite mono and hybrid metal matrix composite systems:

1. The mixed mode of particle addition during hybrid composite synthesis provides better dispersion of particles.
2. The natural graphite is more stable than the synthetic graphite during heat treatment. The synthetic graphite becomes finer during mixing than the natural graphite.
3. There is no remarkable interfacial reaction at the SiC – matrix interface.
4. Addition of both the SiC and graphite particles to the matrix has reduced the size of primary aluminum and eutectic silicon phases compared to the base alloy.

5. Fine dendritic cell size obtained in squeeze cast composite ingots results in better distribution of particles in the matrix than gravity casting.
6. The hindered settling phenomena experienced in hybrid composites due to the presence of low-density carbon reinforcement and high density SiC leads to improved distribution of reinforcements in composites.
7. Introduction of silicon carbide and graphite particles into the Al(356) matrix alloy reduces its liquidus temperature.
8. The graphite mould shows higher peak heat flux values than steel and sand moulds due to the higher thermal conductivity of graphite.
9. Incorporation of additional Mg to the composite melt has multifunction. Apart from its well-known function as a wetting promoter of ceramic particle with the aluminium alloy matrix, it results in better contact at the metal/mould interface, thereby enhancing the heat transfer rate.
10. The addition of graphite particles to the alloy matrix enhances the effective thermal conductivity of the composite system, whereas that of the silicon carbide particles reduces it.
11. Accelerated ageing is observed in both the mono and the hybrid composites.
12. The hardness of composite increases with the introduction of SiC particle, however the hybridization with graphite particle reduces.
13. The compressive strengths of mono and hybrid composite are higher than that of the alloy.

II. Al(356)-SiC-carbon short fibre mono and hybrid metal matrix composite systems:

1. Addition of as received carbon short fibre to the matrix alloy leads to agglomeration and rejection.
2. Among the various surface treatments attempted, sodium silicate treatment is effective in deflocculation of the fibres and maintaining maximum fluffiness for the free flow during the addition into the matrix. The surface treated fibre provides better wetting, separation and distribution of fibre in the matrix.
3. Interfacial reaction occurs at the carbon fibre – matrix interface with the formation of aluminium carbide, which provides better wetting, but degrades the fibre surface.

4. Fibre breakage is observed in the composite due to the shearing induced by the stirrer blade as well as abrasion with the SiC particle in case of hybrid composite.
5. The hardness of the Al(356)-15% SiC_(p)-3% C_(sf) (128 BHN) hybrid composite is increased compared to the Al(356)-15% SiC_(p) (115 BHN) monocomposite.
6. Accelerated ageing is observed in the Al(356)-15% SiC_(p)-3% C_(sf) composites.
7. The tensile and compression strengths of hybrid composite are lowered due to interfacial reaction and breakage of fibre.

III. Al(356)-aluminosilicate short fibre mono and hybrid metal matrix composite systems:

1. Among the various surface treatments studied, the ultrasonic treatment of the fibre in acidic media (pH 4-5 range) has given better dispersion and minimum agglomeration of the reinforcements as well as less porosity in the composite castings.
2. The contact of aluminosilicate fibres with the liquid metal during the synthesis of composites results in interfacial reactions. All the major constituents of the fibre such as Al₂O₃, SiO₂ and ZrO₂ react with the matrix elements.
3. MgAl₂O₄ spinel formation is observed in both the standard and the zirconia grade fibres. The spinel formed is observed both at the interface and the eutectic region.
4. The zirconia grade fibre reacts with aluminium leading to the formation of ZrAl₃ binary and Al-Zr-Si ternary intermetallics, which are observed as coarse precipitates in the matrix alloy. The zirconia grade fibre is more affected by the interfacial reactions than the standard aluminosilicate fibre.
5. The interfacial reactions deplete the Mg content in the matrix, thus reducing the amounts of Mg₂Si available during precipitation hardening and resulting in lower hardness for the composites during aging.
6. The addition of aluminosilicate fibre reduces the liquidus temperature of the matrix. Similarly, the peak heat flux value of ceramic fibre reinforced composite is lower than that of the alloy matrix due to the low thermal conductivity of the fibres.

IV. Al(356)-Fly ash metal matrix composite system:

1. The incorporation of as received spherical fly ash particle of 13 μm APS in 356 Al alloy matrix by liquid metal stir casting process leads to agglomeration of the particles in the composite with high porosity levels.
2. The surface treatment of the particles results in deflocculation and its addition has improved the dispersion of individual particles in the composite and reduced porosity level. However, few agglomerates of particles and high interfacial reaction are observed in liquid metal stir cast composite.
3. By resorting to the semisolid processing / compocasting technique, further improvements in the dispersion of the fly ash and low interfacial reaction are observed. However, formation of coarse α -aluminium and segregation of the particle into the eutectic region have taken place.
4. Modified semisolid processing / compocasting i.e. by reheating the semisolid/compocast composite slurry just above the liquidus and then casting in the permanent mould or squeeze casting give better separation and distribution of the particles and sound casting among the various processes studied.
5. Interfacial reactions between the matrix and the flyash particle are higher in liquid metal stir cast composites than in compocast composites.
6. The Al from the matrix reacts with SiO_2 and Fe_2O_3 and Mg reacts with SiO_2 and Al_2O_3 constituents of the fly ash particles.

8.1 SIGNIFICANT OBSERVATIONS/ CONTRIBUTIONS OF THE PRESENT INVESTIGATION

1. Al(356)- $\text{SiC}_{(p)}$ - $\text{Gr}_{(p)}$ hybrid metal matrix composites have been successfully synthesised using uncoated graphite particle against the currently used Ni coated graphite by the mixed mode of addition using liquid metal stir casting process.
2. The addition of Mg to the aluminium matrix composites has been found to have multifunctional roles. Apart from forming the precipitation hardening phase, Mg_2Si and acting as a wetting promoter between the reinforcement and

the matrix, Mg enhances the heat transfer rate due to improved contact at the metal/mould interface.

3. The surface treatment technique developed has provided better deflocculation of both carbon and aluminosilicate short fibres as well as fine fly ash particles leading to easy processing of respective aluminium matrix composites by liquid metal stir casting with improved wetting and distribution of reinforcements.
4. Modified semisolid processing technique devised enables the fabrication of fine spherical fly ash particle reinforced aluminium matrix composites.
5. The influence of the presence of dispersoids on the solidification curves of hybrid metal matrix composites and the casting/mould interfacial heat flux for both mono and hybrid composites has been studied and reported for the first time.

8.2 SCOPE FOR THE FUTURE WORK

1. Studies on processing and characterisation of discontinuously reinforced hybrid metal matrix composites with other reinforcement combinations.
2. Fabrication of functionally graded mono and hybrid metal matrix composites.
3. Use of nanophase materials as hybridising agent.
4. Mathematical modelling to predict the synergistic effects of the components of HMMCs as an aid for their judicious selection.
5. Product identification and HMMC development with specific property requirements.
6. Use of modified semisolid processing technique and the reinforcement surface treatments for the synthesis of fine SiC, graphite and other dispersoids reinforced composite system.
7. Establishing the reasons and mechanisms for the variation in solidification parameters of cooling curve and metal/ mould interfacial heat transfer in metal matrix composite systems.

REFERENCES

1. S. Deutsch, 23rd National SAMPE Symposium, California, May 2-4, 1978, p.34, Society for the Advancement of Material and Process Engineering, Covina, California, USA.
2. J.D. Muhly, in *The Beginning of the use of Metals and alloys*, R. Maddin (ed) MIT press, Cambridge, pp 2-20.
3. E. Schmidt, German Patents No. 425451, 425452 and 427370, 1924.
4. N. Hansen, *Dispersion strengthened aluminium products – Manufacture, structure and mechanical properties*, Riso National Laboratory, Denmark, 1971.
5. M.D. Maheswari, A. Chatterjee, T. Mukherjee and J.J. Irani, in *Heat Treatment- 1991*, (ed. R.H. Johnson) Inst. of Metals, London, pp. 67-77.
6. T. W. Clyne and P. J. Withers: *An introduction to “Metal Matrix Composites”*, 1993, Cambridge, Cambridge University Press.
7. A. G. Metcalfe: *“Metal Matrix Composites”*, 1974, New York, Academic.
8. K. K. Chawla: *‘Composite Materials – Science and Engineering’*, 1998 (Second Edition), New York, Springer.
9. R. J. Arsenault: *“Thermo Mechanical behaviour of Metal Matrix Composites”*. 1989, New York, Pergamon Press.
10. S. Suresh, A. Mortenson and A. Needleman: *“Fundamentals of Metal Matrix Composites”*, 1993, London, Butterworth - Heinemann.
11. J. N. Fridlyander : *“Metal Matrix Composites”*, 1995, London, Chapman and Hall.
12. P. K. Rohatgi, R. Asthana and S. Das: *Int. Mater. Rev.*, 1986, 31, 115 – 139.
13. D. J. Lloyd: *Int. Mater. Rev.*, 1994, 38, 1 – 23.
14. K. G. Satyanarayana, R. M. Pillai and B. C. Pai *‘Handbook of Ceramics and Composites’* (ed. Chermisinoff), 1990, 1011, 555 – 599.
15. T. S. Srivatsan, T. S. Sudarsan and E. J. Lavernia: *Prog. Mater. Sci.* 1995, 39, 317 - 409.
16. Franck. A. Giroit, J.M. Quenisset and R. Naslain: *Composites Sci. Tech.*, 1987, 30, 155-184.
17. S.V. Nair, J.K. Tien and R.C. Bates: *Int. Met. Rev.*, 1985, 30, 275-90.

18. A. Mortenson and I. Jim: *Int. Mater. Rev.*, 1992, 37, 101 – 128.
19. R. Asthana: *J. Mater. Sci.*, 1998, 33, 1679-1698.
20. F. Delannay, L. Froyen and A. Deruyttere: *J. Mater. Sci.*, 1987, 22, 1-16.
21. E. A. Feest: *Composites*, 1994, 25, 75-86
22. J. M. Howe: *Int. Mater. Rev.*, 1993, 38, 223-256
23. Idem: *Ibid.*, 1993, 38, 257-271
24. B. C. Pai, Geetha Ramani, R. M. Pillai and K. G. Satyanarayana: *J. Mater. Sci.*, 1995, 30, 1903-.
25. R. Mitra and Y. R. Mahajan: *Bull. Mater. Sci.*, 1995, 18, 405-434
26. T. P. D. Rajan, R. M. Pillai and B. C. Pai: *J. Mater. Sci.*, 1998, 30, 3491 – 3503.
27. P. K. Rohatgi, S. Ray and Y. Liu: *Int. Mater. Rev.*, 1992, 37, 129 – 149.
28. R. L. Devis, C. Subramaniam and J. M. Yellup: *Compos. Sci. and Tech.*, 1997, 415 – 435.
29. L.H. Hihara and R.M. Latanision: *Int. Mater. Rev.*, 1994, 39, 245 – 264.
30. M.B.D. Ellis: *Int. Mater. Rev.*, 1996, 41, 41 – 58.
31. A. Mortenson and S. Suresh: *Inter. Mater. Rev.*, 1995, 40, 239 – 265.
32. S. Suresh and A. Mortenson: *Ibid*, 1997, 42, 85 – 116.
33. Z. G. Wei, R. Sandstrom and S. Miyazaki: *J. Mater. Sci.*, 1998, 33, 3743 -- 3762.
34. Idem: *Ibid*, 3763 - 3783.
35. W. Ames and A. T. Alpas: *Metall. Mater. Trans. A*, 1995, 26, 85-98
36. H. C. Park: *Scripta Metall. Mater.*, 1992, 27, 465-470.
37. De-Bondt, L. Froyen and A. Deruyttere: *Mater. Sci., Engg. A*, 1991, 135, 29 – 32.
38. H. M. Cheng, A. Kitahara, S. Akiyama, K. Kobayashi and Z. L. Chou: *J. Mater. Sci.*, 1992, 27, 3617 – 3623.
39. M. D. Skibo and D.M. Schuster, U. S. pat. 475995, 1988.
40. Alcan Aluminium Corporation: U. S. pat. 4786467, 1988.
41. M. D. Skibo, P. C. Morris and D. J. Lloyd, in *Cast Reinforced Metal Composites* (eds S. G. Fishman and A. K. Dhingra) 257 – 61, 1988, ASM, Chicago.
42. W. R. Hoover, in *Metal Matrix Composites – Processing Microstructure and Properties*, 12th Riso International Symposium on Material Science (eds N.

- Hansen, D. Juul Jensen and T. Leffers), 1991, Riso National Laboratory, Roskilde, Denmark, 387 – 392.
43. J. B. Borradaile, S. Skjervold and W. Ruen, in Extended Abstract of Conf., Metal Matrix Composites; Property Optimisation and Applications, London 1989, The Institute of Metals, Paper 10.1.
 44. T. Sritharan, K. Xia, H. Heathcock and J. Mihelich: in Metal and Ceramic Matrix Composites; Processing, Moulding and Mechanical behaviour,' (eds R. B. Bhagat et al.), 1990, Warrendale, PA, AIME, 13 – 22.
 45. S. Caron and J. Masounave, in Fabrication of particulate Reinforced Metal Composites (eds J. Masounave and F. G. Hamel), 1990, ASM International, Materials Park, Ohio, 107 – 113.
 46. N. L. Hansen, T. A. Engh and O. Lohue, in Interfaces in Metal Ceramic Composites, (ed by R. Y. Lin, R. J. Arsenault, G. P. Martins and S. G. Fishman), 1989, Warrendale, PA, The Minerals metals and Materials Society, 241 – 257.
 47. B. C. Pai and P. K. Rohatgi: *J. Mater. Sci*, 1978, 13, 329 – 335.
 48. D. B. Spencer, R. Mehrabian and M. C. Flemings: *Metall. Trans.* 1972, 3, 1925 – 32.
 49. P. A. Joly and R. Mehrabian: *J. Mater. Sci*, 1976, 11, 1393 – 418.
 50. R. Mehrabian, R. G. Rick and M. C. Flemings: *Metall. Trans.* 1974, 5, 1899 – 1905.
 51. Dow Chemical Co. : U. S. Pat 4, 432 936.
 52. J. A. Cornie, H. K. Moon and M. C. Flemings, in 'Fabrication of Particulates Reinforced Metal Composites', (ed. J. Masounave and F. G. Hamel), 1990, ASM International, Materials Park, Ohio, 63 – 78.
 53. P. K. Balsubramaniam, P. S. Rao, B.C. Pai, K.G. Satyanarayana and P. K. Rohatgi: *Comp. Sci. and Tech.*, 1990, 39, 245-260.
 54. C.G. Levi, G.S. Abbaschian and R. Mehrabian: *Metall. Trans.* 1978, 9A, 697-711.
 55. P. K. Rohatgi, R.Q. Guo, T.F. Stephenson and A.E.M. Warner: *Trans. Am. Foundrymen Soc.*, 1998, 106, 191-197.
 56. A. W. Urquhart: *Mater. Sci. and Engg.* , 1991, A144, 75
 57. C. R. Kennedy in Proc. 7th International conference on Modern Ceramic Technologies (ed P. Vincenzine), 1991, Elsevier Science, London, 691 – 700.

58. W. C. Harrigan and R. H. Flowers, in *Fatigue Modes in Composites III* (eds. T. T. Chiao and D. M. Schuster), 1976, New York, The Metallurgical Society of AIME, 212 – 225.
59. E. G. Kendall and R. T. Pepper, U. S. Pat.4082 864, 1978.
60. W. L. Lachman, R. A. Penty and A. F. Jahn, U. S. Pat. 3844863, 1975.
61. T. W. Clyne and J. F. Mason: *Metall. Trans.* 1987, 18A, 1519 – 30.
62. A. Mortenson and V. J. Michaud: *Metall. Trans.* 1990, 21A, 160 - 3.
63. F. Kloucek and R. F. Singer in Proc. 31st International SAMPE Symposium and exhibition of Materials Science for future, (eds. J. L. Baucer and R. Dunaetz), 1986, Covina, CA, SAMPE. 17 01 – 1712.
64. T. Imai, Y. Nishida and S.F. Hansen: *J. Mater. Sci. Lett.*, 1987, 6, 343– 345.
65. N. W. Rasmissen, P. N. Hansen and S. F. Hansen: *Mater. Sci. Engg., A*, 1991, 40, A135, 41 – 43.
66. C. N. Cochran and R. C. Ray: U. S. pat. 3547180, 1970.
67. L. J. Masur, A. Mortenson, J. A. Cornie and M. C. Flemings: *Metall. Trans.* 1989, 20A, 2549 - 2527.
68. S. Nourbakhsh, F. L. Liang and H. Margolin: *Journal of Physics E: Scientific Instruments*, 1988, 21, 898 – 902.
69. W. H. Hunt, in “Interfaces in Metal Matrix Composites”, (ed. A. K. Dhingra and S. G. Fishman), 1986, Warrendale, The Metallurgical Society, 3 – 25.
70. G. D. Lawrence: *AFS Trans.*, 1972, 80, 283 – 286.
71. H. Westengen, D. L. Albright and A. Nygard: SAE Technical Paper Series, Paper No. 900534, 606 – 612, 1990.
72. L. Pennander and C. H. Anderson, in Proc. Conf. of 12th Riso International Symposium on Material Science, Metal Matrix Composites – Processing Microstructure and properties (ed. N. Hansen et al), 1991, Riso National Laboratory, Roskilde, Denmark, 575 - 580.
73. Y. Tsunekawa, M. Okumiya, I. Niimi and K. Yoneyama: *Mater. Sci. Lett.* 1988, 7, 830 – 832.
74. R. M. Andrews and A. Mortenson: *Metall. Trans.* 1988, 22A, 2903 – 2915.
75. J. I. Song. H. D. Bong and K. S. Han: *Metall. Mater. Sci.*, 1995, 33, 1307 – 1313.
76. Shin – Ichi Towata, Hagime Ikuna, and Sen – Ichi, Yamada: *Trans. Japan Inst. Metals*, 1988, 29, 314 – 321.

77. H. Nakanishi, Y. Tsunekawa, M. Okumiya, N. Mohri, I. Niimi and M. Satoh: *J. Japan Inst. Metals*, 1993, 57, 81 – 87.
78. J. W. Wang, T. Hong, G. Y. Li and P. X. Li: *Composites A*, 1997, 28, 943 – 948.
79. Osprey Metals, U. K. Patent, 1379 261, 1975.
80. R. W. Evans, A. G. Leathem and R. G. Brooks: *Powder Metallurgy*, 1985, 28, 13 – 19.
81. T. C. Willis: *Metals and Materials*, 1988, 4, 485 – 8.
82. A. R. E. Singer: *Mater. Sci. Engg.*, 1991, A135, 13 – 17.
83. C. L. Buhmaster, D. E. Clark and H. B. Smartt: *J. of Metals*, 1988, 11, 44 – 45.
84. Y. Tsunekawa, M. Okumiya, I. Niimi and Yoneyama: *J. Mater. Sci. Lett.*, 1988, 7, 30 – 832.
85. R. Tiwari, H. Herman, S. Sampath and B. Gudmundsson: *J. Mater. Sci. & Engg.*, 1991, A144, 127 – 131.
86. J. Zhang, R. J. Freez and E. J. Lavernia: A High Performance Composite-Commodity of Phenomena; (ed. K. K. Chawla) 361 – 376, 1994, Warrendale. The Minerals Metals and Materials Society.
87. Martin Marieta Corp., US. Pat 4710348, 1987.
88. A. R. C. Westwood: *Metall. Trans.* 1988, 19A, 740 – 758.
89. Y. F. Li, D. H. Ling, and C. D. Qin: *J. Mater. Res.*, 1999, 14, 2997 – 3000.
90. M. S. Newark, A. W. Urquhart, H. R. Zwicker and E. Breval: *J. Mater. Res.*, 1986, 1, 81 – 89.
91. P. Xiao and B. Derby, in Surface and Interface, British Ceramic Proceedings (ed. R. Morrel and G. Patridge), 1991, U. K. The Institute of Ceramics, 153-159.
92. P. Sahoo and M. J. Koczak: *Mater. Sci. Engg.*, 1991, A114, 133 – 146.
93. C. F. Feng and L. Froyer: *Acta Mater.*, 1999, 47, 4571 – 4583.
94. W.H. Hunt, Jr., C.R. Cook, K.P. Armanie and T.B. Garganus, in Powder Metallurgy of Composites, (ed. P. Kumar, A. Ritter and K. Vedula), 1987, AIME, Warrendale (TMS).
95. G. S. Upadhyaya: *Met. Mater. Process*, 1989, 1, 217 – 28.
96. Xiaomin Ni, M. S. Maclean and T. N. Baker: *Mater. Sci. Tech.*, 1994, 10, 452 – 459.

97. S. C. Tjong, K. C. Lau and S. Q. Wu: *Metall. Mater. Trans. A*, 1999, 30, 2551 – 2555.
98. L. R. Vishnyakov and V. I. Vodopianov: *Theoretical App. Fract. Mech.*, 1994, 20, 29 –33.
99. L. R. Vishnyakov and V. P. Moroz: *Comp. Sci. Tech.*, 1995, 53, 445 – 447.
100. George Marsh: *Mater. Today*, 2000, 3(3), 21-25.
101. T. F. Stephenson, A. E. M. Warner, S. Wilson, A. T. Alpas and P. K. Rohatgi: In Proc. Conf. Materials Week 1996: Cincinnati. Ohio, October 8 –10, 1996, Joint TMS/ASM conference.
102. J. A. E. Bell, A. E. M. Warner, T. F. Stephenson and E. Siegrist: in proc. Conf. “Materials Week 1996: Cincinnati. Ohio, October 8–10, 1996, Joint TMS/ASM conference.
103. P. K. Rohatgi, J. A. E. Bell and T. F. Stephenson: European Patent EP0567284 A2 April 1993.
104. P. K. Rohatgi, J. A. E. Bell and T. F. Stephenson: US Pat. 5 626 692, 1997.
105. S. Wilson and A. T. Alpas: *Wear*, 1996, 196, 270 – 278.
106. B. C. Pai, R. M. Pillai, K.G. Satyanarayana and H.S. Rao: in Proc. Conf. ‘6th Asian and 47th Indian Foundry Congress, Calcutta, India, January 1999, Institute of Indian Foundryman, vol. 1, p.264-270.
107. M. L. T. Guo and C. Y. A. Tsao: *Comp. Sci. Tech.*, 2000, 60, 65 – 74.
108. I. Carcea, R. Chelariu, M. Mares and C. Roman: *Metallurgia*, 1999, 57, 53 – 38.
109. T. Warner and E. Siegrist: *Adv. Mater. Prog.*, 1996, p.7.
110. J.I. Song and K.S. Han: *J. Comp. Mater.* 1997, 31(4) 316-344.
111. J.I. Song and K.S. Han: *Comp. Structures* 1997, 39(3-4) 309-318.
112. S.V. Prasad and K.R. Mecklenburg: US Pat. 5534044, 1996.
113. B. C. Ko and Y. C. Yoo: *Comp. Sci. Tech.*, 1999, 775 - 779.
114. T. T. Long, T. Nishimura, T. Aisaka and M. Morita: *Mater. Trans. JIM*, 1991, 32, 181 – 188.
115. C. M. Friend, I. Horsfall and C. L. Burrows: *J. Mater. Sci.*, 1991, 26, 225 – 231.
116. T. Tanaka, M. Sakamoto, K. Yamamoto, Y. Sato and E. Kato: US Pat. 5654107, 1997.

117. H. Fang, G. Zhang, R. Chen, Z. Fei, H. Wang, and W. Tian: *Shanghai Jiaotong Daxue Xuebao*, 1998, 32, 10 – 13.
118. T. N. Baker, A. J. Gorton, A. Song, X. Ni M. H. Varvalho, T. M. Amrcello and H. Carvalhihos: *Powder Metallurgy*, 1996, 223 – 229.
119. M. Gu, Z. Mei, Y. Jin, and Z. Wu: *Scripta. Materilia*, 1999, 40, 985 – 991.
120. J. L. Torstad: *AFS Trans.*, 1971, 79, 85 – 90.
121. G. Reninger, D. Abendroth and M. Bolien: in SAE, Tech. Paper Series, SAE 830003.
122. H. H. Hofman, K. Shelmann, E. Wacker and K. Schmidt: in SAE, Tech. Paper Series, SAE 830007.
123. T. Hayashi, H. Ushio and M. Ebisawa: in SAE, Tech. Paper Series, Michigan, 1989, SAE 890557.
124. M. Ebisawa, T. Hara, T. Hayashi and H. Ushio: in SAE, Tech. Paper Series, Detroit, 1991, SAE 910835.
125. K. Shibatha and H. Ushio: *Tribol. Inter.*, 1994, 27, 30 – 34.
126. J. I. Song and K. S. Han: *J. Comp. Mater.* 1997, 31, 316 – 344.
127. J. I. Song and K. S. Han: *Compos. Struc. Mater.* 1997, 39, 309– 318.
128. J. Q. Jiang, N. H. Liu, A. P. Ma and R. S. Tan: *J. Mater. Sci.*, 1994, 29, 3767 – 3773.
129. J. Q. Jiang, N. H. Liu, A. P. Ma and R. S. Tan: *Wear*, 1994, 171, 163 – 168.
130. T. Nakamura, Y. Kato and Y. Watanabe: in Proc. Conf. 'Functionally Gradient Materials ', Dresdan, Germany, October 1998, *Mater. Sci. Forum*, 1999, 308 - 311, 205 – 210.
131. H. M. Cheng, A. Kitahara, K. Kobayashi and B. L. Zhou: *J. Mater. Sci. Lett.*, 1991, 10, 795 – 797.
132. T. Yoshida, S. Kamiya, Y. Kumada, M. Ohkohchi, S. Yamada and S. Towata: in Proc. Conf. '33rd Annual Meeting of Japan Lubrication Society ', Japan, 1988, Japan Lubrication Society, p.197.
133. S. Towata, and S. Yamada: in Proc. 'Japan – U. S. Conf. on Composite Materials', (1986), p. 497.
134. S. Towata, and S. Yamada: *J. Japan Inst. Metals*, 1986, 50, 336.
135. K. U. Kainer and B. L. Mordike: in "Magnesium alloys and their Application" (eds. B. L. Mordike and F. Hehmann), 1992, Clausthal, Germany, DGM Information Gesellschaft, Verlag, 469 – 476.

136. K. Hicks, G. Love, V. D. Scot and R. L. Tramper: in proc. Conf. "9th International conference on Composite Materials (ICCM - 9)", Madrid, July 1993 (eds A. Miarwete), Wood Head Publishing Limited, 325 - 331.
137. B. Inem and G. Polland: in Magnesium alloys and their Applications (eds. B. L. Mordike and F. Hefman), 1992, Clausthal, Germany, DGM Information Gesellschaft, Verlag, 469 – 476.
138. A. Schweighofer, E. Hornboegn, S. Kudela and K. Shemmme: *Ibid*, p 423 - 430.
139. G. Nientit and A. G. Munich: *Ibid*, p 407 – 414.
140. R. Bode and E. Hornboegn: *Ibid*, p 461 – 468.
141. J. Schroder and K. U. Kainer: *Mater. Sci. Engg. A.*, 1991, 135, 33 – 36.
142. X.N. Zhang, D. Zhang, R.J. Wu, Z.G. Zhu and C. Wang: *Scripta Metall.* 1997, 37, 1631-1635.
143. Y.X. CHEN, D.X. LI and G.D. ZHANG: *Scripta Mater.* 2000, 43, 337-341.
144. M. Gu, Z.Wu, Y. Jin and M.Kocak: *J. Mater. Sci.*, 2000, 35, 2499-2505.
145. T. Takai: in proc. Conf. "3rd International conference on New Materials – 90, Osaka, October 1990 New Materials – 90, Japan, p429 - 442.
146. T. Takai: *J. Intelligent. Mater. System Structure*, 1990, 1, 149.
147. Y. Yamada, M. Taya and R. Watanabe: *Mater. Trans. JIM*, 1993, 34, 254.
148. Y. Furuya, A. Sasaki and M. Taya: *Mater. Trans. JIM*, 1993, 34, 224.
149. Y. Furuya: *J. Intelligent Mater. System Structure*, 1996, 7, 321.
150. Y. Watanabe and Y. Fukui: *Aluminium Trans*, 2000, 2(2), 195-208.
151. Y. Watanabe, H. Eryu and K. Matsuura: *Acta. Mater* (in press).
152. Y. Watanabe, N. Yamanaka and Y. Fukui: *Met. Mater. Trans. A* 1999, 30, 3253-3261.
153. K. Yamashita, C. Watanabe, S. Kumai, M. Kato, A. Sato and Y. Watanabe: *Mater. Trans. JIM*, 2000, 41(10) 1322-1328.
154. Y. Fukui, H. Okada, N. Kumazawa and Y. Watanabe: *Met. Mater. Trans. A* 2000, 31, 2627-2636.
155. P. K. Rohatgi: *Modern Casting*, April, 1988, 47 - 50.
156. M. W. Toyas, R. R. Bowles and D. L. Mancini: *Ind. Heat.*, 1987, 54, 17 - 19.
157. R. R. Bowles, D. L. Mancini and M. W. Toyas: *Manuf. Eng.*, 1987, 98, 61 - 62.
158. S. Sampath and R. R. Herman: *J. Metals*, 1993, 45(7), 42 - 49.

159. H. J. Feng and J. J. Moore: *J. Mater. Eng. Perform*, 1993, 2, 645 - 650.
160. Y. Watanabe and T. Nakamura: *Intermetallics*, 2001, 9(1) 33-43.
161. D. Webster, The Erigma of the Lightes: Environment, Econonimics, Energy, SAMPE Series – 2, (1979) 1433 – 50.
162. J. Dinwoodie, E. Morr, C. Langman and W. R. Symes, Proc. ICCM (Eds. W. C. HARRINGAN Jr et. al.), San Diego, California, 29 July – 1 August 1985, Metallurgical Society of AIME, Warren dale, Pennsylvania, Pp 671 – 85.
163. R. J. Arsenault and S. B. Wu: *Mater. Sci. Eng.* 1987, 21, 349 – 354.
164. F. Zok S. Janson, A. G. Evans, A. G. Evans and V. Nardone: *Metall. Trans.* 22A (1991) 2107.
165. R. Dwivedi, G Altland, P. Barron Anatolin, J. Leighton and F. G. Hammel: in Int. off Highway and Power Plant Cong.”, Milwaukee, WI, 1991, SAE.
166. W. H. Hunt, Jr, D. Richmond and R. P. Young: International Conference on ‘Composite Materials – ICC – VI (eds. F. L. Mathews et al.), 2.203, 1987. London, Elsevier Applied Science.
167. D. J. Lloyd: *Acta. Metall. Mater.*, 1991, 39, 59 – 79.
168. R. L. Mohan: *J. Comp. Mater.* 4(1970), 90 – 101.
169. L. Ackerman, J. Charbonnier, G. Desplancher and H. Korslowski: in Proc. Conf. ‘ICCM – 5’, San Diego, CA, July 1985, Metallurgical Society of AIME, Warrendale, 6 87 – 98.
170. G. J. Doorak and W. S. Johnson: *Int. J. Fract.* 1980, 16, 585 – 602.
171. N. Trankarakis, J. M. Sleptz and J. Neens: in “Recent Advances in Composites in United States and Japan”, (eds. J. R. Vinson and M. Taya) 131 - 52, 1985, Philadelphia, ASTM.
172. J. Nunes, E. S. C. Chin, J. M. Sleptz and N. Trankarakis: in Proc. Conf. ‘ICCM – 5’, San Diego, CA, July 1985, TMS – AIME, 723 – 45.
173. U. T. S. Pillai, Ph.D. Thesis, Indian Institute of Technology, New Delhi (1986).
174. A.P. Majidi and T.W. Chou, Proc. ICCM VI, 2, 1987, 422
175. F. M. Horking, F. Folgar – Portillo, R. Wunderlim and R. Mehrabian: *J. Mater. Sci*, 1982, 17, 477 – 98.
176. K. J. Bhansali and R. Mehrabian: *J. Metals*, 1982, 32, 30 – 4.
177. P. P. Trzaskoma: *J. Electrochem. Soc.*, 1982, 129, 1398 – 402.
178. D. J. Lloyd: *Compos. Sci. Technol.*, 1989, 35, 159-179

179. D. J. Lloyd H. Ligas, A. McLeod and P.L Morris: *Mater. Sci. Engg.*, 1989, A107, 73-80.
180. B.C. Pai, S.G.K. Pillai, R.M. Pillai and K.G. Satyanarayana, in *Solidification of Metal Matrix Composites*, (ed. by P.K. Rohatgi), TMS, Warrendale, 1990, 191-203.
181. W. Wang and F. Ajerish, in *Microstructure Formation During Solidification of Metal Matrix Composites*, edited by P.K Rohatgi, TMS, Warrendale, 1993, 63-82.
182. S. Abraham, B.C. Pai, K.G. Satyanarayana and V.K. Vaidhyan: *J. Mater. Sci.*, 1992, 27, 3479.
183. L.A. Masur, A. Mortensen, J.A. Cornie and M.C. Flemings: *Metall. Trans.* 1989, 20A, 2549-2557.
184. A. Mortensen, M.N. Gungar, J.A. Cornis and M.C. Flemings: *J. Met.*, 1986, 38(3), 30-35.
185. N.L. Baturinskaya, N.A. Kalchuk, Yu.D. Sezonenco and V.G. Chenayi: *Russ. Metall.*, 1986, 3, 145-147.
186. T.W. Clyne, M.G. Bader, G.R. Capleman and P.A. Hubert: *J. Met.*, 1985, 20, 85- 96.
187. M. yang and V.D. Scott: *J. Mat. Sci.*, 1991, 26, 2245-2254.
188. G.F. Bolling, J. Cise and G.S. Cole: US patent No: 3607 241, 1971.
189. M.K. Surappa: PhD Thesis, Indian institute of Science, Bangalore, 1979.
190. D.R. Uhlmann, B. Chalmers and K.A. Jackson: *J. Applied Phy*, 1964, 35(10), 2986-2993.
191. G.S. Hanumanth and G.A. Irons: *Met Mater. Trans.*, 1996, 27B, 663
192. Shih-Chang Jeng and Snn-Wen Chen: *Acta. Mater.*, 1997, 45(12), 4887.
193. S. Gowri and F.H. Samuel: *Met. Trans A*, 1992, 23A, 3369-3376
194. H. Kaufmann. E. Neuworth, J. Larcher and H. Pacyna, in *Aluminium Alloys* eds. L. Arnberg, O. Lohne. E. Nes and N. Ryum, NTH and SINTEF, Trondheim, Norway, 1992, p.81.
195. K. Ho and R.D Pehlke: *Met. Trans.*, 1985, 16B, 585-594
196. T.W. Clyne and A. Garcia: *Int. J. Heat Mass Transfer* 1980, 23, 773-782.
197. M. Prates and H. Biloni: *Metall. Trans.* 1972, 3, 1501-1510
198. S.A. Levy, S. Lipson and H. Rosenthal: *AFS Cast Metals Research J.*, 1969, 5, 9-13.

199. R.C. Sen: *AFS Cast Metals Research J.*, 1970, 6, 105- 110.
200. E.S. Tillman and J. T. Berry: *AFS Cast Metals Research J.*, 1972, 8, 1-6.
201. K. Ho and R.D. Pehlke: *Mater. Sci. Tech*, 1987, 3, 466-476.
202. B.G. Thomas, I.V. Somasekhara and J.K. BrimaKombe: *Metall. Trans.* 1984, 15B, 307-318.
203. G.H. Diega and D. R. Poirer, *Transport Phenomena in Metallurgy*, Addition – Wesley Publishing Co., Massachusetts 1974, 585-594.
204. J.Szekely and N.J. Themelis: *Rate Phenomena in Process Metallurgy*, Willey, Intterscience, Newyork, 1971, pp190-196.
205. T.S Prasanna Kumar and K. Narayan Prabhu: *Met. Trans. B*, 1991, 22B, 717-727
206. K. Narayan Prabhu, D. Maheswaran, T.S. Prasanna Kumar and N. Venkataraman: *AFS Trans.*, 1992, 611-617
207. K. Narayan Prabhu: Ph.D. Thesis, Manglore University, India, 1990.
208. H. Srinivasa Rao, B. C. Pai, P. L. Vinod, R. Manoj and S. S. Sreekumar, *Pract. Metall.* 1994, 31, 190.
209. D. J. Lloyd, H. P. Lagace and A. D. Mc Leod, in "Proceedings of the International Conference on Composite Materials", ICCM-III, (ed. by H. Ishida), Elsevier Applied Science, London, 1980, 359.
210. D. J. Lloyd and I. Jin: *Metall. Trans.* 1988, 19A, 3107.
211. R. Warren and C. H. Anderson: *Composites* 1984, 15, 101-111.
212. J. C. Lee, Jung. In Lee and Ho. In. Lee: *Scripta Mater.* 1996, 35, 721-726.
213. L. Salvo, G. L. Esperance, M. Suery and J. G. Legoux: *Mater. Sci. Eng.* 1994, A177, 173.
214. T. Iseki, T. Kameda and T. Muruyama: *J. Mater. Sci.*, 1984, 19, 1692-1698.
215. D. J. Lee, M. D. Vaudin, C. A. Handwerker and U. A. Ka Ttner, in "Proceedings of the Conference of Materials Research Society, 1988, 120, 357.
216. H. J. Rack, in "Proceedings of the Conference of Dispersion Strengthened Aluminium Alloys", edited by Y. M. Kim and W. M. Griffith (TMS, Warrendale, PA, 1988), 649.

217. S. R. Nutt, in "Proceedings of the Conference on Interfaces in Metal Matrix Composites", edited by A. K. Dhingra and S. G. Fishman (TMS, Warrendale, PA, 1986), 157.
218. S. R. Nutt and R. W. Carpenter: *Mater. Sci. Eng.* 1985, 75, 169-177.
219. C. G. Levi, G. J. Abbaschian and R. Mehrabian: *Metal Trans.* 1978, 9A, 697-.
220. T. Sritharan, K. Xia, J. Heathcock and J. Mihelich, in "Proceedings of the Conference on Metal and Ceramic Matrix Composites; Processing, Modelling and Mechanical", edited by R. R. Bhaghat (TMS, Warrendale, PA, 1990), 13.
221. K. K. Chawla, in "Composite Materials Science and Engineering" (Springer, New York, 1987) p83.
222. A. K. Kuruvila, V. V. Bhanu Prasad, K. S. Prasad and Y. R. Mahajan: *Bull. Mater. Sci.* 1989, 12, 495-505.
223. F. Zok, S. Janshon, A. G. Evans and V. Nardone: *Metall. Trans.* 1991, 22A, 2107-2117.
224. P. A. Earvolino, M. E. Fine, J. R. Wecterman and V. R. Parameshwaran: *Scripta Metall. Mater.* 1992, 26, 945.
225. S. R. Gunawardana, S. Jansson and F. A. Leckie, in "Failure mechanisms in high temperature composites" (ASME, New York, NY), 22.
226. Roger, B. Clough, Francis. S. Biancaniello, Hayden. N. G. Wadley and Ursula. R. Kattner: *Metall. Trans.* 1990, 21A, 2747-2757.
227. S. M. Arnold, V. K. Arya and M. E. Metis: *J. Compos. Mater.*, 1992, 26, 1287.
228. L. J. Ghosh and B. A. Lerch, in "NASA Tech. Memo., NASA TM-102295", (1989) 19.
229. R. K. Pandey and U. T. S. Pillai, in "Proceedings of the 4th International Conference on Fatigue Crack Growth (Fatigue 90)" (ed. by H. Kitagawa and T. Tanaka), Vol. 2, MCEP, Hawaii, USA, 1990, 653.
230. U.T.S.Pillai, R.K.Pandey and P.K.Rohatgi: *Engg. Fracture Mechanics*, 1987, 28 (2), 461-477
231. K. Li, X. D. Jim, B. D. Yan and P. X. Li: *Composites* 1992, 23, 54-58.
232. D. P. H. Hasselman and K. Y. Donaldson: *J. Am. Ceram. Soc.* 1992, 75, 3137-3140.

233. A. L. Geiger, D. P. H. Hasselman and K. Y. Donaldson: *J. Mater. Sci. Lett.* 1993, 12, 420.
234. J.V. Beck: *Inst.J.Heat Mass Transfer*, 1967, 10, 1615-1617.
235. J.V. Beck: *Inst.J.Heat Mass Transfer*, 1970, 13, 703-716.
236. Z.Hashin and S.Strikman: *J. App. Phys.*, 1962, 33, 3125.
237. B.W.Rosen and Z.Hashin: *Int. J. Engg. Sci.* 1970, 8, 157
238. R. Taylor: in International Encyclopedia of Composites, Vol.5, Thermophysical properties (ed. by S.M. Lee) CHH publishers, New York, 1991, 530.
239. R.I. Mackay and J.E. Gruzleski: *Int. J.Cast. Metals Res.*, 1997, 10, 131-145.
240. Geetha Ramani, R.M. Pillai, B.C. Pai and T.R. Rammohan: *Composites*, 1991, 22, 143-150.
241. Ning Wang, Zhinui Wang, George C.Weatherly: in Proc. of Intl. Conf. on Fabrication of Particulates Reinforced Metal Composites (ed. J. Masounave and F.G. Hamel), 17-29, Sept.1990, Quebec, Canada, 145-151.
242. N. Eustathopoulos, J.C. Joud, P. Desre and J.M. Hictu: *J. Mater. Sci.* 1974, 9, 1233.
243. J.K. Kim and P.K. Rohatgi: *Met. Mat. Trans A*, 2000, 31A, 1295-1304.
244. B. Maruyama, F.J. Ohuchi and L. Rabenberg: *J. Mater. Sci. Letter.* 1990, 9, 864.
245. B. Maruyama and L. Rabenberg: *Mater, Res. Soc. Symp. Proc.*233
246. R. Asthana: *J. Mater. Sci.*, 1998, 33, 1959-1980.
247. M. Yang and V.D. Scott: *Carbon* 1991, 29, 877.
248. V. Laurent, D. Chatain and N. Eustathopoulos: *Mater. Sci. Engg. A*, 1991, 135, 89-94.
249. Y. Le Petitcorps, J.M. Quenisset, G. Le Borgne and M. Barthole: *Mater. Sci. Eng.* 1991, vol. A135, 37-40.
250. D. Lu: Doctoral Thesis, Shanghai Jiao Tong University, 1999.
251. S. Ciby, B.C. Pai, K.G. Satynarayana, V.K. Vaidyan and P.K. Rohatgi: *J. Mater. Engg. and Perfor.*, 1993, 2, 353-358
252. F. Fogar: *AFS Trans.* 1988, 96, 395-402
253. S.H.J. Lo, S. Dionne, M. Sahoo and H.M. Hawthorne: *J. Mater. Sci.* 1992, 27, 5681-5691

254. S. Dermarkar: *Metals and Materials*, 1986, 2, 144-146
255. Anon: *Auto. Engg.* 1986, 94, 61-65
256. S.O. Lasday: *Ind. Heat.* 1987, 54, 20-21
257. S.V. Prasad and K.R. Mecklenburg: *Wear* 1993, 162, 47-56
258. S. Canumalla, S.A. Dynan, D.J. Green, R.B. Bhagat and R.N. Panborn: *J. of Compos. Materials* 1995, 29, 653-670
259. J.C. Lee, G.H. Kim and H.I. Lee: *Mater. Sci. Tech.* 1997, 13, 182-186
260. W.M. Zhong, G.L. Esperance and M. Suery: *Met. Trans.* 1995, 26A, 2625-2634
261. William. J. Baxter and Anil. K. Sachdev: *Met. Mater. Trans.* 1999, 30A, 815-824
262. J.A. Isaacs, F. Taricco, V.J. Michaud and A. Mortenson: *Met. Trans.* 1991, 22A, 2855-2862
263. T. Lebeau, J.O. Stromolson, J.E. Gruzleski and R.A.L. Drew: *Mater. Char.* 1995, 35, 11-22
264. MMTCL Ceramic Fibre – Thermal Ceramics Products leaflet – Murugappa Morgan Thermal Ceramics Ltd., Chennai 1997.
265. MTDATA Software, National Physical Laboratory, United Kingdom, 2001.
266. A. Banerji and P.K. Rohatgi: *J. Mater. Sci.* 1982, 17 (2), 335-342
267. A.D. Mcleod and C.M. Gabriel: *Met. Trans.* 1992, 23A, 1279-1283
268. L.F. Mondolfo: ‘Aluminium alloys: Structures and properties’, First Edition, Butterworths, London, 1976.
269. H. Ribes and M.Suery: *Scripta Metall.*, 1989, 23, 705-709
270. H. Ribes, R. Da Silva, M. Suery and T. Bretheau: *Mater. Sci. Tech.*, 1990, 6, 621-628.
271. R.I. Mackay and J.E. Gruzleski: *Int. J. Cast Metals Res.*, 1997, 10, 131-145.
272. P.K. Rohatgi: *J. Metals*, 1994, 46, 55-59.
273. P.K. Rohatgi, R. Q. Guo, P. Huang and S. Ray: *Metall. Mater Trans*, 1997, 28, 245-250.
274. P.K. Rohatgi, Z. Grony, J. Sobczak and N. Sobczak: *Transactions of the Foundry Research Institute*, 1993, 143-157.
275. P.K. Rohatgi, R. Q. Guo, B.N. Keshavaram and G. Golden: *AFS Trans*, 1995, 103, 575-579.
276. G. Golden: *EPRI Journal*, 1994, 19, 46-49.

277. B.N. Keshavaram, K.G. Satyanarayana, B. Majumdar, P.K. Rohatgi and B. Duttagune in Proceedings of the 6th Inter. Conf. on Fracture ICF – 6 (eds. S.R.Valluri, D.M.R.Taplin, P.Rama Rao, J.F.Knift and R.Dubey), New Delhi, Dec 1984, Pergamon Publishers, New York, 2979-2988.
278. P. K. Rohatgi: US patent 5 228 494, 1993.
279. P.K. Rohatgi, R Q. Guo, H. Iksan and R. Asthana: *Mater. Sci. Engg.*, 1998, A244, 22-30.
280. P. K. Rohatgi: US patent 5 711 362, 1998.
281. P. K. Rohatgi: US patent 5 899 256, 1999.
282. R.M. Pillai and Geetha Ramani: RRL-T Annual Report, 1990.
283. R. Mehrabian, R.G. Riek and M.C. Flemings: *Met. Trans.* 1974, 5(8), 1899-1905.
284. M.C. Flemings, R.G. Riek and K.P. Young: *Mater. Sci. Engg.* 1976, 25, 103.
285. R.Q. Guo and P.K. Rohatgi: *Met. Mater. Trans. B* 1998, 29B, 519-525.
286. B.P. Krishnan and P.K. Rohatgi: *Met. Technol.*, 1984, 11, 41.

AWARDS, PATENTS AND PUBLICATIONS

AWARDS

1. **“Best Research Paper Award”** for the paper "Processing of short ceramic fibre reinforced aluminium matrix composites", **T.P.D. Rajan**, R.M. Pillai and B.C. Pai presented in the Second National Symposium of Research Scholars on Metals and Materials, IIT Madras, July 3-4, 1998.
2. **“Soli-Commissariat Best Research Paper Award”** for the paper "Casting/Mould interfacial heat transfer during solidification of aluminium matrix composites", **T.P.D. Rajan**, K. Narayan Prabhu, R.M. Pillai and B.C. Pai presented in the 6th Asian Foundry Congress and 47th Indian Foundry, Calcutta, Jan. 23-26 1999.
3. **DST- Young Scientist Fast Track Project Award** (January 2002) on “Processing and Characterization of Hybrid and Functionally Gradient Aluminium Matrix Composites”.
4. **“Best SEM Microstructure Award”** for an SEM structure on Al(356)-Flyash composite at 25th Annual Conference of Electron Microscopic Society of India (EMSI) held at IIT, Mumbai, Feb 19-22, 2002

PATENTS

1. **A novel surface treatment method on the reinforcements for the synthesis of metal matrix composites.**
T.P.D. Rajan, R.M. Pillai and B.C. Pai (to be filed)

PUBLICATIONS (*Published/accepted and communicated*)

1. **Reinforcement coatings and interfaces in aluminium metal matrix composites**
T.P.D. Rajan, R.M. Pillai and B.C. Pai,
Journal of Mat. Sci., Vol. 33 (1998) p3491-3503.
2. **Processing of short ceramic fibre reinforced aluminium matrix composites**
T.P.D. Rajan, R.M. Pillai and B.C. Pai in the Proceedings of Second National Symposium of Research Scholars on Metals and Materials, IIT Madras, July 3-4, 1998. (*Awarded the Best Research Paper Award*)
3. **Casting/Mould interfacial heat transfer during solidification of aluminium matrix composites**
T.P.D. Rajan, K. Narayan Prabhu, R.M. Pillai and B.C. Pai in the Conference proceedings of Asian Foundry Congress-6 / Indian Foundry Congress - 47, Indian Institute of Foundry man, Calcutta, Jan. 23-26, 1999. p 119-128 (*Awarded the Best Research Paper Award*)

4. **Studies on fibre treatments and fabrication of short ceramic fibre reinforced aluminium matrix composites**
T.P.D. Rajan, R.M. Pillai and B.C. Pai,
Journal of Mat. Sci. Letts. Vol. 18 (1999) p1683-1686.
5. **Computer aided cooling curve analysis of aluminium matrix composites**
T.P.D. Rajan, R.M. Pillai and B.C. Pai, in the Proceedings of 4th Pacific Rim International Conference on "Modelling of Casting and Solidification Processes" Seoul, South Korea, Sept. 5-8th 1999. p399-407
6. **Characterisation of Interfaces in aluminosilicate short fibre reinforced aluminum matrix composites**
T.P.D. Rajan, R.M. Pillai and B.C. Pai, International Conference on Advanced Composites – 2000, Bangalore, 24-26, August 2000. p 728-736.
7. **Structural and Interfacial Characteristics of Mono and Hybrid Aluminium Matrix Composites**
T.P.D. Rajan, R.M. Pillai and B.C. Pai, in the Proceedings of Second National Symposium of Research Scholars on Metals and Materials, IIT Madras, Sept 8-9, 2000. p119-128.
8. **Influence of Processing Methods on the structure and properties of Al-7Si-0.35Mg(356)-Flyash composites**
T.P.D. Rajan, R.M. Pillai, B.C. Pai, K.G. Satyanarayana and P. Rohatgi, in the Proceedings of Conference on Recent Advances in Materials Processing- RAMP2001, September 7-8, 2001, Annamalai University, Annamalai Nager, Tamil Nadu, India. p327-334
9. **Interfacial Reactions in Aluminosilicate short fibre reinforced composites**
T.P.D. Rajan, R.M. Pillai and B.C. Pai,
Metallurgical and Materials Transactions, in press (July 2002)
10. **Hybrid Metal Matrix Composites**
T.P.D. Rajan, R.M. Pillai and B.C. Pai,
(Synopsis accepted, Paper communicated to Inter. Mater. Review)
11. **Structural behaviour of Al-7Si-0.3Mg (356)- Fly ash composites processed by liquid and semisolid stir cast composites**
T.P.D. Rajan , R.M. Pillai, B.C. Pai, K.G. Satyanarayana and P. Rohatgi
(Communicated to Mater Sci. Engg. A, under revision)

To be communicated

12. **Solidification Characteristics of discontinuous aluminium matrix composites**
T.P.D. Rajan, K. Narayan Prabhu, R.M. Pillai and B.C. Pai,
(to be communicated to Acta Mater.)

13. **The stability of silicon carbide in metal matrix composites**
T.P.D. Rajan, R.M. Pillai and B.C. Pai
(to be communicated to Journal of Mat. Sci.,)
14. **Processing and Properties of SiC_(p) / graphite reinforced hybrid aluminium matrix composites**
T.P.D. Rajan, R.M. Pillai and B.C. Pai,
(to be communicated to Mat. Sci. and Tech.)
15. **Microstructural characteristics of discontinuously reinforced aluminium matrix composites**
T.P.D. Rajan, R.M. Pillai and B.C. Pai,
(to be communicated to Materials Characterisation).
16. **Solidification behaviour of SiC reinforced cast and wrought aluminium alloy matrix composites**
T.P.D. Rajan, R.M. Pillai and B.C. Pai,
(to be communicated to Metallurgical and Materials Transactions A)
17. **Synthesis and Characteristics of Al(356)-SiC_(p) -C_f mono and hybrid metal matrix composites.**
T.P.D. Rajan, R.M. Pillai and B.C. Pai,
(to be communicated)

PRESENTATIONS

Presented

1. **Reinforcement coating and its influence on interfaces of aluminium metal matrix composites,**
T.P.D. Rajan, R.M. Pillai and B.C. Pai, Presented at the National Conference on Science and Technology of Surface and Interfaces, IIT Kharagpur, Dec. 16-18, 1996
2. **Microstructural Evaluation of surface treated silicon carbide reinforced aluminium matrix composites,**
T.P.D. Rajan, S. R. Santhosh, R.M. Pillai and B.C. Pai, Presented at the National Conference on Characterisation of Materials, IIM Trivandrum Chapter., Aug 20-21, 1998.
3. **Synthesis and Characterisation of 356 Al Alloy- SiC_(p) -Gr_(p) / Al₂O₃ hybrid composites,**
T.P.D. Rajan, R.M. Pillai and B.C. Pai, Presented at 52nd Annual Technical Meeting of Indian Institute of Metals, Bangalore, 16-17 Nov. 1998)

4. **Microstructural aspects of cast hybrid aluminium metal matrix Composites,**
T.P.D. Rajan, R.M. Pillai and B.C. Pai, Presented at 53rd Annual Technical Meeting of Indian Institute of Metals, Kanpur, 13-16 Nov. 1999)
5. **Processing and Characterisation of SiC_(p) and C_(f) reinforced hybrid aluminium matrix composites,**
T.P.D. Rajan, R.M. Pillai and B.C. Pai, National Seminar on Materials Processing and Characterisation – Challenges and Prospects, Trivandrum, February 3-4, 2000.
6. **Studies on Processing of Aluminium-Fly Ash Composites,**
T.P.D. Rajan, R.M. Pillai, B.C. Pai, K.G. Satyanarayana and P. Rohatgi, 54th Annual Technical Meeting, Indian Institute of Metals at Bhilai, 14 – 17th November 2000.
7. **Effect of dispersoid size and loading on solidification curves of Al-SiC_(p) composites by computer aided cooling curve analysis,**
T.P.D. Rajan, R.M. Pillai and B.C. Pai, 55th Annual Technical Meeting, Indian Institute of Metals at Bhuvaneshwar, 17 – 20th November 2001.

To be Presented

8. **Thermal analysis of SiC reinforced cast and wrought aluminium alloy matrix composites**
T.P.D. Rajan, R.M. Pillai and B.C. Pai, International Conference on Non-Ferrous Metals-2002, organised by NFTDC, Hyderabad, India during June 28-29, 2002.